MASS SPECTROMETRIC STUDIES OF NOVEL LIPID-BASED NANOMATERIALS: INVESTIGATIONS OF THE INTRACELLULAR FATE

A Thesis Submitted to the College of Graduate Studies and Research

in Partial Fulfillment of the Requirements

for the Degree of Doctor of Philosophy

in the College of Pharmacy and Nutrition

University of Saskatchewan

Saskatoon

By

McDonald Donkuru

PERMISSION TO USE

In presenting this thesis in partial fulfillment of the requirements for a Postgraduate degree from the University of Saskatchewan, I agree that the Libraries of this University may make it freely available for inspection. I further agree that permission for copying of this thesis in any manner, in whole or in part, for scholarly purposes may be granted by the professor or professors who supervised my thesis work or, in their absence, by the Head of the Department or the Dean of the College in which my thesis work was done. It is understood that any copying or publication or use of this thesis or parts thereof for financial gain shall not be allowed without my written permission. It is also understood that due recognition shall be given to me and to the University of Saskatchewan in any scholarly use which may be made of any material in my thesis.

Requests for permission to copy or to make other uses of materials in this thesis in whole or part should be addressed to:

Dean of the College of Pharmacy and Nutrition
University of Saskatchewan
Saskatoon, Saskatchewan S7N 5E5
Canada

OR

Dean of the College of Graduate and Postdoctoral Studies
University of Saskatchewan
Saskatoon, Saskatchewan S7N 5A2
Canada

ABSTRACT

Dicatonic gemini surfactants have, within the past two decades, demonstrated advancing non-viral gene transfection ability in cell cultures and in animal models. However, knowledge of the intracellular/subcellular fate of gemini surfactants that may further advance gemini surfactant-based gene transfection is very limited. Therefore, my Ph.D. research conducted the investigation of gemini surfactants within transfected PAM212 keratinocytes including the development of *effective* bioanalytical mass spectrometric (MS) methods necessary for such investigations.

For effective mass spectrometric bioanalysis of the gemini surfactants within cellular matrix their fingerprint fragment ions necessary for targeted identification and quantification were first determined through single-stage (MS), tandem (MS/MS) and multi-stage (MS^3) analyses. The molecular composition of gemini surfactants was confirmed. In addition, fragmentation mechanisms of novel dipyridinium and β-cyclodextrin-based diquaternary ammonium molecules (chosen as study compounds) were established in detail, allowing for their qualititive and quantitative analysis.

Hydrophilic interaction liquid chromatography-based (HILIC)-MS/MS methods, alone and in conjunction with the method of standard addition, were subsequently developed/validated by adopting multiple reaction monitoring (MRM), ensuring selectivity alongside the distinctive chromatographic separation. The analytical strategy ensured selectivity/specificity for target gemini surfactants including two lead

compounds, 16(Py)-S-2-S-(Py)16 and 16-3-16. The validated HILIC-MS/MS methods were more sensitive, faster and have simplified isocratic elution relative to recently reported methods.

In the application to nanoparticle-based gene transfection studies, the HILIC-MS/MS and standard addition–HILIC-MS/MS methods allowed a comprehensive investigation of the cellular uptake, intracellular deposition and subcellular distribution of the 16(Py)-S-2-S-(Py)16 and 16-3-16 gemini surfactants. The results showed similar cellular uptake and intracellular depletion trends but different subcellular distribution profiles. Both gemini surfactants showed an initial spike in their concentration within cells upon addition of gemini surfactant-based DNA nanoparticles to the cells, as would be expected to achieve nanoparticle entry into cells during transfection. The intracellular gemini surfactant content, however, underwent a depletion upon removal of the added nanoparticles – a trend observed for the first time and attributable to either gemini surfactant biodegradation or exocytosis from host cells.

Results of subcellular distribution showed higher distribution of 16-3-16 to the mitochondria and nucleus relative to its 16(Py)-S-2-S-(Py)16 counterpart ($p < 0.05$), with the two having similar distribution to the cell membrane, cytosol and the remnant subcellular residue. This differential subcellular distribution, determined for the first time, may explain a suggested higher toxicity for 16-3-16 as its increased distribution to the mitochondria and nucleus could impact their biological integrity and function. Herein, the investigations and findings will benefit further exploration of gemini surfactants

through the established molecular fragmentation fingerprints of novel compounds and comprehensive LC-MRM-MS bioanalytical strategies for studying the biological fate, elucidating varying toxicity and assessing possible metabolite formation.

ACKNOWLEDGEMENTS

My appreciation is first to my supervisor, Dr. Anas El-Aneed, for his professional and moral support, guidance and patience throughout my studies. I have benefited from his knowledge, solid advice and vision, particularly so when we explored new ideas. His confidence in my research inspired me and his careful editing contributed enormously to the production of this thesis.

I also thank the members of my advisory committee, Drs. Ildiko Badea, John Headley and George Katselis. By the same measure, many thanks is extended to Dr. Ed Krol, who chaired my first three committee meetings and to Dr. Dave Blackburn who chaired my final committee meetings. Their solid review and advice on my proposed research and my yearly progress were ultimately beneficial to my overall research and experience.

I thank Dr. Ronald Verrall and Dr. Jackson Chitanda for kindly providing some of the geimi surfactants required for my research and for availing their helpful expertise to me during synthesis of other required gemini surfactants. Here, I extend thanks to Ms. Behshad Vatanparast who undertook and completed the synthesis with me during her summer 2012 research. Equally, I thank Dr. Joshua Buse for thoughtfully providing one gemini surfactant at the time of completing his PhD research, thus helping save time and resources in an otherwise required synthesis.

Sincere appreciation must be extended to Ms. Deborah Michel for the basic training in mass spectrometry provided to me and for the professionaly cordial support throughout my research. Appreciation also goes to my colleagues of the Drug Discovery & Development Research Group (DDDRG) for fruitful friendships, technical assistance and other support; Ms. Mays Al-Dulaymi, Ms. Saniya Alwani, Ms. Mona Hamada, Dr. Amal Makhlouf, Mr. Waleed Mohammed-Saeid and Mr. Hossein Rafiei. In the same vein, I remember and also thank immediate-past colleagues of the DDDRG team: Ms. Hanan Elsayed, Ms. Catherine Hutchinson, Ms. Randeep Kaur, Dr. Isaac Asiamah, Dr. Joshua Buse, Dr. M. Poorghorban, Dr. Istvan Hajdu and Dr. Jagbir Singh.

The following institutions are duly recognized: the College of Pharmacy & Nutrition (University of Saskatchewan, Saskatoon, SK) provided post-graduate scholarship, research workspace/facilities and reputable leadership/mentorship. The College of Graduate Studies & Research also provided funding the form of travel award, enabling me present my research at conferences. The research equipment and supplies were funded by the Natural Sciences and Engineering Research Council of Canada (NSERC), Canadian Foundation for Innovation and College of Pharmacy & Nutrition. The Saskatchewan Structural Science Centre (Saskatoon, SK) also provided the use of their instrumental research facility.

Deep appreciation is owed to a large number of friends, fellows and individuals whose coming together creates a perfect community that fosters a sense of belonging, mutual support and greater impact on society. Much thanks to M. Bagonluri family, E.

Mupondwa family, M. Nketia family, N. Puobi family, A. Salifu family, E. Tuurosong family, Seraphine Kogo, Evelyn Songsore, among numerous others that are not listed simply for lack of space. In the same vein, much appreciation goes to friends and fellows of GCAS, ACCC, KenSask and *Our Lady of Lourdes Church*, Saskatoon, SK [GCAS: Ghanaian-Canadian Association of Saskatoon Inc., ACCC: African-Canadian Catholic Community, KenSask: Community of Kenyans and East-African neighbours in Saskatoon].

Finally and most importantly, I would like to give ultimate gratitude to my parents and siblings (Aaron, Bruce, Ernestina, Martina, Edna) and all my extended family for the continued love, support and prayers throughout my academic pursuits. The first and lasting strength I have had for this journey is that which came from all of my family.

McDonald Donkuru

June 2017, Saskatoon, SK, Canada

DEDICATION

To Micah, Belicia and Beata, who are my *brightest diamonds*. To my parents, Clothilda and Moses Donkuru, who are my roots. And to Uncle Martin Abu, who has been a source of opportunity, goodwill and inspiration.

TABLE OF CONTENTS

LIST OF FIGURES

LIST OF TABLES

LIST OF ABBREVIATIONS

16-3-16 N,N-bis(dimethylhexadecyl)-1,3-propane-diammonium dibromide

16-3-16-$\boldsymbol{d_{66}}$ N,N-bis(dimethylhexadecyl-d_{16})-1,3-propane-diammonium dibromide

12(Py)-S-2-S-(Py)12: 1,1'-[ethane-1,2-diylbis(sulfanediyldodecane-1,2-diyl)]dipyridinium

16(Py)-S-2-S-(Py)16: 1,1'-[ethane-1,2-diylbis(sulfanediylhexadecane-1,2-diyl)]dipyridinium

14(Py)-S-2-S-(Py)14: 1,1'-[ethane-1,2-diylbis(sulfanediyltetradecane-1,2-diyl)]dipyridinium

18(Py)-S-2-S-(Py)18: 1,1'-[ethane-1,2-diylbis(sulfanediyloctadecane-1,2-diyl)]dipyridinium

16(Py)-S-2-S-(Py)16-$\boldsymbol{d_{10}}$: 1,1'-[ethane-1,2-diylbis(sulfanediylhexadecane-1,2-diyl)]dipyridinium-d_{10}

CE Collision energy

CID Collision-induced dissociation

CMC Critical micelle concentration

DART Direct analysis in real time

DESI Desorption electrospray ionization

DNA Deoxyribonucleic acid

DOPE 1,2-dioleoyl-*sn*-glycero-3-phosphoethanolamine

ESI	Electrospray ionization
FC	Fast liquid chromatography
FIA	Flow injection analysis
m-s-m	Composition of diquaternary ammonium gemini surfactants with the structure sequence *hydrocarbon tail–carbon spacer chain–hydrocarbon tail*
HILIC	Hydrophilic interaction lliquid chromatography
HPLC	High performance liquid chromatography
HQC	High quality control
HR-MS	High resolution mass spectrometry
IFN-γ	Interferon-gamma (interferon-γ)
LC	Liquid chromatography
LLOQ	Lowest limit of quantification
LLOD	Lower limit of detection
LQC	Low quality control
MALDI	Matrix assisted laser desorption ionization
MEM	Minimal essential media
MQC	Middle quality control
MRM	Multiple reaction monitoring
MS	Mass spectrometry
MS/MS	Tandem mass spectrometry

MS^n	Multi-stage mass spectrometry
m/z	Mass-to-charge ratio
PAM212	Murine epidermal keratinocyte cells
PEG	Polyethylene glycol
P/G/L	Plasmid/gemini surfactant/DOPE nanoparticle formulation
ppm	Parts per million
QqQ-LIT-MS	Triple quadrupole-linear ion trap mass spectrometer
Q-ToF-MS	Quadrupole time of flight mass spectrometer
RNA	Ribonucleic acid
RSD	Relative standard deviation
ToF	Time of Flight
USFDA	United States of America Food and Drug Administration
UV	Ultraviolet

CHAPTER 1:

Literature Review and Proposed Research

1. Introduction

As the development and biomedical application of novel lipid-based nanoparticles intensifies, there is a need to evaluate the intracellular deposition and biological fate of such nanoparticles. Mass spectrometry (MS) is capable of investigating the intracellular fate/profiles of lipid-based nanoparticles with highthroughput capabilities. MS, as an analytical technique, allows for screening, detection and quantification of targeted molecular species.

Used in the form of supramolecular aggregates, biomedical nanoparticles inevitably enter or accumulate in cells wherein the exact intracellular fate of the foreign chemical material is largely unknown.[(1)] Mass spectrometric analysis can be conducted on lipid-based nanoparticles extracted from simple, highly purified samples or within highly complex, multi-component biological extracts[(2)]. Unlike other methods, MS offers high sensitivity and specificity to its qualitative and quantitative analysis even for unrefined, complex biological samples.[(3, 4)] Thus, various mass spectrometric-based analytical methods are proposed for studying the intracellular fate of gemini surfactant-based nanoparticles as outlined in this report.

1.1 Nanomedical drug delivery: an overview

Safe and efficient delivery of therapeutic agents, such as cytotoxic anti-cancer drugs and therapeutic DNA, into diseased cells remains a critical objective of an increasingly intense drug

delivery research within both academia and the pharmaceutical industry.[5-7] However, when introducing any foreign chemical substances into cells, there is an accompanying imperative to determine their intracellular profiles and safety. In this regard, MS provides a suitable and sensitive means of investigating the biotransformation and safety profiles of foreign substances found within cells.

Developments in nanotechnology is enabling the design of new molecules (biological, biomimetic), and their novel complex aggregates, at the nanometer (nm) scale (Figure 1.1), to achieve desired structures, functions and applications. Such new molecules include new amphiphilic lipids,[8-12] surfactants (conventional[13] and the so-called "gemini" types[14-17]), peptides[18-23], polymers[24-28] and dendrimers[29-32]. On the other hand, the complex aggregates include micelles, liposomes (or vesicles), cubosomes and similar supramolecular aggregates[33-35] (covered under *Section 1.3.2*). These supramolecular structures fulfill functions including drug solubilization, encapsulation, transmembrane transport and delivery into target cells.[33-35]

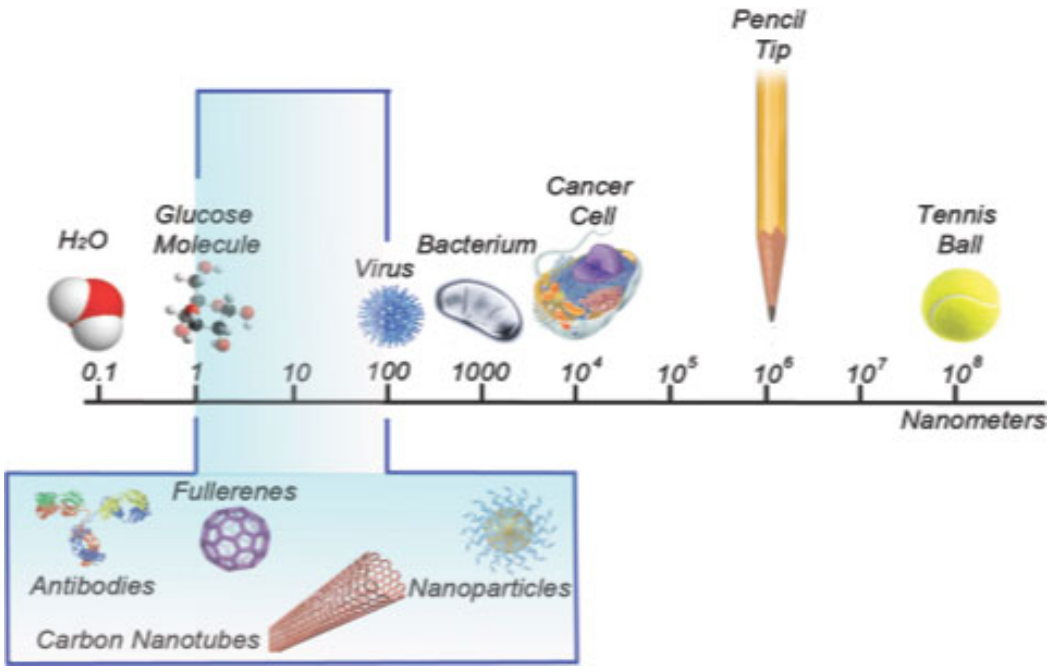

Figure 1.1: A logarithmic scale depiction of matter at the nanometer scale (see blue outline). Much smaller unit H_2O molecule and larger-sized entities are included for comparisons. Adopted from International Iberian Nanotechnology Laboratory (official website: "http://inl.int/what-is-nanotechnology-2").

The novelty with these supramolecular nanomaterials is the ability to precisely control their functions by fine-tuning specific parameters such as particle size, shape (morphology), structure (internal, external), surface properties (coating, zeta potential, binding specificity), chemical composition and concentrations.[36-44] Although liposomes and similar nanoparticles, with these fine-tunable parameters, can encapsulate and deliver active ingredients to cells to elicit therapeutic effect, the nanoparticles are also known to cause cytotoxicity following *in vitro*

and *in vivo* treatments. In addition, the fate of the delivery agent (i.e., nanoparticle carrier) is still not fully studied or understood.[45-50]

While this research focuses on nanoparticle drug carriers that serve biomedical purpose, it is worth noting that the lack of clarity on biological fate also surrounds environmentally released nanoparticles which become passively incorporated within organisms.[1, 51-53] Biological uptake of nanoparticles from nanoparticle-polluted environments represents an unintended consequence, but it nonetheless happens from the continuous interaction between organisms (skin, lungs, gut) and the environment.

Given the above knowledge gap, my research will implement a range of analytical ***mass spectrometric*** methods to study the intracellular persistence/retention and bio-localization properties of novel gemini surfactant molecules recently reported to possess effective drug-delivery capabilities. The broader research on biological fate of xenobiotics also involves investigating their biodegradation profiles. But for the chosen novel gemini surfactants, their intracellular persistence and subcellular distribution must first be determined so as to guide future studies on the gemini surfactant biotransformation.

Specifically, my research focus is to screen, identify and quantify nanoparticles' constituent amphiphiles (discussed in *Section 2.2.2*) after introduction into the cells via transfection. This will be achieved by developing and validating MS-based methods, which will then be used to analyze the nanoparticle-treated cells. Ultimately, an understanding of the gemini surfactant biological fate will be useful for the development of safer, less toxic and more efficient gemini surfactants; and, for establishing safety guidelines regarding nanoparticle composition and application.

1.2 Nanotechnology, its scope and principles

A unique craftsmanship of nature is that, matter has the ability to be organized at various scales of structural build-up (Figure 1.1). Nanotechnology, in a classical sense, involves the "understanding and control of matter at dimensions of roughly 1-100 nm, where unique phenomena enable novel applications" (NNI, USA)[54]. In a wider context, nanotechnology, covers matter having dimensions measuring up to 100–500 nm.[55] A reason for this is that, the *nano-scale* properties can remain undiminished for dimensions ranging up to 500 nm (or more) when focusing nanotechnology on drug delivery.

It should be recognized that the ***nanometer-scale*** (1 nm: 10^{-9} m) is next to the angstrom-scale (1 Å: 10^{-10} m) for bond lengths or interatomic distances. Thus naturally, when dimensions decreases to the nanometer range, the building blocks of the nano-materials are arranged at just few layers of atoms or molecules.[56-60] Intense fabrication of nanomaterials, nanoparticles and nanodevices has evolved based on the concept of atom-by-atom or molecule-by-molecule organization of matter.[56, 57, 59] Nanotechnology itself is traced back to the late 1950s when scientists began to conceptualize the *nano-scale* realm of matter and the immense synthetic approach in being able to "re-create" matter by directly assembling or organizing atoms.[61]

Nanomaterials, nanoparticles or nanodevices may be described, summarily, as: 1) originating by natural, incidental or engineered phenomena;[62] 2) existing as or containing particulate entities (or films) that are discrete or aggregated/agglomerated, but not covalently bonded;[62, 63] 3) having one or more dimensions (of the particles, films) breaking into the classic threshold of 1-100 nm;[62, 63] 4) having parameters that can constitute productive functionalities to

fulfill novel applications. In undesired cases, however, nanoparticles can pose toxicological properties that could threaten health and safety.[62-65]

The practical (experimental) development of engineered nanoscale structures broadly follows two alternative approaches, namely, **bottom-up** and **top-down** manufacturing. The bottom-up approach covers fabrication schemes that drive nanoparticle formation solely from the constituent building blocks, such as atoms and molecules, which aggregate into particles. Bottom-up approach may encompass self-assembly, positional assembly and chemical synthesis as all these bring constituent units together to fulfill nanostructure formation.[61, 66-69] The top-down approach refers to the downsizing of bulk matter into nanostructures which can be achieved by such processes as milling, etching and pulverization.[70] In both approaches, control of size and other parameters is critical toward achieving desired functionality.[55, 71-73]

The crucial aspect of nanotechnology lies in the small size and the associated large surface area-to-volume ratio of matter organized at the *nano-scale*. With extreme small sizes, a change occurs in the relative strength of acting forces; influence of gravity diminishes, whereas major influence arises for forces such as surface tension and non-covalent forces such as *Van der Waals* interaction.[74-76] In addition, the extreme reduction of solid particle sizes consequently results in the *quantum size effect*: 1) characterized by the presence of confined electrons and their quantized energy that exerts strong influence on nanoparticles; and, 2) noticed by dramatic changes in optical, electrical, magnetic and mechanical properties, as well as, physical, chemical, thermal and biological behaviour.[77] To illustrate, copper in bulk is opaque and it becomes transparent at the nanoscale. Similarly, bulk properties yield to nano-properties in other materials: solid gold becomes liquid at room temperature; stable aluminum becomes

combustible; inert platinum becomes a catalyst; and, the insulator silicon becomes a conductor.[77-80]

Although nanotechnology has been mostly driven by the applications enabled by unique nanoparticle properties, an increasing recognition has arisen regarding the uncertainties or potential hazards in the context of some applications or exposure to humans.[64, 81] Nanoparticles have a high propensity to penetrate and accumulate in large loads within organisms, where toxicity could be observed. However, as noted above, the exact fate of nanoparticles (within cells, body or environment) is still unknown.[64, 65, 82, 83] As a result, *nanotoxicology* has emerged; it aims to measure the magnitude, characterize the correlations and mechanisms of toxicity associated with nanomaterials and, trace the end-fate of nanomaterials.[84, 85]

1.3 Nanomaterial compostion and origins

Nanomaterials exist in the atmosphere, waters (underground, surface, sea, ocean), soils, organisms and laboratories. In particular, engineered nanomaterials are being increasingly researched and their fabrication has been demonstrated using matter ranging from living virus particles to lifeless colloidal particles.[62] They exhibit varied functional attributes and so can be categorized by many different criteria. Based on chemical composition, that is, nature of constituent ingredients, the following categories arise: **1**) *soft*, organic nanoparticles which are developed from synthetic or naturally-derived organic amphiphiles (and other molecules), and engineered microbiological components; **2**) allotropic carbon nanoparticles such as nanodiamonds, carbon nanotubes, and fullerenes; and, **3**) inorganic nanoparticles made of rigid core cluster of metal atoms, metal oxides or semiconductor core material such as silicon.[62, 86]

Added to the above categories, newer platform nanoparticles are evolving that incorporate aspects of all three conventional categories to yield unique nanoparticles. These "hybrid" nanoparticles fall somewhat under an integrated nanoparticle category.[14, 86] The focus of this research is on lipid-based nanoparticles which are widely used for drug delivery. Lipid-based nanoparticles fall under the category of organic amphiphilic nanoparticles (*CATEGORY 1*).

1.3.1 Organic amphiphilic nanoparticles

The organic nanoparticle category covers such supramolecular systems as micelles, liposomes (or vesicles), cubosomes and other amphiphile aggregates (Figure 1.2). They typically arise through self-assembly and self-organization (in aqueous media) of tailored amphiphile molecules such as gemini surfactants.[87] The particular aggregate type depends on governing factors such as concentration, molecular structure of the amphiphile, temperature, and characteristics of solvent media including pH, ionic strength, composition and nature of the solvent components.[87, 88] The formed amphiphile aggregates may then be loaded with a measured proportion of, for instance, active drugs. The self-assembly-formation and maintenance of these organic nanoparticles is driven by a combination of non-covalent forces and hydrocarbon–water unfavourable interactions, which both induce aggregate formation and allow unfavourable interactions to be minimized, resulting in thermodynamic stability.[87, 89, 90]

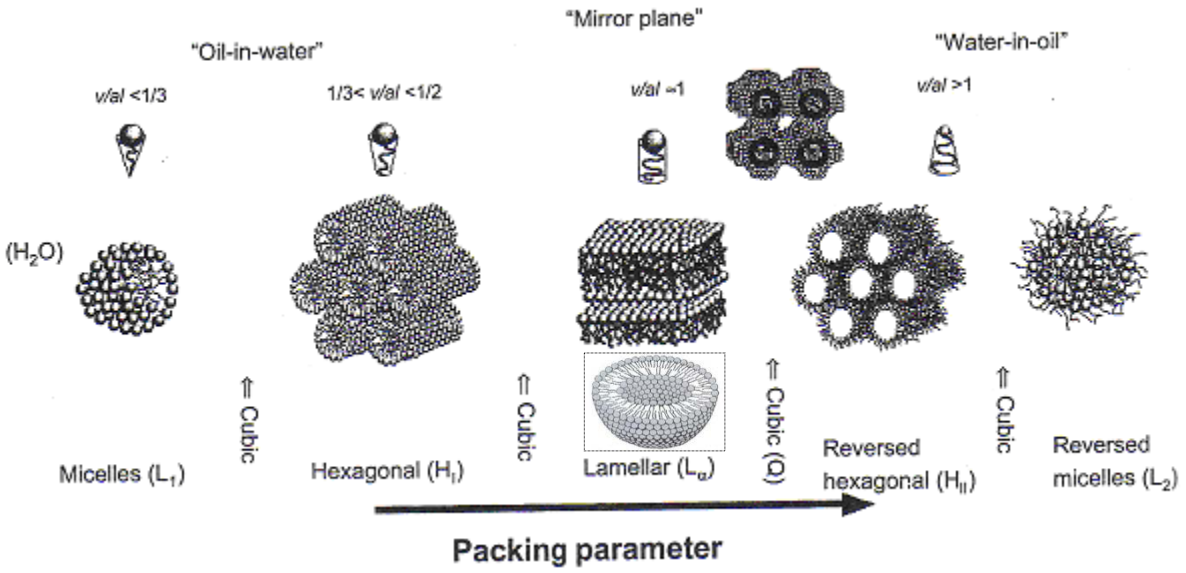

Figure 1.2: Lipid-based nanoparticles.

A complex array of nanoparticle structures can be obtained depending on a number of factors. The nanoparticles shown here have varying structural phases as function the packing parameter of different lipid molecules. Packing parameter is a characteristic related to architecture and structure of the amphiphile compounds; it is mathematically defined by v/al ; where v = volume of alkyl tail, a = headgroup area, l = alky tail length. Adopted from ref.[91]

Self-assembly is both dynamic and reversible, that is, the starting primary building blocks (molecules, ingredients) aggregate into complex secondary structures, which the system can integrates into its next level of organization. This organizational scheme then continues (Figure

1.2), and can produce one of two effects.[90] First, it allows for the incorporation of any added ingredients, and helps attain an equilibrium characterized by greater stability and lower Gibbs free energy.[88, 89] Second, it can also allow the aggregates to disintegrate back into the constituent building blocks due to a perturbation of thermodynamic variables arising from external forces such as excessive dilution.[92-94] Extending such combined character, organic amphiphilic nanoparticle systems are able to interact with biological components such as cell membrane, organelles as well as the physiological environment within cells, and respond to stimuli such as change in pH, temperature and ionic strength. Such behaviour accounts for the function and use of organic nanoparticles as cellular drug delivery systems.[87, 89, 90]

As noted earlier, the molecular building-blocks for organic nanoparticles range from lipids to gemini surfactants, peptides, polymers, dendrimers and anti-oxidants such as vitamin E. The drug transporter portion, which mainly comprises the amphiphiles, generally constitutes the bulk of these nanoparticles, accounting for about 90 mol% of the *dry weight* of drug-loaded nanoparticles.[14, 39, 95, 96] The active ingredients, namely, therapeutic DNA or small molecule anti-cancer drugs, make up the other portion. The molecular structure of the amphiphiles is known to strongly correlate with the nanoparticle properties, starting from the formulation stages to downstream *in vitro*/*in vivo* drug delivery and toxicity.[16, 17, 97, 98] In terms of compound structural effects, the wide range of lipids that exists, including natural and synthetic or semi-synthetic lipid compounds, can be organized in groups for MS investigations of both the similar and different intracellular profiles among the different compound structures.

1.3.2 Lipid-based nanoparticles and drug delivery

The field of lipid-based nanoparticle drug delivery now has several established strategies through which the drug delivery function and safety of the nanoparticles can be improved.[6, 18, 32, 39, 95, 99, 100] These strategies include the design of novel lipids capable of efficient nanoparticle formation and drug packaging (Figure 1.3, top panel);[98] the optimization of nanoparticle behaviour via improved preparation and processing;[12, 101] and uncovering the intracellular behaviour of nanoparticles to circumvent challenges such as toxicity.[102]

Lipid-based nanoparticle development is ultimately aimed to give safe and effective drug delivery systems. To this end, the gap in ongoing research is to determine the best compound structures needed for both efficient lipid-based drug delivery and non-toxic effects. An increasing variety of lipids are being investigated in this regard, including, several phospholipids with long hydrocarbon chains,[103, 104] the unique steroid-based lipid cholesterol,[105, 106] and several synthetic compounds such as gemini surfactants.[14, 16]

As the analytical capability of MS-based techniques has improved, their application has also widened to allow analysis of an increasing variety of lipids and lipid-based drug delivery nanoparticles.[107, 108] Lipid molecules that are naturally produced within cells help form/maintain biological membranes and films, among other roles.[109] These natural cellular lipids, with their unique molecular structure and chemistry, lend themselves to routine use and metabolic processing within cells. In general, natural cellular lipid compounds are being progressively studied using MS,[110] and the information gained has given a better understanding of the function, deposit locations and distribution of some natural lipids.

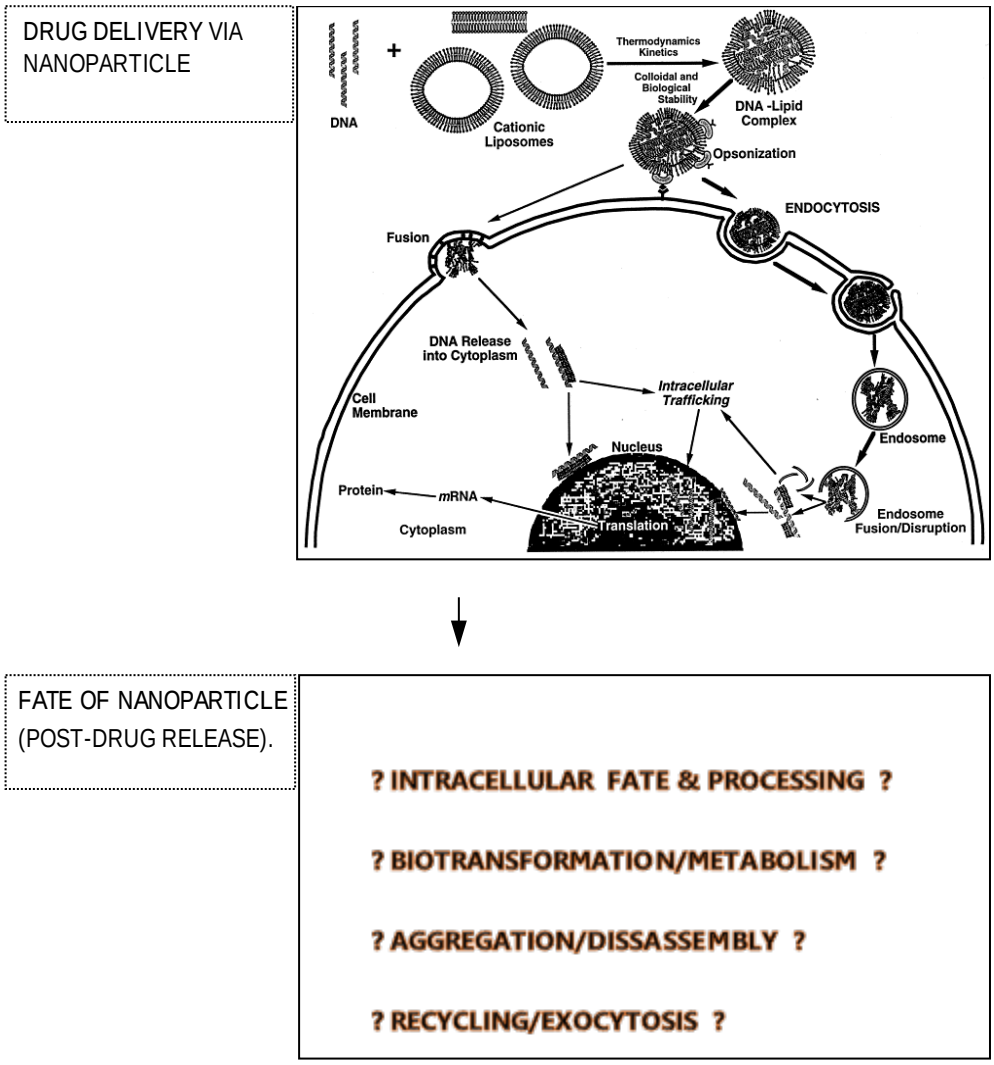

Figure 1.3: The interactions between a target cell and a nanoparticle.

Three mechanisms of interaction, which represent different means of entry of the whole nanoparticle or only its contents into the cell, are endocytosis, lipid-mediated poration and lipid fusion. Entry into cells triggers further events including intracellular trafficking and/or unpacking of the internalized material, entry of DNA into the nucleus and

subsequent protein expression. NOTE: Here, the DNA–lipid complex nanoparticle (also termed lipoplex) is made of cationic liposomes and a load of DNA that is neutralized, condensed and encapsulated within interior cavity of liposomes. Adopted from ref.[111]

There is a broad similarity in the nature of analyte between lipid components of nanoparticles and natural cellular lipids. Therefore, MS is expected to be effective in analyzing lipid-based nanoparticles found within cells. In this context, data for intact and authentic lipids standards can be examined in parallel with data for lipid components of nanoparticles (such as gemini surfactants) that have been incorporated into cells. Gemini surfactant (a class of amphiphiles) present unlimited versatility in compound structures and this could be exploited using mass spectrometry[112-114] for the assessment of their intracellular deposition and fate, and the effects of different compound structures.

1.3.3 Gemini surfactant-based nanomaterials

Gemini surfactants, or simply bis-surfactants, are compounds in which two conventional surfactants (each bearing one polar head and one hydrocarbon chain) are covalently incorporated into one molecule or chemical compound. A gemini surfactant therefore has structural components that include two polar, hydrophilic head-groups and two hydrophobic, hydrocarbon tails, whereby the two head-tail segments are connected by a chosen linker chain.[16, 17, 115] An illustration is given by the N,N-bis(dimethylalkyl)-α,ω-alkanediammonium surfactants (denoted as **m-s-m**; where **m** = alkyl tail length, **s** = alkyl spacer length; Figure 1.4).

One characteristic effect of the "gemini" structural scheme is that it allows a pairing of different head, tail and linker groups, leading to unlimited number of possible gemini surfactants. A second effect is that gemini surfactants have greatly reduced critical micelle concentration (CMC) values. Therefore, their nanoparticle formation ability is far greater than that of the corresponding conventional surfactants bearing one polar head and one hydrocarbon chain.[16, 17, 115] Also, low CMC means that lower gemini surfactant concentrations are adequate for efficient drug delivery and minimized concentration dependent-toxicity.

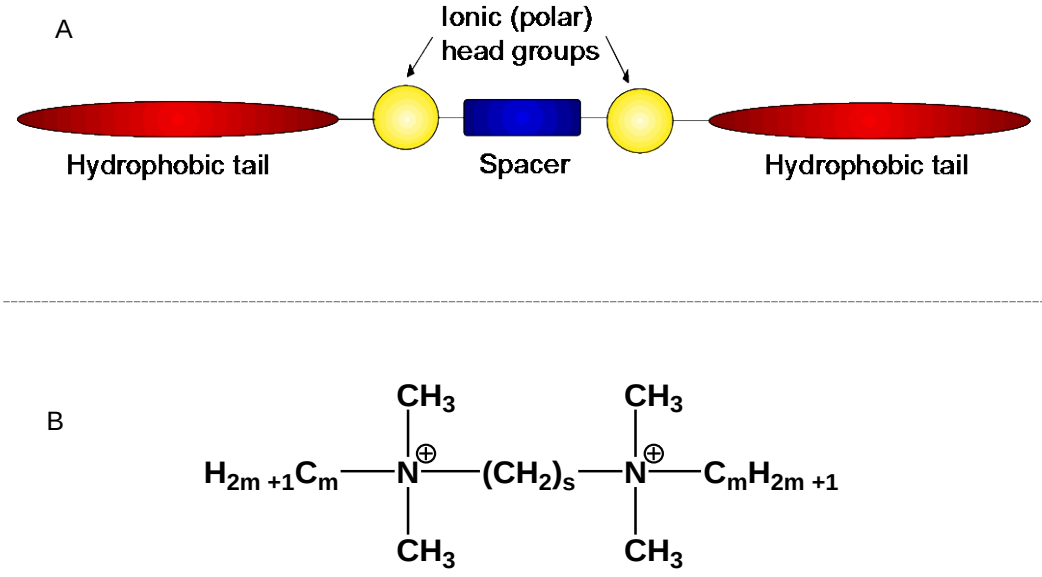

Figure 1.4: General structural scheme of ***m-s-m*** gemini surfactants.

A) General structure, showing how any two monomer surfactants can be connected using a spacer group. B) Structure of the m-s-m gemini surfactants. Two traditional monomeric surfactants with C_m alkyl tails (where m = chain length) are connected at their quaternary

ammonium heads via a polymethylene C_s chain containing **s** methylene units. Adopted from ref.[15]

Among a wide variety of customized gemini surfactants that have evolved for use as drug delivery nanomaterials, many are reported to possess suitable structural attributes. The gemini surfactants being investigated in this research exhibit different molecular structures – Figure 1.5. These include: **i**) m-s-m gemini surfactants (currently the most studied types);[14, 96] **ii**) bis-pyridinium-containing dialkyl compounds;[116-119] and, **iii**) cyclodextrin-substituted gemini surfactants.[120] The three compound series are reported to have drug delivery efficiency.[14, 96, 119-121] Other reported gemini surfactants with efficient activity are those with amino acid/peptide-moieties,[95, 122-124] sugar-/saccharide-based substituents,[125-127] and amine-groups.[14, 128, 129]

The above range of compounds display chemical groups that include amines, amides, esters and ethers, carboxylates, phosphates, disulphide-bond-bearing units and quaternary ammoniums. These functional groups give gemini surfactants useful traits such as being cationic, anionic, nonionic, zwitterionic, pH-sensitive and interactive with other molecules.[16, 17] For example, a recently reported series of gemini surfactants (abbreviated as m-7NH-m) bearing two cationic ammonium headgroups and a pH-sensitive amino group have demonstrated effective DNA encapsulation and its delivery into cells.[14] Selected gemini surfactants with compound structures containing select chemical groups and characteristics, as listed above, will be good candidates for investigations aimed at probing the intracellular profiles/fate of gemini surfactant-based nanoparticles.

Gemini surfactant series	General structure
R-7N(*X*-suc-**β**-CD)-R (β-cyclodextrin-substituted series) R, *x* = n-$C_{12}H_{25}$, O. = n-$C_{12}H_{25}$, NH. = n-$C_{16}H_{33}$, O. = n-$C_{18}H_{35}$, O.	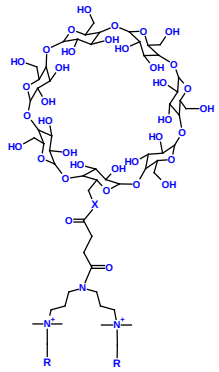
R(Py)-S-2-S-(Py)R (Bis-pyridinium series) R (total) = n-$C_{12}H_{24}$. = n-$C_{14}H_{28}$. = n-$C_{16}H_{32}$. = n-$C_{18}H_{36}$.	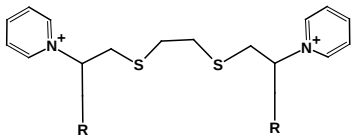
m-s-m series R = n-$C_{16}H_{33}$ and s = 3	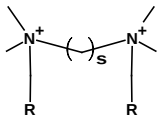

Figure 1.5: Structure scheme of the three series of gemini surfactants.

The specific compounds from each series being investigated in this research are as follows. **R-7N(*x*-suc-β-CD)-R** series, four compounds: R, *x* = n-$C_{12}H_{25}$, O; n-$C_{12}H_{25}$,

NH; n-$C_{16}H_{33}$, O; n-$C_{18}H_{35}$, O. **R(Py)-S-2-S-(Py)R** series, four compounds: R = -$C_{10}H_{22}$, -$C_{12}H_{24}$, -$C_{14}H_{28}$, -$C_{16}H_{32}$. ***m-s-m*** series, one compound: R = n-$C_{16}H_{33}$ with *s* = 3. The structural variations when correlated with the various characteristics to be determined from the studies will present vital information on the biological fate of these nanomaterials. Abbreviations: Py, pyridinium ring.

Studies and understanding of the intracellular (or biological) fate of gemini surfactants used in the form of lipid-based drug delivery nanoparticles can allow for structural modification to improve function. For instance, insights into their intracellular biodegradation profiles will enable safer, less toxic and more efficient gemini surfactants to be developed. Currently, most efforts at improving gemini surfactant nanoparticles for efficient and safe drug delivery rely on data relating to drug packaging efficiency, biological/cell membrane penetration effectiveness (Figure 1.3, top panel), and cell death (toxicity).[15] For instance, groups of gemini surfactants are frequently screened in nanoparticle drug delivery experiments to identify those factors resulting in the highest efficacy and lowest toxicity.[14, 95, 122, 128] Such investigations mainly arrive at findings that emphasize the importance of compound structure and nanoparticle formulation methods, among other factors. However, little or no attention is paid to how the nanoparticles and the constituent amphiphiles are distributed or metabolized in cells (Figure 1.3, bottom panel) despite the potential correlation to both efficacy and toxicity.

To better understand cell death induced by gemini surfactant nanoparticles and to control it, an understanding of the gemini surfactant intracellular fate or metabolism is needed (Figure

1.3, bottom panel). The application of MS has recently been shown to allow for the determination of fragmentation mechanisms of gemini surfactants where the collision-induced dissociation yielded product ions that included unique product ion species (fingerprints) for specific compound structures.[112-114] With known (pre-established) mass spectrometric fingerprints and fragmentation mechanisms, a highthroughput investigation of the subcellular deposition and intracellular fate of gemini surfactants can be conducted.

1.4 Mass spectrometry

1.4.1 Bio-analytical Mass spectrometry

Mass spectrometry attracts much application as a bio-analytical tool and is ideal for the identification and quantification of target molecular species – xenobiotics or endogenous cellular compounds.[113, 130-133] In drug delivery, soft amphiphilic organic nanoparticles are commonly assumed to unpack and/or disassemble after incorporation (entry) into cells so as to release their cargo (drug). Therefore, the constituent amphiphiles (herein, gemini surfactants, Figure 1.5) can be reasonably expected to localize or be distributed to various sites within cells. In reality, quantitative experimental data supporting disassembly of nanoparticles and/or distribution to subcellular sites is yet to be reported.[46, 47]

As proposed, studies to help address the above issue include: investigation of the intracellular persistence/retention and the subcellular localization of the 16(Py)-S-2-S-(Py)16 gemini surfactant in comparison with its structurally contrasting and counterpart, 16-3-16. This will allow for future work to screen, detect and quantify possible metabolites of these gemini surfactants. The possible metabolites will include species whose *m/z* values, compared with that of the intact compounds, reflect certain conjugation or cleavage products from metabolism. For the chosen gemini surfactants, 16-3-16 and 16(Py)-S-2-S-(Py)16 (Figure 1.5), the former was recently found to be less toxic.[119] This observation is neither understood nor expected.[134-138] My work will focus ***mainly*** on the cytotoxicity, intracellular persistence, subcellular deposition in relation to the molecular structure of tested compounds.

Data on the subcellular localization for gemini surfactants is essential: (1) it provides insights into the intracellular trafficking, elimination, recycling or other processes that the gemini surfactants may undergo; (2) it will enable a comparison of the measured cytotoxicity levels with the observed intracellular distribution of the lipids to give insights into how different molecular structures influence toxicity or other *in vitro* parameters. To determine the subcellular localization, treated PAM 212 cell sample will be fractionated and analyzed to quantify the proportion of 16(Py)-S-2-S-(Py)16 and 16-3-16 present within various intracellular compartments.

1.5 Mass spectrometric studies of *in vitro* profile of nanoparticles

In this research, MS is being implemented for investigating the intracellular fate of gemini surfactant nanoparticles previously found to give good drug delivery efficiency and varying cytotoxic profile depending on the molecular structure.[119, 120] MS as an analytical technique that has evolved and improved since the late 1880s, allows for the detection, identification and quantification of samples containing chemical analytes.[130] MS operates by a fundamental design that consists of three modular parts which are laid out in the order: 1) ionization source, 2) mass analyzer and 3) detector.[139] It works by generating vapourized ions of the analyte, followed by measuring their mass-to-charge ratio, *m/z*, and providing data in the form of mass spectra.[112, 113, 140]

In addition to MS, several alternative techniques exist that may be applied to study and characterize nanoparticles. These include fluorescent and electron microscopies, atomic force microscopy (AFM), dynamic light scattering (DLS), fluorescent and UV-vis spectroscopy (UV

spec), nuclear magnetic resonance (NMR) and synchrotron techniques.[141, 142] But each of these techniques alone does not appear suitable for the specific purpose of studying the biodegradative transformation and intracellular fate of gemini surfactant-based nanoparticles. This is due to their inability to track nanoparticles up to a stage of disassembly; lack of UV-active or fluorescent moieties or probes in gemini surfactants typically used in drug delivery applications; and, complexity or unrefined state of ***actual*** biological samples containing the gemini surfactants. Aims of my research include the screening, detection and measurement of gemini surfactants, contained within unrefined, complex cellular extracts.

Given the considerations above, MS emerges as a means of investigating gemini surfactant nanoparticle bio-fate, but with challenges. ***First*:** in metabolic studies, the anticipated degradation of the nanoparticles can be speculated to differ from simple metabolic breakdown or transformations of dispersed, non-aggregated molecules introduced into cells. A wide variety of xenobiotics (foreign compounds in cells) including drugs and delivery agents, are subject to phase I or phase II biotransformation and consequent detoxification and/or elimination.[143, 144] In some cases the metabolic derivatives, the parent xenobiotic compounds or both result in toxicity.[144, 145]

In the case of molecules aggregated or bound together as nanoparticles, their metabolism may not be feasible until there is disintegration of the nanoparticle into the individual molecules.[144, 146] Thus, a limiting step in nanoparticle metabolism could, speculatively, be identified as the disassembly of nanoparticles into the corresponding dispersed, non-aggregated molecules which may then readily undergo metabolic breakdown. For investigations using MS,

the common assumption is that organic nanoparticles disassemble into the constituent molecules (dispersed) during or after uptake into cells.[17, 147, 148]

The ***second*** challenge is related to the complexity of the biological matrix with the possibility of interfering with MS analysis. Even for cellular samples which have experienced some refinement such as solid phase and/or liquid phase extraction, co-extracted natural cellular compounds can still interfere with the analysis.[149-151] Given the above potential challenges, several analytical *modes* and *methods* in MS, detailed ahead, will be utilized in this research.

The MS techniques that will be used in my research are hybrid quadrupole–time-of-flight MS and triple quadrupole-linear ion trap MS which are suitable for studies of the intracellular profile of gemini surfactants. These two techniques offer high resolution and highthroughput that are immensely beneficial to the proposed analysis. They also allow for both qualitative and quantitative analysis either alone or in conjunction with HPLC.

1.5.1 Qualitative and quantitative analysis in mass spectrometry

Over the past few decades, qualitative and quantitative MS has improved due to new and *versatile* ionization sources, mass analyzers and detectors.[130, 163] Tandem or hybrid MS systems allow for tandem MS (MS/MS) analysis; this can be combined with other analytical techniques such liquid chromatography to add analytical separation of compounds. Qualitative MS-based analysis covers identification and differentiation of known and unknow analytes, and the determination of molecular formulae and structures including metabolic changes to compound structures.

Quantitative MS-based analysis detrermines and monitors analyte concentrations and/or changes in concentrations to study analytes in biological tissues where the analyte may

quantitatively show a bio-distribution, depletion and metabolic profile. The analyte's bio-distribution, depletion and metabolic profile may then reveal its biological role, fate or impact. A number of assorted instrumental platforms in analytical MS, considered for this research, are briefly reviewed below. This includes a discussion of the selected modular parts, that is, ionization sources and mass analyzers.

Electrospray Ionization (ESI):

ESI technique primarily achieves ionization of polar analytes (dissolved in organic solvents: mostly methanol, with or without acetic acid) via generation of fine aerosol of very small, charged droplets, using high voltage, temperature and a nebulizing gas. The charged droplets become smaller by solvent evaporation from their surfaces, making the droplet gain increasing charge density and instability, ultimately leading to the threshold Rayleigh limit at which point the droplet explodes (Coulumbic explosion) into even smaller droplets. Repeated cycles of the solvent evaporation, droplet contraction and Coulombic explosions lead to the final droplet from which the molecular adducts or charged ions are released in gaseous form. Ionization in positive ion mode generates positive ions including $[\mathbf{M}+nH]^{n+}$, $[\mathbf{M}+Na]^{+}$ or $[\mathbf{M}]^{n+}$; while a negative mode ionization generates negative ions including $[\mathbf{M}–nH]^{n-}$ or $[\mathbf{M}]^{n-}$. The $[\mathbf{M}]^{n+}$ and $[\mathbf{M}]^{n-}$ ions (n = 1, 2, etc) are for analytes which bear permanent charge (n+, n-) and gain no additional charge from the ionization process. Positive ionization uses positive voltage and negative uses negative voltage.[142]

ESI is a soft ionization technique, allowing for the formation of intact protonated or deprotonated ions, which are singly or multiply charged. ESI is suitable for analyzing large molecules such as peptides/proteins and non-covalent complexes.[143] ESI operates at ambient conditions and offers an ease of interfacing with HPLC.

Time-of-flight (ToF) mass analyzers:

In ToF mass analyzers, ions are freely accelerated through a flight tube toward the detector using uniform electric field. The time-of-flight through the tube (of fixed distance) is measured for the ions. A ToF analyzer allow all ions (entering it from the ionization source) to be detected

as opposed to other mass analyzers (e.g., quadrupole and linear ion trap analyzers) that act as ion filter. Use of a uniform electric field imparts the same kinetic energy to ions, but the observed velocity of ions through the flight tube is dependent on the *m/z* values: ions with smaller *m/z* reach detector before "heavier" ions. [144, 145]

To give superior resolution, ToF analyzers often have *delayed ion extraction* capability and/or a ***reflectron*** for eliminating undesired kinetic energy variations for ions with identical *m/z* values.[132, 144, 145] *Delayed ion extraction* implies that ions are briefly delayed to correct (or minimize) the variations in initial kinetic energies before entering the mass analyzer where ion separation occurs.[132, 144, 145] *Reflectron* also serves to correct kinetic energy variation but for ions already extracted into the flight tube: ions having identical *m/z* values but different energies travel into a "reflectron" region at varying depths so that they emerge with equal energy and reach the detector at the same time. Commonly encountered systems with an interfaced ToF analyzer include ESI-ToF-MS, MALDI-ToF-MS. Also in existence are tandem ToF-ToF-MS and hybrid system such as Qq-ToF-MS (Q = quadrupole analyzer, discussed ahead). Tandem and hybrid systems generally allow precursor ions to be isolated in the first analyzer, then fragmented in a collision cell, followed by analysis of the product ions in the second analyzer.[144, 145]

Quadrupole mass analyzers

Quadrupole mass analyzers consist of four circular, parallel metal rods which are arranged at the corners of a square. The rods carry oscillating electric fields between them and filter (analyze) ions based on their *m/z* values. The oscillating electric field is created by connecting a positive electrical charge to one pair of opposite rods, while remaining pair is connected a

negative electrical charge. A radio-frequency (*rf*) voltage and a direct current voltage that will superimpose on the *rf* voltage are then applied to the rods. The result of this setting is that ions are permitted through the four rods to a detector based on thier trajectories within the analyzer. Only ions with the right trajectory will reach the dectector while all other ions will collide with the rods and be removed. Quadrupole mass analyzers can operate either in the scanning mode scanning all ionized species or as ion filiter with particular *m/z* values selected for .[146]

Linear ion trap (LIT) mass analyzers:

A linear quadrupole ion trap (LIT) analyzer is similar to quadrupole analyzer being made of four parallel rod electrodes supplied with oscillating electric fields and thus is geometrically similar to a quadrupole analyzer. However, an LIT analyzer can scan ions too. By design, LIT analyzers provide a *potential well* bound by the four quadrupole rod electrodes, such that, ions that enter the LIT are confined in two ways: radially and axially. Radial confinement is provided by an appropriate *rf* voltage while axial confinement is provided by DC voltage at both ends of the rod electrodes. Ion ejection to the detector is permitted by manipulations of the two voltages. Ideally, ions entering LIT analyzers are: 1) stably trapped in the right amounts; 2) undergo collisional cooling due to the presence of He damping gas; 3) confined into a packet of ions (as opposed to a diffuse cloud) and focused at the center of the trap; and, 4) ejected (mass selective ejection: in order of increasing *m/z*) to a detector to yield mass spectra data.[112, 139, 140]

The ion detection can also be done *in situ* using Fourier Transform techniques. Ion trapping, mass selective ejection and detection underpin the capability of ion trap MS for MS^n experiments in structural elucidation studies.[112, 139, 140] LIT analyzers have advantages, such as high ion storage capacity (related to dimensions of internal volume space), ideal scan times, wide

dynamic range and simplicity of construction. In addition, they can be used as stand-alone analyzers or interfaced with other analyzers to give hybrid MS instruments as demonstrated by hybrid triple quadrupole–linear ion trap Q-LIT-MS systems[112, 138] described below.

1.5.2 Molecular structure elucidation using mass spectrometry

Quadrupole–time-of-flight MS (Qq-ToF-MS) equipped with an electrospray ionization source (ESI-Qq-ToF-MS) has the unique capability of recording mass spectra with high mass accuracy, particularly if compared with triple quadrupole instruments.[164, 165] ESI is commonly chosen as it is easily interfaced with HPLC and because it is a soft ionization technique that allows the conversion of analytes into intact precursor ions (singly or multiply charged).[166, 167] Other ionization techniques such as matrix-assisted laser desorption ionization (MALDI) may also be used depending on the analysis.[168, 169]

The arrangement of the Qq-ToF hybrid mass analyzer allows the first quadrupole Q to receive and isolate target ions (e.g., precursor ion) generated from the ionization source, followed by CID-fragmentation of ions within a linear hexapole or octapole collision cell (regarded as the second "quadrupole", q).[170, 171] The product ions are then analyzed in a *reflectron* ToF analyzer with orthogonal acceleration, bringing about superior ion separation and detection of high resolution signal.[172]

The ion separation provided by *reflectron* ToF analyzer accounts for a relatively high resolution and mass accuracy. Mass accuracy of the newest ToF systems is routinely better than 1 ppm after both external and internal calibration, while resolution is routinely over 60,000 ($m/\Delta m$; Δm = the full peak width at half-maximum, FWHM).[173, 174] Qq-ToF-MS offers high

resolution and accuracy and is widely used for analysis of known and unknown analytes within complex biological matrices.[164, 165, 171]

1.5.3 Highthroughput bio-analysis using mass spectrometry

Triple quadrupole–linear ion trap MS (QqQ-LIT-MS, Figure 1.6) is based on the format of three-linearly-connected (in-tandem) quadrupole analyzers, termed **triple quadrupole** ($Q_1q_2Q_3$). However, in this case the standard triple quadrupole system is modified such that the third quadrupole Q_3 has both quadrupole (mass filtering) and linear ion trap operational functions. As a result the QqQ-LIT-MS platform combines the sensitivity of conventional QqQ-MS with the capability of ion trap MS^n. Therefore, qualitative and quantitative analysis can be performed simultaneously.[175] An electrospray ionization source is frequently used (i.e., an ESI-QqQ-LIT-MS), but other ionization methods such as atmospheric pressure chemical ionization (APCI) can also be employed.

Using the QqQ-LIT-MS system (Figure 1.6), the first quadrupole can isolate a precursor ion, with the ion entering into and undergoing CID-fragmentation in the second quadruople (collision cell) which is supplied with Ar, He, or N_2 collision gas. This is followed by analysis of product ions in the third quadruople-linear ion trap analyzer, which then releases the ions for detection by mass selective ejection.[130, 176, 177] The process also allows further trapping and fragmentation of initial product ions into smaller ions (multiple-stage MS) before detection.

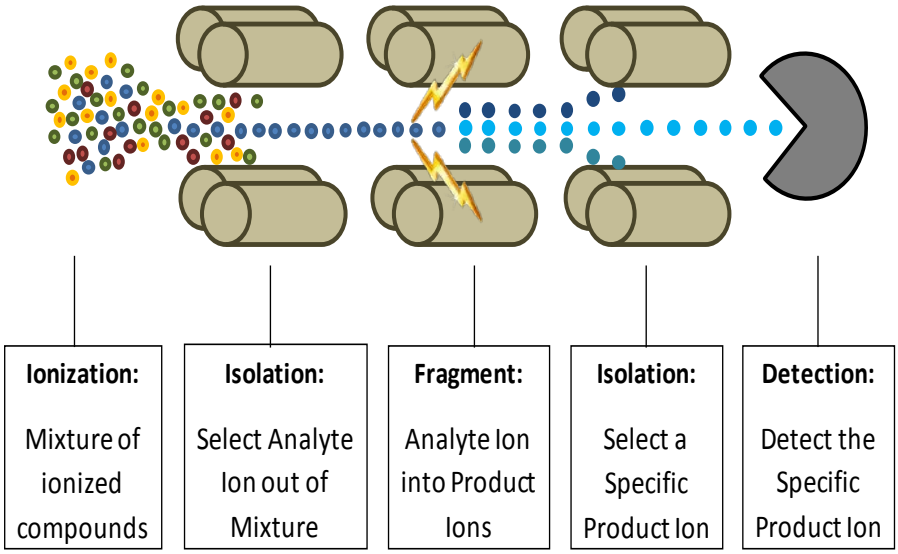

Figure 1.6: Illustration of MS experimentation process using a triple quadrupole–linear ion trap (QqQ-LIT-MS) instrument.

The stepwise process allows selection of precursor (or target) ion, its fragmentation into product ions and detection of the product ions. Also, the process allows further fragmentation (multiple-stage) of initial product ions into smaller fragment ions before detection. Adopted from ref.[147]

The mechanism, as described above, allows QqQ-LIT-MS systems to give highthroughput analysis. QqQ-LIT-MS systems also perform neutral loss scans and selected reaction monitoring to strengthen its use for obtaining information on compound structure, fragmentation mechanism and molecular fingerprints. Triple quadruople systems typically have a mass range in the limit of ≤ 4 kDa, and are characterized by low mass resolution. QqQ-LIT-MS systems are easily interfaced with HPLC and GC.[178] An alternative type of ion trap analyzer is the 3D (i.e.,

spherical) quadrupole ion trap analyzer. However, it has an inferior ion storage capacity relative to LIT analyzers.[130]

In bio-analysis, liquid chromatography (LC: conventional HPLC) is commonly coupled to tandem MS instruments, giving the hyphenated LC-MS/MS system. LC-MS/MS systems have the combined capabilities of multiplexed analyte separation and high-speed, sensitive mass-selective determination of analytes.[179, 180] LC-MS/MS is widely used in the analysis of complex mixtures to separate, identify and quantify the constituent analytes (known, unknown) including compounds in their intact form, their derivatized or breakdown products as in the pharmaceutical industry.[2, 149, 181-183] One class of separation technologies to be used in this research is hydrophilic liquid chromatography (HILIC) and is discussed below.

1.5.4 HILIC-HPLC-tandem mass spectrometry (HILIC-LC-MS/MS)

In LC-MS/MS, the ability of the liquid chromatographic step to effectively separate target analytes within complex mixtures is critical and requires suitable HPLC separation columns (i.e., stationary phase), mobile phases, and optimized analytical conditions.[184-186] Among liquid chromatographic separation modes, HILIC (utilizes a uniquely different separation mechanism) has given the highest sensitivity for analysis of polar compounds.[184-186] In other words, HILIC-HPLC is a more sensitive variant of traditional reversed-phase (RP-HPLC) and normal-phase liquid chromatography (NP-HPLC) in terms of application to polar analytes.[187-189] Consistent with the above, the hyphenated HILIC-LC-MS/MS method is expected to be superior to its RP-LC-MS/MS and NP-LC-MS/MS counterparts.[187, 190] As a result, HILIC-based LC methods are

generally established as the separation mode of choice for polar/ionic analytes and also as complimentary option for other analytes.[191]

HILIC-HPLC draws similarities from RP-HPLC and NP-HPLC as well as ion-exchange chromatography.[189, 192-195] It uses polar stationary phases to retain polar analytes similar to typical NP-HPLC systems; but for the elution, organic mobile phases (mostly acetonitrile, containing at least 3% water) are used.[192, 196, 197] In RP-HPLC systems, nonpolar stationary phases (e.g., octadecyl silane) are used to retain nonpolar analytes, with the elution driven by mobile phases that are mixtures of aqueous and organic solvents.[192] Thus HILIC-HPLC is similar to NP-HPLC based on column polarity and to RP-HPLC based on the use of water in the mobile phase.[189] HILIC-HPLC is also similar to ion-exchange chromatography as it is compatible with charged analytes.[189, 193] The inclusion of water in the HILIC mobile phases permits the use of ionic additives. Organic acids and salts (acetic, formic; and ammonium acetate and formate) allow, for instance, the control of mobile phase pH, ionic strength, and charge of analytes.[198]

A major modification in HILIC-HPLC is its separation mechanism, although the exact interactions between its two phases (stationary, mobile) and analytes are under debate. Typically, RP-HPLC mode separation involves partitioning of analytes between the two chromatographic phases, while NP-HPLC mode separation involves adsorption of analytes onto the stationary phase. For HILIC, various combined interactions account for the separation, including adsorption, partitioning, hydrogen bonding, and electrostatic interactions.[189, 192-195] The exact interactions depend on the polarity of the HILIC stationary phase while the order of retention and elution depends directly on the polarity of analytes and inversely on the polarity of mobile

phases.[189] Partitioning is believed to be a major HILIC interaction particularly for simple nonionic, neutral stationary phases. The aqueous mobile phase forms a semi-immobilized, water-enriched layer on the hydrophilic stationary phase, allowing analytes to partition into the water-enriched layer.[189]

1.5.5 HILIC-LC-MS/MS for intracellular analysis of gemini surfactants

The suitability of HILIC-LC-MS/MS for the analysis of gemini surfactants depends on the polar chemistry of the gemini surfactants in question. The gemini surfactants in this research (Figure 1.5) contain alkyl tails along with either quaternary ammonium or pyridinium head-groups, which both have a cationic nitrogen atom, $\mathbf{N}^{+}$. Recently, the suitability of HILIC-LC-MS/MS for the analysis of representative quaternary amine compound(s) has been remarkably demonstrated. In the study, HILIC-LC-MS/MS gave higher sensitivity over RP-LC-MS/MS by 75 times.[187, 190] Based on broader scale, HILIC-LC-MS/MS is generally projected to be at least 10× more sensitive than RP-LC-MS/MS when working at optimal analytical conditions.[188, 189, 199]

Currently, multi-functional HILIC stationary phases such as those with sulfoalkylbetaine (zwitterionic) functional groups are gaining increasing use in HILIC-LC-MS/MS applications. Multi-functional HILIC columns employ mixed-mode interactions (adsorption, partitioning, hydrogen bonding, electrostatic interaction), allowing for the analysis of different polar analytes.[200-203] Compared with simple/single-mode HILIC columns, mixed-mode HILIC stationary phases (branded commercial example: ZIC®-HILIC column, Figure 1.7) gives very efficient separations through differential retention of polar, ionic, neutral and zwitterionic

analytes.[200-203] For the ZIC®-HILIC column (evaluated and chosen for this research), its obvious compatibility with the gemini surfactants involves electrostatic interaction, $^{+}N\cdots SO_3^{-}$.

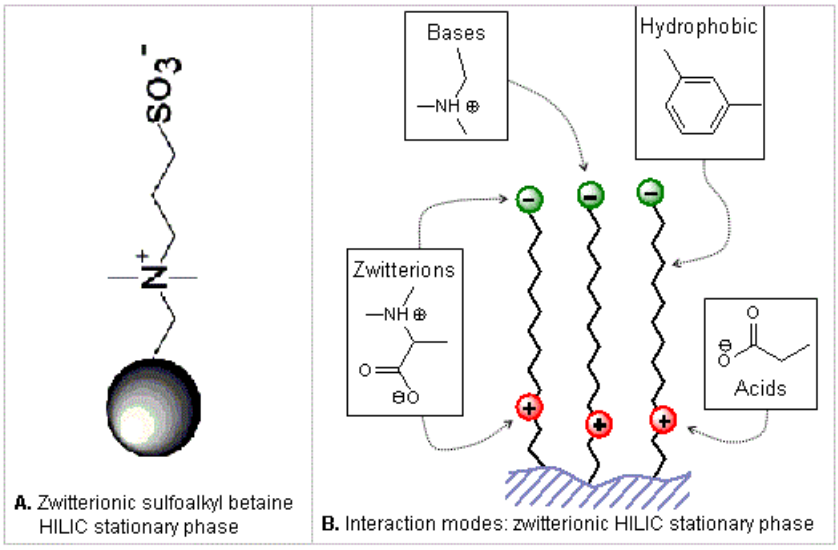

Figure 1.7: Multi-functional HILIC stationary phases.

A) Zwitterionic sulfoalkylbetaine-based HILIC stationary phase – created by covalent attachment of a sulfoalkylbetaine group onto silica particles. **B**) Interaction modes of a zwitterionic HILIC stationary phase – interactions are shown for different functional polarities that are representative of acidic, basic, hydrophobic and zwitterionic analyties. HILIC: hydrophilic interaction liquid chromatography. Adopted with modifications from ref.[203]

The improved sensitivity of HILIC-LC-MS/MS methods is partly due to their highly organic mobile phases (typically, ≥ 60% acetonitrile) since highly organic solvents promote desolvation and ensure efficient ionization. In addition, the low viscosities of relatively organic

mobile phases affords a low pressure drop across a working HILIC column and allows the use of high flow rates for maximizing throughput.[187, 189, 190] HILIC mobile phases do not require ion-pairing reagents (e.g., triethylamine, TEA) and this eliminates the associated ion suppression and ion source contamination.[204] In contrast, the less volatile, highly aqueous RP-HPLC mobile phases and their frequent use of ion-pairing reagents significantly compromises sensitivity.[189]

Despite the many advantages described, the HILIC mode has a disadvantageous trade-off in one aspect − a specificity to retain only polar/ionic analytes but not hydrophobic compounds. As a result, HILIC separation typically resolves only the hydrophilic components of a mixture. For equilibration, HILIC stationary phases may require short or lengthy equilibrations depending on the case. When switching mobile phase or sample types, a lengthy equilibration (e.g., 200[205] and 400[206] column volumes) can be required. The long equilibration process however did not deteriorate subsequent retention ability. Overall, the HILIC mode offers strong compatibility and better sensitivity for studying the bio-fate (intracellular persistence, distribution) of the chosen gemini surfactants when considering the advantages[189, 192-195] and the demonstrated sensitivity in the analysis of representative quaternary ammonium compounds.[187]

1.6 Biological fate of nanoparticles

The biological fate of nanoparticles begins from the port of entry into the host organism. It is influenced by events including ***bio***distribution, interaction with endogenous components and ***bio***transformation or ***bio***persistence before or after translocation into specific cell types or to subcellular structures. The nature and effects of these events vary depending mainly on the

nanoparticle characteristics, the biological environment/host and the port of entry. The nature and effects of these events can studied using mass spectrometry.

In biomedicine, lipid-based nanoparticles for drug delivery or diagnostic nanoparticles with inner metal/metal-oxide core and outer organic coating are introduced into organisms through injections, topical application or inhalation. But with small size and superior diffusion, nanoparticles can also enter organisms via the skin,[64] lungs[64] and gastrointestinal (GI)[64] tract through exposure to nanoparticles released into the environment during production, storage and disposal. Exposure to nanoparticle-polluted environment including food and water, exposes organisms to complex mixtures of nanoparticles, including those used biomedically.

Once in host organisms, nanoparticles can migrate by active or passive diffusion from the entry port into or away from blood circulation. They can theoretically be destroyed by enzymes, cleared by macrophage and/or excreted in feces or in urine, as noted for particles in very small size range ($\leq$ 20 nm).[207-211] It has been established that nanoparticles mainly with evasive *stealth* surface can reach the circulatory system from the lungs (respiratory tract) as an entry port.[64] In the blood, they can circulate freely, reaching the liver, heart, spleen, bone marrow, tumours, and other sensitive sites.[64, 212-214]

For the GI tract and skin as entry ports, systemic distribution is curtailed or eliminated depending on the skin integrity and the penetration capability of the nanoparticles. The skin barrier limits entry of nanoparticles and has dermal macrophages for phagocytotic clearance of transgressive nanoparticles.[62, 64] Similarly, the GI tract either destroys nanoparticles or carries them along for clearance in feces.[64] However, nanoparticle translocation from the outer skin into circulation may be possible particularly if transdermal penetration is strong or if skin is

unhealthy (e.g., cancer, lesions); and from GI tract into circulation if the particle size is sufficiently small.[64]

1.6.1 Intracellular fate of biomedical lipid nanoparticles

Both the properties of nanoparticles and cell type (*i.e.*, biological environment), strongly influences the intracellular fate of nanoparticles. The PAM 212 epidermal keratinocytes (predominant cell type in epidermis) chosen for my work are found in the basal layer of the skin which is estimated at ~0.07 mm[215-219] beneath the outer skin surface. *In vivo* targeting of keratinocytes using topical nanoparticles relies on ***good*** transdermal diffusion from outer skin to keratinocytes in the basal layer. Nanoparticles may, in some cases, penetrate beneath the basal layer (made of keratinocytes) into the deeper skin and distribute its native cells.[64]

For *in vitro* studies, the applied nanoparticles readily interact or bind to cells resulting in cellular uptake. Uptake into cells, leads to intracellular trafficking and distribution to various subcellular compartments, with or without eventual metabolism, recycling or exocytosis from cells. Within cells, drug-loaded lipid-based nanoparticles should ideally release their drug contents and undergo biodegradation. In reality, these nanoparticles impose toxic or benign effects; the toxicity is often higher when nanoparticles are tested as drug-free excipients relative to when drugs are incorporated.[122]

1.6.2 Trafficking and distribution of lipid nanoparticles in cells

The most accepted mechanism of cellular uptake, intracellular trafficking and drug release for drug-encapsulated lipid nanoparticles focuses on major steps as given in bulleted summary below and illustrated in Figure 1.8.

1) Binding to outer cell membrane.[6, 98] Binding is driven by the biomembrane-binding ability of nanoparticles – an ability explained by large surface area-to-volume ratio along with cationic surface charge and/or surface-attached ligands for targeting cell-membrane receptors.[6, 98]

2) Endocytosis leading to enveloping within endosomes (early, late).[6, 98] Other entry modes (minor ones) include cell–particle fusion and lipid-mediated membrane poration.[6, 98]

3) Release from late endosome into cytoplasm (completed delivery if drug is small-molecule).[6, 98] The release stage competes with non-release and/or imminent fusion with lysosomes.[6, 98]

4) Movement from cytoplasm to the nucleus– drug either free or still in nanoparticle.[6, 98] In case of nucleic acid drugs, further migration into nucleus is needed, except for RNAs.[6, 98]

5) Entry across nuclear membrane into nucleus (final destination if drug is DNA).[6, 98] It should be noted that the integrity of freed nucleic acid is susceptible to degradation by endonucleases.[6, 98]

DRUG DELIVERY VIA NANOPARTICLE

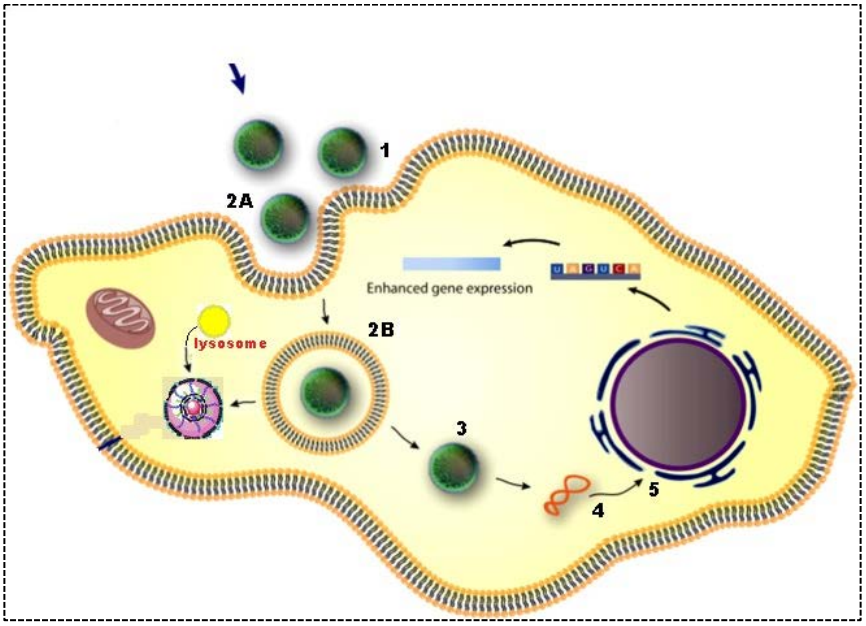

Figure 1.8: Cellular uptake mechanism and intracellular distribution of lipid/DNA nanoparticle complexes.

The multi-step interaction process begins with binding of nanoparticle to cell, leading to internalization. Endocytosis (step **2A**) accounts for internalization of majority of nanoparticles into the cells. However, other important but minor internalization routes are lipid-mediated poration and cell–nanoparticle fusion. After entry into cells, unpacking of the nanoparticle and intracellular trafficking occurs are required to propel the DNA ***drug*** into the nucleus for subsequent protein expression. Adopted with minor modifications from ref[(220)]

Most likely, **steps 1−5** only indicate part of nanoparticle distribution and fate in cells. The subcellular distributions implied by these steps are discussed below, with an added discussion on

other plausible distributions which may ***not*** be inferable from the above steps. The nanoparticle distribution around subcellular compartments most likely changes with time.[64, 221-223] The distributions can be revealed by quantitative changes of the nanoparticles or the constituent lipids around subcellular compartments. Using differential centrifugation[224] for isolation of subcellular compartments from homogenized, treated cells and LC-MS/MS for quantitative and qualitative analysis,[225, 226] knowledge of intracellular distribution of nanoparticles can be advanced.

1.6.2.1 *Whole cells*

An important aim in drug delivery is efficient uptake of drug-loaded lipid-based nanoparticles by target cells.[6, 98] As recently reported,[227] studies of intracellular fate can begin with LC-MS/MS analysis of nanoparticle uptake by quantitative detection of the constituent lipids in whole cell lysates. The report observed a plateaued-persistence of gemini surfactants in cells 55-hours after treatment with gemini surfactant-based nanoparticles.[227] Also, uptake often requires optimization based on several factors (e.g., lipid molecular structure, applied dose, particle size, surface charge, and targeting ligands).[6, 98] Quantitative uptake data from LC-MS/MS methods ***could*** contribute to understanding the correlations and to defining optimal conditions.

1.6.2.2 *Subcompartment of the plasma membrane*

Interaction of lipid nanoparticles with target cells begins from the binding of the two entities, followed by internalization ***mainly*** via endocytosis and ***marginally*** via cell–particle fusion and lipid-mediated poration (opening of connecting pores)[98, 111, 228, 229] Consequently, the

cell–nanoparticle binding and the three internalization modes can create a distribution of nanoparticles around the plasma membrane.[230] The quantitative changes of the nanoparticles or the constituent lipids at the plasma membrane that show the distribution can be determined by LC-MS/MS analysis of the outer cell membranes isolated by differential centrifugation[224] (Figure 1.9).

1.6.2.3 *Microsomal subcompartment*

The possible microsomal localization of nanoparticles, which is currently unknown, merits investigation for two reasons. Microsomes (vesicles, 20−200 nm) represent valuable tool for studying the metabolism of xenobiotics including nanoparticles.[231, 232] Microsomes are formed from the reorganization of fragmented pieces of endoplasmic reticulum (ER) after cell homogenization/disruption. In the re-aggregation process, the broken pieces of ER envelope cytochrome P450 enzymes along with their bound xenobiotic substrate reassemble, resulting in microsomal viscles.[231, 233, 234] The metabolism of lipid nanoparticles ***will*** require the assembly of their constituent lipids from various intracellular sites to the CYP450 enzymes, known to metabolize over 90% of drugs and other xenobiotics in humans.[235-237]

Nanoparticles made from natural biological lipids or other molecules may easily undergo biotransformation (metabolism) upon disassembly of the nanoparticles into separated molecules. For synthetic lipid nanoparticles, the constituent synthetic lipids similarly undergo metabolism.[235-237] LC-MS/MS analysis can allow a quantitative determination of nanoparticle sequestration into microsomal vesicles.[238-240] Microsomes of nanoparticle-treated cells are be obtained by homogenization and differential centrifugation (Figure 1.9).[224]

1.6.2.4 *Endosomes, transport/endocytotic vesicles*

Endosomes which arise from endocytotic uptake of nanoparticles represent the first intracellular nanoparticle accumulation site; they partly determine the subsequent distribution of the nanoparticles to other organelles.[202, 241] In general, various exogenous materials internalized by cells go through different intracellular processes. For lipid nanoparticles, they may be confined within endosomes for subsequent low-pH hydrolytic destruction involving the fusion of endosomes with lysosomes.[242] Alternatively, the nanoparticles may also be released into the cytosol[6, 98] or removed from cells by endosomal exocytosis.[243]

Ideally, endocytosed drug-loaded nanoparticles should interface with the endosomal environments in order to escape from endosomes or allow only the drug molecule to escape. One example of ***interfacing*** is the ability of pH-sensitive nanoparticles to expand in response to endosomal acidification, with resultant endosomal rupture and release of the nanoparticles in the cytosol.[6, 98] Therefore, nanoparticles from endosomes may lead into the cytosol, lysosomes or may be exocytosed from cells.[244, 245]

The accumulation of nanoparticles from extracellular environments into endosomes can be studied using LC-MS/MS quantitative analysis. The endosomal accumulation data can be compared with the ones obtained for nanoparticle deposition in the cytosol in order to help refine nanoparticle characteristics that allows optimal release into cytosol.[246, 247] Comparisons can also be conducted between the endosomal accumulation and efficiency of drug release/deposition from nanoparticles into the cytosol.

Intact endosomes from nanoparticle-treated cells can be isolated for LC-MS/MS analysis using cell disruption and differential centrifugation[224] in conjunction density with shift

techniques.[248-250] As noted (*Section 3.3*, ahead) density shift techniques will help to effectively separate endosomes from organelles whose sedimentation coefficients often overlap with that of endosomes.[243, 248, 250, 251]

1.6.2.5 *Lysosomal subcompartment*

Lysosomes are major host organelles within which biomedical nanoparticles are detected via fluorescence microscopy after their uptake into cells.[6, 252, 253] As noted, nanoparticles found in lysosomes are normally transited from the endosomes, with this transfer channel representing an intracellular clearance pathway in which foreign materials are targeted for destruction.[6, 242, 243, 245, 254, 255] Nanoparticles that are channeled into lysosomes may undergo degradation through the activity of lysosomal hydrolases at low pH; they may be exocytosed (or recycled[256]) as degraded products or as undegraded materials if they are not degradable.[242, 257]

Nanoparticle entry into lysosomes can impact nanoparticle-mediated drug delivery in two ways: ***i***) entry into lysosomes before the release of the drug from the nanoparticles will result in the destruction of the drugs if they are nucleic acids or hydrolytically-susceptible molecules; ***ii***) entry into lysosomes after the release of the drug from the nanoparticles will have no effect on the drug.[6, 242, 258] The later scenario represents a desired end in nanoparticle-mediate drug delivery since it allows for successful drug delivery as well as for the degradation and/or exocytosis of the nanoparticles.[6, 242]

Since lysosomal exocytosis occurs routinely in some cells, an inhibition of this process may be necessary in order to determine the total nanoparticle distribution to the lysosomes.[259-261] In the absence of this inhibition, the determinations can reveal time-dependent quantitative

decreases of lysosome-entrapped nanoparticles or constituent lipids that may or may not be linked to lysosomal degradation and/or exocytosis.[242, 257] Similar to endosomes, lysosomes to be used for LC-MS/MS analysis can be isolated from nanoparticle-treated cells using differential centrifugation in conjunction density shift techniques.[224, 253, 262-264]

1.6.2.6 *Ribosomal structures*

To date, no reported study has sought to investigate ribosomal structures within cells as a potential site of nanoparticle localization. Ribosomes are compact, non-membrane bound structures (25-30 nm diameter, eukaryotic 80S);[265, 266] they represent molecular machines that provide the site, structural support and catalysis for the assembly of amino acids into polypeptides during protein synthesis.[265, 266] This role requires that the surfaces and space around ribosomes should be free to allow the ribosomes to interact with mRNA and tRNA to bring about the assembly of amino acids into proteins, which perform several intracellular functions.[265, 266]

With ribosomes' roles as 'protein factory' of cells, a possible nanoparticle migration and localization at the surface of ribosomes could obstruct their function and therefore inhibit protein synthesis with or without consequent toxicity.[267, 268] In nanoparticle-mediated delivery of siRNA (strategy for **cancer** gene therapy via targeted gene suppression), the widely established concept is that the nanoparticles mediate the intracellular delivery of siRNA which disrupts expression of targeted mRNA before or after it reaches the ribosomes.[268-273] However, the propensity of nanoparticles to freely migrate within cells and localize at various subcellular sites could generate steric blocking effects around ribosomes, leading to gene supression.[98, 267, 268]

The suggested/possible dual effect of nanoparticles (steric obstruction of ribosomalprotein synthesis along with intracellular delivery of siRNA) is desirable in cancer cells. But there is a crucial need to investigate the nature and impact of possible nanoparticle distribution to ribosomes especially for applications in non-cancer cells where interference in ribosomal function is undesirable. To investigate the nature of possible nanoparticle distribution to ribosomes, these subcellular structures can isolated by differential centrifugation[224] from nanoparticle-treated cells and subjected to quantitative LC-MS/MS analysis.

1.6.2.7 *Cytosolic fluid fraction*

Upon cellular uptake, nanoparticles emerge into a cell's cytoplasm, where they may be bagged within organelles or suspended within the cytosolic fluid.[252, 274] If the uptake occurs through endocytosis (main uptake mode), the nanoparticles appear in the cytoplasm being initially enveloped in endosomes, from which their release into the cytosol follows. On the other hand, if uptake occurs through non-endocytotic internalization (i.e., nanoparticle–cell fusion[8] or lipid-mediated poration[275, 276]) the nanoparticles are deposited directly into the cytosol.[6, 98, 277]

Cytosolic deposition of freely suspended lipid nanoparticles following cellular uptake (endocytotic, non-endocytotic[252, 277, 278]) and endosomal release enables the imported nanoparticles to migrate and localize within cytoplasmic organelles. These organelles such as mitochondria and nucleus (discussed below) play critical functions which can be affected by the presence of nanoparticles. The nature of cytosolic deposition of nanoparticles and its impact on nanoparticle distribution to organelles can be studied using LC-MS/MS analysis. Prior to analysis, the cytosolic fluid from homogenized, nanoparticle-treated cells can be isolated by differential centrifugation.[224]

1.6.2.8 *Nuclear subcompartment*

In nanoparticle-mediated *in vitro* gene transfection, migration of nanoparticles into the nucleus is typically ***not*** expected. Instead, the nanoparticles should ideally transport the entrapped DNA cargo into cells and facilitate nuclear entry of the DNA, without the nanoparticle itself entering the nucleus.[98] This is because the successful protein expression has been demonstrated from microinjection of *naked* DNA[279] into the nucleus, rather than DNA entrapped in nanoparticles.[280, 281] In addition, DNA-encapsulated nanoparticles are not sufficiently small to enter through the tiny nuclear pores.[98, 147, 282-284]

While nuclear entry of only the DNA cargo is widely supported by published data,[98, 147, 282-284] a few reports suggest that nuclear entry can involve both the DNA/lipid nanoparticles complex.[285-287] Consequently, an apparent debate arises regarding the nature of nuclear entry: DNA alone *vs.* nanoparticle/DNA complexes. This debate can be clarified using LC-MS/MS analysis of intact nucleus from nanoparticle-treated cellsmin.[224]

1.6.2.9 *Mitochondrial subcompartment*

Currently, only ***qualitative***, fluorescence microscopic data indicate that nanoparticles which are internalized by cells translocate into mitochondria. Initially, non-targeted distribution of micellar nanoparticles to mitochondria was reported in studies (*in vitro*),[252] supporting previously held hypothesis.[288, 289] Subsequently, strategies emerged for targeted mitochondrial entry and accumulation of *mitochondriotropic* nanoparticles.[290-293] Mitochondriotropic nanoparticles (first reported in 2003[294, 295]) are designed with surface-tethered residues for recognition and binding to mitochondria.[290-293] Mitochondria have, consequently, become a

recognized intracellular distribution site of nanoparticles which are designed with or without mitochondrial targeted ligands.[64, 285]

Mitochondria which is the main site of lipid oxidation and generation of reactive oxygen species (ROS) play host to crucial events of cell death.[296, 297] Mitochondrial generation of ROS can be induced (but not always[298, 299]) by oxidation of lipids (by mitochondrial CYP450 enzymes),[300] which can include the lipids used as nanoparticle building blocks. Although lipid nanoparticle-induced toxicity is still to be fully understood by molecular mechanism, the toxicity and intracellular production of ROS in the presence of nanoparticles are well-correlated.[301-305]

LC-MS/MS analysis of intact mitochondria from treated cells (isolated by differential centrifugation[224]) will reveal the quantitative nanoparticle distribution to mitochondria and the distribution kinetics, among others. Such quantitative data can contribute to understanding nanoparticle-associated toxicity.

1.6.2.10 *Extracellular space/supernatant*

After nanoparticle incorporation into cells, the total intracellular nanoparticle content can decrease progressively.[306] Two main processes may account for a gradual disappearance of engineered nanoparticles from the cell interior: **i**) biotransformation;[307] **ii**) exocytosis of the nanoparticles or their constituent amphiphiles.[306] Exocytosis of nanoparticles can be significant in two ways: first, exocytosis of drug-loaded nanoparticles before drug release within cells is not beneficial. Second, exocytosis of nanoparticles after drug release within cells can provide strategic platform for development and use '***exocytose-able***' nanoparticles.

In the *in vitro* treatment of cells with nanoparticles, the administration of nanoparticles to cells is usually followed by changing of the supernatant cell culture media to fresh, nanoparticle-free media.[14] To investigate the occurrence or non-occurrence of exocytosis, the '***freshly added***' supernatant media can be collected after selected incubation periods and probed by LC-MS/MS analysis, which can reveal any exocytosed nanoparticles.[308]

1.7 Isolation of subcellular organelles and structures for LC-MS/MS bioanalysis

The LC-MS/MS determination of gemini surfactants in subcellular organelles and compartments of nanoparticle-treated cells (*Section 3.2.1–3.2.10*) requires isolation of the target organelles and sub-structures. Similar to native intracellular molecules, xenobiotics such as gemini surfactants may occur in subcellular organelles and compartments at different abundance. For organelles/compartments with a low abundance of the gemini surfactants, their separation will particularly be beneficial for LC-MS/MS detections and quantifications. In addition, absence of the bulk of cellular matrix improves LC-MS/MS sensitivity and helps give reproducible quantitative and qualitative analysis in target organelles.[309, 310]

Experimentally, the isolation of subcellular organelles and structures is achieved mainly through differential centrifugation (Figure 1.9). Differential centrifugation involves subjecting of cells (homogenized gently and effectively) to different centrifugal forces in different steps that exert differential pull on subcellular structures due to their distinct densities, sizes and shapes.[311, 312] As a result, the cell substructures selectively pellet (or sediment) and are collected as separate subcellular fractions in sequence with the centrifugation steps. The collected subcellular fractions

may contain enriched contents of a particular organelle or may represent mixtures of a few organelles which can further be separated.[313, 314]

The centrifugation steps adopted for fractionation of homogenized nanoparticle-treated cells herein is summarized below (Figure 1.9), taking PBS buffer as suspension medium. **Step 1:** the centrifugation will be performed at 6,300 × *g* for 5 min to give crude nuclei & debris (pellet 1) and supernatant 1 containing membranes, organelles & cytoplasm. **Step 2:** pellet 1 will be rehomogenized, resuspended in media, then centrifugated at 4,000 × *g* for 5 min to give **nuclear fraction** (pellet 2). The supernatant from this step is typically a *buffer*/*cellular remnant*, containing mainly the used suspension buffer with or without cellular remnants.[313, 315] Residual materials as well as target subcellular fractions will be saved (-80 ^{o}C) for subsequent analysis.

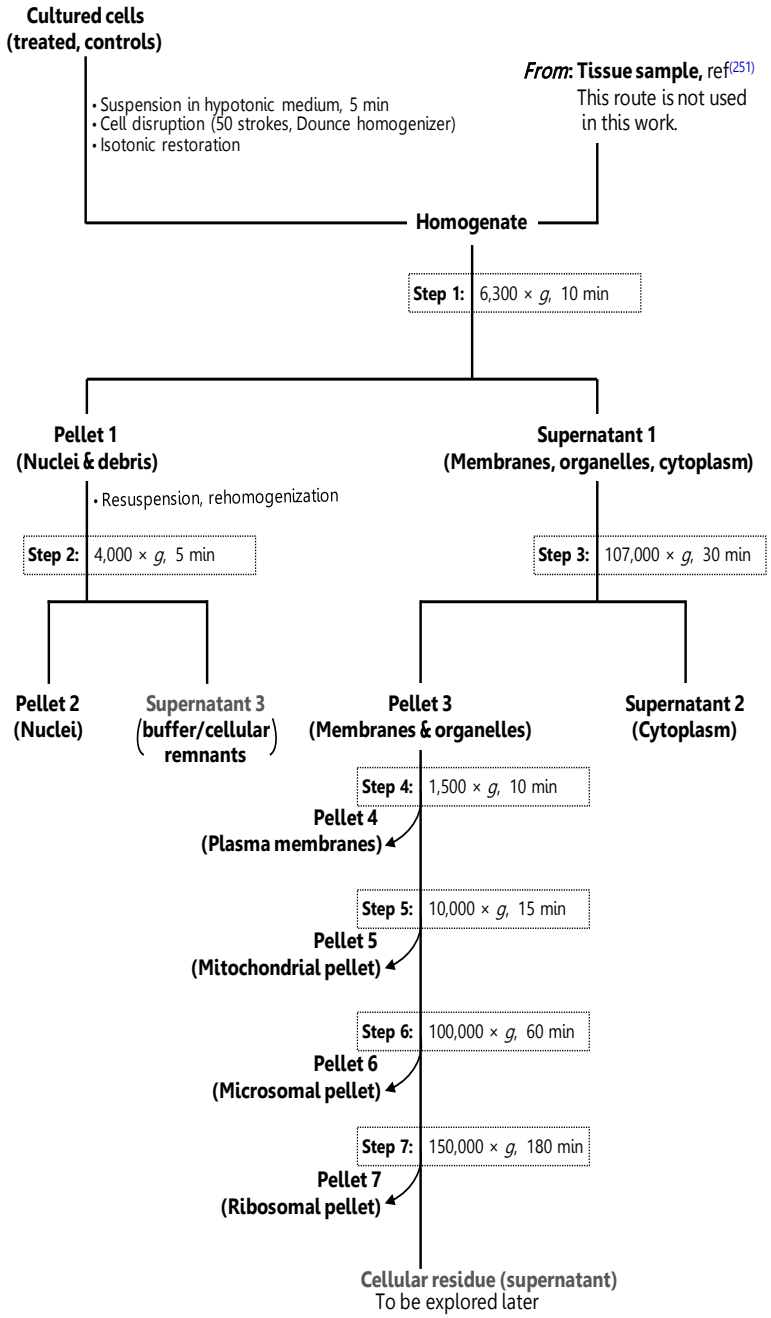

Figure 1.9: Subcellular fractionation scheme based on differential centrifugation. Adopted with some modifications from refs.[251, 313, 314]

In **Step 3**, supernatant 1 from **step 1** will be subjected to further centrifugation at 107,000 × *g* for 30 min to give **cytosolic fluid** (supernatant 2) and pellet 3 containing membranes & organelles. A well-mixed suspension of pellet 3 will be centrifugated in sequential steps to pellet the following subcellular fractions: **4**) 1,500 × *g* for 10 min, plasma membranes; **5**) 10,000 × *g* for 15 min, mitochondrial fraction; **6**) 100,000 × *g* for 60 min, microsomal fraction; **7**) 150,000 × *g* for 3 hr, ribosomal fraction.[224, 314] The supernatant from step **7** typically represents ***cellular residue*** with little chance of further recovery of intact organelles as their innate integrity deteriorates with continuous manipulation.[313-315]

Differential centrifugation will be used in conjunction with density shift techniques to separate organelles with overlapping sedimentation coefficients if signs of overlap exist, such as cross-contamination between organelle fractions.[316] Overlaps can be caused by certain similarities among few organelles, some cell media types or *in vitro* cell treatments.[314, 317] Organelles (as a group) often affected include endosomes, lysosomes, peroxisomes and mitochondria.[248-250] Density shift involves altering the buoyant density of an organelle away from that of others to allow effective centrifugal separation. Buoyant densities will be altered by attaching dense metal nanoparticles (or other tailored probes) to target organelles via organelle-selective ligands.[243, 248, 250, 251]

The composition and purity of subcellular fractions will be assessed using immunoblot assays with antibodies for detecting the presence and/or absence of organelle-specific marker proteins.[313, 316] A drawback of differential centrifugation for subcellular fractionation relates to purity: that is, isolated subcellular fractions can contain other cellular components in minor or appreciable amounts. In addition, cell homogenization and step-to-step manipulations increase

chances of ruptured organelles, making it difficult to recover every organelle in intact form from the same batch of homogenized cells.[264, 309, 314, 318, 319]

To circumvent the above-stated drawback, desired collections of different organelles can be obtained by pooling together subcellular fractions from replicate batch of cells – a useful strategy to be employed in this research. Toward downstream analysis, the obtained subcellular fractions will be homogenized by probe-tip ultrasonication. The homogenized organelles will be subjected to liquid–liquid extraction (LLE) to recover target analytes, gemini surfactants, which will then be determined using LC-MS/MS analysis.

1.8 The proposed research

1.8.1 Rationale of the proposed research

Numerous research has been conducted to investigate nanoparticle function and efficiency.[9] However, there is a lack of *in vitro*, *in vivo* and *ex vivo* data on the biological fate of medical nanoparticles.[54, 56, 69] In drug delivery applications of nanoparticles, the nanoparticles transport and release drugs into cells via the unpacking of the nanoparticles into the individual molecules (i.e., dispersed).[14, 115, 116] However, investigations to trace the amphiphile constituents and give an indication of the nanoparticle biological fate are generally not pursued.[54, 56, 69] Such studies could give a better understanding of nanoparticle-associated cytotoxicity and present an opportunity of averting it.

My research is focused on developing and implementing tandem mass spectrometric methods to study the intracellular/subcellular fate of gemini surfactant-based nanoparticles known to yield efficient *in vitro* drug delivery.[119, 120] As research to address the unknown fate of nanoparticles at the intracellular/subcellular level is still lacking,[45-50] my research findings will help solve the unknown nanoparticle bio-fate and help model possible correlations between nanoparticle intracellular distribution and nanoparticle-associated toxicity.

1.8.2 Research Hypotheses

1.8.2.1 *CID-MS/MS fragmentation behaviour and structural confirmation of dipyridinium and β-cyclodextrin-based diquaternary ammonium gemini surfactants*

HYPOTHESIS 1 of 3: β-cyclodextrin-substituted- and bis-pyridinium-based gemini surfactant compounds with broad structural similarities will show similarity in their CID-MS/MS fragmentation, and thus, will reveal a universal fragmentation pattern with similarities in the sequence and the structure of the product ions.

1.8.2.2 *Development and evaluation of liquid chromatograph-tandem mass spectrometry methods for bioanalysis of dipyridinium and diquaternary ammonium gemini surfactants*

HYPOTHESIS 2 of 3: LC-MS/MS methods employing a combination of sulfoalkylbetaine HILIC stationary phase and methanol/chloroform-based analyte recovery will show compatibility with gemini surfactants through significantly enhanced analytical sensitivity of the resultant methods relative to comparable methods without a demonstrated amphiphile-compatibility.

1.8.2.3 *Determination of the intracellular deposition and subcellular distribution profiles of representative dipyridinium and diquaternary ammonium gemini surfactants*

HYPOTHESIS 3 of 3: The two structurally contrasting gemini surfactant counterparts, 16(Py)-S-2-S-(Py)16 and 16-3-16 (dipyridinium *versus* diquaternary ammonium,

respectively) will exhibit different (i.e., non-identical) intracellular deposition and/or subcellular distribution profiles.

1.8.3 Research Objectives

1.8.3.1 *Specific Objective 1 – Based on Hypothesis 1*

Under **Specific Objective 1**, the molecular structure and composition of the chosen gemini surfactants (Figure 1.5) will be analyzed using QqQ-LIT-MS and Qq-ToF-MS plaftforms. The QqQ-LIT-MS system has a capability of MS^3 analysis, while the capability of the Qq-ToF-MS system includes high resolution full scan MS and MS/MS analysis. Their combined use will generate data for validating the molecular composition of the compounds and for the determination of CID-MS/MS distinct fragmentation products (i.e., fingerprints). Similar structural elucidation studies were recently conducted by our group for other gemini surfactants having quaternary ammonium headgroups, that is, alkanediyl-α,ω-bis(dimethyl alkylammonium halide) gemini surfactants.[95-97] In addition, data from **Objective 1** will indicate suitable fragment ions for multiple reaction monitoring (MRM) MS/MS quantitative analysis.

Two specific goals under **Objective 1** will be achieved:

- Confirmation of gemini surfactant molecular structures and determination of their diagnostic fragment ions through single-stage MS, tandem MS/MS, and multi-stage MS^3 analysis.
- Establishment of both universal and distinct MS/MS fingerprints.

1.8.3.2 *Specific Objective 2 – Based on Hypothesis 2*

Quantitative LC-ESI-MS/MS methods will be developed and evaluated toward the analysis of representative gemini surfactants contained in PAM 212 cell cultures after treatment with nanoparticles of these amphiphiles. The gemini surfactants are 16(Py)-S-2-S-(Py)16 and 16-3-16 (compound structures: Figure 1.5). Recently, MS-based methods for quantification were developed by our group for a group of alkanediyl-α,ω-bis(dimethyl alkylammonium halide) gemini surfactants,[147] but no methods are yet available for the bis-pyridinium-based-gemini surfactants. LC-ESI-MS/MS offers prior purification/separation for analytes within biological samples and this improves the detection of the analyte due to its relative purity. The methods will be applied for screening, detection and quantification of 16(Py)-S-2-S-(Py)16 and 16-3-16 present within PAM 212 cells. To do this, the two gemini surfactants will first be recovered from PAM 212 cell cultures in the form of cell lysates after cell treatments (i.e., transfection for varied durations) using separate nanoparticle formulations of the two gemini surfactants. The cell lysates will then be analyzed to quantify the amount of intact 16(Py)-S-2-S-(Py)16 and 16-3-16 at pre- and post-treatment times. Here, the information gained will give insights into any intracellular metabolism or elimination of gemini surfactants and this will, in turn, help define the biological fate of these representative lipids.

There are two specific goals under **Specific Objective 2**:

- Development and evaluation of HILIC-EIS-MS/MS platform for the bioanalysis of gemini surfactants with varying molecular structures.
- Development and full validation of HILIC-EIS-MS/MS quantitative methods for the bioanalysis of two lead gemini surfactants, 16(Py)-S-2-S-(Py)16 and 16-3-16.

1.8.3.3 *Specific Objective 3 – Based on Hypothesis 3*

In drug delivery, soft amphiphile organic nanoparticles are commonly assumed to unpack and/or disassemble after incorporation (entry) into cells so as to release their cargo (drug). Therefore, the constituent amphiphiles, which in this case are gemini surfactants, can be reasonably expected to localize or be distributed to various sites within cells. In this regard, **Specific Objective 3** seeks to investigate subcellular localization of 16(Py)-S-2-S-(Py)16 in comparison with structurally contrasting counterpart, 16-3-16. Data on both the subcellular localization for structurally contrasting gemini surfactants is essential: (1) it provides insights into the intracellular trafficking, elimination, recycling or other processes that the gemini surfactants may undergo; (2) it will enable a comparison of the measured cytotoxicity levels with the observed intracellular distribution of the lipids to give insights into how different molecular structures influence toxicity or other *in vitro* parameters. To determine the subcellular localization, treated PAM 212 cell sample will be fractionated and analyzed to quantify the proportion of 16(Py)-S-2-S-(Py)16 and 16-3-16 present within various fractions.

Two specific goals under **Specific Objective 3** include:

- Quantitative determination of 16(Py)-S-2-S-(Py)16 and 16-3-16 as lead gemini surfactants within transfected PAM 212 cells using developed/validated HILIC-ESI-MS/MS methods.
- Quantitative determination of 16(Py)-S-2-S-(Py)16 and 16-3-16 within treated PAM212 subcellular fractions using developed/validated HILIC-ESI-MS/MS methods in conjunction with standard addition approach.

1.9 REFERENCES:

1. Sargent Jr. JF. Nanotechnology and Environmental, Health, and Safety: Issues for Consideration. CRS Report for U.S. Congress, 2011 Contract No.: RL34614.

2. Covey TR, Lee ED, Henion JD. High-speed liquid chromatography/tandem mass spectrometry for the determination of drugs in biological samples. Anal Chem. 1986;58(12):2453-60.

3. Raith K, Schmelzer CEH, Neubert RHH. Towards a molecular characterization of pharmaceutical excipients: Mass spectrometric studies of ethoxylated surfactants. International Journal of Pharmaceutics. 2006;319(1–2):1-12.

4. Ehehalt R, Wagenblast J, Erben G, Lehmann W, Hinz U, Merle U, et al. Phosphatidylcholine and lysophosphatidylcholine in intestinal mucus of ulcerative colitis patients. A quantitative approach by nanoElectrospray-tandem mass spectrometry. Scand J Gastroenterol. 2004;39(8):737–42.

5. Edelhauser HF, Rowe-Rendleman CL, Robinson MR, Dawson DG, Chader GJ, Grossniklaus HE, et al. Ophthalmic drug delivery systems for the treatment of retinal diseases: basic research to clinical applications. Invest Ophthalmol Vis Sci. 51. United States2010. p. 5403-20.

6. Donkuru M, Badea I, Wettig S, Verrall R, Elsabahy M, Foldvari M. Advancing nonviral gene delivery: lipid- and surfactant-based nanoparticle design strategies. Nanomedicine (Future Medicine). 2010;5(7):1103−27.

7. Singh J, Mohammed-Saied W, Kaur R, Badea I. Nanoparticles in Gene Therapy: From Design to Clinical Applications. Reviews in Nanoscience and Nanotechnology. 2013;2(4):275-99.

8. Felgner PL, Ringold GM. Cationic liposome-mediated transfection. Nature. 1989;337(6205):387-8.

9. Subramanian M, Holopainen JM, Paukku T, Eriksson O, Huhtaniemi I, Kinnunen PK. Characterisation of three novel cationic lipids as liposomal complexes with DNA. Biochim Biophys Acta. 1466. Netherlands2000. p. 289-305.

10. Wetzer B, Byk G, Frederic M, Airiau M, Blanche F, Pitard B, et al. *Reducible cationic lipids for gene transfer*. Biochem J. 2001;*356*:747–56.

11. Sola B, Staedel C, Remy J-S, Bahr A, Behr J-P. Lipospermine-mediated gene transfer technique into murine cultured cortical cells. Journal of Neuroscience Methods. 1997;71(2):183-6.

12. Donkuru M, Badea I, Wettig S, Verrall R, Elsabahy M, Foldvari M. Advancing nonviral gene delivery: lipid- and surfactant-based nanoparticle design strategies. Nanomedicine (Future Medicine). 2010;5(7):1103-27.

13. Zhang S, Xu Y, Wang B, Qiao W, Liu D, Li Z. Cationic compounds used in lipoplexes and polyplexes for gene delivery. *Journal of Controlled Release*. 2004;100.

14. Donkuru M, Wettig SD, Verrall RE, Badea I, Foldvari M. Designing pH-sensitive gemini nanoparticles for non-viral gene delivery into keratinocytes. J Mater Chem. 2012;22:6232-44.

15. Donkuru M. Non-viral gene delivery with pH-sensitive gemini nanoparticles: synthesis of gemini surfactant Building blocks, characterization and *in vitros*creening of transfection efficiency and toxicity. Saskatoon, SK, Canada: Univeristy of Saskatchewan; 2008.

16. Wettig SD, Verrall RE, Foldvari M. Gemini surfactants: a new family of building blocks for non-viral gene delivery systems. Curr Gene Ther. 2008;8(1):9-23.

17. Kirby AJ, Camilleri P, Engberts JB, Feiters MC, Nolte RJ, Soderman O, et al. Gemini surfactants: new synthetic vectors for gene transfection. Angew Chem Int Ed Engl. 2003;42(13):1448-57.

18. Chen Z, Deng J, Zhao Y, Tao T. Cyclic RGD peptide-modified liposomal drug delivery system: enhanced cellular uptake in vitro and improved pharmacokinetics in rats. Int J Nanomedicine. 7. New Zealand2012. p. 3803-11.

19. Hart SL, Collins L, Gustafsson K, Fabre JW. Integrin-mediated transfection with peptides containing arginine-glycine-aspartic acid domains. Gene Ther. 1997;4(11):1225-30.

20. **Mason A**, **Martinez A**, **Glaubitz C**, **Danos O**, **Kichler A**, **Bechinger B**. **The antibiotic and DNA-transfecting peptide LAH4 selectively associates with, and disorders, anionic lipids in mixed membranes**. **FASEB J**. 2006;20(2):320–2.

21. Gupta B, Levchenko TS, Torchilin VP. Intracellular delivery of large molecules and small particles by cell-penetrating proteins and peptides. Advanced Drug Delivery Reviews. 2005;57(4):637-51.

22. Deshayes S, Morris MC, Divita G, Heitz F. Cell-penetrating peptides: tools for intracellular delivery of therapeutics. Cell Mol Life Sci. 2005;62(16):1839-49.

23. Li W, Nicol F, Szoka Jr FC. GALA: a designed synthetic pH-responsive amphipathic peptide with applications in drug and gene delivery. Advanced Drug Delivery Reviews. 2004;56(7):967-85.

24. Sakae M, Ito T, Yoshihara C, Iida-Tanaka N, Yanagie H, Eriguchi M, et al. Highly efficient in vivo gene transfection by plasmid/PEI complexes coated by anionic PEG derivatives bearing carboxyl groups and RGD peptide. Biomed Pharmacother. 62. France2008. p. 448-53.

25. Kumar MN, Mohapatra SS, Kong X, Jena PK, Bakowsky U, Lehr CM. Cationic poly(lactide-co-glycolide) nanoparticles as efficient in vivo gene transfection agents. J Nanosci Nanotechnol. 2004;4(8):990-4.

26. Jeong JH, Kim SW, Park TG. Biodegradable triblock copolymer of PLGA-PEG-PLGA enhances gene transfection efficiency. Pharm Res. 2004;21(1):50-4.

27. Zaliauskiene L, Bernadisiute U, Vareikis A, Makuska R, Volungeviciene I, Petuskaite A, et al. Efficient Gene Transfection Using Novel Cationic Polymers Poly(hydroxyalkylene imines). Bioconjugate Chemistry. 2010;21(9):1602-11.

28. Amiji MM. Polymeric Gene Delivery: Principles and Applications. Boca Raton, FL, USA: CRC Press LLC; 2004. 704 p.

29. Shcharbin DG, Klajnert B, Bryszewska M. Dendrimers in gene transfection. Biochemistry (Mosc). 74. United States2009. p. 1070-9.

30. Dean DA, Gasiorowski JZ. Dendrimer-Mediated Transfection. Cold Spring Harbor Protocols. 2011;2011(3):prot5584.

31. Shakhbazau A, Isayenka I, Kartel N, Goncharova N, Seviaryn I, Kosmacheva S, et al. Transfection efficiencies of PAMAM dendrimers correlate inversely with their hydrophobicity. International Journal of Pharmaceutics. 2010;383(1–2):228-35.

32. Choia JS, Namb K, Park J-y, Kim J-B, Lee J-K, Park J-s. Enhanced transfection efficiency of PAMAM dendrimer by surface modification with l-arginine. Journal of Controlled Release. 2004; 99:445–56.

33. Faraji AH, Wipf P. Nanoparticles in cellular drug delivery. Bioorganic & Medicinal Chemistry. 2009;17(8):2950-62.

34. Lasic DD. Novel applications of liposomes. Trends in Biotechnology. 1998;16(7):307-21.

35. Coombs RRH, Robinson DW. Nanotechnology in Medicine and the Biosciences. Bowen DK, editor. Amsterdam, Netherlands: Gordon and Breach Publishers SA; 1996.

36. Ma B, Zhang S, Jiang H, Zhao B, Lv H. Lipoplex morphologies and their influences on transfection efficiency in gene delivery. Journal of Controlled Release. 2007;123(3):184-94.

37. Xu Y, Hui SW, Frederik P, Szoka FC, Jr. Physicochemical characterization and purification of cationic lipoplexes. Biophys J. 77. United States1999. p. 341-53.

38. Peng SF, Su CJ, Wei MC, Chen CY, Liao ZX, Lee PW, et al. Effects of the nanostructure of dendrimer/DNA complexes on their endocytosis and gene expression. Biomaterials. 31. England: 2010 Elsevier Ltd; 2010. p. 5660-70.

39. Caracciolo G, Pozzi D, Caminiti R, Marchini C, Montani M, Amici A, et al. Enhanced transfection efficiency of multicomponent lipoplexes in the regime of optimal membrane charge density. J Phys Chem B. 2008;112(36):11298–304.

40. Ciani L, Ristori S, Salvati A, Calamai L, Martini G. DOTAP/DOPE and DC-Chol/DOPE lipoplexes for gene delivery: zeta potential measurements and electron spin resonance spectra. Biochimica et Biophysica Acta (BBA) - Biomembranes. 2004;1664(1):70-9.

41. Martin-Herranz A, Ahmad A, Evans HM, Ewert K, Schulze U, Safinya CR. Surface functionalized cationic lipid-DNA complexes for gene delivery: PEGylated lamellar complexes exhibit distinct DNA-DNA interaction regimes. Biophys J. 86. United States2004. p. 1160-8.

42. Li W, Huang Z, MacKay JA, Grube S, Szoka FC, Jr. Low-pH-sensitive poly(ethylene glycol) (PEG)-stabilized plasmid nanolipoparticles: effects of PEG chain length, lipid composition and assembly conditions on gene delivery. J Gene Med. 2005;7(1):67-79.

43. Kim TW, Chung H, Kwon IC, Sung HC, Jeong SY. Optimization of lipid composition in cationic emulsion as in vitro and in vivo transfection agents. Pharm Res. 2001;18(1):54-60.

44. Frerix A, Schonewald M, Geilenkirchen P, Muller M, Kula MR, Hubbuch J. Exploitation of the coil-globule plasmid DNA transition induced by small changes in temperature, pH salt, and poly(ethylene glycol) compositions for directed partitioning in aqueous two-phase systems. Langmuir. 2006;22(9):4282-90.

45. Huth US, Schubert R, Peschka-Süss R. Investigating the uptake and intracellular fate of pH-sensitive liposomes by flow cytometry and spectral bio-imaging. Journal of Controlled Release. 2006;110(3):490-504.

46. Borm P, Klaessig FC, Landry TD, Moudgil B, Pauluhn J, Thomas K, et al. Research strategies for safety evaluation of nanomaterials, part V: role of dissolution in biological fate and effects of nanoscale particles. Toxicol Sci. 2006;90(1):23-32.

47. Gemeinhart RA, Luo D, Saltzman WM. Cellular fate of a modular DNA delivery system mediated by silica nanoparticles. Biotechnol Prog. 2005;21(2):532-7.

48. Prokop A, Davidson JM. Nanovehicular intracellular delivery systems. J Pharm Sci. 2008;97(9):3518-90.

49. Smiljanic N, Yockot D, Cendret V, Francois-heude M, Moreau V, Djedaini-pilard F. Oligosaccharide-cyclodextrin conjugates: synthesis and biological affinity torward lecithins. Carbohydrate Chemistry. 2012;37:374-97.

50. Kadam RS, Bourne DW, Kompella UB. Nano-advantage in enhanced drug delivery with biodegradable nanoparticles: contribution of reduced clearance. Drug Metab Dispos. 2012;40(7):1380-8.

51. Colvin LV. The potential environmental impact of engineered nanoparticles. Nature Biotechnology. 2003;21:1166-70.

52. Smita S, Gupta KS, Bartonova A, Dusinska M, Gutleb CA, Rahman Q. Nanoparticles in the environment: assessment using the causal diagram approach. Environ Health. 2012;11((Suppl 1)):1–13.

53. Schmidt WC. Nanotechnology-Related Environment, Health, and Safety Research: Examining the National Strategy. Environ Health Perspect. 2009;117(4):A158–A61.

54. Council NST. National Natechnology Initiative: Strategic Plan. 2011.

55. Buse J, El-Aneed A. Properties, engineering and applications of lipid-based nanoparticle drug-delivery systems: current research and advances. Nanomedicine (Lond). 2010;**5**(8):1237-60.

56. Drexler KE. Engines of Creation 2.0: The Coming Era of Nanotechnology. Los Angeles, USA: WOWIO LLC; 2007. 646 p.

57. Baum RM. "Nanotechnology: Drexler and Smalley make the case for and against 'molecular assemblers". *Chemical & Engineering News* (American Chemical Society). 2003; **81**(48):37–42.

58. Klaessig F, Marrapese M, Abe S. Current Perspectives in Nanotechnology Terminology and Nomenclature. In: Murashov V, Howard J, editors. Nanotechnology Standards: Nanostructure Science and Technology2011. p. 21-52.

59. Taniguchi N, editor On the Basic Concept of 'Nano-Technology'. Proc Intl Conf Prod Eng; 1974; Tokyo, Japan.

60. Nanotechnology: Integrated Processing Systems for Ultra-precision and Ultra-fine products. Taniguchi N, editor. Cary, NC, USA: Oxford University Press; 1996. 424 p.

61. Feynman RP. There's Plenty of Room at the Bottom. *Engineering and Science* magazine. 1960;XXIII(5).

62. Buzea C, Pacheco I, Robbie K. Nanomaterials and nanoparticles: Sources and toxicity. Biointerphases. 2007;2(4):MR17-MR71.

63. Somasundaran P, Fang X, Ponnurangam S, Li B. Nanoparticles: Characteristics, Mechanisms and Modulation of Biotoxicity. KONA Powder and Particle Journal No28. 2010:38 – 49.

64. Oberdörster G, Oberdörster E, Oberdörster J. Nanotoxicology: An Emerging Discipline Evolving from Studies of Ultrafine Particles. Environmental Health Perspectives. 2005;113(7):823 - 39.

65. Houdy BP, Lahmani M, Marano F. **Nanoethics and Nanotoxicology**. Berlin: Springer-Verlag; 2011. 1-613 p.

66. Minelli C. Bottom-up approaches for organizing nanoparticles with polymers: École Polytechnique Fédérale de Lausanne (EPFL), Switzerland; 2004.

67. Whitesides G, Kriebel J, Mayers B. Self-Assembly and Nanostructured Materials. In: Huck WS, editor. Nanoscale Assembly. Nanostructure Science and Technology: Springer US; 2005. p. 217-39.

68. Zhang J, Wang Z-l, Liu J, Chen S, Liu G-y. Self-Assembled Nanostructures: Springer Line (eBooks); 2002.

69. Lee YS. Self-Assembly and Nanotechnology Systems: Design, Characterization, and Applications: John Wiley & Sons, Inc.; 2011. 459 pp p.

70. Raab C, Simkó M, Fiedeler U, Nentwich M, Gazsó A. Production of nanoparticles and nanomaterials. **NANO** TRUST DOSSIERS. 2011;006-EN.

71. L. Parker Alan, Newman C, Briggs S, Seymour L, Paul JS. Nonviral gene delivery: techniques and implications for molecular medicine. *Expert Rev Mol Med*. 2003;5:1-15.

72. Donkuru M, Badea I, Wettig S, Verrall R, Elsabahy M, Foldvari M. Advancing nonviral gene delivery: lipid- and surfactant-based nanoparticle design strategies. 2010;5(7):1103-27.

73. Srinivasan C, Burgess DJ. Optimization and characterization of anionic lipoplexes for gene delivery. J Control Release. 136. Netherlands2009. p. 62-70.

74. Zhang J, Wang Z-l, Liu J, Chen S, Liu G-y. Synthetic Self-Assembled Materials: Principles and Practice. Self-Assembled Nanostructures. Nanostructure Science and Technology. New York: Kluwer Academic Publishers; 2004. p. 7-52.

75. Sastry M, Rao M, Ganesh KN. Electrostatic Assembly of Nanoparticles and Biomacromolecules. Accounts of Chemical Research. 2002;35(10):847-55.

76. Fullam S, Rensmo H, Rao SN, Fitzmaurice D. Noncovalent Self-Assembly of Silver and Gold Nanocrystal Aggregates in Solution. Chemistry of Materials. 2002;14(9):3643-50.

77. Pertsov EI. Nanomaterials: New Research Developments. Far**go, North Dakota, USA**: Nova Science Pub Incorporated; 2008. 348 p.

78. Buffat P, Borel JP. Size effect on the melting temperature of gold particles. Phys Rev A. 1976;13:2287-98.

79. Reed M, Randall J, Aggarwal R, Matyi R, Moore T, AE W. Observation of discrete electronic states in a zero-dimensional semiconductor nanostructure. *Phys Rev Lett*. 1988;60(6):535–7.

80. Ekimov AI, Onushchenko AA. Quantum size effect in three-dimensional microscopic semiconductor crystals. *JETP Lett*. 1981;34:345–9.

81. "Nanoscience and nanotechnologies: opportunities and uncertainties": Royal Society and Royal Academy of Engineering; July 2004 [cited 2012 4 July]. Available from: http://www.nanotec.org.uk/finalReport.htm.

82. Sayes C, Reed K, Warheit D. Assessing toxicity of fine and nanoparticles: comparing in vitro measurements to in vivo pulmonary toxicity profiles. Toxicol Sci. 2007;97(1):163-80.

83. Union SE. What are the potential environmental effects of nanomaterials? 2009 [cited 2012 11 September]. Official document of European Union via its The Scientific Committee on Emerging and Newly Identified Health Risks (SCENIHR) on the stated subject]. Available from: http://ec.europa.eu/health/scientific_committees/opinions_layman/nanomaterials/en/l-3/6.htm#0.

84. Hussain SM, Hess KL, Gearhart JM, Geiss KT, Schlager JJ. In vitro toxicity of nanoparticles in BRL 3A rat liver cells. Toxicology in Vitro. 2005; 19:975–83.

85. Wani MY, Hashim MA, Nabi F, Malik MA. **Nanotoxicity: Dimensional and Morphological Concerns**. Advances in Physical Chemistry. 2011;2011:1-15.

86. Hochella Jr. MF, Lower SK, Maurice PA, Penn RL, Sahai N, Sparks DL, et al. Nanominerals, Mineral Nanoparticles, and Earth Systems. Science. 2008;319(5870):1631-5.

87. Whitesides MG, Boncheva M. Beyond molecules: Self-assembly of mesoscopic and macroscopic components. PNAS. 2002;99(8):4769–74.

88. Nagarajan R, Ruckenstein E. Theory of Surfactant Self -Assembly: A Predictive Molecular Thermodynamic Approach. Langmuir. 1991;7:2934-69.

89. Lehn J-M. Toward self-organization and complex matter. Science. 2002;295(5564):2400–3.

90. Whitesides MG, Kriebel KJ, Love JC. Molecular engineering of surfaces using self-assembled monolayers. Science Progress. 2005;88(Pt. 1):17–48.

91. Israelachvili NJ. Intermolecular and Surface Forces. 3rd Ed. ed. London: Academic Press; 2011.

92. Valignat M-P, Theodoly O, Crocker CJ, Russel BW, Chaikin MP. **Reversible self-assembly and directed assembly of DNA-linked micrometer-sized colloids**. PNAS, USA. 2005;102(12)):4225–9.

93. Grinthal A, Kang SH, Epstein AK, Aizenberg M, Khan M, Aizenberg J. Steering nanofibers: An integrative approach to bio-inspired fiber fabrication and assembly. Nano Today. 2011;7:35–52.

94. Matsunaga M, Aizenberg M, Aizenberg J. Controlling the Stability and Reversibility of Micropillar Assembly by Surface Chemistry. *J Am Chem Soc*. **2011**;133(*14*):*5545–53*.

95. Yang P, Singh J, Wettig S, Foldvari M, Verrall RE, Badea I. Enhanced gene expression in epithelial cells transfected with amino acid-substituted gemini nanoparticles. European Journal of Pharmacuetics & Biopharmacuetics. 2010;75(3):311–20.

96. Badea I, Verrall R, Baca-Estrada M, Tikoo S, Rosenberg A, Kumar P, et al. *In vivo* cutaneous interferon-γ gene delivery using novel dicationic (gemini) surfactant–plasmid complexes. Journal of Gene Medicine. 2005;7(9):1200–14.

97. Byk G, Dubertret C, Escriou V, Frederic M, Jaslin G, Rangara R, et al. Synthesis, activity, and structure--activity relationship studies of novel cationic lipids for DNA transfer. J Med Chem. 1998;41(2):229-35.

98. Niculescu-Duvaz D, Heyes J, Springer CJ. Structure-activity relationship in cationic lipid mediated gene transfection. Curr Med Chem. 2003;10(14):1233-61.

99. *Mohammed-Saeid W*, M*ichel D*, El-*Aneed A*, *Ve*rral*l ER*, *Low* HN, *Badea I*. Development of Lyophilized Gemini Surfactant-Based Gene Delivery Systems: Influence of Lyophilization on the Structure, Activity and Stability of the Lipoplexes. J Pharm Pharm Sci. 2012;15(4):548-67.

100. Chen S, Zhuo RX, Cheng SX. Enhanced gene transfection with addition of a cell-penetrating peptide in substrate-mediated gene delivery. J Gene Med. 2010;12(8):705-13.

101. **Cannon BJ**. Strategies to Formulate Lipid-based Drug Delivery Systems. *American Pharmaceutical Review*. 2011;14(4):pp13.

102. Allen MT. Pharmacokinetics and Biopharmaceutics of Lipid-Based Drug Formulations. In: Gregoriadis G, editor. Liposome Technology, Volume III. Interactions of Liposomes with the Biological Milieu. III. 3rd ed. New York, USA: Informa Healthcare; 2006. p. 49 – 64 (of 434).

103. Wheeler CJ, Felgner PL, Tsai YJ, Marshall J, Sukhu L, Doh SG, et al. A novel cationic lipid greatly enhances plasmid DNA delivery and expression in mouse lung. Proc Natl Acad Sci U S A. 1996;93(21):11454–9.

104. Ewert K, Slack NL, Ahmad A, Evans HM, Lin AJ, Samuel CE, et al. Cationic lipid-DNA complexes for gene therapy: understanding the relationship. Curr Med Chem. 2004;11(2):133-49.

105. Yu J-M, Li Y-J, Qiu L-Y, Jin Y. Self-aggregated nanoparticles of cholesterol-modified glycol chitosan conjugate: Preparation, characterization, and preliminary assessment as a new drug delivery carrier. European Polymer Journal. 2008;44(3):555-65.

106. Ji B, Peacock G, Lu DR. Synthesis of cholesterol-carborane conjugate for targeted drug delivery. Bioorg Med Chem Lett. 2002;12(17):2455-8.

107. Kane DB, Oktem B, Johnston MV. Nanoparticle Detection by Aerosol Mass Spectrometry. Aerosol Science and Technology. 2001;34(6):520-7.

108. Chiang C-K, Chen W-T, Chang H-T. Nanoparticle-based mass spectrometry for the analysis of biomolecules. Chem Soc Rev. 2011;40:1269-81.

109. Berg MJ, Tymoczko LJ, Stryer L. Biochemistry. 7 (revised international edn.) ed. New York, USA: W. H. Freeman & Co Ltd.; 2011. 1026 p.

110. Butovich IA, Uchiyama E, McCulley JP. Lipids of human meibum: mass-spectrometric analysis and structural elucidation. J Lipid Res. 2007;48(10):2220-35.

111. Lasic DD. Recent developments in medical applications of liposomes: sterically stabilized liposomes in cancer therapy and gene delivery in vivo. Journal of Controlled Release. 1997;48(2-3):203–22.

112. Mohammed-Saeid W, Buse J, Badea I, Verrall R, El-Aneed A. Mass spectrometric analysis of amino acid/di-peptide modified gemini surfactants used as gene delivery agents: Establishment of a universal mass spectrometric fingerprint. *Int J Mass Spectrom*. 2012;309:182–91.

113. Buse J, Badea I, Verrall RE, El-Aneed A. Tandem mass spectrometric analysis of novel diquaternary ammonium gemini surfactants and their bromide adducts in electrospray-positive ion mode ionization. J Mass Spectrom. 2011;46(10):1060-70.

114. Buse J, Badea I, Verrall ER, El-Aneed A. Tandem Mass Spectrometric Analysis of the Novel Gemini Surfactant Nanoparticle Families G12-s and G18:1-s. Spectroscopy Letters. 2010;43:447–57.

115. Menger FM, Keiper JS. Gemini Surfactants. Angew Chem Int Ed Engl. 392000. p. 1906-20.

116. Ilies MA, Seitz WA, Ghiviriga I, Johnson BH, Miller A, Thompson EB, et al. Pyridinium cationic lipids in gene delivery: a structure-activity correlation study. J Med Chem. 2004;47(15):3744-54.

117. Ilies MA, Seitz AW, Caproiu TM, Wentz M, Garfield ER, Balaban TA. Pyridinium-Based Cationic Lipids as Gene-Transfer Agents. Eur J Org Chem. 2003:2645–55.

118. van der Woude I, Wagenaar A, Meekel AA, ter Beest MB, Ruiters MH, Engberts JB, et al. Novel pyridinium surfactants for efficient, nontoxic in vitro gene delivery. Proc Natl Acad Sci U S A. 1997;94(4):1160-5.

119. Bhadani A, Singh S. Novel gemini pyridinium surfactants: synthesis and study of their surface activity, DNA binding, and cytotoxicity. Langmuir. 2009;25(19):11703-12.

120. Michel D, Chitanda JM, Balogh R, Yang P, Singh J, Das U, et al. Design and evaluation of cyclodextrin-based delivery systems to incorporate poorly soluble curcumin analogs for the treatment of melanoma. Eur J Pharm Biopharm. 81. Netherlands: 2012 Elsevier B.V; 2012. p. 548-56.

121. Ilies MA, Sommers TV, He LC, Kizewski A, Sharma VD. Pyridinium Amphiphiles in Gene Delivery – Present and Perspectives. Amphiphiles: Molecular Assembly and Applications. ACS Symposium Series. 1070: American Chemical Society; 2011. p. 23-38.

122. Singh J, Yang P, Michel D, Verrall RE, Foldvari M, Badea I. Amino acid-substituted gemini surfactant-based nanoparticles as safe and versatile gene delivery agents. Curr Drug Deliv. 8. United Arab Emirates2011. p. 299-306.

123. Fan H-M, Zhu X-M, Li Z-C, Han F, Liu Z, Huang J-B. Synthesis and Characterization of Cystine-based Gemini Surfactants. Acta Phys Chim Sin. 2007;23(07):969–72.

124. Ikeda I. Synthesis of gemini (dimeric) and related surfactants. In: Zana R, Xia J, editors. Gemini Surfactants: Synthesis, Interfacial and Solution-Phase Behavior and Applications. New York, USA: Marcel Dekker, Inc; 2004. p. 9 – 35.

125. Fielden ML, Perrin C, Kremer A, Bergsma M, Stuart MC, Camilleri P, et al. Sugar-based tertiary amino gemini surfactants with a vesicle-to-micelle transition in the endosomal pH range mediate efficient transfection in vitro. Eur J Biochem. 268. Germany2001. p. 1269-79.

126. Wasungu L, Scarzello M, van Dam G, Molema G, Wagenaar A, Engberts JB, et al. Transfection mediated by pH-sensitive sugar-based gemini surfactants; potential for in vivo gene therapy applications. J Mol Med (Berl). 2006;84(9):774-84.

127. Chierici S, Boullanger P, Marron-Brignone L, Morelis RM, Coulet PR. Synthesis and interfacial behaviour of a gemini neoglycolipid. Chemistry and Physics of Lipids. 1997;87(2):91-101.

128. Wettig SD, Badea I, Donkuru M, Verrall RE, Foldvari M. Structural and transfection properties of amine-substituted gemini surfactant-based nanoparticles. J Gene Med. 2007;9(8):649-58.

129. Wettig SD, Wang C, Verrall RE, Foldvari M. Thermodynamic and aggregation properties of aza- and imino-substituted gemini surfactants designed for gene delivery. Phys Chem Chem Phys. 2007;9(7):871-7.

130. Watson JT, Sparkman OD. Introduction to Mass Spectrometry: Instrumentation, Applications, and Strategies for Data Interpretation. 4th ed. Chichester, England: John Wiley & Sons; 2007. 862 p.

131. Want E, Compton JB, Hollenbeck T, Siuzdak G. The application of mass spectrometry in pharmacokinetic studies. Spectroscopy. 2003;17:681–91.

132. Ramanathan R. Mass Spectrometry in Drug Metabolism and Pharmacokinetics. Hoboken, New Jersey, USA.: John Wiley & Sons Ltd; 2008. 390 p.

133. Liang Y, Wang G, Xie L, Sheng L. Recent development in liquid chromatography/mass spectrometry and emerging technologies for metabolite identification. Current Drug Metabolism. 2011;12(4):329–44.

134. Damani LA, Crooks PA, Shaker MS, Caldwell J, D'Souza J, Smith RL. **Species differences in the metabolic C- and N-oxidation , and N-methylation of [^{14}C]pyridine in vivo**. Xenobiotica. 1982;12(8):527–34.

135. D'Souza J, Caldwell J, Smith RL. **Species variations in the N-methylation and quaternization of [^{14}C]pyridine**. Xenobiotica. 1980;10(2):151–7.

136. Roper LW. Toxicological Profile for Pyridine. Agency for Toxic Substances and Disease Registry, U.S. Public Health Service, 1992.

137. Brazda FG, Coulson RA. Toxicity of nicotinic acid and some of its derivatives. Proc Soc Exp Biol Med. 1946;62:19–20.

138. Smyth HFJ, Carpenter CP, Weil CS. Range-finding toxicity data: List IV. AMA Arch Ind Hyg Occup Med. 1951;4(2):119-22.

139. Griffiths J. A Brief History of Mass Spectrometry. Anal Chem. 2008;80(15):5678–83.

140. Antignac J-P, Le Bizec B, Monteau F, Andre F. Validation of analytical methods based on mass spectrometric detection according to the “2002/657/EC” European decision: guideline and application. Analytica Chimica Acta. 2003;483(1–2):325-34.

141. (E-MRS) EMRS, editor ALTECH 2014 (Symposium H): Analytical Techniques for Precise Characterization of NanoMaterials. E-MRS Spring Meeting 2014; 2014; Lille, France.

142. Lin P-C, Lin S, Wang PC, Sridhar R. Techniques for physicochemical characterization of nanomaterials. Biotechnology Advances. 2013.

143. Hodgson E. A Textbook of Modern Toxicology. 4 ed: John Wiley & Sons; 2011. 672 p.

144. Omiecinski CJ, Vanden Heuvel JP, Perdew GH, Peters JM. Xenobiotic Metabolism, Disposition, and Regulation by Receptors: From Biochemical Phenomenon to Predictors of Major Toxicities. Toxicological Sciences. 2011;120(suppl 1):S49-S75.

145. Macherey A-C, Dansette PM. Biotransformations Leading to Toxic Metabolites: Chemical Aspect. In: Wermuth CG, editor. The Practice of Medicinal Chemistry. 3 ed. Burlington, MA, USA: Academic Press; 2011. p. 674–96 (982 pp, whole book).

146. Wermuth CG. The Practice of Medicinal Chemistry. 3 ed. Burlington, MA, USA: Academic Press/Elsevier Science; 2011. 982 p.

147. Singh J, Michel D, Chitanda MJ, Verrall ER, Badea I. Evaluation of cellular uptake and intracellular trafficking as determining factors of gene expression for amino acid-substituted gemini surfactant-based DNA nanoparticles. J Nanobiotechnology.
2012;10(7):1–14.

148. Anno T, Higashi T, Motoyama K, Hirayama F, Uekama K, Arima H. Possible enhancing mechanisms for gene transfer activity of glucuronylglucosyl-β-cyclodextrin/dendrimer conjugate. Int J Pharm. 2012;426(1-2):239-47.

149. Lim CK, Lord G. Current developments in LC-MS for pharmaceutical analysis. Biol Pharm Bull. 2002;25(5):547-57.

150. Kadavil J, Booth B. Bioanalytical Method Validation - Biopharmaceutics (guidance for Industry). Food and Drugs Administration, United States of America, 2013.

151. Tiwari G, Tiwari R. Bioanalytical method validation: An updated review Pharm Methods. 2010;1(1):25–38.

152. Aebersold R, Mann M. Mass spectrometry-based proteomics. Nature. 422. England2003. p. 198-207.

153. Ma M, Gard AL, Xiang F, Wang J, Davoodian N, Lenz PH, et al. Combining in silico transcriptome mining and biological mass spectrometry for neuropeptide discovery in the Pacific white shrimp Litopenaeus vannamei. Peptides. 2010;31(1):27-43.

154. Dettmer K, Aronov PA, Hammock BD. Mass spectrometry-based metabolomics. Mass Spectrom Rev. 2007;26(1):51-78.

155. Gstaiger M, Aebersold R. Applying mass spectrometry-based proteomics to genetics, genomics and network biology. Nat Rev Genet. 10. England2009. p. 617-27.

156. Meng Z, Simmons-Willis TA, Limbach PA. The use of mass spectrometry in genomics. Biomolecular Engineering. 2004;21(1):1-13.

157. Blanksby SJ, Mitchell TW. Advances in mass spectrometry for lipidomics. Annu Rev Anal Chem (Palo Alto Calif). 2010;3:433-65.

158. Murphy RC, Merrill Jr AH. Lipidomics and Imaging Mass Spectrometry. Biochimica et Biophysica Acta (BBA) - Molecular and Cell Biology of Lipids. 2011;1811(11):635-6.

159. Zaia J. Mass spectrometry and glycomics. OMICS. 2010;14(4):401-18.

160. Morelle W, Michalski JC. Glycomics and mass spectrometry. Curr Pharm Des. 2005;11(20):2615-45.

161. Zaia J. Mass Spectrometry and the Emerging Field of Glycomics. Chemistry & Biology. 2008;15(9):881–92.

162. Liu X, McNally JD, Nothaft H, Li J, Szymanski MC, Brisson J-R. Mass Spectrometry-Based Glycomics Strategy for Exploring N-Linked Glycosylation in Eukaryotes and Bacteria. Anal Chem. 2006;78(17):6081–7.

163. Louris JN, Cooks RG, Syka JEP, Kelley PE, Stafford GC, Todd JFJ. Instrumentation, applications, and energy deposition in quadrupole ion-trap tandem mass spectrometry. Analytical Chemistry. 1987;59(13):677–1685.

164. Li R, Zhou Y, Wu Z, Ding L. ESI-QqTOF-MS/MS and APCI-IT-MS/MS analysis of steroid saponins from the rhizomes. J Mass Spectrom. 2006;41(1):1-22.

165. Chernushevich IV, Loboda AV, Thomson BA. An introduction to quadrupole-time-of-flight mass spectrometry. J Mass Spectrom. 2001;36(8):849-65.

166. Kebarle P, Verkerk UH. Electrospray: from ions in solution to ions in the gas phase, what we know now. Mass Spectrom Rev. 2009;28(6):898-917.

167. Ho CS, Lam CW, Chan MH, Cheung RC, Law LK, Lit LC, et al. Electrospray ionisation mass spectrometry: principles and clinical applications. Clin Biochem Rev. 2003;24(1):3-12.

168. Marvin LF, Roberts MA, Fay LB. Matrix-assisted laser desorption/ionization time-of-flight mass spectrometry in clinical chemistry. Clin Chim Acta. 337. Netherlands2003. p. 11-21.

169. Knochenmuss R. Ion formation mechanisms in UV-MALDI. Analyst. 2006;131(9):966-86.

170. Krutchinsky AN, Chernushevich IV, Spicer VL, Ens W, Standing KG. Collisional Damping Interface for an Electrospray Ionization Time-of-Flight Mass Spectrometer. Journal of the American Society for Mass Spectrometry. 1998;9(6):569-79.

171. Shevchenko A, Chernushevich I, Ens W, Standing KG, Thomson B, Wilm M, et al. Rapid ‘de novo’ peptide sequencing by a combination of nanoelectrospray, isotopic labeling and a quadrupole/time-of-flight mass spectrometer. Rapid Commun Mass Spectrom. 1997;11:1015 - 24.

172. Guilhaus M, Selby D, Mlynski V. Orthogonal Acceleration Time-Of-Flight Mass Spectrometry. Mass Spectrometry Reviews. 2000;19:65 – 107.

173. Bristow T. EVOLUTION & REVOLUTION in time-of-flight mass spectrometry and its impact on research within the pharmaceutical industry. European Pharmaceutical Review. 2011;16(3):13 – 5.

174. Toyoda M, Okumura D, Ishihara M, Katakuse I. Multi-turn time-of-flight mass spectrometers with electrostatic sectors. J Mass Spectrom. 2003;38:1125–42.

175. Zhang MY, Pace N, Kerns EH, Kleintop T, Kagan N, Sakuma T. Hybrid triple quadrupole-linear ion trap mass spectrometry in fragmentation mechanism studies: application to structure elucidation of buspirone and one of its metabolites. J Mass Spectrom. 2005;40(8):1017-29.

176. Douglas DJ, Frank AJ, Mao D. Linear ion traps in mass spectrometry. Mass Spectrom Rev. 2005;24(1):1-29.

177. Schwartz JC, Senko MW, Syka JEP. A two-dimensional quadrupole ion trap mass spectrometer. Journal of the American Society for Mass Spectrometry. 2002;13(6):659-69.

178. Yost RA, Enke CG. Selected ion fragmentation with a tandem quadrupole mass spectrometer. *Journal of the American Chemical Society*. 1978;**100**(7):2274–5.

179. Arpino P. Combined liquid chromatography mass spectrometry. Part III. Applications of thermospray. Mass Spectrometry Reviews. 1992;11(1):3-40.

180. Arpino P. Combined liquid chromatography mass spectrometry. Part I. Coupling by means of a moving belt interface. Mass Spectrometry Reviews. 1989;8(1):35-55.

181. Lee MS, Kerns EH. LC/MS applications in drug development. Mass Spectrom Rev. 1999;18(3-4):187-279.

182. Hsieh Y, Korfmacher WA. Increasing speed and throughput when using HPLC-MS/MS systems for drug metabolism and pharmacokinetic screening. Curr Drug Metab. 2006;7(5):479-89.

183. Covey TR, Crowther JB, Dewey EA, Henion JD. Thermospray liquid chromatography/mass spectrometry determination of drugs and their metabolites in biological fluids. Anal Chem. 1985;57(2):474-81.

184. Lopez de Alda MJ, Diaz-Cruz S, Petrovic M, Barcelo D. Liquid chromatography-(tandem) mass spectrometry of selected emerging pollutants (steroid sex hormones, drugs and alkylphenolic surfactants) in the aquatic environment. J Chromatogr A. 2003;1000(1-2):503-26.

185. Grebe SK, Singh RJ. LC-MS/MS in the Clinical Laboratory - Where to From Here? Clin Biochem Rev. 2011;32(1):5-31.

186. Vogeser M, Seger C. Pitfalls associated with the use of liquid chromatography-tandem mass spectrometry in the clinical laboratory. Clin Chem. 2010;56(8):1234-44.

187. Guo Y. Analysis of Quaternary Amine Compounds by Hydrophilic Interaction Chromatography/Mass Spectrometry (HILIC/MS). Journal of Liquid Chromatography & Related Technologies. 2005;28(4):497-512.

188. Heckendorf A, Gilar M, Krull IS, Rathore A. HILIC and Its Applications for Biotechnology, Part II. LCGC NORTH AMERICA. 2014;32(1):38–53.

189. Buszewski B, Noga S. Hydrophilic interaction liquid chromatography (HILIC)—a powerful separation technique. Analytical and Bioanalytical Chemistry. 2012;402(1):231-47.

190. Jian W, Edom RW, Lin ZJ, Weng N. Chromatographic separation methods. In: Zhang D, Surapaneni S, editors. ADME-Enabling Technologies in Drug Design and Development. Hoboken, New Jersey, USA: John Wiley & Sons, Inc.,; 2012. p. 381–400.

191. Zhang CE, Xiong Y, Dong Q, Gao D, Zhang LL, Ma LN, et al. Comparison of reversed-phase liquid chromatography and hydrophilic interaction chromatography for the fingerprint analysis of Radix isatidis. J Sep Sci. 2014.

192. Hemström P, Irgum K. Hydrophilic interaction chromatography. Journal of Separation Science. 2006;29(12):1784-821.

193. Alpert AJ. Electrostatic repulsion hydrophilic interaction chromatography for isocratic separation of charged solutes and selective isolation of phosphopeptides. Anal Chem. 2008;80(1):62-76.

194. Alpert AJ. Hydrophilic-interaction chromatography for the separation of peptides, nucleic acids and other polar compounds. Journal of Chromatography A. 1990;499(0):177-96.

195. Grumbach ES, Wagrowski-Diehl DM, Mazzeo JR, Alden B, Lraneta PC. Hydrophilic Interaction Chromatography Using Silica Columns for the Retention of Polar Analytes and Enhanced ESI-MS Sensitivity. LCGC North America. 2004;22(10):1010–23.

196. Dejaegher B, Vander Heyden Y. HILIC methods in pharmaceutical analysis. J Sep Science. 2010;33(6-7):698–715.

197. Dejaegher B, Mangelings D, Vander Heyden Y. Method development for HILIC assays. J Sep Sci. 2008;31(9):1438-48.

198. Heckendorf A, Krull IS, Rathore A. HILIC and Its Applications for Biotechnology, Part I. LCGC NORTH AMERICA. 2013;31(12):998–1007.

199. Periat A, Boccard J, Veuthey JL, Rudaz S, Guillarme D. Systematic comparison of sensitivity between hydrophilic interaction liquid chromatography and reversed phase liquid chromatography coupled with mass spectrometry. J Chromatogr A. 2013;1312(49–57).

200. Wang X, Ding K, Yang C, Lin X, Lu H, Wu X, et al. Sulfoalkylbetaine-based monolithic column with mixed-mode of hydrophilic interaction and strong anion-exchange stationary phase for capillary electrochromatography. Electrophoresis. 2010;31(17):2997-3005.

201. Wang X, Lin X, Xie Z. Preparation and evaluation of a sulfoalkylbetaine-based zwitterionic monolithic column for CEC of polar analytes. Electrophoresis. 2009;30(15):2702-10.

202. Chen Y, Wang K, Liu Y, Yang H, Yao S, Chen B, et al. Improved sulfoalkylbetaine-based organic-silica hybrid monolith for high efficient hydrophilic interaction liquid chromatography of polar compounds. Electrophoresis. 2013;34(13):1877-85.

203. Chen C-C, Su W-C, Huang B-Y, Chen Y-J, Tai H-C, Obena RP. Interaction modes and approaches to glycopeptide and glycoprotein enrichment. Analyst. 2014;139:688–704.

204. Pereira L. HILIC–MS Sensitivity without Silica. LCGC North America. 2011;29(3):262.

205. Appelblad P, Jonsson T, Jiang W, Irgum K. Fast hydrophilic interaction liquid chromatographic separations on bonded zwitterionic stationary phase. J Sep Sci. 2008;31(9):1529−36.

206. Corporation W. Atlantis™ columns (HILIC) – Applications Notebook, 720000472EN. Milford, MA, USA: Waters Corporation, 2004.

207. Hak Soo Choi, Wenhao Liu, Preeti Misra, Eiichi Tanaka, John P. Zimmer, Binil Itty Ipe, et al. Renal Clearance of Nanoparticles. Nat Biotechnol. 2007;25(10):1165–70.

208. Liu J, Yu M, Zhou C, Zheng J. Renal clearable inorganic nanoparticles: a new frontier of bionanotechnology. Materials Today. 2013;16(12):477-86.

209. Abdelhalim MA. Uptake of gold nanoparticles in several rat organs after intraperitoneal administration in vivo: a fluorescence study. (2314-6141 (Electronic)).

210. Longmire M, Choyke PL, Kobayashi H. Clearance properties of nano-sized particles and molecules as imaging agents: considerations and caveats. Nanomedicine (Lond). 2008;3(5):703-17.

211. Boyer C, Davis T. A new generation of nanoparticles for image enhancement. Australian Biochemist. 2012;43(3):13–6.

212. Reszka R, Beck P, Fichtner I, Hentschel M, Richter J, Kreuter J. Body distribution of free, liposomal and nanoparticle-associated mitoxantrone in B16-melanoma-bearing mice. J Pharmacol Exp Ther. 1997;280(1):232-7.

213. Lee MJ, Veiseh O, Bhattarai N, Sun C, Hansen SJ, Ditzler S, et al. Rapid pharmacokinetic and biodistribution studies using cholorotoxin-conjugated iron oxide nanoparticles: a novel non-radioactive method. PLoS One. 2010;5(3):e9536.

214. Enright HA, Malfatti MA. Detection methods for the in vivo biodistribution of iron oxide and silica nanoparticles – effect of size surface chemistry and shape. Nanotoxicology: Progress toward Nanomedicine. 2014:177–200.

215. Martin J. Butson, Tsang Cheung, Peter K.N. Yu, Martin Carolan, Peter E. Metcalfe. Simulation and measurement of air generated electron contamination in radiotherapy. Radiation Measurements. 2000;32:105–11.

216. Butson MJ, Cheung T, Yu PKN. Skin dose delivered in megavoltage external beam therapeutic radiology. Austral-Asian J Cancer. 2006;5(2):101–4.

217. Turesson I, Thames HD. Repair capacity and kinetics of human skin during fractionated radiotherapy: erythema, desquamation, and telangiectasia after 3 and 5 year's follow-up. Radiother Oncol. 1989;15(2):169-88.

218. Kry SF, Smith SA, Weathers R, Stovall M. Skin dose during radiotherapy: a summary and general estimation technique. J Appl Clin Med Phys. 2012;13(3):3734.

219. Williams PL, Warwick R, Dyson M, Bannister LH. Gray's Anatomy (305 × 235mm). 37 ed. Edinburgh, Scotland: Churchill Livingstone; 1989. p. 1598 pp.

220. Gaspar VM, Marques JG, Sousa F, Louro RO, Queiroz JA, Correia IJ. Biofunctionalized nanoparticles with pH-responsive and cell penetrating blocks for gene delivery. Nanotechnology. 2013;24(27):275101.

221. Zhu MT, Feng WY, Wang Y, Wang B, Wang M, Ouyang H, et al. Particokinetics and extrapulmonary translocation of intratracheally instilled ferric oxide nanoparticles in rats and the potential health risk assessment. Toxicol Sci. 2009;107(2):342-51.

222. Geiser M, Kreyling WG. Deposition and biokinetics of inhaled nanoparticles. Particle & Fibre Toxicology. 2010;7(2):1–17.

223. Choi HS, Ashitate Y, Lee JH, Kim SH, Matsui A, Insin N, et al. Rapid translocation of nanoparticles from the lung airspaces to the body. Nat Biotechnol. 2010;28(12):1300-3.

224. Lodish H, Berk A, Zipursky LS, Matsudaira P, Baltimore D, Darnell J. Biomembranes and the Subcellular Organization of Eukaryotic Cells. Molecular Cell Biology. 6 ed. New York: W. H. Freeman & Company; 2000. p. 973.

225. Andreyev AY, Fahy E, Guan Z, Kelly S, Li X, McDonald JG, et al. Subcellular organelle lipidomics in TLR-4-activated macrophages. J Lipid Res. 2010;51(9):2785-97.

226. Brugger B. Lipidomics: Analysis of the Lipid Composition of Cells and Subcellular Organelles by Electrospray Ionization Mass Spectrometry. Annu Rev Biochem. 2014.

227. Buse J, Badea I, Verrall RE, El-Aneed A. A general liquid chromatography tandem mass spectrometry method for the quantitative determination of diquaternary ammonium Gemini surfactant drug delivery agents in mouse keratinocytes' cellular lysate. Journal of Chromatography A. 2013;1294:98–105.

228. Lasic DD, Papahadjopoulos D. Liposomes Revisited. Science. 1995;267(1275–1276).

229. Lasic DD. Liposomes. American Scientis. 1992;80(1):20–31.

230. Garcia-Garcia E, Andrieux K, Gil S, Kim HR, Doan TL, Desmaële D, et al. A methodology to study intracellular distribution of nanoparticles in brain endothelial cells. International Journal of Pharmaceutics. 2005;298(2):310-4.

231. Jia L, Liu X. The conduct of drug metabolism studies considered good practice (II): in vitro experiments. Curr Drug Metab. 2007;8(8):822-9.

232. Lohr JW, Willsky GR, Acara MA. Renal Drug Metabolism. Pharmacological Reviews. 1998;50(1):107−42.

233. Conney AH. Pharmacological implications of microsomal enzyme induction. Pharmacological Reviews. 1967;19(3):317−66.

234. Voet D, Voet JG. Biochemistry. Hokoben, NJ, USA: John Wiley & Sons; 2011.

235. Bains RK. African variation at Cytochrome P450 genes: Evolutionary aspects and the implications for the treatment of infectious diseases. Evol Med Public Health. 2013;2013(1):118-34.

236. Lewis DF. 57 varieties: the human cytochromes P450. Pharmacogenomics. 2004;5(3):305-18.

237. Ingelman-Sundberg M. Human drug metabolising cytochrome P450 enzymes: properties and polymorphisms. Naunyn Schmiedebergs Arch Pharmacol. 2004;369(1):89-104.

238. Zhang Y, Wu W, Han F, Chen Y. LC/MS/MS for identification of in vivo and in vitro metabolites of jatrorrhizine. Biomed Chromatogr. 2008;22(12):1360-7.

239. Dooley AN, Seto C, Ghobarah H, Jones EB. Simultaneous Metabolite Identification and Quantitation with UV Data Integration Using LightSight® Software v2.2, № 1038610-01. Foster City, CA: AB SCIEX Pte. Ltd.; 2010.

240. Zientek M, Youdim K. Simultaneous determination of multiple CYP inhibition constants using a cocktail-probe approach. Methods Mol Biol. 2013;987:11-23.

241. Sorkin A, von Zastrow M. Endocytosis and signalling: intertwining molecular networks. Nat Rev Mol Cell Biol. 2009;10(9):609-22.

242. Saftig P, Klumperman J. Lysosome biogenesis and lysosomal membrane proteins: trafficking meets function. Nat Rev Mol Cell Biol. 2009;10(9):623-35.

243. Vasir JK. Nanoparticle-cell interactions, intracellular trafficking, and protein therapy for restenosis. Omaha, Nebraska, USA2008.

244. Yokoyama M. Novel passive targetable drug delivery with polymeric micelles. In: Okano T, editor. Biorelated Polymers and Gels: Controlled Release and Applications in Biomedical Engineering. San Diego, CA, USA: Academic Press; 1998. p. 193–230.

245. Bremnes T, Paasche JD, Mehlum A, Sandberg C, Bremnes B, Attramadal H. Regulation and intracellular trafficking pathways of the endothelin receptors. J Biol Chem. 2000;275(23):17596-604.

246. Erazo-Oliveras A, Muthukrishnan N, Baker R, Wang T-Y, Pellois J-P. Improving the Endosomal Escape of Cell-Penetrating Peptides and Their Cargos: Strategies and Challenges. Pharmaceuticals. 2012;5:1177−209.

247. Serda RE, Mack A, van de Ven AL, Ferrati S, Dunner K, Jr., Godin B, et al. Logic-embedded vectors for intracellular partitioning, endosomal escape, and exocytosis of nanoparticles. Small. 2010;6(23):2691-700.

248. Ajioka RS, Kaplan J. Characterization of Endocytic Compartments Using the Horseradish Peroxidase-Diaminobenzidine Density Shift Technique. The Journal of Cell Biology. 1987;104:77–85.

249. Guimaraes de Araujo ME, Fialka I, Huber LA. Endocytic Organelles: Methods for Preparation and Analysis: eLS - Wiley Online Library; 2010.

250. Tjelle TE, Brech A, Juvet LK, Griffiths G, Berg T. Isolation and characterization of early endosomes, late endosomes and erminal lysosomes: their role in protein degradation. Journal of Cell Science. 1996;109:2905–14.

251. Manunta M, Izzo L, Duncan R, Jones AT. Establishment of subcellular fractionation techniques to monitor the intracellular fate of polymer therapeutics II. Identification of

endosomal and lysosomal compartments in HepG2 cells combining single-step subcellular fractionation with fluorescent imaging. J Drug Target. 2007;15(1):37-50.

252. Savić R, Luo L, Eisenberg A, Maysinger D. Micellar nanocontainers distribute to defined cytoplasmic organelles. Science. 2003;300(5619):615–8.

253. Wu HY, Chung MC, Wang CC, Huang CH, Liang HJ, Jan TR. Iron oxide nanoparticles suppress the production of IL-1beta via the secretory lysosomal pathway in murine microglial cells. Part Fibre Toxicol. 2013;10:46.

254. Coffey GP, Stefanich E, Palmieri S, Eckert R, Padilla-Eagar J, Fielder PJ, et al. In vitro internalization, intracellular transport, and clearance of an anti-CD11a antibody (Raptiva) by human T-cells. J Pharmacol Exp Ther. 2004;310(3):896-904.

255. Dell'Angelica EC, Mullins C, Caplan S, Bonifacino JS. Lysosome-related organelles. Faseb j. 2000;14(10):1265-78.

256. Wright JR. Clearance and recycling of pulmonary surfactant. Am J Physiol. 1990;259(2 Pt 1):L1-12.

257. Yanes RE, Tarn D, Hwang AA, Ferris DP, Sherman SP, Thomas CR, et al. Involvement of lysosomal exocytosis in the excretion of mesoporous silica nanoparticles and enhancement of the drug delivery effect by exocytosis inhibition. Small. 2013;9(5):697-704.

258. Moghimi SM, Hunter AC, Murray JC. Nanomedicine: current status and future prospects. The FASEB Journal. 2005;19(3):311-30.

259. Bagshaw RD, Mahuran DJ, Callahan JW. A proteomic analysis of lysosomal integral membrane proteins reveals the diverse composition of the organelle. Mol Cell Proteomics. 2005;4(2):133-43.

260. Yates JR, 3rd, Gilchrist A, Howell KE, Bergeron JJ. Proteomics of organelles and large cellular structures. Nat Rev Mol Cell Biol. 2005;6(9):702-14.

261. Sant'Anna C, Nakayasu ES, Pereira MG, Lourenco D, de Souza W, Almeida IC, et al. Subcellular proteomics of Trypanosoma cruzi reservosomes. Proteomics. 2009;9(7):1782-94.

262. Mušálková D, Lukáš J, Majer F, Hřebíček O, Svobodová E, Kuchař L, et al. Rapid Isolation of Lysosomal Membranes from Cultured Cells. Folia Biologica (Praha). 2013;59:41–6.

263. Nikos P. Subcellular Fractionation. Mater Methods. 2013;3:562.

264. Graham JM. Subcellular Fractionation and Isolation of Organelles (Chptr. 3). Current Protocols in Cell Biology (ebook). 1999.

265. Alberts B, Johnson A, Lewis J, Raff M, Roberts K, Walter P. The Molecular Biology of the Cell. 5 ed. Anderson M, Granum S, editors. New York, NY, USA: Garland Science; 2008. 1392 pp p.

266. Hardesty B, Kramer G. Structure, Function, and Genetics of Ribosomes. 1 ed. New York, NY, USA: Springer (Springer –Verlag); 1986. 810 p.

267. Brown KA, Park S, Hamad-Schifferli K. Nucleotide−Surface Interactions in DNA-Modified Au−Nanoparticle Conjugates: Sequence Effects on Reactivity and Hybridization. The Journal of Physical Chemistry C. 2008;112(20):7517-21.

268. Dias N, Stein CA. Antisense oligonucleotides: basic concepts and mechanisms. Mol Cancer Ther. 2002;1(5):347-55.

269. Lee J-M, Yoon T-J, Cho Y-S. Recent Developments in Nanoparticle-Based siRNA Delivery for Cancer Therapy. BioMed Research International. 2013;2013(782041):1–10.

270. Goldberg MS, Xing D, Ren Y, Orsulic S, Bhatia SN, Sharp PA. Nanoparticle-mediated delivery of siRNA targeting Parp1 extends survival of mice bearing tumors derived from Brca1-deficient ovarian cancer cells. Proc Natl Acad Sci U S A. 2011;108(2):745-50.

271. Kolli S, Wong SP, Harbottle R, Johnston B, Thanou M, Miller AD. pH-triggered nanoparticle mediated delivery of siRNA to liver cells in vitro and in vivo. Bioconjug Chem. 2013;24(3):314-32.

272. Gilleron J, Querbes W, Zeigerer A, Borodovsky A, Marsico G, Schubert U, et al. Image-based analysis of lipid nanoparticle-mediated siRNA delivery, intracellular trafficking and endosomal escape. Nat Biotech. 2013;31(7):638-46.

273. Hou KK, Pan H, Ratner L, Schlesinger PH, Wickline SA. Mechanisms of Nanoparticle-Mediated siRNA Transfection by Melittin-Derived Peptides. ACS Nano. 2013;7(10):8605–15.

274. Zelphati O, Szoka FC, Jr. Intracellular distribution and mechanism of delivery of oligonucleotides mediated by cationic lipids. Pharm Res. 1996;13(9):1367-72.

275. Xu Y, Szoka FC, Jr. Mechanism of DNA release from cationic liposome/DNA complexes used in cell transfection. Biochemistry. 1996;35(18):5616-23.

276. Lu JJ, Langer R, Chen J. Mechanism of DNA Release from Cationic Liposome/DNA Complexes Used in Cell Transfection. Biochemistry. 1996;35:5616–23.

277. Khalil IA, Kogure K, Akita H, Harashima H. Uptake pathways and subsequent intracellular trafficking in nonviral gene delivery. Pharmacol Rev. 2006;58(1):32-45.

278. Elouahabi A, Ruysschaert JM. Formation and intracellular trafficking of lipoplexes and polyplexes. Mol Ther. 2005;11(3):336-47.

279. Capecchi MR. High efficiency transformation by direct microinjection of DNA into cultured mammalian cells. Cell. 1980;22(2 Pt 2):479-88.

280. Zabner J, Fasbender AJ, Moninger T, Poellinger KA, Welsh MJ. Cellular and molecular barriers to gene transfer by a cationic lipid. J Biol Chem. 1995;270(32):18997-9007.

281. Pollard H, Remy JS, Loussouarn G, Demolombe S, Behr JP, Escande D. Polyethylenimine but not cationic lipids promotes transgene delivery to the nucleus in mammalian cells. J Biol Chem. 1998;273(13):7507-11.

282. Zanta MA, Belguise-Valladier P, Behr JP. Gene delivery: a single nuclear localization signal peptide is sufficient to carry DNA to the cell nucleus. Proc Natl Acad Sci U S A. 1999;96(1):91-6.

283. Ciolina C, Byk G, Blanche F, Thuillier V, Scherman D, Wils P. Coupling of nuclear localization signals to plasmid DNA and specific interaction of the conjugates with importin alpha. Bioconjug Chem. 1999;10(1):49-55.

284. Aissaoui A, Oudrhiri N, Petit L, Hauchecorne M, Kan E, Sainlos M, et al. Progress in gene delivery by cationic lipids: guanidinium-cholesterol-based systems as an example. Curr Drug Targets. 2002;3(1):1-16.

285. Xia T, Kovochich M, Brant J, Hotze M, Sempf J, Oberley T, et al. Comparison of the abilities of ambient and manufactured nanoparticles to induce cellular toxicity according to an oxidative stress paradigm. Nano Lett. 2006;6(8):1794-807.

286. Zhang F, Andreassen P, Fender P, Geissler E, Hernandez J-F, Chroboczek J. A transfecting peptide derived from adenovirus fiber protein free. Gene Therapy. 1999;6(171–181).

287. Pitard B, Oudrhiri N, Vigneron JP, Hauchecorne M, Aguerre O, Toury R, et al. Structural characteristics of supramolecular assemblies formed by guanidinium-cholesterol reagents for gene transfection. Proc Natl Acad Sci USA. 1999;96:2621–6.

288. Weissig V, Torchilin VP. Mitochondriotropic cationic vesicles: a strategy towards mitochondrial gene therapy. Curr Pharm Biotechnol. 2000;1(4):325-46.

289. Yokoyama Ma, Okano Te, editors. Biorelated Polymers and Gels: Controlled Release and Applications in Biomedical Engineering. San Diego, CA, USA: Academic Press; 1998.

290. Carreira RS, Lee P, Gottlieb RA. Mitochondrial therapeutics for cardioprotection. Curr Pharm Des. 2011;17(20):2017-35.

291. Boddapati SV, D'Souza GG, Weissig V. Liposomes for drug delivery to mitochondria. Methods Mol Biol. 2010;605:295-303.

292. Wallace DC, Fan W, Procaccio V. Mitochondrial energetics and therapeutics. Annu Rev Pathol. 2010;5:297-348.

293. Yamada Y, Harashima H. Delivery of bioactive molecules to the mitochondrial genome using a membrane-fusing, liposome-based carrier, DF-MITO-Porter. Biomaterials. 2012;33(5):1589-95.

294. Boddapati SV, Tongcharoensirikul P, Hanson RN, D'Souza GG, Torchilin VP, Weissig V. Mitochondriotropic liposomes. J Liposome Res. 2005;15(1-2):49-58.

295. Weissig V, D'Souza GGM. Cationic Mitochondriotropic Vesicles for DNA Delivery to Mitochondria. Molecular Therapy. 2004;9:S259–S.

296. Kadirvela G, Kumara S, Kumaresana A. Lipid peroxidation, mitochondrial membrane potential and DNA integrity of spermatozoa in relation to intracellular reactive oxygen species in liquid and frozen-thawed buffalo semen. Animal Reproduction Science. 2009;114(1-3):125–34.

297. Voet D, Judith GV, Charlotte WP. Fundamentals of Biochemistry: Life at Molecular level. 4th ed. New York, NY, USA: John Wiley & Sons, Inc.; 2013.

298. Dix TA, Aikens J. Mechanisms and biological relevance of lipid peroxidation initiation. Chem Res Toxicol. 1993;6(2–18).

299. Ghersi-Egea JF, Perrin R, Leininger-Muller B, Grassiot MC, Jeandel C, Floquet J, et al. Subcellular localization of cytochrome P450, and activities of several enzymes responsible for drug metabolism in the human brain. Biochem Pharmacol. 1993;45(3):647–58.

300. Porter NA. Mechanisms for the autoxidation of polyunsaturated lipids. Acc Chem Res. 1986;19:262–8.

301. Takiguchi N, Takahashi Y, Nishikawa M, Matsui Y, Fukuhara Y, Oushiki D, et al. Positive correlation between the generation of reactive oxygen species and activation/reactivation of transgene expression after hydrodynamic injections into mice. Pharm Res. 2011;28(4):702-11.

302. Audouy SA, de Leij LF, Hoekstra D, Molema G. In vivo characteristics of cationic liposomes as delivery vectors for gene therapy. Pharm Res. 2002;19(11):1599-605.

303. Brown DM, Wilson MR, MacNee W, Stone V, Donaldson K. Size-dependent proinflammatory effects of ultrafine polystyrene particles: a role for surface area and oxidative stress in the enhanced activity of ultrafines. Toxicol Appl Pharmacol. 2001;175(3):191-9.

304. Molina MD, Anchordoquy TJ. Formulation strategies to minimize oxidative damage in lyophilized lipid/DNA complexes during storage. J Pharm Sci. 2008;97(12):5089-105.

305. Molina MD, Anchordoquy TJ. Degradation of lyophilized lipid/DNA complexes during storage: the role of lipid and reactive oxygen species. Biochim Biophys Acta. 2008;1778(10):2119–26.

306. Wu Y, Ho YP, Mao Y, Wang X, Yu B, Leong KW, et al. Uptake and intracellular fate of multifunctional nanoparticles: a comparison between lipoplexes and polyplexes via quantum dot mediated Forster resonance energy transfer. Mol Pharm. 2011;8(5):1662-8.

307. Koch AM, Reynolds F, Kircher MF, Merkle HP, Weissleder R, Josephson L. Uptake and metabolism of a dual fluorochrome Tat-nanoparticle in HeLa cells. Bioconjug Chem. 2003;14(6):1115-21.

308. Jang A, Lee HJ, Suk JE, Jung JW, Kim KP, Lee SJ. Non-classical exocytosis of alpha-synuclein is sensitive to folding states and promoted under stress conditions. J Neurochem. 2010;113(5):1263-74.

309. Michelsen U, von Hagen J. Isolation of subcellular organelles and structures. Methods Enzymol. 2009;463:305-28.

310. Frezza C, Cipolat S, Scorrano L. Organelle isolation: functional mitochondria from mouse liver, muscle and cultured fibroblasts. Nat Protoc. 2007;2(2):287-95.

311. Alberts B, Johnson A, Lewis J, Raff M, Roberts K, Walter P. Part III - Methods: Chptr 8 - Fractionation of Cells. In: Anderson M, Dilernia B, editors. The Molecular Biology of the Cell. 4 ed. New York, NY, USA: Garland Science; 2002 p. 469–581 (1616 pp, whole book).

312. Nikos P. Subcellular Fractionation. Nature Methods. 2013;3:562.

313. Guillemin I, Becker M, Ociepka K, Friauf E, Nothwang HG. A subcellular prefractionation protocol for minute amounts of mammalian cell cultures and tissue. Proteomics. 2005;5(1):35-45.

314. Graham JM, Rickwood D. Subcellular Fractionation: A Practical Approach. New York, NY, USA: Oxford University Press; 2002 (reprinted). 1–360 pp p.

315. Hinton RH, Mullock BM. Isolation of subcellular fractions. In: Graham JM, Rickwood D, editors. Subcellular Fractionation: A Practical Approach. New York, NY, USA: Oxford University Press; 2002 (reprinted). p. 31–70 (360 pp, whole book).

316. Salvi D, Rolland N, Joyard J, Ferro M. Assessment of organelle purity using antibodies and specific assays : the example of the chloroplast envelope. Methods Mol Biol. 2008;432:345-56.

317. Della Valle MC, Sleat DE, Zheng H, Moore DF, Jadot M, Lobel P. Classification of subcellular location by comparative proteomic analysis of native and density-shifted lysosomes. Mol Cell Proteomics. 2011;10(4):M110.006403 · 1–14.

318. Singal HR. Cell Fractionation. In: Sawhney SK, Singh R, editors. Introductory Practical Biochemistry. New Delhi, India: Alpha Science International Limited; 2002. p. 158–94 (452 pp, whole book).

319. Gauthier DJ, Lazure C. Complementary methods to assist subcellular fractionation in organellar proteomics. Expert Rev Proteomics. 2008;5(4):603-17.

...

CHAPTER 2:

RESEARCH PUBLICATION 1

***Citation*:** McDonald Donkuru, Jackson Chitanda, Ronald Verrall, Anas El-Aneed.
Multi-stage tandem mass spectrometric analysis of novel β-cyclodextrin-substituted and novel bis-pyridinium gemini surfactants designed as nanomedical drug delivery agents.
Rapid Communication in Mass Spectrometry, 2014, **28**, 757–772.

The work presented in this chapter is a verbatim copy of a peer-review research article with the citation below. It was published exclusively from work conducted within my Ph.D. research and describes the multi-stage tandem mass spectrometric analysis of novel β-cyclodextrin-substituted and novel bis-pyridinium gemini surfactants designed as nanomedical drug delivery agents. I designed, initiated and completed all experimental work including gemini surfactant synthesis, analytical sample preparation and subsequent multi-stage mass spectrometric analysis. For the gemini surfactant synthesis, technical advice was provided by by co-authors Jackson Chitanda and Ronald Verrall. In addition, the synthesis of β-cyclodextrin-based gemini surfactants, was done by co-author, Jackson Chitanda under the superversion of Ronald Verrall. As first author, I wrote all draft versions of the manuscript and incorporated revision advised by co-authors. This work was fully supervised by Dr. Anas El-Aneed.

2. Multi-stage tandem mass spectrometric analysis of novel β-cyclodextrin-substituted and novel bis-pyridinium gemini surfactants designed as nanomedical drug delivery agents

McDonald Donkuru[1], Jackson Chitanda[2], Ronald Verrall[3], Anas El-Aneed[1]

1. Drug Design & Discovery Group, College of Pharmacy and Nutrition, University of Saskatchewan, 110 Science Place, Saskatoon, SK S7N 5C9, Canada
2. Department of Chemical & Biological Engineering, College of Engineering, University of Saskatchewan, 57 Campus Drive, Saskatoon, SK S7N 5A9, Canada
3. Department of Chemistry, University of Saskatchewan, 110 Science Place, Saskatoon, SK S7N 5C9, Canada

–

Corresponding author:

Drug Design & Discovery Group, College of Pharmacy and Nutrition, University of Saskatchewan, 110 Science Place, Saskatoon, SK S7N 5C9, Canada.

Email: Anas.El-Aneed@usask.ca

Tel: 306-966-2013

Fax: 306-966-6370

SHORT TITLE:

Multi-stage tandem MS analysis of novel gemini surfactants

KEYWORDS:

Gemini surfactants,

Tandem mass spectrometry,

CID-fragmentation,

Mass accuracy

2.1 Abstract

RATIONALE: This study aimed at evaluating the CID-MS/MS fragmentation patterns of novel β-cyclodextrin-substituted- and bis-pyridinium gemini surfactants currently being explored as nanomaterial drug delivery agents. In the β-cyclodextrin-substituted gemini surfactants, a β-cyclodextrin ring is grafted on to a N,N-bis(dimethylalkyl)-α,ω-*amino*alkane-diammonium moiety using variable succinyl linkers. Contrastively, the bis-pyridinium gemini surfactants are based on a 1,1'-**(**1,1'-(ethane-1,2-diylbis(sulfanediyl))bis(alkane-2,1-diyl)**)**dipyridinium template, defined by two symmetrical N-alkylpyridinium parts connected through a fixed ethane dithiol spacer.

METHODS: Detection of the precursor ion $[M]^{2+}$ species of the synthesized compounds and the determination of measurement accuracies were conducted using a QqToF-MS instrument. A multi-stage tandem analysis of the detected $[M]^{2+}$ species was conducted using a QqQ-LIT-MS instrument. Both instruments were equipped with an electrospray ionization source (ESI).

RESULTS: Abundant precursor ion $[M]^{2+}$ species were detected for all compounds at sub-1ppm mass accuracies. The β-cyclodextrin-substituted compounds, fragmented via two main pathways: *Pathway 1*: the loss of one head-tail region produces a $[M - (N(Me)_2\text{-}R)]^{2+}$ ion, from which sugar moieties (Glc) are sequentially cleaved; Pathway 2: both head-tail regions are lost to give $[M - 2(N(Me)_2\text{-}R)]^{+}$, followed by consecutive loss of Glc units. Alternatively, the cleavage of the Glc units could also have occurred simultaneously. Nevertheless, the fragmentation evolved around the quaternary ammonium cations, with characteristic cleavage of Glc moieties. For the bis-pyridinium gemini compounds, they either lost neutral pyridine(s) to give doubly-charged

ions (*Pathway A*) or formed complementary pyridinium and alongside other singly-charged ions (*Pathway B*). Similar to β-cyclodextrin-substituted compounds, the fragmentation was centered on the quaternary amine functional groups.

CONCLUSIONS: The MS^n analyses of these novel gemini surfactants, reported here for the first time, revealed diagnostic ions for each compound, with a universal fragmentation pattern for each compound series. The diagnostic ions will be employed within LC-MS/MS methods for screening, identification, and quantification of these compounds within biological samples.

2.2 Introduction

Amphiphilic compounds such as 'gemini' surfactants have been extensively developed and tested for applications in gene therapy,[1] drug delivery,[2] drug targeting[3] and antimicrobial treatments.[4-6] Gemini surfactants contain two conventional monomer surfactant molecules which are incorporated into a single molecule via a spacer chain.[7] The drug delivery function of gemini surfactants is increasingly attracting intense research including design and formulation of supramolecular nanoparticles,[8-10] and encapsulation of therapeutic agents such as DNA and cytotoxic anti-cancer molecules.[2, 11, 12] As the biomedical application of gemini surfactants evolve toward the stage of clinical trials,[9, 13] there is a critical need for methods of identifying, quantifying and characterizing these compounds and their metabolites within biological tissues and organs. It should be noted that gemini surfactants are also known to cause toxicity;[14, 15] as such, analytical methods are needed for the investigation of their pharmacokinetic and other properties that may influence their *in vivo* application.

Mass spectrometry (MS) is ideally suited for the identification and quantification of small pharmaceuticals.[16, 17] It offers the capability of sensitive, selective and high throughput analyses of chemical analytes.[18] Recently, our group reported the collision-induced dissociation-(CID) tandem mass spectrometric (MS/MS) fragmentation mechanisms and fingerprints of traditional *m-s-m* type gemini surfactants and their amino acid-/dipeptide-substituted analogues.[19-21] The *m-s-m* abbreviation defines compounds in which two N,N-dimethylalkylammonium moieties of alkyl chain length *m* are joined by a poly(methylene) spacer of carbon chain length *s*, resulting in N,N-bis(dimethylalkyl)-α,ω-alkanediammonium structures (Figure 2.1A). Subsequent to these previous studies,[19-21] diagnostic ions were identified for the development of a LC-MS/MS quantification method to analyze diquaternary ammonium gemini surfactants in treated cells.[22]

A: Structure of *m-s-m* compounds

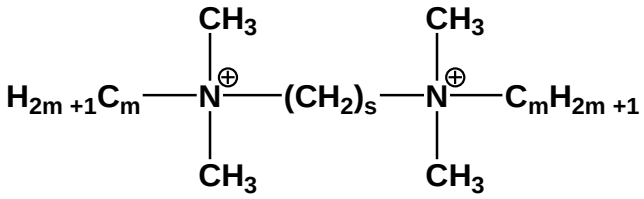

B: R-7N(*X*-suc-β-CD)-R compounds

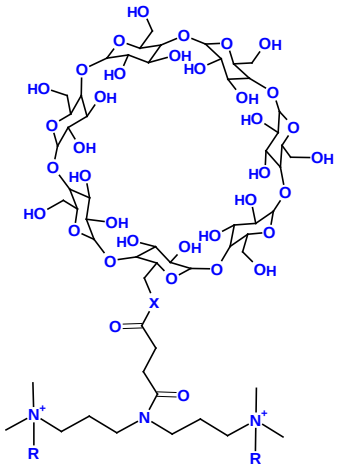

R = $C_{12}H_{25}$, *X* = O

= $C_{12}H_{25}$, *X* = NH

= $C_{16}H_{33}$, *X* = O

= $C_{18}H_{35}$, *X* = O

= $C_{12}D_{25}$, *X* = O

C: R̂(Py)-S-2-S-(Py)R̂ compounds

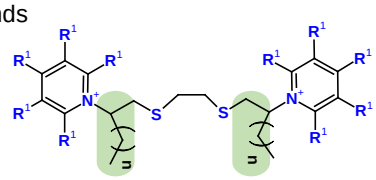

n = 9 ($C_{12}H_{24}$), R^1 = H

= 11 ($C_{14}H_{28}$), R^1 = H

= 13 ($C_{16}H_{32}$), R^1 = H

= 15 ($C_{18}H_{36}$), R^1 = H

= 11 ($C_{16}H_{32}$), R^1 = D

Figure 2.1: Gemini surfactant structural schemes.

A) Structure of the m-s-m gemini surfactants. Two traditional monomeric

surfactants with C_m alkyl tails (where m = chain length) are connected at their quaternary ammonium heads via a polymethylene C_s chain containing **s** methylene units. **B**) Structure of the R-7N(*x*-suc-β-CD)-R gemini surfactants. The attached R groups represent alkyl tails. **C**) R̂(Py)-S-2-S-(Py)R̂ gemini surfactants. Here, the R̂ groups (shaded) comprise the hydrocarbon chains attached to S atoms at one end, bonded to Py head groups (on C-2 from S-atom) and having a terminal methyl on the other end. Thus, the full length alkyl tails R̂ are: $C_{12}H_{24}$, for n = 9; $C_{14}H_{28}$, n = 11; $C_{16}H_{32}$, n = 13; $C_{18}H_{36}$, n = 15.

The *m-s-m* gemini surfactants have traditionally been used in non-viral DNA transfection,[1, 23] but newer compounds are needed for optimal cellular uptake, target cell binding specificity, enhanced transfection efficiency and low toxicity. Our laboratory has recently designed/synthesized novel β-cyclodextrin-substituted-gemini surfactants in which a β-cyclodextrin ring (β-CD) is attached to a N,N-bis(dimethylalkyl)-α,ω-*amino*alkane-diammonium base structure via a succinyl linker (Figure 2.1B).[2] Also, Bhadani and Singh have recently designed bis-pyridinium gemini surfactants which contain two identical N-alkylpyridinium moieties and an ethane dithiol spacer (Figure 2.1C), whereby the pyridinium head groups present a contrast to ammonium head groups of *m-s-m* compounds.[24, 25] The β-cyclodextrin-substituted-gemini surfactants have demonstrated efficient drug delivery,[2] while their bis-pyridinium counterparts gave efficient DNA transfection,[25, 26] with both families showing low toxicity.[2, 25]

The β-cyclodextrin moiety of the β-cyclodextrin-substituted-compounds and the pyridinium head groups of the bis-pyridinium compounds introduce unique structural

characteristics which is instrumental to their efficient drug delivery ability.[2, 25] The MS/MS fragmentation pattern of the two compound types has not been reported. MS/MS analysis allows for the confirmation of their molecular structure and the identification of diagnostic ion pair (precursor → diagnostic fragments) needed for the development of quantitative MRM (multiple reaction monitoring) methods. The quantitative methods will be applied for high throughput sub-cellular identification and quantification of tested compounds as well as aid in metabolite identification.

As noted in the literature, gemini surfactants (and other amphipiles) have shown varying degrees of cytotoxicity within their biomedical applications.[14, 15] Therefore, understanding their intracellular metabolic profile and subcellular distribution could offer explanations into observed toxicities. Evaluation of the gemini surfactant fragmentation behaviour as a prior step has the advantage of revealing distinctive gemini surfactant fingerprint fragments that can allow for compound identification and the development of quantification methods.

The aim of this study is to investigate the CID-MS/MS fragmentation behaviour of the β-cyclodextrin-substituted and bis-pyridinium gemini surfactants. We have previously employed CID-MS/MS analyses to establish the fragmentation profile of the *m-s-m* gemini surfactants and their amino acid-/dipeptide-substituted analogues.[19-21] However, the β-cyclodextrin-substituted and bis-pyridinium gemini surfactant series introduce structural and chemical modifications from these earlier investigated compounds and we have observed, as anticipated, a different CID-MS/MS behaviour for the two new series.

2.3 Materials and Methods

2.3.1 Gemini surfactants

Four β-cyclodextrin-substituted compounds (R-7N(*X*-suc-β-CD)-R, Figure 2.1B) were synthesized using previously reported synthetic methods.[2] As well, four bis-pyridinium-based compounds were synthesized as previously described,[25] and are denoted R̂(Py)-S-2-S-(Py)R̂ (Figure 2.1C), where the special symbol R̂ denotes the uniquely bonded alkyl tails. Also, deuterated gemini surfactants analogues, to serve as internal standards, were synthesized according to the respective methods above[2, 25]. These include a deuterated-pyridine(-$\mathbf{d}_5$)-bearing compound for the R̂(Py)-S-2-S-(Py)R̂ series and a deuterated-dodecyl(-$\mathbf{d}_{25}$)-bearing compound for the R-7N(*X*-suc-β-CD)-R series.

In the R̂(Py)-S-2-S-(Py)R̂ and R-7N(*X*-suc-β-CD)-R series (Figure 2.1), there is a variation of both the alkyl groups R and the head group/spacer region. In the R-7N(*X*-suc-β-CD)-R compounds, the alkyl tails, R, are attached to quaternary ammonium head groups that are joined by a di(propyl)amine spacer, onto which a β-CD substituent is grafted via a succinyl linker. In the R̂(Py)-S-2-S-(Py)R̂ series, pyridinium units (Py) are incorporated as head groups, an ethane-dithiol chain is the spacer, and the alkyl tails, R̂, are bonded differently. They are attached at one end to an S atom; and on C-2 position from this end, the pyridinium head groups are bonded as substituents. On the other end of the R̂ chains are terminal methyl groups (Figure 2.1). Thus for the "R̂(Py)-S-2-S-(Py)R̂" designation (Figure 2.1C), the full length R̂ chains are: $C_{12}H_{24}$, for n = 9; $C_{14}H_{28}$, n = 11; $C_{16}H_{32}$, n = 13; $C_{18}H_{36}$, n = 15.

Methanol (Fisher Scientific) and formic acid (EMD Chemicals) were used as solvents. The water used was organic-free and prepared form a Milli-Q purification system (Millipore Corp).

2.3.2 Sample preparation

Stock solutions of each surfactant, 3 mM, in 50:50 methanol/water (v/v) and containing 0.1% formic acid were prepared and stored at –20 ^{o}C prior to analysis. For MS (single-stage), MS/MS, and MS^3 analysis, each sample was further diluted by 1000–5000× prior to sample injection and MS analysis.

2.3.3 Mass spectrometric analysis

2.3.3.1 *Single-stage MS analysis*

Positive ion mode, single stage MS analysis of gemini surfactants was conducted using an Applied Biosystems API QSTAR® XL MS/MS quadrupole time-of-flight hybrid tandem mass spectrometer (QqToF-MS/MS). The declustering potential was varied between 40.0 and 50.0 V, while the focusing potential was fixed at 290.0 V. Using an integrated Harvard Syringe pump (Havard Apparatus, MA, USA), sample aliquots were infused into the mass spectrometer at a rate of 10 µL/min through a Turbo Ionspray Source, having a needle voltage of 5500 V and a temperature of 80–100 ^{o}C. Nitrogen was used both as the drying gas and ESI nebulizing gas.

Similar to previous work,[19, 20] a two-point internal calibration was performed for all gemini surfactants using two doubly charged calibration standards, given that the tested gemini surfactants are doubly-charged species. The two calibrants were [Glu^1]-Fibrinopeptide B Human (amino acid sequence EGVNDNEEGFFSAR, $[M + 2H]^{2+}$ *m/z* 785.8421, $C_{66}H_{95}N_{19}O_{26}$; Sigma-Aldrich, Oakville, ON, Canada) and N,N-bis(dimethyldodecyl)-1,3-propanediammonium dibromide (12-3-12, $[M]^{2+}$ *m/z* 234.2685), an in-house pure-grade standard.[27] Unlike our previous calibration methods, each single analyte was infused simultaneously with the two

calibrants under optimized conditions such that the three detected species (two calibrants, one analyte) are within 5% variation in their recorded ion counts. This was to ensure high mass accuracy and minimal error.

In addition, we employed our previous calibration method[19, 20] which involved infusion of the two calibrants along with multiple analytes (≥4) and the mass accuracy results were compared with the method of single-analyte and two-calibrant infusion, described above. With the single analyte infusion approach, the peak intensities of the analyte and two calibrants could be optimized to reduce the variation in their ion count to about 5% of each other. In contrast, optimization of peak intensities to such a narrow margin for multiple analytes, infused simultaneously, was not attainable, using the same calibrants and solvents.

2.3.3.2 *CID-MS/MS analysis*

The collision-induced dissociation (CID) tandem MS/MS analysis of each compound was conducted using a QTRAP® 4000 LC/MS/MS system (Applied Biosystems, Foster City, CA, USA). This hybrid triple quadrupole–linear ion trap mass spectrometer (QqQ-LIT) was equipped with a "Turbo V Ion Spray" ESI source and used nitrogen as collision gas. A freshly diluted sample of each compound (1000–5000× dilution of 3 mM stock) was infused directly into the ionization source at a flow rate of 10 μL/min using a model 11 Plus syringe pump (Harvard Apparatus, MA, USA). The declustering potential was varied in the range 30–100 V, while the collision energy was optimized for each compound in the range 16–55 eV to induce fragmentation while the precursor ion remained abundant. It should be note that MS/MS experiments using the API QSTAR® XL did not yield informative spectra regardless of the experimental conditions.

2.3.3.3 *Multi-stage MS^3 analysis*

MS^3 experiments were conducted on the QTRAP® 4000 LC/MS/MS system using the optimized conditions/settings stated above. The QqQ-LIT system is suitable for obtaining vital structural information due to its ability to trap ions in the LIT analyzer and, subsequently, to perform MS^3 experiments.[28, 29] In the MS^3 mode, the excitation energy (AF2) used to fragment of selected second generation ions was fixed at 100 mV. The QqQ-LIT system has up to MS^3 capability. To further probe the sequential fragmentation patterns, multiple MS^3 experiments were performed.

2.4 Results

2.4.1 *Single-stage QToF MS analysis*

Abundant doubly-charged species $[M]^{2+}$ were detected for all tested gemini surfactants by full scan MS analysis in the positive ion mode. The observation signifies the presence of'ionized' compounds with two positive charges, as expected for the β-cyclodextrin-substituted- and bis-pyridinium gemini surfactants which contain either two diquaternary ammonium or two pyridinium headgroups (Figure 2.1), respectively. The exact masses of the $[M]^{2+}$ species were detected with mass accuracies of less than 1 ppm mass error (Table 2.1) using a two-point internal calibration method and analyzing the compounds individually. Such level of mass accuracy exceeds previous mass accuracies reported for similar compound analysis.[19, 20] In contrast, when the mass accuracy analysis with two-point calibration was done for multiple compounds (infused all at once), the observed mass accuracies were less strong as previously shown (Table 2.1).[19, 20]

The level of high mass accuracy for single-analyte infusion was achieved through peak intensity optimization for the analyte and two calibrants such that a minimized variation (≤5%) in their absolute ion count is attained in each calibration step. The highest measure of mass accuracy is normally achieved when the detected ions of the calibrants and the analyte(s) are approximately of the same abundance.[30] In contrast, fluctuations in ion abundance and peak shape can both significantly compromise the measured mass accuracy when using internal calibrants.[30, 31] These results clearly illustrate that very robust data can be achieved using the QSTAR® QqToF-MS/MS system.

Table 2.1. Detected doubly charged precursor ion species **$[M]^{2+}$** for β-CD-based and bis-pyridinium gemini surfactants in the positive ion mode. Mass accuracy analysis was conducted on a QSTAR® QqToF-MS/MS system.

Gemini surfactant	**Molecular formula**	**Mono-isotopic mass**	**$[M]^{2+}$ *m/z*, calculated**	**Method A: single analyte infusion**		**Method B: multi-analyte infusion**	
				$[M]^{2+}$ *m/z*, exp'tal[A]	**Mass accuracy (ppm)[A]**	**$[M]^{2+}$ *m/z*, exp'tal[B]**	**Mass accuracy (ppm)[B]**
12-7N(*O*-suc-β-CD)-12	$C_{80}H_{147}N_3O_{37}^{2+}$	1741.9702	870.98512	870.98517	0.05741	870.98940	4.91398
12-7N(*NH*-suc-β-CD)-12	$C_{80}H_{148}N_4O_{36}^{2+}$	1740.9862	870.49311	870.49313	0.02298	870.49110	-2.30904
16-7N(*O*-suc-β-CD)-16	$C_{88}H_{163}N_3O_{37}^{2+}$	1854.0954	927.04772	927.04776	0.04315	927.04830	0.62564
18:1-7N(*O*-suc-β-CD)-18:1*	$C_{92}H_{167}N_3O_{37}^{2+}$	1906.1267	953.06337	953.06349	0.12591	953.06001	-3.52547
12(Py)-S-2-S-(Py)12	$C_{36}H_{62}N_2S_2^{2+}$	586.4343	293.21717	293.21719	0.06821	293.21701	-0.54567
14(Py)-S-2-S-(Py)14	$C_{40}H_{70}N_2S_2^{2+}$	642.4969	321.24847	321.24849	0.06226	321.24893	1.43191
16(Py)-S-2-S-(Py)16	$C_{44}H_{78}N_2S_2^{2+}$	698.5595	349.27977	349.27974	-0.08589	349.27821	-4.46633
18(Py)-S-2-S-(Py)18	$C_{48}H_{86}N_2S_2^{2+}$	754.6221	377.31107	377.31111	0.10601	377.30812	-7.81848

[A]From the method of single analyte infusion with two internal calibrants. [B]From the method of multiple analyte infusion with two internal calibrants. *18:1 denotes mono-unsaturated C_{18} tails (***oleyl*** − $C_{18}H_{35}$).

2.4.2 *Multi-stage MS analysis*

Using positive ion mode ESI-QqQ-LIT-MS^n analysis, distinct multi-stage CID-MS^n fragmentation patterns were observed for the β-cyclodextrin-subsituted and the bis-pyridinium gemini surfactant series. The different spacer types as well as the incorporated substituent, β-CD, in one of the series would be expected to give rise to different fragmentation patterns and specific product ions that can serve as diagnostic fragments. However, the compounds from the same series showed a similar fragmentation pattern.[19]

For the β-cyclodextrin-subsituted gemini surfactants, the compound-specific product ions originate from the neutral loss of ***only*** one quaternary ammonium head group along with the attached alkyl tail region, $N(CH_3)_2$-R. Additional neutral losses from the β-CD substituent of the remaining fragment leads to further compound-specific product ions. But the loss of the remaining head group–tail unit results in a fragment ion which is identical for these surfactants except where the structural variable *X* alternates between O (16 Da) and NH (15 Da) (Figure 2.1B). Surprisingly, the ester linkage connecting the β-CD ring to the rest of the compound structure remained intact during fragmentation.

For the bis-pyridinium compounds R̂(Py)-S-2-S-(Py)R̂, the observed diagnostic product ions originated from the loss of either one or both pyridinium head group(s). Pyridinum was either eliminated as chared or neutral species. In addition, the loss of one N-alkylpyridinium (a combined head group–tail unit) or the cleavage of portions of the alkyl tail resulted in compound-specific product ions. Overall, the observed diagnostic product ions authenticated the molecular structures of tested compounds, confirming the presence of pyridinium head groups and other unique structural features.

Table 2.2. Major product ions of the R-7N(*X*-suc-β-CD)-R gemini surfactants and their theoretical *m/z* values from CID-MS/MS analysis of the precursor ions $[M]^{2+}$. The distinctive product ions include those numbered **1–7**. Several minor product ions are also observed (not listed); they include those corresponding to neutral loss of H_2O, CO or CO_2 from the listed ions.

Product ion	Designation of fragment structure	12-7N(*O*-suc-β-CD)-12 *m/z*, (CE: 50 V)	$12_{\mathbf{D25}}$-7N(*O*-suc-β-CD)-$12_{\mathbf{D25}}$ *m/z*, (CE: 50 V)	12-7N(*NH*-suc-β-CD)-12 *m/z*, (CE: 50 V)	16-7N(*O*-suc-β-CD)-16 *m/z*, (CE: 53 V)	18:1-7N(*O*-suc-β-CD)-18:1 *m/z*, (CE: 55 V)
	$[M]^{2+}$	870.99	896.14	870.49	927.05	953.06
1	$[M-(R-H)]^{2+}$	786.89	789.44	786.37	814.89	827.90
2	$[M-(R-H)-NH(Me)_2]^{2+}$	764.36	766.94	763.87	792.39	805.40
3^{i1}	$[M-(R-H)-NH(Me)_2-Glc]^{+}$	1365.66	1421.73	1364.68	1421.73	1447.74
3^{i2}	$[M-(R-H)-NH(Me)_2-2Glc]^{+}$	1203.62	1259.67	1202.63	1259.67	1285.69
⋮						
3^{i6}	$[M-(R-H)-NH(Me)_2-6Glc]^{+}$	717.45	773.52	716.47	773.52	799.53
4^{i1}	$[M-2(R-H)-2(NH(Me_2))-Glc]^{+}$	555.39	611.46	554.42	611.46	637.48
4^{i2}	$[M-2(R-H)-2(NH(Me_2))-2Glc]^{+}$	1152.56	1152.56	1151.43	1152.56	1152.56
⋮						
4^{i6}	$[M-2(R-H)-2(NH(Me_2))-6Glc]^{+}$	504.21	504.21	503.21	504.21	504.21
5^{i1}	$[M-2(R-H)-NH(Me_2)-Glc]^{+}$	342.15	342.15	341.15	342.15	342.15

5^{i2}	$[M-2(R-H)-NH(Me_2)-2Glc]^+$	314.16	314.16	313.17	314.16	314.16
⋮						
5^{i6}	$[M-2(R-H)-NH(Me_2)-6Glc]^+$	522.22	522.22	521.22	522.22	522.22
7^{i1}	$[M-2(R-H)-2(NH(Me_2))-(Glc-H_2O)]^+$	198.11	198.11	197.11	198.11	198.11
7^{i2}	$[M-2(R-H)-2(NH(Me_2))-2(Glc-H_2O)]^+$	170.12	170.12	169.11	170.12	170.12
⋮						
7^{i6}	$[M-2(R-H)-2(NH(Me_2))-6(Glc-H_2O)]^+$	648.25	648.25	647.26	648.25	648.25
8	$[M-2(R-H)-2(NH(Me_2))-6(Glc-H_2O)-CO]^+$	306.16	306.16	359.16	306.16	306.16
9^{i1}	$[M-2(R-H)-2(NH(Me_2))-H_2O-Glc]^+$	486.20	486.20	485.20	486.20	486.20
9^{i2}	$[M-2(R-H)-2(NH(Me_2))-H_2O-2Glc]^+$	324.14	324.14	323.14	324.14	324.14
⋮						
9^{i6}	$[M-2(R-H)-2(NH(Me_2))-H_2O-6Glc]^+$	324.14	324.14	324.14	324.14	324.14
10	$[M-2(R-H)-2(NH(Me_2))-H_2O-6Glc-CO]^+$	296.15	296.15	296.15	296.15	296.15

Table 2.3. Major product ions of the R̂(Py)-S-2-S-(Py)R̂ gemini surfactants and their theoretical *m/z* values from CID-MS/MS analysis of the precursor ions $[M]^{2+}$. The *m/z* values differ for all product ions except for product ion number **5**. Other, but minor, product ions were also observed, resulting from various neutral losses in the form $C_{\chi}H_{2\chi-y}$, y = 0 or 2.

Product ion	Designation of fragment structure	12(Py)-S-2-S-(Py)12 *m/z*, (CE: 16 V)	14(Py)-S-2-S-(Py)14 *m/z*, (CE: 17 V)	16(Py)-S-2-S-(Py)16 *m/z*, (CE: 19 V)	16(Py_{D5})-S-2-S-(Py_{D5})16 *m/z*, (CE: 24 V)	18(Py)-S-2-S-(Py)18 *m/z*, (CE: 25 V)
	$[M]^{2+}$	293.28	321.25	349.28	354.65	377.31
1^{f1}	$[M-{}^{*}Py]^{2+}$	253.83	281.80	309.77	302.24	337.74
1^{f2}	$[M-Py-C_3H_6]^{2+}$	232.77	260.74	290.71	293.34	318.64
1^{f3}	$[M-Py-C_3H_6-CH_2]^{2+}$	225.69	253.66	283.61	291.27	311.67
2^{f1}	$[M-2Py]^{2+}$	214.17	269.14	299.11	299.32	327.12
2^{f2}	$[M-2Py-C_3H_6]^{2+}$	193.15	221.12	251.12	251.49	279.94
2^{f3}	$[M-2Py-C_3H_6-CH_2]^{2+}$	186.14	214.11	244.09	244.26	272.06
3^{f1}	$[M-Py]^{+}$	506.28	562.34	618.44	623.84	674.55
3^{f2}	$[M-Py-C_3H_6]^{+}$	464.28	520.36	576.46	581.56	632.57
3^{f3}	$[M-Py-C_3H_6-CH_2]^{+}$	450.24	506.41	562.63	567.73	618.74
4^{f1}	$[M-2Py]^{+}$	427.81	483.87	539.97	539.77	596.08

4^{f2}	$[M-2Py-C_3H_6]^+$	385.73	441.79	497.89	497.99	554.05
4^{f3}	$[M-2Py-C_3H_6-CH_2]^+$	371.28	427.44	483.54	483.64	539.65
5	$[Py+H]^+$	80.10	80.17	80.11	85.21	80.31
6^{f1}	$[M-2Py-2(CH_2)]^+$	399.76	455.82	511.92	502.02	568.03
6^{f2}	$[M-2Py-C_3H_6-2(CH_2)]^+$	357.24	413.31	469.41	470.05	525.52
6^{f3}	$[M-2Py-C_3H_6-3(CH_2)]^+$	343.26	399.37	455.43	455.75	511.54
7^{f1}	$[3^{i1}-(\hat{R}-H_2)]^+$ or $[M-Py-(\hat{R}-H_2)]^+$	340.65	396.69	452.79	457.89	508.90
7^{f2}	$[M-2Py-(\hat{R}-H_2)]^+$	261.27	317.33	373.43	373.59	429.54
7^{f3}	$[M-2Py-(\hat{R}-H_2)-C_2H_2S_2]^+$	203.19	259.25	315.35	315.54	371.46
7^{f4}	$[M-2Py-(\hat{R}-H_2)-C_2H_2S_2-H_2]^+$	201.27	257.33	313.43	313.55	369.54
7^{f5}	$[M-2Py-\hat{R}-C_2H_2S_2-CH_2]^+$	189.18	245.23	301.33	301.48	357.44
7^{f6}	$[M-2Py-\hat{R}-C_2H_2S_2-2(CH_2)]^+$	175.17	231.25	287.35	287.63	343.64
7^{f7}	$[M-2Py-\hat{R}-C_2H_2S_2-3(CH_2)]^+$	161.10	217.16	273.26	273.66	329.36

* Py: indicates pyridine, i.e., either hydrogenated pyridine Py, or deuterated pyridine, Py_{D5}.

The gemini surfactant fragmentation patterns are detailed below using two representative examples, namely 12-7N(*O*-suc-β-CD)-12 and 12(Py)-S-2-S-(Py)12 from the β-cyclodextrin-substituted and bis-pyridinium compound series, respectively. The major product ions are tabulated for the β-cyclodextrin-subsituted (Table 2.2) and bis-pyridinium gemini surfactants (Table 2.3). In addition, data is given for deuterated gemini surfactant analogues that confirm the proposed fragmentation patterns by revealing increased *m/z* values for deuterated fragments in comparison with the corresponding non-deuterated fragments of test compounds.

2.4.3 *R-7N(X-suc-β-CD)-R compounds: MS/MS fragmentation pathway*

The five R-7N(*X*-suc-β-CD)-R compounds include 12-7N(*O*-suc-β-CD)-12, 12-7N(*NH*-suc-β-CD)-12, 16-7N(*O*-suc-β-CD)-16, 18:1-7N(*O*-suc-β-CD)-18:1 and 12_{D25}-7N(*O*-suc-β-CD)-12_{D25}, the latter being an isotope-labeled analogue of 12-7N(*O*-suc-β-CD)-12 (Figure 2.1B). Because of the identical pattern of fragmentation within this series, the compound 12-7N(*O*-suc-β-CD)-12 is chosen as a representative example of the series. Figure 2.2 shows the ESI-QqQ-LIT-MS/MS analysis of the compound, while Scheme 2.1 shows its proposed fragmentation pathway. Ions were designated based on the fragmentation type and Table 2.4A provides the definition of relationships between fragments ions which were produced by the 12-7N(O-suc-β-CD)-12 compound in a serial pattern.

The 12-7N(*O*-suc-β-CD)-12 compound (precursor ion $[M]^{2+}$: *m/z* 870.99) fragmented readily, generating a first product ion observed at *m/z* $[786.89]^{2+}$, designated as $[M–(R–H)]^{2+}$ (**1**). It represents the loss of one full alkyl tail in the form of a neutral dodecene molecule (R–H = $C_{12}H_{24}$). The observed peak for the product ion *m/z* $[786.89]^{2+}$ has relatively weak intensity

(Figure 2.2). The substantially low abundance for this fragment ion suggests that it is unstable and instantly fragments (further explanation in the *Discussion* section).

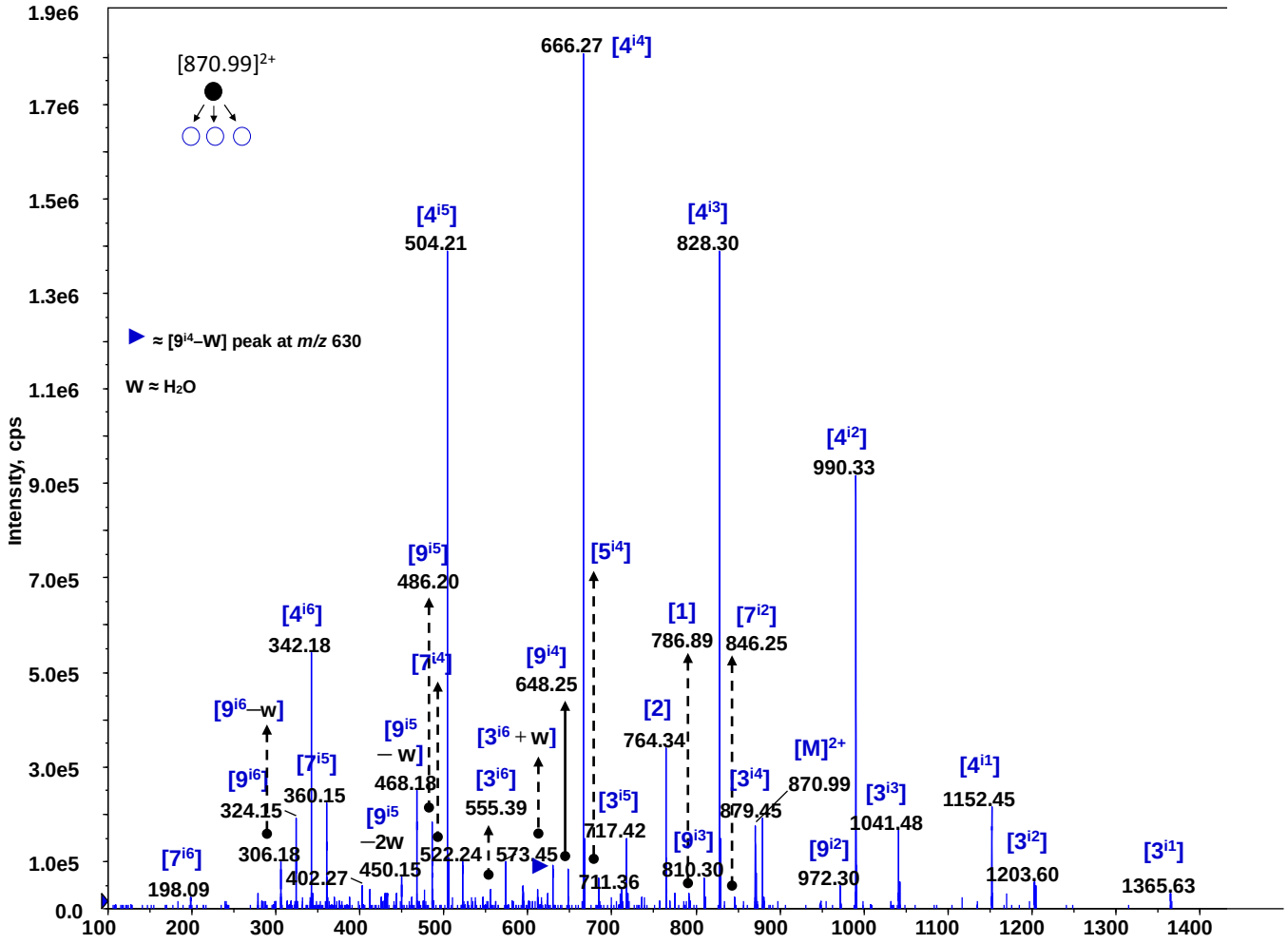

Figure 2.2: MS/MS spectrum of 12-7N(*O*-suc-β-CD)-12 as a representative example of the β-CD-substituted gemini surfactants. This compound may also be designated by: 12-$^{+}$N(Me)$_2$-7N(*O*-suc-β-CD)-$^{+}$N(Me)$_2$-12.

Table 2.4. The structure of various fragment ions series illustrated in Schemes 1 and 2. **A)** Fragment ion series for the 12-7N(O-suc-β-CD)-12 gemini surfactant; **B)** fragment ion series for the 12(Py)-S-2-S-(Py)12 gemini surfactant.

Part A:

Gemini surfactant	**Fragment ion series**	**General structure of fragment ion series**	**Variation among serial fragment ions**
12-7N(*O*-suc-β-CD)-12	$\mathbf{3^{i1}}$ – $\mathbf{3^{i6}}$	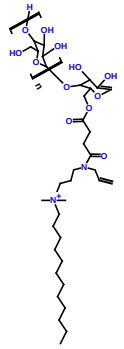	Ion $\mathbf{3^{i1}}$, n = 6 Ion $\mathbf{3^{i2}}$, n = 5 Ion $\mathbf{3^{i3}}$, n = 4 Ion $\mathbf{3^{i4}}$, n = 3 Ion $\mathbf{3^{i5}}$, n = 2 Ion $\mathbf{3^{i6}}$, n = 1
	$\mathbf{4^{i1}}$ – $4^{\mathbf{i6}}$	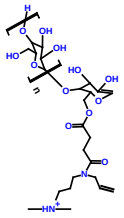	Ion $4^{\mathbf{i1}}$, n = 6 Ion $4^{\mathbf{i2}}$, n = 5 Ion $4^{\mathbf{i3}}$, n = 4 Ion $4^{\mathbf{i4}}$, n = 3 Ion $4^{\mathbf{i5}}$, n = 2 Ion $4^{\mathbf{i6}}$, n = 1
	$\mathbf{5^{i1}}$ – $5^{\mathbf{i6}}$	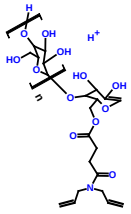	Ion $5^{\mathbf{i1}}$, n = 6 Ion $5^{\mathbf{i2}}$, n = 5 Ion $5^{\mathbf{i3}}$, n = 4 Ion $5^{\mathbf{i4}}$, n = 3 Ion $5^{\mathbf{i5}}$, n = 2

			Ion 5^{i6}, n = 1
	7^{i1} – 7^{i6}	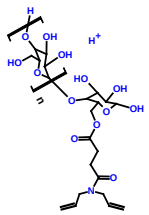	Ion 7^{i1}, n = 6 Ion 7^{i2}, n = 5 Ion 7^{i3}, n = 4 Ion 7^{i4}, n = 3 Ion 7^{i5}, n = 2 Ion 7^{i6}, n = 1
	9^{i1} – 9^{i6}	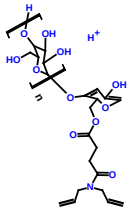	Ion 9^{i1}, n = 6 Ion 9^{i2}, n = 5 Ion 9^{i3}, n = 4 Ion 9^{i4}, n = 3 Ion 9^{i5}, n = 2 Ion 9^{i6}, n = 1

Table continued on next page…

Part B:

Gemini surfactant	Fragment ion series	General structure of fragment ion series	Variation among serial fragment ions
12(Py)-S-2-S-(Py)12	$\mathbf{1^{f1}}$ – $\mathbf{1^{f3}}$	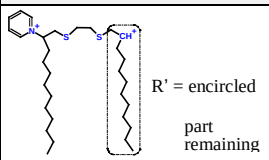 R' = encircled part remaining	Ion $\mathbf{1^{f1}}$, R' = C_{12} Ion $\mathbf{1^{f2}}$, R' = C_9 Ion $\mathbf{1^{f3}}$, R' = C_8
	$\mathbf{2^{f1}}$ – $\mathbf{2^{f3}}$	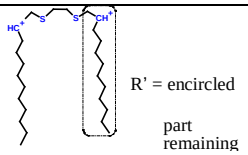 R' = encircled part remaining	Ion $\mathbf{2^{f1}}$, R' = C_{12} Ion $\mathbf{2^{f2}}$, R' = C_9 Ion $\mathbf{2^{f3}}$, R' = C_8
	$\mathbf{3^{f1}}$ – $\mathbf{3^{f3}}$	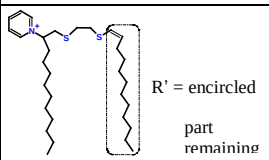 R' = encircled part remaining	Ion $\mathbf{3^{f1}}$, R' = C_{12} Ion $\mathbf{3^{f2}}$, R' = C_9 Ion $\mathbf{3^{f3}}$, R' = C_8
	$\mathbf{4^{f1}}$ – $\mathbf{4^{f3}}$	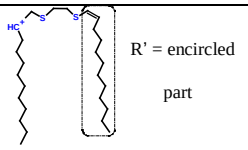 R' = encircled part	Ion $\mathbf{4^{f1}}$, R' = C_{12} Ion $\mathbf{4^{f2}}$, R' = C_9 Ion $\mathbf{4^{f3}}$, R' = C_8
	$\mathbf{6^{f1}}$ – $\mathbf{6^{f3}}$	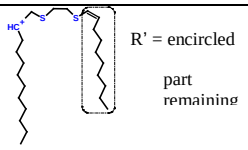 R' = encircled part remaining	Ion $\mathbf{6^{f1}}$, R' = C_{10} Ion $\mathbf{6^{f2}}$, R' = C_7 Ion $\mathbf{6^{f3}}$, R' = C_6
	$\mathbf{7^{f1}}$	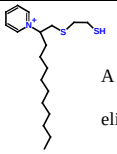 A full alkyl tail R̂ eliminated	N/A

	7^{f2}		N/A
	7^{f3}	 A full alkyl tail	N/A
	8^{f1} – 8^{f3}	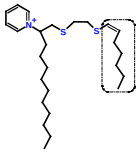 R' = encircled part	Ion **8^{f1}**, R' = C_7 Ion **8^{f2}**, R' = C_6 Ion **8^{f3}**, R = C_5 Ion **8^{f4}**, R' = C_4

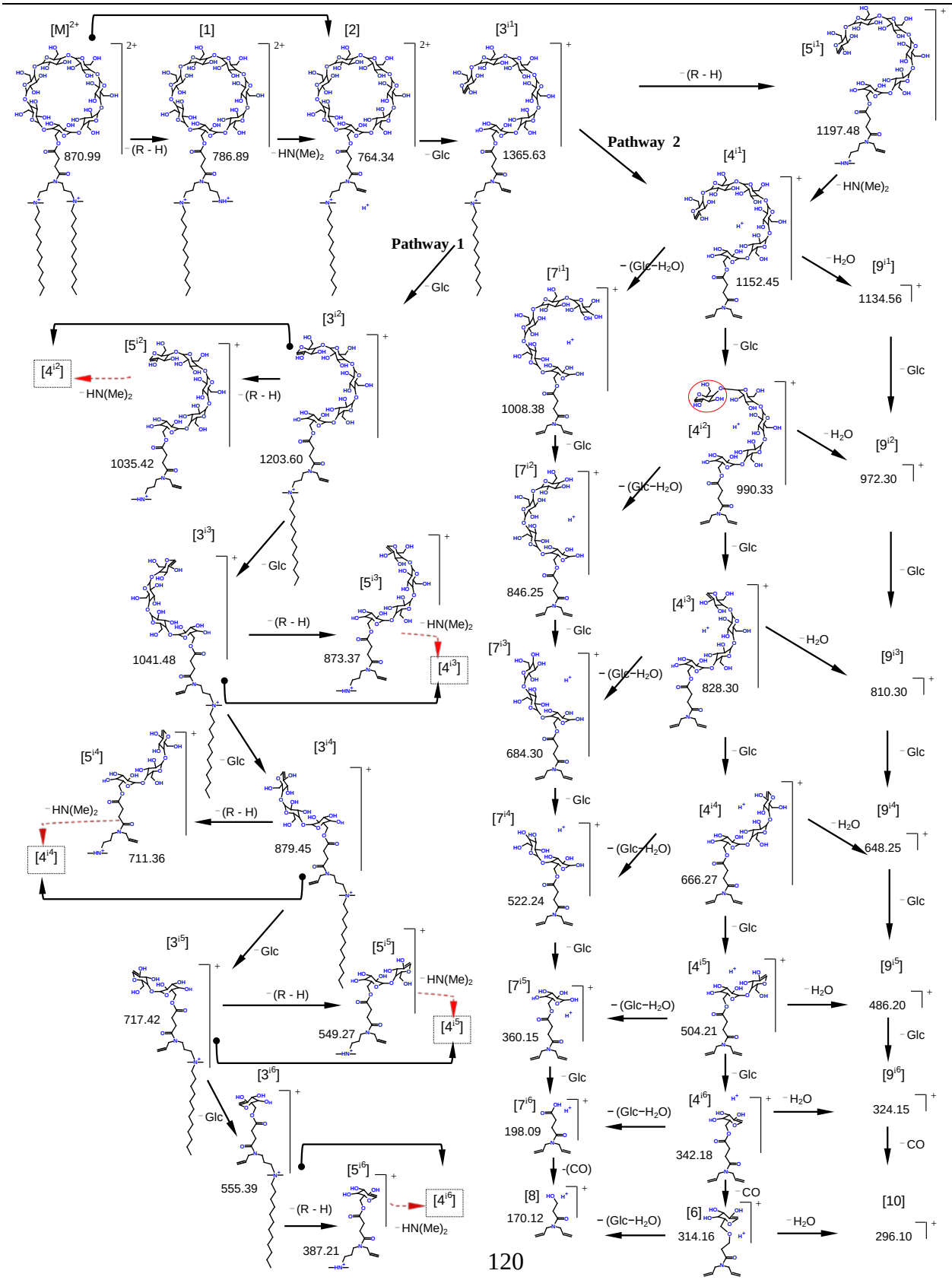

Scheme 2.1: Multi-stage fragmentation pattern of 12-7N(O-suc-β-CD)-12 as a representative example of the β-CD-substituted gemini surfactant.

Legend:

3^{i1}–3^{i6}: Product ions retaining ***one*** headgroup–tail region;

4^{i1}–4^{i6}: Product ions retaining ***no*** headgroup–tail region;

5^{i1}–5^{i6}: Product ions retaining ***one*** dimethylammonium headgroup but ***no*** tail region;

7^{i1}–7^{i6}: Product ions related to 4^{i1}–4^{i6} by neutral loss of 144 Da glycosyl residue (Glc– H_2O);

9^{i1}–9^{i6}: Product ions related to 4^{i1}–4^{i6} by neutral loss of H_2O molecule.

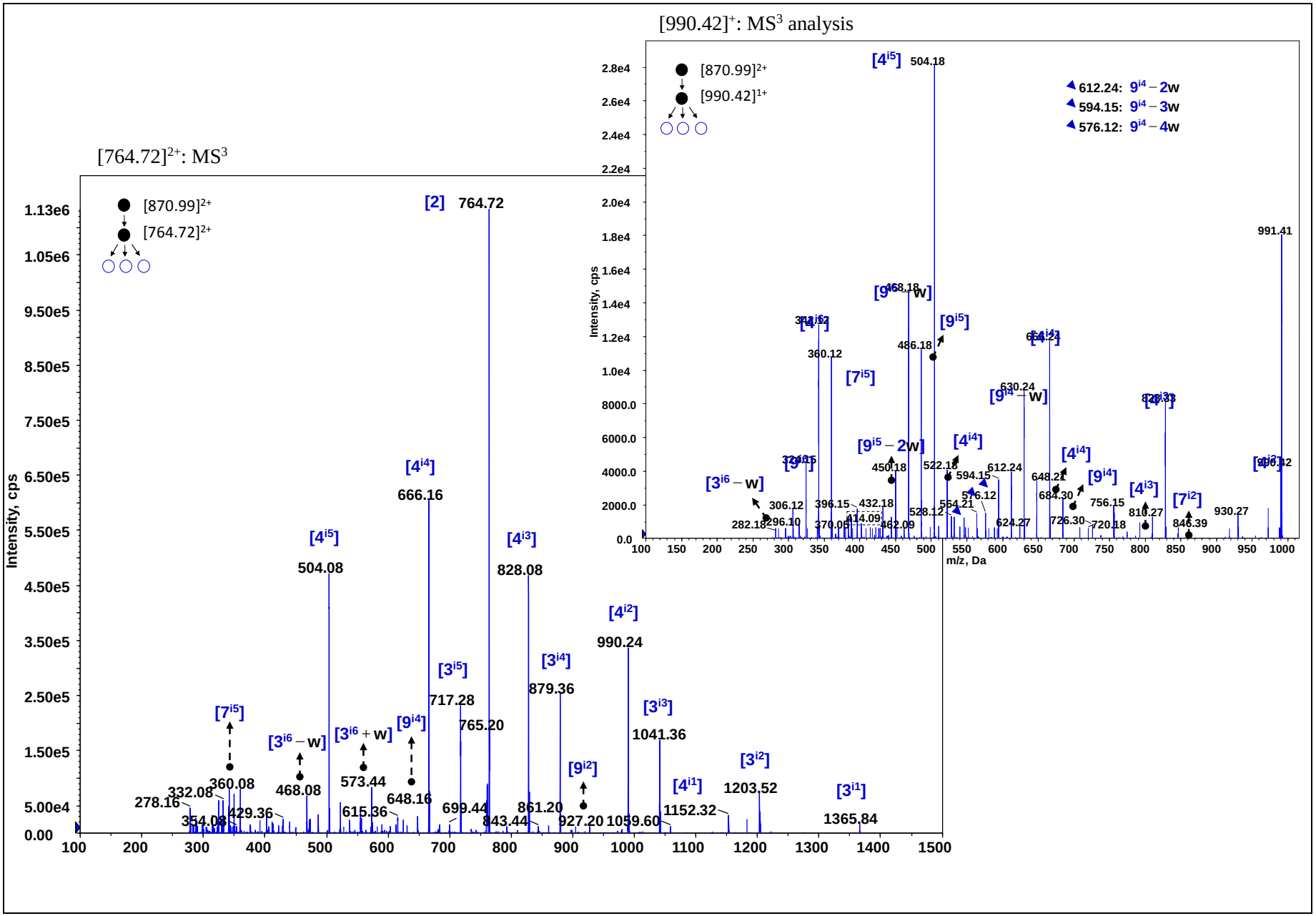
[764.72]2+: MS3
[870.99]2+
[764.72]2+
[2] 764.72
[4i4] 666.16
[4i5] 504.08
[4i3] 828.08
[4i2] 990.24
[3i5] 717.28
[3i4] 879.36
[3i3] 1041.36
[3i2] 1203.52
[3i1] 1365.84
[7i5]
[3i6 − w]
[3i6 + w]
[9i4]
[9i2]
[4i1] 1152.32
360.08
332.08
278.16
354.08
429.36
468.08
573.44
615.36
648.16
699.44
765.20
843.44
861.20
927.20
1059.60
Intensity, cps
m/z, Da
[990.42]+: MS3 analysis
[870.99]2+
[990.42]1+
[4i5] 504.18
612.24: 9i4 − 2w
594.15: 9i4 − 3w
576.12: 9i4 − 4w
[9i4 − w] 468.18
[9i5] 486.18
[7i5] 360.12
[9i5 − 2w] 450.18
[3i6 − w] 306.12
630.24
991.41
Intensity, cps
m/z, Da

Figure 2.3: MS^3 spectrum of product ion *m/z* $[764.72]^{2+}$ which originates from MS/MS fragmentation of the compound 12-7N(*O*-suc-β-CD)-12, with precursor ion $[M]^{2+}$ *m/z* 870.99. Insert: MS^3 spectrum of product ion *m/z* $[990.42]^{2+}$ which was also observed in the MS^3 fragmentation of the product ion *m/z* $[764.72]^{2+}$.

[M]2+
m/z 293.28
Pathway A
Pathway B
[5]
m/z [80.10]+
[1f1]
m/z [253.83]2+
[2f1]
m/z [214.17]2+
[1f2]
m/z [232.77]2+
[2f2]
m/z [193.15]2+
[1f3]
m/z [225.69]2+
[2f3]
m/z [186.14]2+
[3f1]
m/z [506.28]+
[3f2]
m/z [464.28]+
[3f3]
m/z [450.24]+
[4f1]
m/z [427.81]2+
[4f2]
m/z [385.73]2+
[4f3]
m/z [371.28]2+
[6f1]
m/z [399.76]2+
[6f2]
m/z [357.24]2+
[6f3]
m/z [343.26]2+
[7f1]
m/z [340.26]+
[7f2]
m/z [261.27]+
[7f3]
m/z [203.19]+
[7f4]
m/z [201.27]+
[7f5]
m/z [189.18]+
[7f6]
m/z [175.17]+
[7f7]
m/z [161.10]+
[8f1]
m/z [436.26]+
[8f2]
m/z [422.28]+
[8f3]
m/z [408.30]+
[8f4]
m/z [394.70]+

Scheme 2.1: Major multi-stage fragmentation pathways of 12(Py)-S-2-S-(Py)12 as representative example of the bis-pyridinium gemini surfactants. Fragment ions observed are mainly of two kinds: **1**) singly-charged product ions $[M–Py]^+$, $[M–Py–(R–H)]^+$, $[M– Py–(R–H)–(C_\chi H_{2\chi–y})]^+$; and **2**) doubly-charged products ions $[M–Py]^{2+}$, $[M–Py–(R–H)]^{2+}$, $[M– Py–(R–H)–(C_\chi H_{2\chi–y})]^{2+}$.

2.4.4 *R̂(Py)-S-2-S-(Py)R̂ compounds: MS/MS fragmentation pathway*

The R̂(Py)-S-2-S-(Py)R̂ family fragmentation behaviour was studied by using multi-stage tandem ESI-QqQ-LIT-MS analysis. Five member compounds of the series (including an isotopic analogue), were investigated: 12(Py)-S-2-S-(Py)12, 14(Py)-S-2-S-(Py)14, 16(Py)-S-2-S-(Py)16, 16(Py_{D5})-S-2-S-(Py_{D5})16 and 18(Py)-S-2-S-(Py)18. The fragmentation pattern was similar for all of these compounds and 12(Py)-S-2-S-(Py)12 is used as an example for illustration. The MS/MS analysis of the precursor ion $[M]^{2+}$ *m/z* 293.28 for this compound is given in Figure 2.4. Ions were designated based on the fragmentation type and Table 2.4B provides the definition of relationships between fragment ions which were produced by the 12(Py)-S-2-S-(Py)12 compound in a serial pattern.

The 12(Py)-S-2-S-(Py)12 compound readily fragmented (Scheme 2.2); however, its fragmentation is markedly different and begins with two alternate fragmentation routes, designated Pathways *A* and *B*. *Pathway A* shows the fragmentation of the precursor ion $[M]^{2+}$ *m/z* 293.22, leading to a series of doubly-charged product ions, initiated by the elimination of a neutral pyridine moiety. *Pathway B*, on the other hand, leads to a series of singly-charged product ions including the initial generation of two complementary ions (Scheme 2.1).

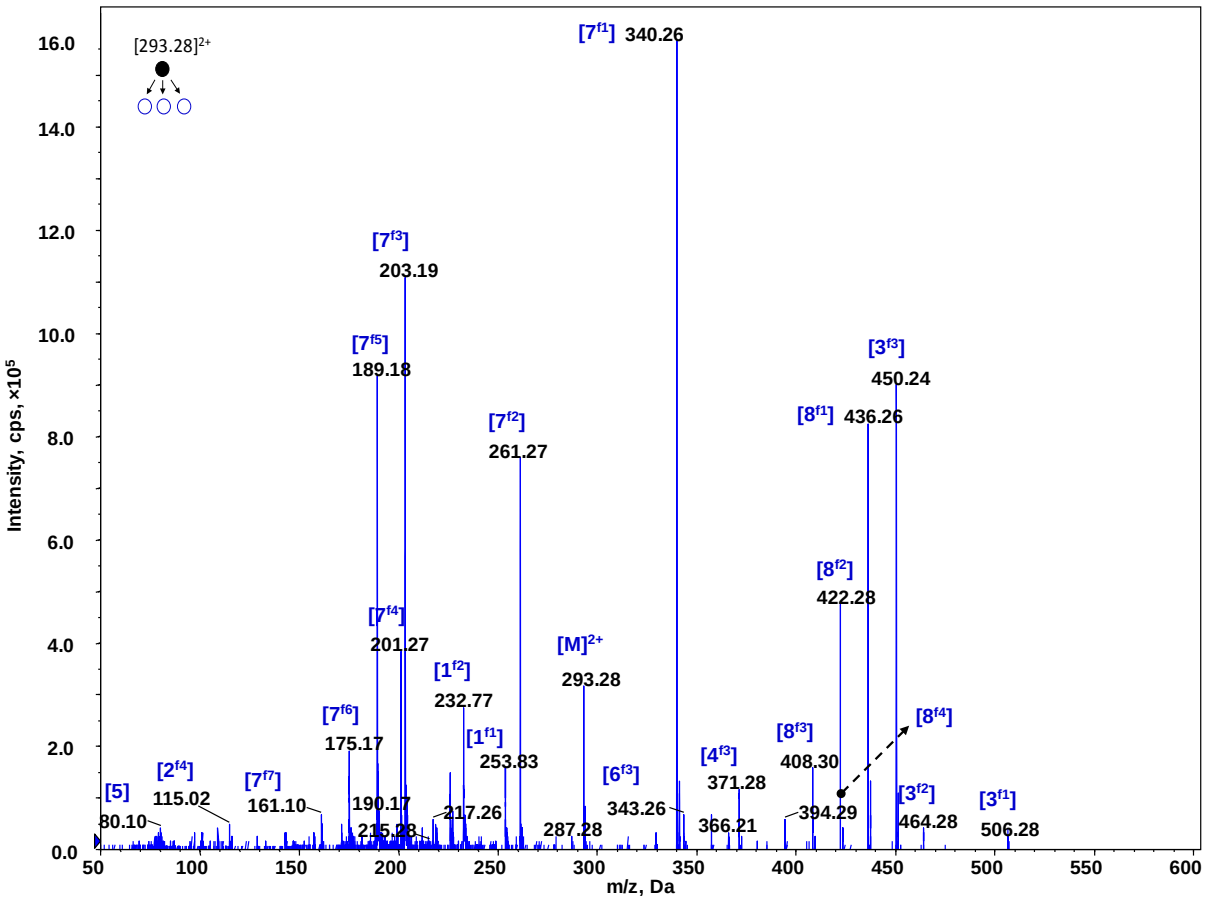

Figure 2.4: MS/MS spectrum of 12(Py)- S-2-S-(Py)12 as a representative example of the bis-pyridinium gemini surfactants. Inset: full MS scan of the precursor ions $[M]^{2+}$ of four bis-pyridinium gemini surfactants: *m/z* 293.28, 321.27, 349.29, 377.32. Analysis: positive mode.

For *Pathway A*, the first stage is the neutral loss of a pyridinium head group, leading to the doubly-charged diagnostic ion *m/z* $[253.83]^{2+}$ ($\mathbf{1^{f1}}$: $[M–Py]^{2+}$). Although a pyridinium head group is cleaved, fragment ion $\mathbf{1^{f1}}$ remains doubly-charged because of one positive charge from the remaining cationic pyridinium headgroup and another positive charge created on the carbon atom originally bonded to the cleaved pyridinium head group.

Ion $\mathbf{1^{f1}}$ then fragments via successive cleavage of portions of the alkyl tail or via the neutral elimination of the remaining pyridinium head group, followed by successive cleavage of segments from the alkyl tails. The series of ions observed through stepwise breakage of alkyl tails with the retention of ***one*** pyridinium head group is designated as the $[M–Py–(C_\chi H_{2\chi–y})]^{2+}$ ($\mathbf{1^f}$-series). The other series observed through stepwise breakage of alkyl tails with no remaining pyridinium head group conforms to the designation $[M–2(Py)–(C_\chi H_{2\chi–y})]^{2+}$ ($\mathbf{2^f}$-series); $C_\chi H_{2\chi–y}$ represents the cleaved portions of the alkyl tail such as propene, ethene or methylene (Table 2.4B). It should be noted that ions formed via *Pathway A* were doubly-charged and of relatively low abundance.

Unlike *Pathway A* which produced relatively low abundant doubly-charged ions (via elimination of neutral pyridine and neutral hydrocarbon species), *Pathway B* gives rise to abundant singly-charged product ions. The precursor ion $[M]^{2+}$ *m/z* 293.28 first produces two positively, singly-charged complementary ions, namely *m/z* $[506.28]^+$ ($\mathbf{3^{f1}}$: $[M–Py–H]^+$) and *m/z* $[80.10]^+$ (**5**: $[Py+H]^+ \approx C_5H_6N^+$). This complementary loss was confirmed with the analysis of the deuterated pyridinium-bearing compound which revealed the formation of the ion *m/z* $[85.09]^+$ ($C_5H\mathbf{D}_5N^+$, data not shown), confirming the formation of fragment ion **5**.

Subsequently, ion $\mathbf{3^{f1}}$ fragments to yield multiple product ions which either **i**) bear two partial or complete tail regions (Series $\mathbf{3^{f}}$, $\mathbf{4^{f}}$, or $\mathbf{8^{f}}$), or **ii**) bear one partial or complete tail region (i.e. $\mathbf{7^{f}}$**-series** ions). Most fragment ions generally arise from similar sequential breakage of portions of the alkyl tail regions. Despite this, the observed ions still had different fragment structures due to differences in the exact nature of structural parts that are cleaved and/or retained.

For product ions of the $\mathbf{4^{f}}$-series, designated as [M–2Py–H with/without $-(C_{\chi}H_{2\chi-y})]^{+}$, ion $\mathbf{4^{f1}}$ (*m/z* $[427.81]^{+}$) is first formed through the loss of a neutral pyridine molecule (C_5H_6N, 79 Da) from the preceding ion $\mathbf{3^{f1}}$. The other $\mathbf{4^{f}}$-series ions, including $\mathbf{4^{f2}}$ and $\mathbf{4^{f3}}$, similarly evolved through the loss of a neutral pyridine moiety from corresponding $\mathbf{3^{f}}$-series ions (Scheme 2.1, Table 2.4B). The **7-series** ions (dominant ions), $[M–n\text{Py}–R–H–(C_{\chi}H_{2\chi-y})]^{+}$, originate from the loss of a full alkyl tail as a neutral dodecyne molecule ($C_{\chi}H_{2\chi-y} = C_{12}H_{22}$, $x = 12$, $y = 2$) from ion $\mathbf{3^{f1}}$ to first yield the major product ion $\mathbf{7^{f1}}$ *m/z* $[340.26]^{+}$. Ion $\mathbf{7^{f1}}$ then leads to a succession of ions: $\mathbf{7^{f2}}$ *m/z* $[261.27]^{+}$, $\mathbf{7^{f3}}$ *m/z* $[203.19]^{+}$, $\mathbf{7^{f4}}$ *m/z* $[189.18]^{+}$, $\mathbf{7^{f5}}$ *m/z* $[175.17]^{+}$ and $\mathbf{7^{f6}}$ *m/z* $[161.10]^{+}$ via neutral losses as illustrated in Scheme 2.1.

Finally, the **8-series** ions $[M–2(\text{Py})–(R–H)–(C_{\chi}H_{2\chi-y})]^{+}$, Table 2.4B) resulted from neutral loss of ethene from the partially fragmented hydrocarbon tail of ion $\mathbf{3^{f2}}$ to give ion $\mathbf{8^{f1}}$. Fragment ion $\mathbf{8^{f1}}$ then subsequently produces smaller ions $\mathbf{8^{f2}}$ **-** $\mathbf{8^{f4}}$ via a stepwise cleavage of neutral ethene, methylene or other small units from the partially fragmented hydrocarbon tail. Regardless of the tail length, the overall CID-MS^n results for the R̂(Py)-S-2-S-(Py)R̂ compounds showed a universal fragmentation (Table 2.3).

2.5 Discussion

2.5.1 *Mass accuracy and compound structural confirmation*

The achievement of high mass accuracies in this work using the QSTAR® system (up to less than 1 ppm error, Table 2.1) is particularly important as high mass accuracies can strongly confirm/establish a compound's identity.[30, 31] The level of mass accuracy given by the single analyte infusion method exceeded that given by multiple analyte infusion obviously due to the minimization of peak intensity variations.

2.5.2 *Multi-stage tandem MS/MS fragmentation patterns*

The bioanalysis (identification, quantification and intracellular fate investigation) of gemini surfactants within cells/tissues requires an understanding of their MS fragmentation behaviour. The fragmentation patterns for both the R̂(Py)-S-2-S-(Py)R̂ and the R-7N(*X*-suc-β-CD)-R gemini surfactant series (Schemes 2.1, 2.2) established by using multi-stage tandem CID-MS^n analysis has revealed unique behaviour and diagnostic fragment ions. This has led to confirmation of the molecular structure of tested compounds For instance, the structures of the R-7N(*X*-suc-β-CD)-R compounds were adequately confirmed with the detection of eight diagnostic fragment ions including **1**, **2**, and $\mathbf{3^{i1}}$–$\mathbf{3^{i6}}$ series (Scheme 2.1, Table 2.2) for each compound. These ions reflect the distinct alkyl tails R, β-CD substituent and the presence of either the *O*- or *N*-succinyl linker (Figure 2.1, Table 2.2).

In addition, identical fragment ions were also observed (e.g., ions in *Pathway 2*, Scheme 2.1) following complete collision-induced cleavage of the distinct structural parts. This further confirms the molecular structures since the stepwise cleavage of specific structural parts matched

the observed changes in *m/z* values. For instance, the fragment ion $\mathbf{4^{i1}}$, which was a prominent recurring ion among the R-7N(*X*-suc-β-CD)-R compounds with *X* = *O*, was obtained via the loss of neutral alkene molecules that depended on the carbon length of the alkyl tail region. The identified alkene molecules (denoted R–H, in the $[\mathbf{M}]^{2+}\rightarrow[\mathbf{1}]$ and $[\mathbf{3^{i1}}]\rightarrow[\mathbf{5^{i1}}]$ transitions, Scheme 2.1) included dodecene (168.19 Da), dodecene-$\mathbf{d_{24}}$ (192.34 Da), hexadecene (224.25 Da) and octadecadiene (250.27 Da). Each specific alkene molecule (i.e., the neutral loss) occurred only for a specific compound, and thus helped confirm the molecular identity of the compound(s).

For the R̂(Py)-S-2-S-(Py)R̂ compounds, the occurrence of several diagnostic product ions including $\mathbf{1^{f1}}$, $\mathbf{1^{f2}}$, $\mathbf{1^{f3}}$, $\mathbf{3^{f1}}$, $\mathbf{3^{f2}}$ and $\mathbf{3^{f3}}$ (Scheme 2.2, Figures 2.4, 2.5) marks a distinct identity for each of these compounds. The cleavage of pyridinium head groups both as a neutral pyridine moiety and as a pyridinium ion gives confirmation of the bis-pyridinium content of the R̂(Py)-S-2-S-(Py)R̂ compounds. Similarly, the loss of neutral aliphatic alkyne molecules (e.g., dodecyne) also confirms the presence of two alkyl tails. The loss of neutral alkyne molecules from the R̂(Py)-S-2-S-(Py)R̂ compounds, when compared with the loss of neutral alkenes from the corresponding R-7N(*X*-suc-β-CD)-R compounds, is consistent with the difference in bonding of the alkyl tail within the two series.

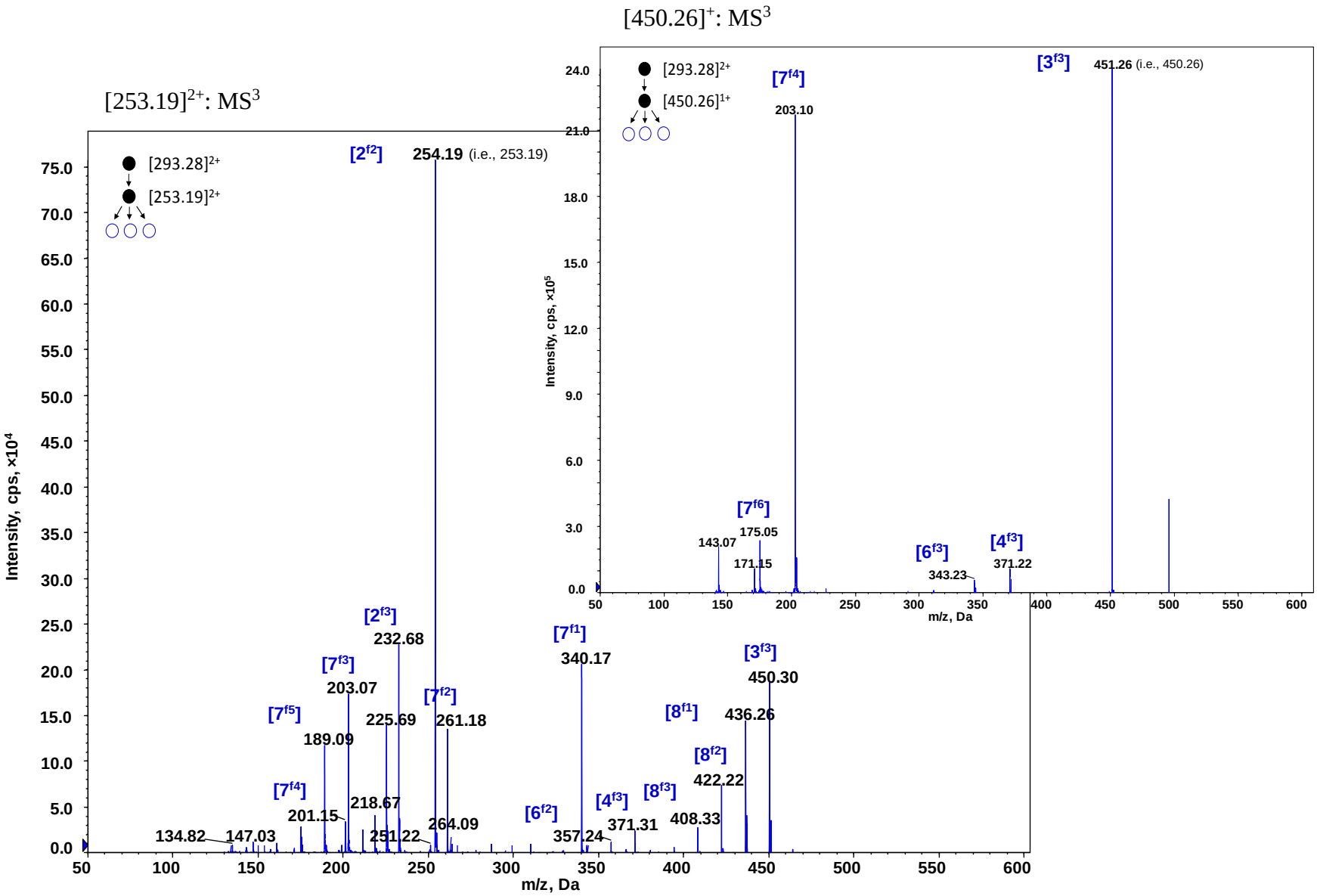
[253.19]2+: MS3
[293.28]2+
[253.19]2+
[2f2] 254.19 (i.e., 253.19)
[2f3] 232.68
[7f3] 203.07
[7f5] 189.09
[7f2] 261.18
225.69
[7f4] 218.67
201.15
134.82
147.03
251.22
264.09
[6f2]
[7f1] 340.17
[4f3] 371.31
357.24
[8f3] 408.33
[8f1] 436.26
[3f3] 450.30
[8f2] 422.22
Intensity, cps, ×10^4
m/z, Da
[450.26]+: MS3
[293.28]2+
[450.26]1+
[7f4] 203.10
[3f3] 451.26 (i.e., 450.26)
[7f6] 175.05
143.07
171.15
[6f3] 343.23
[4f3] 371.22
Intensity, cps, ×10^5
m/z, Da

Figure 2.5: MS^3 spectrum of product ion *m/z* $[253.19]^{2+}$ which originates from MS/MS fragmentation of the compound 12(Py)-S-2-S-(Py)12, with precursor ion $[M]^{2+}$ *m/z* 293.28. Insert: MS^3 spectrum of product ion *m/z* $[450.26]^{+}$ originating from MS^3 fragmentation of the product ion *m/z* $[253.19]^{2+}$.

2.5.3 Fragmentation: *R-7N(X-suc-β-CD)-R vs. R̂(Py)-S-2-S-(Py)R̂*

The difference in molecular structure between the R-7N(*X*-suc-β-CD)-R and R̂(Py)-S-2-S-(Py)R̂ compounds was evident from their different tandem CID-MS/MS fragmentation behaviour. The quaternary ammonium head groups in the R-7N(*X*-suc-β-CD)-R compounds were lost as neutral N-methylmethanamine molecules (Me-N(H)-Me, 45 Da; Scheme 1). On the other hand, the pyridinium head groups in the R̂(Py)-S-2-S-(Py)R̂ compounds were cleaved either as a neutral pyridine moiety (C_5H_5N, 79 Da) or as a pyridinium ion (ion **5**, $C_5H_6N^+$, *m/z* 80 Da; Figure 2.4, Scheme 2.2). Also, the neutral loss of full alkyl tail moieties gave different forms of neutral aliphatic molecules for the R-7N(*X*-suc-β-CD)-R *vs.* R̂(Py)-S-2-S-(Py)R̂ compounds. To illustrate this, the R-7N(*X*-suc-β-CD)-R compounds showed the loss of full alkyl tail groups R as alkene molecules (C_nH_{2n}, e.g., dodecene, 168 Da, Scheme 2.1). The corresponding neutral loss for the R̂(Py)-S-2-S-(Py)R̂ compounds, gave alkyne molecules (C_nH_{2n-2}, e.g., dodecyne, 166 Da, Scheme 2.2).

In addition, several small fragment ions obtained after the complete loss of both alkyl tail groups or head group-tail regions showed more distinct differences among the R-7N(*X*-suc-β-CD)-R and R̂(Py)-S-2-S-(Py)R̂ compounds. For instance, the ammonium head group/tail-free fragment ions of the R-7N(*X*-suc-β-CD)-R compounds underwent further fragmentation, giving rise to smaller ions along with neutral loss of glycosyl residues, CO and H_2O. In the case of the R̂(Py)-S-2-S-(Py)R̂ compounds, further fragmentation of the pyridinium head group-free fragments ions showed cleavage (neutral losses) of segments of the alkyl tails as neutral hydrocarbon species such as CH_2=CH_2, CH_2=CH-CH_3. Thus, using a mixture of the R-7N(*X*-suc-

β-CD)-R and R̂(Py)-S-2-S-(Py)R̂ compounds as a prototype multi-component sample, the respective individual compounds were screened and identified based on the distinct tandem CID-MS/MS fragmentation patterns.

2.5.4 *Conclusion*

The analysis of novel R-7N(*X*-suc-β-CD)-R and R̂(Py)-S-2-S-(Py)R̂ compounds using a combination of ESI-QqToF-MS and ESI-QqQ-LIT-MS^n enabled a complete characterization of these doubly-charged gemini surfactants. Using the ESI-QqToF-MS system with two-point internal calibration, the tested compounds were detected with sub-1 ppm accuracy, an accuracy level that is sufficient for unambiguously confirming the compound's molecular formula.

The in-depth fragmentation patterns, which were established using ESI-QqQ-LIT-MS^n (up to MS^3), revealed diagnostic product ions which are characteristic of the individual R-7N(*X*-suc-β-CD)-R and R̂(Py)-S-2-S-(Py)R̂ compounds, thus providing further confirmation of the compound structure. Within the R-7N(*X*-suc-β-CD)-R series, eight common diagnostic product ions were observed, while six common diagnostic product ions were observed for the R̂(Py)-S-2-S-(Py)R̂ series. The fragmentation pathways established in this work (especially the $[M]^{2+} \rightarrow$ diagnostic ion transitions) can be used as a fingerprint pattern for rapid and accurate bioanalysis (identification and quantification) of these test compounds within complex biological samples. We are currently evaluating the intracellular localization and metabolic fate of the tested gemini surfactants which will be reported upon completion.

2.6 *Acknowledgements*

The authors acknowledge the technical assistance of Ms. Bheshad Vantarparrast in parts of the compound synthesis within this study. Acknowledgement is also due to Mr. Ken Thoms for his technical assistance and to the Saskatchewan Structural Sciences Centre for use of the QSTAR® system. Ms. Deborah Michel and Mr. Joshua Buse provided basic training on the MS instrumentation and are also acknowledged. Funding from the Natural Sciences and Engineering Research Council (NSERC) through an NSERC Discovery Grant is duly recognized. Funding for the purchase of the AB Sciex QTRAP® 4000 LC-MS/MS instrument was obtained through a Canada Foundation for Innovation (CFI) grant – Leaders Opportunity Fund.

2.7 References

1. H.S. Rosenzweig, V.A. Rakhmanova, R.C. MacDonald. Diquaternary ammonium compounds as transfection agents. *Bioconjug. Chem*. **2001**, 12(2), 258.

2. D. Michel, J.M. Chitanda, R. Balogh, P. Yang, J. Singh, U. Das, A. El-Aneed, J. Dimmock, R. Verrall, I.Badea. Design and evaluation of cyclodextrin-based delivery systems to incorporate poorly soluble curcumin analogs for the treatment of melanoma. *Eur. J. Pharm. Biopharm*. **2012**, 81(3), 548.

3. C. McGregor, C. Perrin, M. Monck, P. Camilleri, A.J. Kirby. Rational approaches to the design of cationic gemini surfactants for gene delivery. *J. Am. Chem. Soc*. **2001**,123, 6215.

4. S. He, B. Wang, H. Chen, C. Tang, Y. Feng. Preparation and antimicrobial properties of gemini surfactant-supported triiodide complex system. *ACS. Appl. Mater Interfaces*. **2012**, 4(4), 2116.

5. L. Caillier, E. Taffin de Givenchy, R. Levy, Y. Vandenberghe, S. Geribaldi, F. Guittard. Polymerizable semi-fluorinated gemini surfactants designed for antimicrobial materials. *J. Colloid. Interface Sci.* **2009**, 332(1), 201.

6. J. Chlebicki, J. Węgrzyńska, I. Maliszewska, M. Oświęcimska. Preparation, surface-active properties, and antimicrobial activities of bis-quaternary ammonium salts from amines and epichlorohydrin. *J. Surfactants Detergs*. **2005**, 8(3), 227.

7. F.M. Menger, J.S. Keiper. Gemini Surfactants. *Angew. Chem. Int. Ed. Engl*. **2000**, 39(11), 1906.

8. S.D. Wettig, C. Wang, R.E. Verrall, M. Foldvari. Thermodynamic and aggregation properties of aza- and imino-substituted gemini surfactants designed for gene delivery. *Phys. Chem. Chem. Phys.* **2007**, 9(7), 871.

9. A.J. Kirby, P. Camilleri, J.B. Engberts, M.C. Feiters, R.J. Nolte, O. Soderman, M. Bergsma, P.C. Bell, M.L. Fielden, C.L. García Rodríguez, P.Guédat, A. Kremer, C. McGregor, C. Perrin, G. Ronsin, M.C.van Eijk. Gemini surfactants: new synthetic vectors for gene transfection. *Angew. Chem. Int. Ed. Engl.* **2003**, 42(13), 1448.

10. I. Ikeda. in *Gemini Surfactants: Synthesis, Interfacial and Solution-Phase Behavior and Applications*. (Eds: R. Zana, J. Xia). Marcel Dekker, Inc., New York, **2004**, pp. 9–35.

11. L.S. Saroj. Novel glucose derived non-ionic gemini surfactants as reverse micellar systems for encapsulation of d- and l-enantiomers of some aromatic α-amino acids in n-hexane. *J. Incl. Phenom. Macrocycl. Chem.* **2012**, 74(1-4), 251.

12. K. Ruckmani, B. Jayakar, S.K. Ghosal. Nonionic surfactant vesicles (niosomes) of cytarabine hydrochloride for effective treatment of leukemias: encapsulation, storage, and in vitro release. *Drug Dev. Ind. Pharm.* **2000**, 26(2), 217.

13. C.Bombelli, L. Giansanti, P. Luciani, G. Mancini Gemini Surfactant Based Carriers in Gene and Drug Delivery. Curr. Med. Chem. **2009**, 16(2), 171.

14. J. Singh, P. Yang, D. Michel, R.E. Verrall, M. Foldvari, I. Badea. Amino acid-substituted gemini surfactant-based nanoparticles as safe and versatile gene delivery agents. *Curr Drug Deliv.* **2011**, 8(3), 299.

15. M. Donkuru, S.D. Wettig, R.E. Verrall, I. Badea, M. Foldvari. Designing pH-sensitive gemini nanoparticles for non-viral gene delivery into keratinocytes. *J. Mater. Chem.* **2012**, 22, 6232.

16. M. Persike, M. Karas. Rapid simultaneous quantitative determination of different small pharmaceutical drugs using a conventional matrix-assisted laser desorption/ionization time-of-flight mass spectrometry system. *Rapid Commun. Mass Spectrom.* **2009**, 23, 3555.

17. B.Toussaint, C. Pitti, B. Streel, A. Ceccato, P. Hubert, J. Crommen. Quantitative analysis of N-acetylcysteine and its pharmacopeial impurities in a pharmaceutical formulation by liquid chromatography-UV detection-mass spectrometry. *J. of Chromatogr. A.* **2000**, 896, 191.

18. B. Krastins, A. Prakash, D.A. Sarracino, D. Nedelkov, E.E. Niederkofler, U.A. Kiernan, R. Nelson, M.S. Vogelsang, G. Vadali, A. Garces, J.N. Sutton, S. Peterman, G. Byram, B. Darbouret, J.R. Pérusse, N.G. Seidah, B. Coulombe, J. Gobom, E. Portelius, J. Pannee, K. Blennow, V. Kulasingam, L. Couchman, C. Moniz, M.F. Lopez. Rapid development of sensitive, high-throughput, quantitative and highly selective mass spectrometric targeted immunoassays for clinically important proteins in human plasma and serum. *Clin. Biochem.* 2**013**, 46(6), 399.

19. Mohammed-Saeid W, Buse J, Badea I, Verrall R, El-Aneed A. Mass spectrometric analysis of amino acid/di-peptide modified gemini surfactants used as gene delivery agents: Establishment of a universal mass spectrometric fingerprint. *Int. J. Mass Spectrom.* **2012**, 309, 182.

20. J. Buse, I. Badea, R.E. Verrall, A. El-Aneed. Tandem mass spectrometric analysis of novel diquaternary ammonium gemini surfactants and their bromide adducts in electrospray-positive ion mode ionization. *J. Mass Spectrom.* **2011**, 46(10), 1060.

21. J. Buse, I. Badea, E.R. Verrall, A. El-Aneed. Tandem Mass Spectrometric Analysis of the Novel Gemini Surfactant Nanoparticle Families G12-s and G18:1-s. *Spectrosc. Lett.* **2010**, 43, 447.

22. J. Buse, I. Badea, R.E. Verrall, A. El-Aneed. A general liquid chromatography tandem mass spectrometry method for the quantitative determination of diquaternary ammonium Gemini

surfactant drug delivery agents in mouse keratinocytes' cellular lysate. *J. Chromatogr. A.* **2013**, 1294, 98.

23. S.D. Wettig, R.E. Verrall, M. Foldvari Gemini surfactants: a new family of building blocks for non-viral gene delivery systems. *Curr. Gene Ther.* **2008**, 8(1), 9.

24. Mahajan RK, Mahajan S, Bhadani A, Singh S. Physicochemical studies of pyridinium gemini surfactants with promethazine hydrochloride in aqueous solution. *Phys. Chem. Chem. Phys.* **2012**, 14, 887.

25. A.Bhadani, S. Singh. Novel gemini pyridinium surfactants: synthesis and study of their surface activity, DNA binding, and cytotoxicity. *Langmuir.* **2009**, 25(19), 11703.

26. M.A. Ilies, T.V. Sommers, L.C. He, A. Kizewski, V.D. Sharma. Pyridinium Amphiphiles in Gene Delivery – Present and Perspectives. Amphiphiles: Molecular Assembly and Applications. *ACS Symp. Ser.* **2011**, 1070, 23.

27. S.D. Wettig, R.E. Verrall. Thermodynamic studies of aqueous m-s-m gemini surfactant systems. *J. Colloid. Interface Sci.* **2001**, 235, 310.

28. J.W. Hager. A new linear ion trap mass spectrometer. *Rapid Commun. Mass Spectrom.* **2002**, 16, 512.

29. G. Hopfgartner, E. Varesio, V. Tschäppät, C. Grivet, E. Bourgogne, L.A. Leuthold. Triple quadrupole linear ion trap mass spectrometer for the analysis of small molecules and macromolecules. *J. Mass Spectrom.* **2004**, 39, 845.

30. K. Webb. *Methodology for accurate mass measurements of small molecules – best practice guide.* LGC Limited, Teddington (UK), **2004**.

31. G.L. Glish, R.W. Vachet. The basics of mass spectrometry in the twenty-first century. *Nat. Rev. Drug Discov.* **2003**, 2(2), 140.

CHAPTER 3:

RESEARCH PUBLICATION 2

***Citation*:** McDonald Donkuru, Deborah Michel, Hanan Awad, George Katselis, Anas El-Aneed. Novel HILIC-LC-MS/MS quantitative method for the cellular analysis of varying structures of gemini surfactants designed as nanomaterial drug carriers. *Journal of Chromatography A*, 2016, **1446**, 114–124.

The work presented in this chapter is a verbatim copy of a peer-reviewed research article with the citation above. It was published exclusively from work conducted within my Ph.D. research and describes new HILIC-based LC-MS/MS methods for the bio-analysis of gemini surfactants. It also presents quantitative cellular uptake and intracellular deposition profile of two lead gemini surfactatns, 16(Py)-S-2-S-(Py)16 and 16-3-16, within transfected PAM212 epidermal keratinocytes analysed using the HILIC-LC-MS/MS methods. I designed, initiated and completed all experimental work including HILIC-LC-MS/MS method development/validation, gemini surfactant nanoparticle-based cell transfections, analytical sample preparation and subsequent determination of gemini surfactants within the treated cells. Co-athors Deborah Michel and Hanan Awad provided confirmatory evaluation of the developed/validated LC-MS/MS methods; they also did check the produced data and its quality. Some data were removed/redone based on their contributions. Relating to sample preparation, valuable technical input was made by co-

author George Katselis with this contributing to efficient analyte recovery. As the first author, I wrote all draft versions of the manuscript and incorporated revision advised by co-authors. This work was fully supervised by Dr. Anas El-Aneed.

Manuscript:

3. Novel HILIC-LC-MS/MS quantitative method for the cellular analysis of varying structures of gemini surfactants designed as nanomaterial drug carriers.

McDonald Donkuru[1], Deborah Michel[1], Hanan Awad[1], George Katselis[2], Anas El-Aneed[1]

1. Drug Design & Discovery Group, College of Pharmacy and Nutrition, University of Saskatchewan, 107 Wiggins Road, Saskatoon, SK S7N 5E5, Canada
2. Canadian Centre for Health and Safety in Agriculture (CCHSA), and Department of Medicine, University of Saskatchewan, 104 Clinic Place, Saskatoon, SK S7N 2Z4, Canada

3.1 Abstract

Diquaternary gemini surfactants have successfully been used to form lipid-based nanoparticles that are able to compact, protect and deliver genetic materials into cells. However, there is an absence of information about what happens to the gemini surfactants after they have released their therapeutic cargo. Such knowledge is critical in order to assess quality, safety and efficacy of gemini surfactant nanoparticles. Herein, we developed simple and rapid liquid chromatography tandem mass spectrometry (LC–MS/MS) method for the quantitative determination of various structures of gemini surfactants in cells. Hydrophilic interaction liquid chromatography (HILIC) was employed allowing for a short, simple isocratic run of only 4 minutes, linearity range of 50 – 5000 ng/mL, and a 3 ng/mL lower limit of detection (LLOD). The method was applicable to 18 structures of gemini surfactants belonging to two different structural families with full validation for two lead compounds according to USFDA guidelines. The HILIC-MS/MS was ideally compatible with the physicochemical properties of gemini surfactants that bear permanent positive change with both hydrophilic and hydrophobic elements within their molecular structure. In addition, the chromatographic separation was combined with effective liquid-liquid extraction method (98% recovery) that surpasses previously used methods. Data from the analysis of nanoparticle-treated cells showed an initial rise in the analyte intracellular concentration followed by a maximum and a somewhat more gradual decrease of the intracellular concentration. Two events that may account for the seeming intracellular depletion of the gemini surfactants are bio-transformation into metabolites and exocytosis from the host cells.

3.2 Introduction

Dicationic gemini surfactants are a promising class of lipids currently being investigated for nanoparticle-mediated gene delivery.[1,2,3] They can effectively be complexed with DNA into therapeutic nano-lipoplexes which in turn can transfect cells. Gemini surfactants are structurally defined a general molecular architecture in which two monomer surfactants with polar or ionic head-groups are connected via a spacer moiety (Figure 3.1A). In dicationic gemini surfactants (frequently used as the bromide salts), the head-groups are positively charged to allow DNA complexation. Structural modification in gemini surfactants aims at increasing transfection efficiency while at the same time reducing toxicity. In fact, an expanding variety of gemini surfactants demonstrates effectiveness as non-viral DNA delivery agents.[4,5,6,7] However, there is an absence of information about what happens to the gemini surfactants after they have released their therapeutic cargo. Such knowledge is critical in order to assess quality, safety and efficacy of gemini surfactant nanoparticles. Therefore, effective analytical methods are urgently needed.

Liquid chromatography coupled to tandem mass spectrometry (LC-MS/MS) offers the combined capability of analyte separation alongside sensitive, high-throughput and selective analysis.[8,9,10] Gemini surfactants are not compatible with fluorescent/UV-detection due to the lack of fluorescent or UV-active moieties. Therefore, LC-MS/MS is an ideal platform for the quantitative determination of the nanoparticles' amphiphilic constituents within complex biological mixtures. In addition, LC-MS/MS analysis with the use of multiple reaction monitoring (MRM) allows gemini surfactants to be monitored using precursor ion → product ion diagnostic transitions which provides specificity to target gemini surfactant analytes.

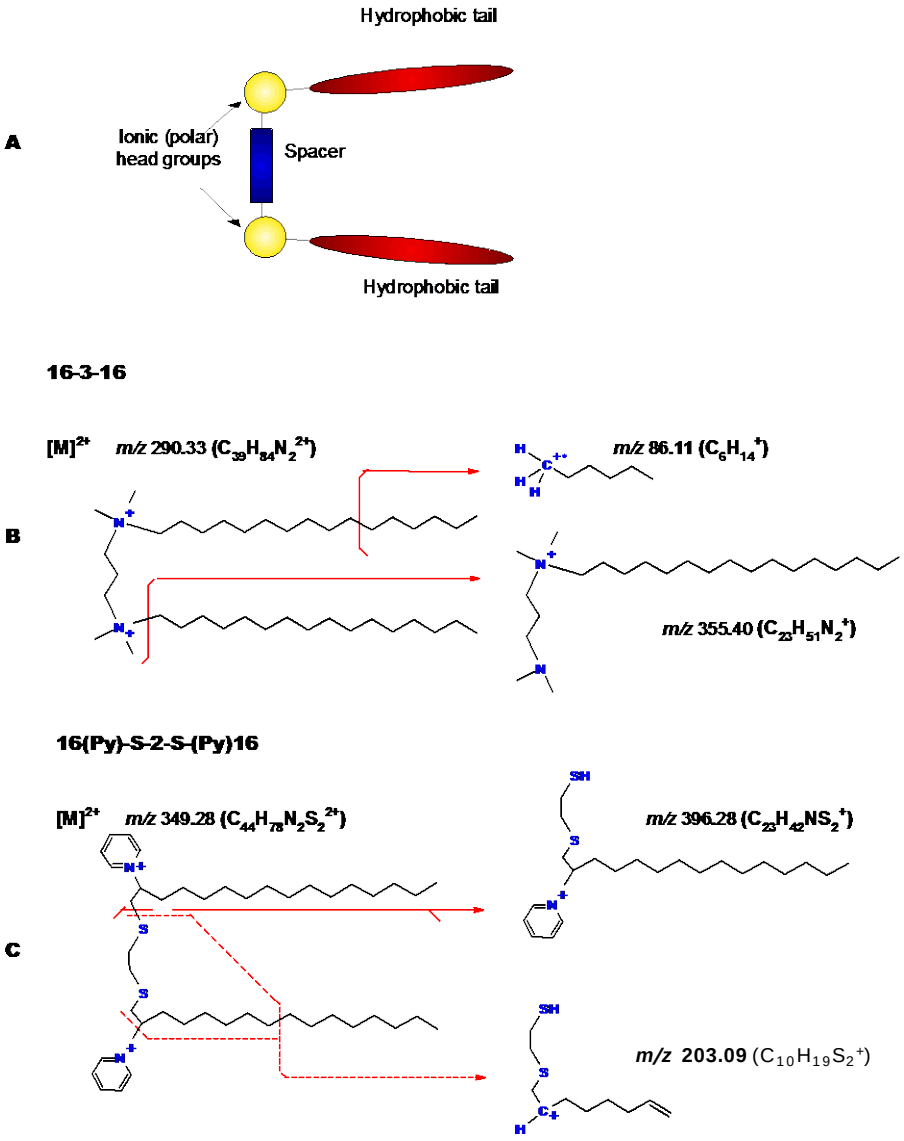

Figure 0.1: A) Schematic representation of gemini surfactant general structure; B) The exact molecular structures of intact compounds and monitored product ions during HILIC-MS/MS of 16-3-16: N,N-bis(dimethylhexadecyl)-1,3-propanediammonium; C) 16(Py)-S-2-S-(Py)16: 1,1'-[ethane-1,2-diylbis(sulfanediylhexadecane-1,2-diyl)]dipyridinium.

To allow for the assessment of the cellular fate of gemini surfactants, our laboratory initiated studies to first establish the collision-induced dissociation (CID)-MS/MS fragmentation patterns and fingerprint ions of several gemini surfactant structures.[11,12,13,14] These qualitative studies allowed for the subsequent development of an LC-MS/MS method employing a *cyano* chromatographic column for the quantification of gemini surfactants in epidermal keratinocytes.[15] However, this method suffered from drawbacks, such as ion suppression due to the addition of an ion pairing reagent, long run times, relatively low sensitivity and the use of gradient elution. Other MS-based quantification methods, such as fast chromatography (FC)-MS, desorption electrospray ionization (DESI-MS/MS) and matrix assisted laser desorption (MALDI)-MS were also developed in our lab and their analytical capabilities were compared;[16] however, all the developed methods were only applicable to one structural family of gemini surfactants with full validation possible for the *N*,*N*-bis(dimethylhexadecyl)-1,3-propanediammonium compound, denoted as 16-3-16 (Figure 3.1B). In fact, the fastest MS quantification method,[16] MALDI-MS, was not applicable to gemini surfactant structures that have more than three carbons within their spacer region due to the incomplete dissociation of the gemini surfactants within the MALDI source, preventing the possibility of developing quantification methods. Hence, there is need for a universal method that can produce quantitative data for varying gemini surfactant structures through the adoption of suitable chromatography platform such as hydrophilic interaction liquid chromatography (HILIC). HILIC is an ideal stationary phase that can combine the benefits of both the normal and reversed-phases of separation.[17] It has been widely used for the analysis of polar compounds including those bearing quaternary amines.[18]

In addition to traditional, non-substituted alkanediyl-*α,ω*-bis(dimethyl alkyl-ammonium) gemini surfactants (designated as *m-s-m*), other classes of gemini surfactants especially bis(alkyl-pyridinum) compounds have emerged.[19,20] The latter is reported to be less toxic when comparing *m-s-m* and *bis(alkyl-pyridinum)* representative bromide compounds.[19] The representative *m-s-m* compound is *N,N*-bis(dimethylhexadecyl)-1,3-propanediammonium (denoted 16-3-16; Figure 3.1B), while the *bis(alkyl-pyridinum)* counterpart is 1,1'-[ethane-1,2-diylbis(sulfanediylhexadecane-1,2-diyl)]dipyridinium (denoted 16(Py)-S-2-S-(Py)16; Figure 3.1C). The 16-3-16 compound imposed higher toxicity than 16(Py)-S-2-S-(Py)16 [19,21] without a logical explanations based on their molecular structures. It is reasonable to speculate that possible differences in gemini surfactant nanoparticle entry into cells, nano-bio interactions, bio-distribution, bio-transformation or bio-persistence could explain differences in toxicity. Therefore, we aimed at developing simple and fast LC-MS/MS method that can effectively quantify varying structures of gemini surfactants within treated cells.

Herein, we report the utilization of HILIC-LC-MS/MS to allow for the quantitative determination of variable structures of gemini surfactants within cells. We were able, for the first time, to quantify gemini surfactants that belong to two different structural families with full method validation for 16-3-16 and 16(Py)-S-2-S-(Py)16 (Figure 3.1).

3.3 Materials and Methods

3.3.1 Materials

The diquaternary ammonium and dipyridinium gemini surfactants, as well as their deuterated internal standards, used in this study were synthesized based on established

methods.[19,22,23] For the 16-13-6 analyte, the internal standard (16-13-6-$\boldsymbol{d_{66}}$) incorporated deuterated alkyl tails resulting in mass difference of +66 Da; while in the case of 16(Py)-S-2-S-(Py)16, deuteration was within the pyridinium heads accounting for +10 Da mass difference for the internal standard, 16(Py)-S-2-S-(Py)16-$\boldsymbol{d_{10}}$ (Figure S3.6 in the supplementary information).

The neutral lipid 1,2-Dioleoyl-sn-glycero-3-phosphoethanolamine (DOPE) was purchased from Avanti Polar Lipids Inc. (Alabaster, AL, USA). Chloroform, methanol and 1-Octanol (99%) were purchased from Fisher Scientific (Ottawa, ON, Canada). Ammonium formate, formic acid, mass spectrometric-grade water and acetonitrile were purchased from Fisher Scientific (Ottawa, ON, Canada). PAM 212 cells were kindly provided by Dr. S. Yuspa, National Cancer Institute, Bethesda, MD, USA. The cell growth medium contained minimum essential media (MEM), fetal bovine serum albumin (FBS) and antibiotic-antimycotic which were obtained from Sigma-Aldrich (Oakville, ON, Canada). Tissue culture flasks (with capacities: 150-cm^3, 75-cm^3, 25-cm^3) as well as 6-well plates, were purchased from Fisher Scientific (Ottawa, ON, Canada).

3.3.2 LC-MS/MS instrumentation

The hybrid LC-MS/MS analytical system comprised of an Agilent 1200 Series HPLC having a quaternary pump, a degasser and auto sampler (Agilent Technologies, Mississauga, ON, Canada) coupled to an AB Sciex API 4000 QTRAP mass spectrometer (AB Sciex, Concord, ON, Canada). The chromatography step used a ZIC®-HILIC column (150 × 2.1 mm, 5 µm, 200 Å; Merck SeQuant AB) held at 50 ˚C and an isocratic mobile phase flowing at 500 µL/min to analyze 2 µL injected aliquots. The mobile phase was 80:20 (v/v) acetonitrile/buffer, with the buffer containing 2.5 mM ammonium formate and 25 mM formic acid. No sample carryover was

detected and to eliminate any chances of carryover, double blank injections were run after the injection of the highest calibration curve concentration.

The AB Sciex QTRAP 4000 mass spectrometer is equipped with an electrospray (ESI) source set at 5500 V ionspray voltage and 600 ◦C at the ion source interface, with 30 psi being set as the curtain gas pressure and 40 psi as the pressures for both GS1 (nebulizer gas) and GS2 (heater gas). The mass spectrometer was operated in the multiple reaction monitoring (MRM) mode to monitor the analytes and the deuterated internal standards as $[M]^{2+}$ species, including the following transitions: 16-3-16 $[M]^{2+}$ *m/z* 290.33 → 355.40, 86.11; 16-3-16-***d*$_{66}$** $[M]^{2+}$ *m/z* 323.54 → 388.61; and, 16(Py)-S-2-S-(Py)16 $[M]^{2+}$ *m/z* 349.28 → 396.28, 203.09; 16(Py)-S-2-S-(Py)16-***d*$_{10}$** $[M]^{2+}$ *m/z* 354.31 → 401.31. The MRM conditions and fingerprint structures for the monitored transitions are presented below (Table 3.1, Figure 3.1, and Figure S3.6 in the supplementary information).

Table 1.1. Conditions for MRM transitions of the analytes on AB Sciex 4000 QTRAP® System.

Analyte		MRM Transition		DP*	CE*	CXE*
Gemini surfactant	Molecular Formula	$[M]^{2+} \rightarrow [M - X]^{+}$	*m/z* → *m/z*	(eV)	(eV)	(eV)
16(Py)-S-2-S-(Py)16	$C_{44}H_{78}N_2S_2^{2+}$	$[M]^{2+} \rightarrow [M - C_{21}H_{36}N]^{+}$	*m/z* 349 → 396	30	22	10
16(Py)-S-2-S-(Py)16	$C_{44}H_{78}N_2S_2^{2+}$	$[M]^{2+} \rightarrow [M - C_{34}H_{59}N_2]^{+}$	*m/z* 349 → 203	30	22	10
16(Py)-S-2-S-(Py)16-***d*$_{10}$**	$C_{44}H_{68}\mathbf{D_{10}}N_2S_2^{2+}$	$[M]^{2+} \rightarrow [M - C_{21}H_{31}\mathbf{D_5}N]^{+}$	*m/z* 354 → 401	30	25	10
16-3-16	$C_{39}H_{84}N_2^{2+}$	$[M]^{2+} \rightarrow [M - C_{16}H_{33}]^{+}$	*m/z* 290 → 355	40	21	10
16-3-16	$C_{39}H_{84}N_2^{2+}$	$[M]^{2+} \rightarrow [M - C_{33}H_{70}N_2]^{+}$	*m/z* 290 → 86	40	35	6
16-3-16-***d*$_{66}$**	$C_{39}H_{18}\mathbf{D_{66}}N_2^{2+}$	$[M]^{2+} \rightarrow [M - C_{16}\mathbf{D_{33}}]^{+}$	*m/z* 323 → 388	35	25	10

***Abbreviation:**

DP: declustering potential, CE: collision energy, CXE: collision cell exit potential; X: neutral loss

3.3.3 Preparation of standard solutions

Aqueous stock solutions of all gemini surfactants at molarity of 3 mM were prepared, used with or without dilutions and routinely stored at −20 ˚C under darkness. The mass concentrations (equivalent to the 3 mM molarity) for purpose of analytical quantitation are detailed on Table S3.1. DOPE vesicles, a 1 mM solution, was prepared fresh in 9.25% w/v isotonic sucrose solution which had pH 9. Plasmid DNA (pGT·IFN-GFP) solution, 40 μg/mL, was prepared in ultrapure, organic-free water and was stored at −20 ˚C. The DOPE and plasmid DNA solutions were used without further dilutions.

3.3.4 Preparation of nanoparticle formulations

Plasmid DNA/gemini surfactant/lipid DOPE (P/G/L) nano-lipoplex formulations were prepared to a 1:10:100 molar ratio of the ingredients (combined in the order given) as previously described.[22] The mole of DNA is calculated per DNA base-pair with an average molecular weight of 660 Da.[24] Briefly, the required transfection dose of plasmid DNA was measured, to which the appropriate amount of gemini surfactant was added with an allowed 30-minute incubation at room temperature. DOPE was then added to the binary mixture, followed by further 15-minute incubation at room temperature to obtain a ternary (final) P/G/L system. The transfection dose of plasmid DNA was 0.3 μg for 1×10^6 cells/treatment.

3.3.5 PAM 212 cell treatment and sample collection

PAM 212 cells were routinely cultured inside humidified 95% air/5% CO_2 incubators at 37 ˚C. The culture medium was MEM that was supplemented with 10% FBS and 1 unit/mL antibiotic-antimycotic. Cells cultured to 80% confluence were harvested by trypsinization and

either subcultured or prepared for treatment. At 24 h before treatment, cells were seeded at 1 × 10^6 cells/mL/well within 6-well plate format. At 1 h to transfection, the cell supernatant media was replaced with FBS-free media. Nanoparticle formulations, freshly prepared (*Section 2.3*), were added and allowed to interact with cells by placing the cells in the CO_2 incubator (37 ˚C). This marked the reference point for recording any post-treatment incubation time-points where further steps are taken.

After 5 h, the nanoparticle-dosed cell media was replaced with supplemented media (MEM with 10% FBS, 1 unit/mL), followed by a continued incubation of cells. All treatments were carried out in replicates ($n \geq 3$) along with appropriate controls on at least three separate days. The controls included cells that underwent no treatment as well as cells that received formulation prepared without the inclusion of the gemini surfactant component. During the incubation period, replicates of treated cell samples were, at different time-points, trypsinized and collected into 1.5 mL volumes. The collected cells were pelleted (14,000 rpm, 5 min, 4 ˚C), rinsed with phosphate-buffered saline (PBS) and reconstituted into smaller sample volumes of 200 µL in (PBS), and then stored at −80 ˚C prior to analyte extraction and LC-MS/MS analysis.

To better conduct sample collection and reduce tediousness in the process, an alternative approach was also used. During the post-treatment incubation period, replicates of treated cells were, at different time-points, retrieved from the CO_2 incubator, rinsed (3×) with PBS and placed at −80 ˚C. All cells kept at −80 ˚C were then thawed, trypsinized and collected into 1.5-mL volumes. The 1.5-mL samples were reduced into smaller sample volumes of 200 µL using centrifugal evaporation (speed vacuum concentration). Results were identical using both approaches.

3.3.6 Sample Preparation for LC-MS/MS analysis

The 200-µL treated cell samples kept at −80 ˚C were lysed by six freeze/thaw cycles along with 1-h sonication at 25 kHz. The samples were spiked with constant amounts of the internal standards by addition of 50-µL solutions obtained from a dilution of $^1/_{250}$ parts of the pure stock internal standard in water; the resultant concentration was 1,938 ng/mL for 16-3-16-$\boldsymbol{d}_{66}$ and 2,086 ng/mL for 16(Py)-2-S-2-(Py)16-$\boldsymbol{d}_{10}$. For the construction of calibration curves, 200-µL cell lysates (equivalent to 1×10^6 cells each) which had not received any nanoparticle treatment were used. The untreated samples were spiked with 50-µL solutions containing the analyte and the corresponding internal standard. The resultant volume was 250 µL for all samples prior to subsequent steps.

Liquid-liquid extraction (LLE) of the analytes and internal standards from the cellular matrix was achieved using the Bligh/Dyer method.[25] Briefly, the 250-µL samples were mixed with 950 µL (3.8 vols) of 2:1 (v/v) methanol/chloroform, followed by mixing with 310 µL (1.24 vols) of both chloroform and water, in that order. Mixing was achieved by vortexing in all cases. The combined mixtures were centrifuged at 14,000 rpm for 1 min at room temperature to obtain separate aqueous and organic phases. The bottom organic phase (80% portion) was retrieved and dried using a gentle N_2 gas stream, followed by reconstitution of the extracted analytes in 200 µL of n-octanol prior to LC-MS/MS analysis.

For comparison, a recently reported alternative method, *octanol* extraction, was also used.[15] For the *octanol* extraction, which involves extracting samples with equal volumes of n-octanol, the 250-µL samples were mixed with 250 µL of n-octanol. Separation of the aqueous

and organic phases was achieved by centrifugation as above. The organic phase (200-µL, i.e., 80% portion) was retrieved for LC-MS/MS analysis.

3.3.7 LC-MS/MS method validation

The LC-MS/MS method was fully validated for the 16-3-16 and 16(Py)-2-S-2-(Py) gemini surfactants in accordance with USFDA guidelines.[26,27] To establish specificity and rule out interference due to co-eluting endogenous species, six different batches of PAM 212 cell samples were analyzed. Linearity was probed over a wide range of analyte concentrations, including 50 – 5,000 ng/mL. Using least-square analysis along with $1/\chi$ as the weighting factor, data was processed by plotting the ratio of summed peak areas for 16-3-16 and 16(Py)-2-S-2-(Py)16 over the peak areas for their respective internal standards, 16-3-16-$\boldsymbol{d_{66}}$ and 16(Py)-2-S-2-(Py)16-$\boldsymbol{d_{10}}$. Linearity was established with the slope, intercept and coefficient of determination (r^2). The limit of detection (LLOD) was set as the lowest detectable concentration with a signal-to-noise (S/N) ratio of 3, while the lowest limit of quantification (LLOQ) was set at the lowest concentration having $S/N \geq 5$, with precision and accuracy within ±20% of the nominal value as per the USFDA guidelines.[27]

The intra- and inter-day precision and accuracy of the method was established through the analysis of six replicates of samples at four different concentrations (lower limit of quantification, LLOQ; lower quality control, LQC; middle quality control, MQC; and high quality control, HQC) on three different days. Single assay runs were accepted only when the relative standard deviation (RSD) was found to be less than ±15% at concentrations other than the LLOQ, which is allowed at ±20%. The criterion for accuracy was set at ±15% of the nominal

concentration of the QC samples and ±20% for LLOQ. In no case did more than one third of the QC samples violate these criteria.

Studies involving freeze/thaw stability, bench-top stability and long-term stability were undertaken at LQC, MQC, and HQC. Freeze/thaw stability was tested after three freeze/thaw cycles spaced at least 24 h apart with sample storage at −20 ± 5 ˚C between sample thawing. Twenty-four hour stability of 16-3-16 and 16(Py)-2-S-2-(Py)16 in PAM212 cell lysate under bench-top conditions was evaluated. Predicted concentrations were calculated using newly prepared calibration curves. Samples were stored at −20 ± 5 ˚C for 105 days prior to analysis of long-term stability. Samples were considered stable when the USFDA criteria for precision and accuracy were met.[27]

3.4 Results

3.4.1 HILIC-LC-MS/MS specificity for gemini surfactant bio-analysis

HILIC-LC-MS/MS method provided selectivity through the observed analyte-specific retention times and specificity through the MRM mode which monitors the analytes using precursor → product ion transitions. The specific retention times established for each analyte and the elimination of carryover effects made the HILIC chromatographic separation an ideal choice for the analysis of gemini surfactants. In addition, the HILIC-LC-MS/MS method was applicable to various gemini surfactant structures as shown in Table 3.2.

A characteristic chemical structure-dependent elution order was observed, establishing predictable HILIC retention time trends important for distinguishing the gemini surfactants. For instance, the alkyl tail length of three gemini surfactants with the same spacer moiety increase in

the order 12(Py)-S-2-S-(Py)12 (tail: *dodecyl*), 14(Py)-S-2-S-(Py)14 (tail: *tetradecyl*) and 16(Py)-S-2-S-(Py)16 (tail: *hexadecyl*); the corresponding retention times (R_t) decreased in the reverse order, 2.88 min, 2.80 min, and 2.62 min, respectively (Table 3.2). Such trend was also notable in the case of the alkyl spacer portions. The increase in the alkyl spacer chains led to shorter retention times as observed for gemini surfactants: 12-3-12 (spacer: *propyl*) R_t = 2.96, 12-8-12 (spacer: *octyl*) R_t = 2.56, 12-12-12 (spacer: *dodecyl*) R_t = 2.43 min (Table 3.2). Thus, gemini surfactants with longer hydrophobic alkyl tails or longer alkyl spacer chains showed shorter retention times on the HILIC column.

Table 1.2. HILIC-LC-MS/MS bio-analysis of 17 gemini surfactants with varying molecular structures.

Gemini surfactant Symbol	Spacer region		Tail region		MRM transitions $m/z \rightarrow m/z$	Retention time (min)
	Name	Molecular formula	Name	Molecular formula		
12-3-12	Propyl	C_3H_6	Dodecyl	$C_{12}H_{25}$	234 → 299	2.96
12-4-12	Butyl	C_4H_8	Dodecyl	$C_{12}H_{25}$	241 → 313	2.91
12-8-12	Octyl	C_8H_{16}	Dodecyl	$C_{12}H_{25}$	269 → 369	2.57
12-12-12	Dodecyl	$C_{12}H_{24}$	Dodecyl	$C_{12}H_{25}$	297 → 425	2.43
12-16-12	Hexadecyl	$C_{16}H_{32}$	Dodecyl	$C_{12}H_{25}$	325 → 481	2.42
16-3-16	Propyl	C_3H_6	Hexadecyl	$C_{16}H_{33}$	290 → 355	2.86
16-7-16	Heptyl	C_7H_{14}	Hexadecyl	$C_{16}H_{33}$	318 → 411	2.52
18-3-18	Propyl	C_3H_6	Octadecyl	$C_{18}H_{37}$	318 → 383	2.44
18-7-18	Heptyl	C_7H_{14}	Octadecyl	$C_{18}H_{37}$	346 → 439	2.37
18:1-3-18:1	Propyl	C_3H_6	Octadec-9-ene	$C_{18}H_{35}$	316 → 381	2.57
18:1-6-18:1	Hexyl	C_6H_{12}	Octadec-9-ene	$C_{18}H_{35}$	337 → 423	2.50
12(Py)-S-2-S-(Py)12	1,2-ethanedithiol	$C_2H_4S_2$	Dodecyl	$C_{12}H_{25}$	293 → 340	2.86
14(Py)-S-2-S-(Py)14	1,2-ethanedithiol	$C_2H_4S_2$	Tetradecyl	$C_{14}H_{29}$	321 → 368	2.79
16(Py)-S-2-S-(Py)16	1,2-ethanedithiol	$C_2H_4S_2$	Hexadecyl	$C_{16}H_{33}$	349 → 396	2.78
18(Py)-S-2-S-(Py)18	1,2-ethanedithiol	$C_2H_4S_2$	Octadecyl	$C_{18}H_{37}$	377 → 424	2.63
12-7NH-12	Dipropylamine	$C_6H_{13}N$	Dodecyl	$C_{12}H_{25}$	263 → 356	7.12
Py-3-12	Propyl	C_3H_6	Dodecyl, Hexapyrenyl,	$C_{12}H_{25}$, $C_{22}H_{23}$	293 → 417	2.96

All tested compounds eluted before 4 minutes making the analysis a very fast approach for varying gemini surfactant structures. The only exception is 12-7NH-12 eluting at 7.12 min (Table 3.2); this compound contains a secondary amine within the spacer region. Therefore, it bears increased polarity within its structure leading to an overall stronger interaction and retention on the zwitterionic sulfoalkylbetaine stationary phase (ZIC®-HILIC column).

In addition, the HILIC-LC-MS/MS platform demonstrated a capability in allowing for the analysis and differentiation of isobaric gemini surfactants, namely 16-7-16 and 18-3-18 (identical composition $C_{43}H_{92}N_2^{2+}$, $[M]^{2+}$ *m/z* 318). The differentiation of the isobaric gemini surfactants

relied on the established characteristic chromatographic retention behaviour in combination with the analyte's unique mass spectrometric fingerprints (Table 3.2). Finally, it is worth noting that the developed method was not only applicable to the two classes of gemini surfactants, but it was also capable of separating the gemini surfactant Py-3-12, which contains two asymmetric tails, dodecyl chain and fluorescent pyrenyl-hexyl tail. The gemini surfactant Py-3-12 is generally used as a fluorescence probe for studying DNA complexation with gemini surfactants in addition to its gene transfection potential.[28,29]

3.4.2 Method validation for bio-analysis of 16(Py)-S-2-S-(Py)16 and 16-3-16

The method validation established the robustness of the HILIC-LC-MS/MS method for the bio-analysis of two specific gemini surfactants, 16(Py)-S-2-S-(Py)16 and 16-3-16, in accordance with USFDA guidelines.[27] Full method validation was established for these two promising molecules as they are currently being evaluated at the pre-clinical stage, assessing their toxicity alongside gene transfer capabilities. All method validation parameters are summarized in Table S3.2 (supplementary materials).

3.4.3 Selectivity and matrix effects

Selectivity was achieved as illustrated for both 16(Py)-S-2-S-(Py)16 and 16-3-16 gemini surfactants as shown in Figure 3.2 and Figure S3.7 (supplementary materials), respectively. Figure 3.2A shows that no analyte peaks were detected in "double blank" samples, which represent the matrix background and contain neither the analyte nor the internal standard. This indicates the absence of interference from endogenous cellular components against the selective bio-determination of the 16(Py)-S-2-S-(Py)16. Also, no cross-interference occurred between the

analytes and the internal standards as show by Figure 3.2B and Figure 3.2C, representing separate LC-MS/MS runs for 16(Py)-S-2-S-(Py)16-$\boldsymbol{d_{10}}$ and 16(Py)-S-2-S-(Py)16, respectively. Similar data for 16-3-16 is shown in the supplementary materials (Figure S3.2).

The cellular matrix did not have an effect on the ionization efficiency, that is, neither ionization enhancement nor suppression was observed. The matrix effect was calculated to be approximately 101% for both 16(Py)-S-2-S-(Py)16 and 16-3-16 (criteria: >100% indicates enhancement, <100% indicates suppression). Determination of the matrix effect followed the method of Matuszewski *et al*,[30] as given below:

$$\text{Matrix effect}(\%) = \frac{\text{Response post-extraction spiked sample}}{\text{Response non-extracted neat sample}} \times 100 \qquad (1);$$

where the post-extraction spiked sample refers to standards spiked after extraction and contains the standard analyte added to extracted blank cell lysate. The non-extracted neat sample contains the analyte added to octanol (pure, cellular matrix-free). The determined value is the average for a set of 6 replicates.

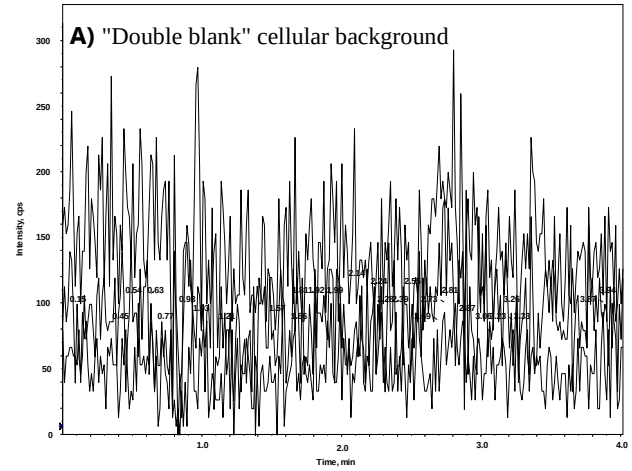
A) "Double blank" cellular background
Intensity, cps
Time, min

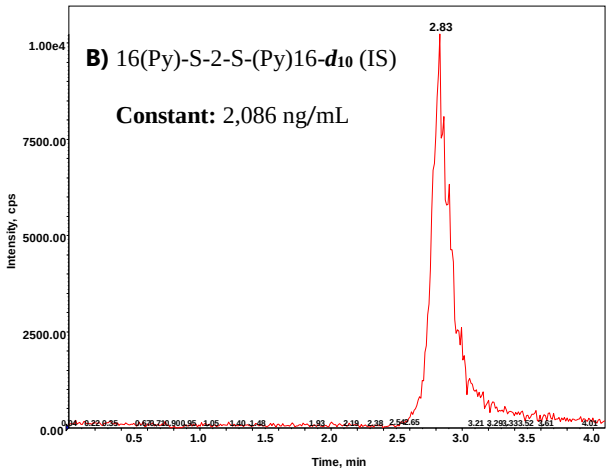
B) 16(Py)-S-2-S-(Py)16-d10 (IS)
Constant: 2,086 ng/mL
2.83
Intensity, cps
Time, min

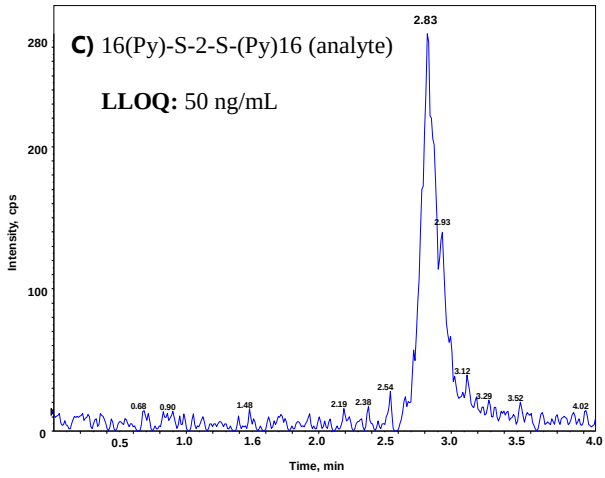
C) 16(Py)-S-2-S-(Py)16 (analyte)
LLOQ: 50 ng/mL
2.83
2.93
Intensity, cps
Time, min

Figure 1.2: Chromatograms of the 16(Py)-S-2-S-(Py)16 and 16(Py)-S-2-S-(Py)16-d_{10} gemini surfactants, i.e., the analyte and IS, respectively. Panel **A** indicates the absence of any interference against the selective determination of both 16(Py)-S-2-S-(Py)16 and 16(Py)-S-2-S-(Py)16-d_{10} by showing the detection of no signals around the established HILIC-LC-MS/MS elution times of these compounds within "double blank" cell samples. **B**) chromatogram from an injection of only 16(Py)-S-2-S-(Py)16-d_{10} and **C**) Chromatogram from an injection of only 16(Py)-S-2-S-(Py)16 at lower limit of quantitation, LLOQ. No cross-interference occurred between 16(Py)-S-2-S-(Py)16 and 16(Py)-S-2-S-(Py)16-d_{10}.

3.4.4 Calibration curve linearity and sensitivity

The calibration curves for the 16(Py)-S-2-S-(Py)16 and 16-3-16 gemini surfactant analytes were linear at a concentration range of 50 – 5000 ng/mL, with an r^2 value ≥ 0.997 as shown in Figure S3.8 (supplementary materials). Figure 3.3 shows a representative chromatograms for 16(Py)-S-2-S-(Py)16 at 6, 50 and 5,000 ng/mL. The lower limit of quantitation (LLOQ), 50 ng/mL, was accepted as it met the USFDA guideline for the 20% reproducibility for accuracy and precision. The concentration determined as the lower limit of detection (LLOD) was based on a set limit of S/N ≥ 3; this led to an LLOD of 6 ng/mL for 16(Py)-S-2-S-(Py)16, (Figure 3.3C). The LLOD for 16-3-16 was 3 ng/mL, with corresponding chromatograms given in the supplementary information (Figure S3.9).

HILIC-LC-MS/MS showed a substantially higher sensitivity in comparison with a recent cyano-based stationary phase LC-MS/MS method for the cellular analysis of 16-316 gemini

surfactant, with reported LLOD of 180 ng/mL and LLOQ of 300 ng/mL.[15] With the reported cyano-LC-MS/MS method, triethylamine (TEA) along with gradient elution were needed and the analyte extraction from aqueous medium utilized *n*-octanol which had a 71% recovery.[15] In the current work, the increased limit of detection up to 60-fold over previous work can be attributed to the change to the utilization of HILIC chromatography, coupled with the exclusion of the ion-pairing reagent, TEA, and better analyte recovery using the Bligh/Dyer lipid extraction method.[25]

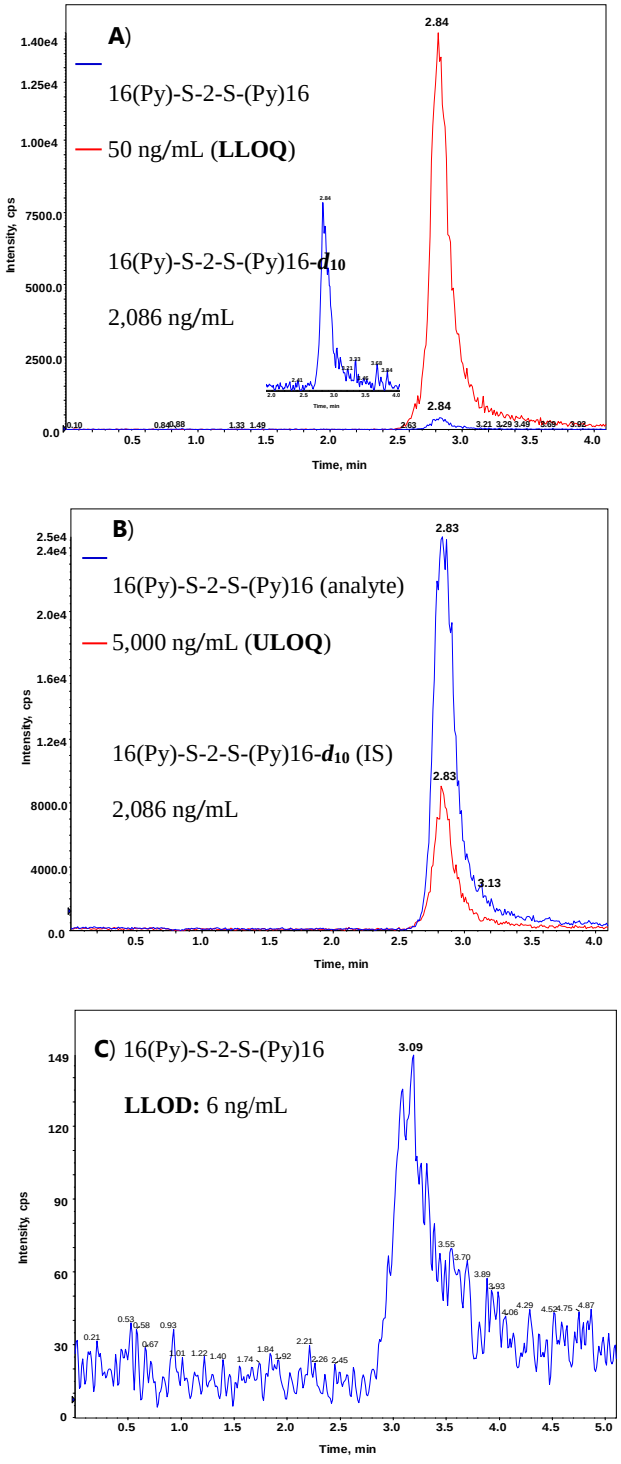

Figure 1.3: Chromatograms of the 16(Py)-S-2-S-(Py)16 gemini surfactant at LLOQ, ULOQ and LLOD. The relative response signal is shown for the analyte at: **A**) LLOQ – insert is a

zoomed in spectrum of the analyte and **B**) ULOQ in relation to the internal standard, 16(Py)-S-2-S-(Py)16-d_{10}, which was present at a constant concentration. **C**) Extracted ion chromatogram for 16(Py)-S-2-S-(Py)16 at LLOD.

3.4.5 Recovery

Liquid-liquid extraction of the 16(Py)-S-2-S-(Py)16 gemini surfactant analytes gave more than 96% recovery using the Bligh⁄Dyer lipid extraction method while the recovery was 67.5-73.9% for octanol extraction (Table 3.3). The corresponding data for 16-3-16 is available in the supplementary materials (Table S3.3) showing similar trends. The recovery values were computed as proposed by Matuszewski *et al*,[30]:

$$\text{Recovery}(\%) = \frac{\text{Response from extracted cells}}{\text{Response from spiked extracted cells}} \times 100 \qquad (2);$$

where the response from extracted cells refers to standards spiked before extraction where samples were processed as per the extraction procedure. Response from spiked extracted cells refers to known standards spiked after the extraction procedure was employed on cells.

Table 1.3. Recovery of 16(Py)-S-2-S-(Py)16 from the aqueous cellular matrix.

Theoretical concentration	Bligh⁄Dyer extraction			***Octanol*** extraction		
	Extracted cells (mean ± SD, ng⁄mL)	**Spiked extracted cells** (mean ± SD, ng⁄mL)	Recovery (%)	**Extracted cells** (mean ± SD, ng⁄mL)	**Spiked extracted cells** (mean ± SD, ng⁄mL)	Recovery (%)
16(Py)-S-2-S-(Py)16						
50 ng⁄mL (LLOQ)	47.44 ± 4.73	48.31 ± 3.74	96.2	32.88 ± 4.42	48.73 ± 4.74	67.5
150 ng⁄mL (LQC)	151.16 ± 10.61	155.36 ± 9.31	97.3	104.51 ± 11.02	145.36 ± 8.98	71.9
375 ng⁄mL (MQC)	369.75 ± 41.33	377.68 ± 37.93	97.9	270.87 ± 19.16	375.68 ± 47.92	72.1
4375 ng⁄mL (HQC)	4309.51 ± 359.41	4344.25 ± 222.53	99.2	3209.64 ± 179.11	4343.22 ± 182.33	73.9

For the separate extraction methods, the average recoveries were consistent for replicate determinations and were equal for the analyte (at three concentrations: lower, middle and upper limit of quantitation). With such improved recovery (Figure 3.4 and Figure S3.10 in supplementary materials), our routine analyte extractions adopted the Bligh/Dyer extraction for its better efficiency, increasing the sensitivity of the LC-MS/MS method.

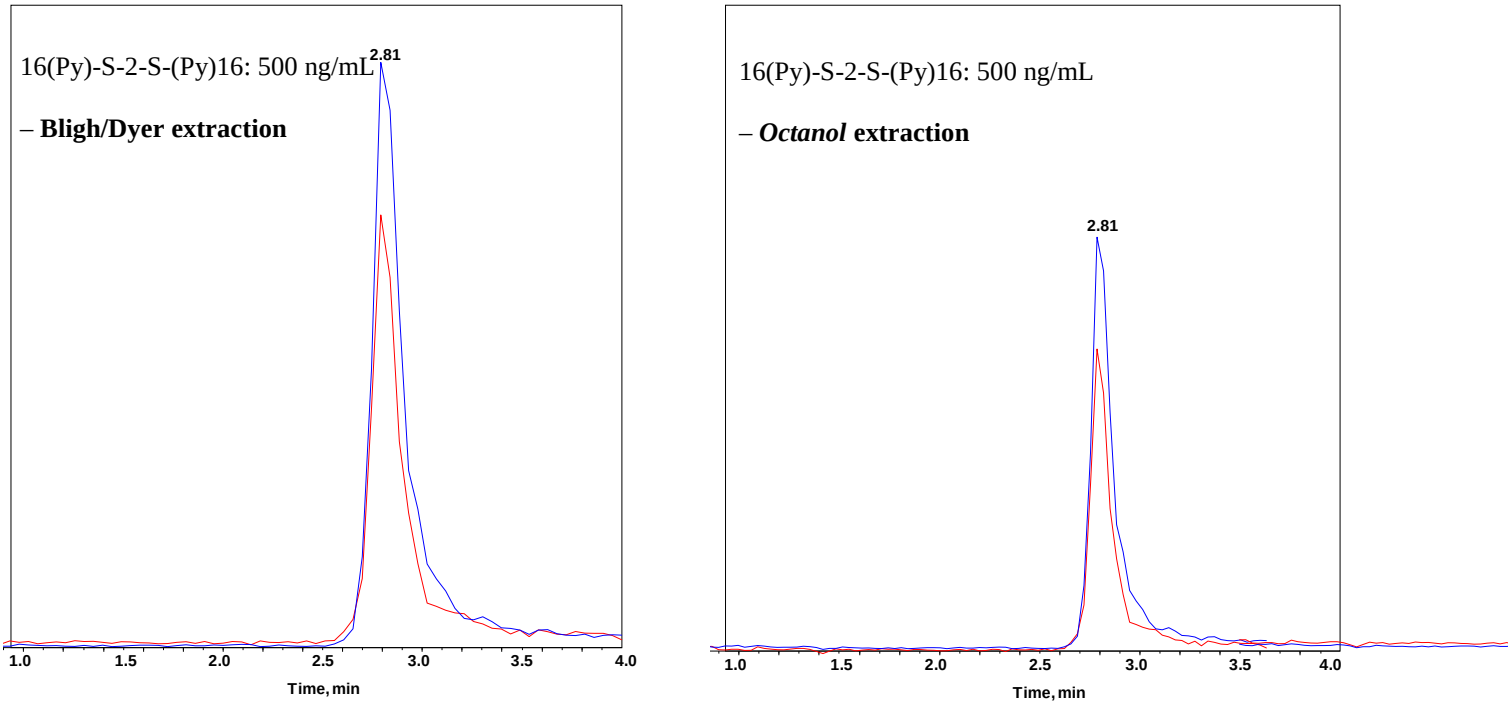

Figure 1.4: Analyte recovery efficiencies for Bligh/Dyer lipid extraction vs octanol extraction. Bligh/Dyer lipid extraction gave a better recovery (typically 98%) of the analyte and was the chosen liquid-liquid extraction method, departing from a recent report in which

octanol extraction (70% efficiency) was used. Unsurprisingly, the new HILIC-LC-MS/MS methods reported herein show better sensitivity (60-fold increase).

3.4.6 Accuracy and precision

In general, the validated method satisfied the USFDA-recommended accuracy and precision limits for all standard curve and quality control samples. Table 3.4 shows the accuracy and precision obtained for 16(Py)-S-2-S-(Py)16 gemini surfactant at four concentrations chosen per USFDA guidelines: LLOQ, LQC, MQC and HQC (corresponding data for 16-3-16 are available in the supplementary information, Table S3.4). For both the intra- and inter-day experiments, the accuracy (computed by expressing the observed concentrations as percentage of the theoretical values) varied between ~92 – ~110%. For precision, the values were within ~3 – ~11% relative standard deviation for both intra- and inter-day cases.

Table 1.4. Intra- and inter-day accuracy and precision in the analysis of 16(Py)-S-2-S-(Py)16.

Quality Control		Observed concentration (mean ± SD, ng/mL)	Accuracy (%)	Precision (%RSD)
INTRA-DAY:	Analysis Day (#)			
LLOQ: 50 ng/mL	Day 1	46.44 ± 4.73	92.9	10.2
	Day 2	51.26 ± 5.08	102.5	9.9
	Day 3	55.06 ± 3.33	110.1	6.0
LQC: 150 ng/mL	Day 1	145.96 ± 8.61	97.3	9.0

	Day 2	154.64 ± 13.9	103.1	8.4
	Day 3	161.14 ± 9.99	107.4	6.2
MQC: 375 ng/mL	Day 1	363.75 ± 11.33	97.0	3.1
	Day 2	393.36 ± 21.73	104.9	5.5
	Day 3	369.03 ± 19.77	98.4	5.4
HQC: 4375 ng/mL	Day 1	4032.50 ± 359.41	92.2	8.9
	Day 2	4411.38 ± 272.55	100.8	6.2
	Day 3	4321.99 ± 323.09	98.8	7.5
INTER-DAY:				
	Concentration			
LLQC	50 ng/mL	51.15 ± 4.84	102.3	9.7
LQC	150 ng/mL	157.25 ± 10.84	104.8	7.7
MQC	375 ng/mL	375.38 ± 17.61	100.1	4.7
HQC	4375 ng/mL	4255.29 ± 318.53	97.3	7.5

3.4.7 Stability

Both the 16(Py)-S-2-S-(Py)16 and 16-3-16 analytes were stable beyond 24 h when stored at room temperature (bench top stability) and long-term stability when stored at –20 ˚C (Table 3.5, Table S3.5). The analytes also showed very good freeze/thaw stability after three freeze/thaw cycles. The autosampler stability was within USFDA guidelines for accuracy/precision and was determined for samples re-injected for analysis for up to two consecutive days. Overall, the stabilities were within ~96 – ~105% accuracy and ~2 – ~9% precision for all the determinations (Table 3.5, Table S3.5).

Table 1.5. Stability of 16(Py)-S-2-S-(Py)16 analyte within the sample matrix.

Quality Control	Storage condition/ period	Observed concentrations (mean ± SD, ng/mL)	Accuracy (%)	Precision (%RSD)
LQC: 150 ng/mL	0 h	150.33 ± 11.14	102.3	9.7
	24 h on bench top	148.83 ± 10.04	99.3	7.7
	Three freeze/thaw cycles	145.87 ± 13.13	94.3	8.5
	–20 ˚C for 105 days (LT)	146.16 ± 9.91	96.7	10.1
	48 h extract in autosampler	150.15 ± 8.43	96.6	9.2
MQC: 375 ng/mL	0 h	365.03 ± 18.18	102.3	9.7
	24 h on bench top	381.73 ± 17.98	99.3	7.7
	Three freeze/thaw cycles	355.05 ± 18.17	94.3	8.5
	–20 ˚C for 105 days (LT)	355.22 ± 18.68	96.7	10.1
	48 h extract in autosampler	375.88 ± 15.76	96.6	9.2
HQC: 4375 ng/mL	0 h	4358.23 ± 198.08	102.3	9.7
	24 h on bench top	4398.23 ± 201.27	99.3	7.7
	Three freeze/thaw cycles	4151.53 ± 229.38	94.3	8.5
	–20 ˚C for 105 days (LT)	4324.56 ± 186.83	96.7	10.1
	48 h extract in autosampler	4308.93 ± 191.77	96.6	9.2

LT (long term): –20 ˚C for 105 days

3.4.8 Bio-analysis of P/G/L-nanoparticle-treated cells

Using the validated HILIC-LC-MS/MS methods, the uptake and intracellular deposition profile of the 16(Py)-S-2-S-(Py)16 and 16-3-16 gemini surfactants was studied within PAM 212 cells which had been treated with the gemini surfactant-containing P/G/L-nanoparticles. Figure 3.5 shows the intracellular concentration vs. time profile for 16(Py)-S-2-S-(Py)16 and 16-3-16. The intracellular concentration of the analyte increased rapidly throughout the 5-h duration when the administered nanoparticles remain in contact with cells, followed by a noticeable decrease within the next 5 h after removal of the nanoparticle-dosed supernatant culture media. The intracellular amount rose to 900 ng (maximum) with the initial increase followed by subsequent decreased by ~60%. A similar trend was observed in the case of 16-3-16; however, its intracellular amount rose to 400 ng (maximum) while its subsequent decrease of ~40% occured less rapidly than that observed for 16(Py)-S-2-S-(Py)16.

The above observations are consistent with a progressive nanoparticle uptake, which reached a maximum before a seeming depletion of the intracellular analyte. For both analytes, an observed intracellular remnant proportion did not undergo further depletion within the intracellular investigation lasting 54-h. For the 16-3-16 gemini surfactant, its partial depletion from the host cells is in disagreement with our recent reports[15,16] showing no depletion of this compound. The apparent discrepancy is attributed to differences in the extraction method and the extensive washing of treated cell cultures in the present work. Adequate washing steps were not conduced in the past work. Gemini surfactants tend to be adherent to bio-membranes and to plastics including walls of plastic cell culture containers. The washing was thus critical for

eliminating potential gemini surfactant that is adherent to plastic walls or loosely adsorbed to exterior cell surfaces.

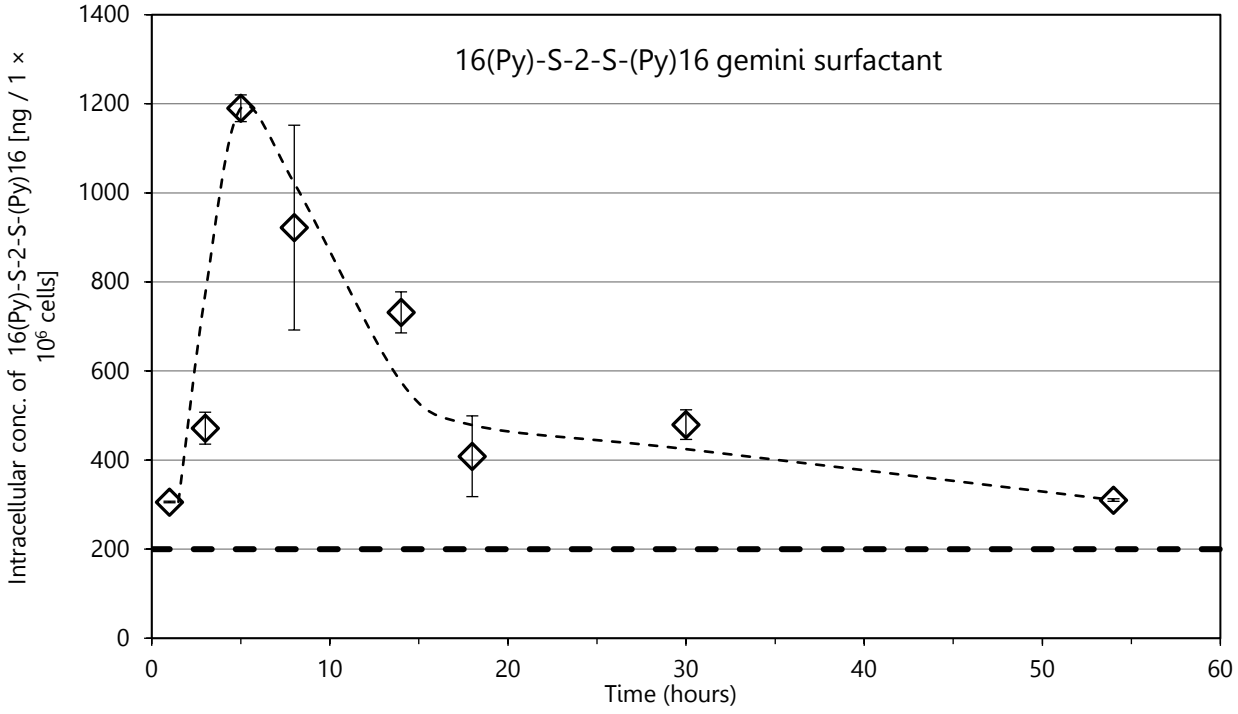

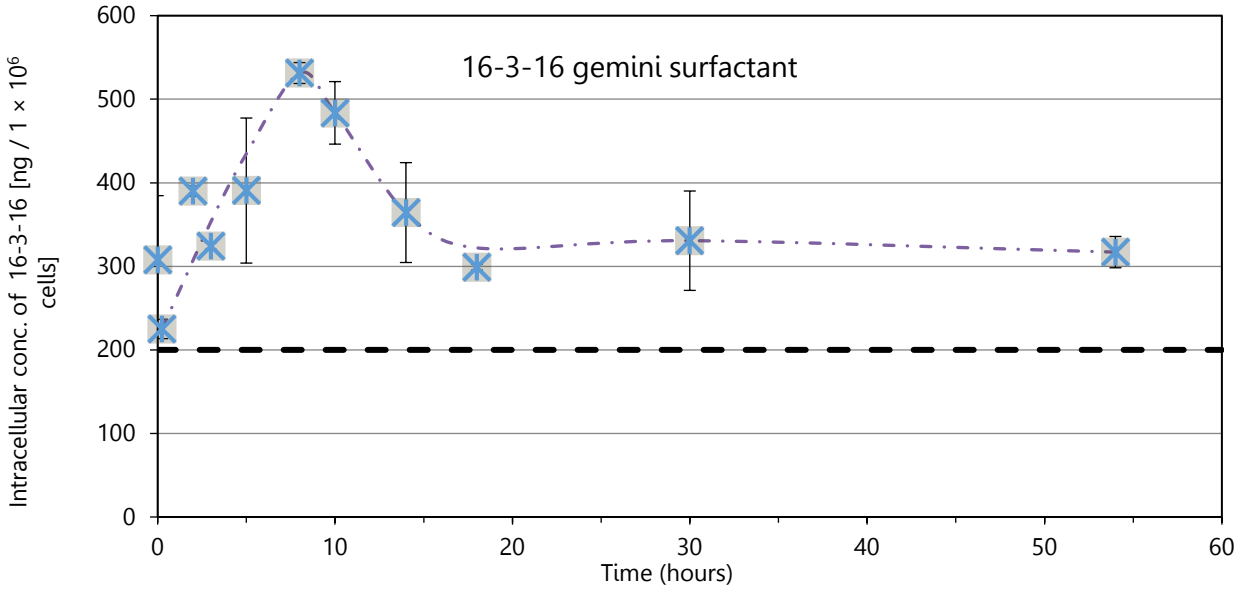

Figure 1.5: Representative experiments showing the intracellular concentration vs. time profile of the gemini surfactants, 16(Py)-S-2-S-(Py)16 (top panel) and 16-3-16 (bottom panel). The intracellular concentration increased progressively throughout the duration of nanoparticle administration to cells, followed by a gradual decrease after removal of the nanoparticle-dosed supernatant culture media. The dashed horizontal line "y-axis = 200 ng/mL" shows that the results is reported only for data with concentration above 200 ng/mL as noted under *Section 3.8*. Each plotted data point represents mean ± SD, n = 3.

To verify the methodology and results, the cell transfection experiments and the subsequent LC-MS/MS quantification procedures were repeated. The results reported attests to the reproducibility of the methods and consistency of the quantitative results on the uptake and subsequent intracellular profile of the investigated gemini surfactants.

3.5 Discussion

The present study describes the development of novel fast and simple HILIC-MRM-MS/MS methods that were applicable to 18 gemini surfactants with varying molecular structures (Table 3.2). To-date, only one LC-MS/MS method has been reported for the quantification of gemini surfactants[15] but was only applicable to one class of gemini surfactants, the m-s-m family. This gives importance to the demonstrated applicability of the HILIC-LC-MS/MS platform to different structures of gemini surfactants.

The choice of HILIC chromatography (with sulfoalkyl betaine-based zwitterionic stationary phase, ZIC-HILIC column[31,32]) contributed to a high sensitivity, which is 60-fold higher in terms of LLOD relative to the sensitivity of the method reported for the analysis of 16-3-16.[15] Our choice of the ZIC-HILIC column, based on its compatibility with the diquaternary ammonium gemini surfactant analytes through $^{+}N/^{-}SO_3$ HILIC mode interaction, led to more efficient chromatographic separation. Unlike the previous method,[15] no ion pairing reagent (i.e. TEA) was needed resulting in better ionization efficiency within the ESI source. TEA can compete for ionization within the ESI source resulting in undesirable ion suppression. Another major advantage of the HILIC-MS/MS is the use of isocratic elution rather than gradient system. In fact, the isocratic option was not possible when the *cyano* column was utilized.[15]

The mobile phase was optimized to ensure that retention times are established to correlate with the gemini surfactant structural properties; a low buffer concentration (2.5 mM formate) was used. This buffer concentration (lower than concentrations of up to 50 mM in some cases) allows the chance for dominant interaction between the stationary phase and the analyte so that the gemini surfactants can display specific retention times as a result of their different structural

features. Here, an added potential benefit is that low buffer concentrations are associated with better sensitivity as opposed to high buffer concentrations. In addition, the buffered mobile phase was optimized to pH 6.2; deviation from this pH resulted in weak and inconsistent response as well as unstable retention times. The HILIC system is very sensitive to variations in analytical conditions including pH and temperature. In fact, deviation from the optimized column temperature resulted in increased pressure within the column thus preventing chromatographic separation.

In addition to adopting HILIC chromatography, a high efficiency analyte recovery was achieved through the use of Bligh/Dyer lipid extraction. Bligh/Dyer method uses 2:1 (v/v) methanol/chloroform binary extractant-solvent allowing for high compatibility with the gemini surfactants' amphiphilic nature[25] (as defined by having both hydrophobic and hydrophilic moieties, Figure 3.1). In fact, we have previously employed liquid-liquid extraction using either methanol or octanol with 63% and 70% recoveries[16], respectively. While methanol may favor the solubilisation of the hydrophilic component within gemini surfactants, octanol is more compatible with the hydrophobic elements. The methanol/chloroform system of the Bligh/Dyer method can, therefore, solubilize both components within gemini surfactants resulting in approximately 98% extraction efficiency. The high recovery is clearly illustrated in Figures 3.6 and S3.11 in which a direct comparison with octanol extraction is shown. Overall, the superior sensitivity achieved for the reported HILIC-LC-MS/MS method underscores a strategic use of HILIC chromatography in conjunction with high analyte extraction efficiency and a suitable mobile phase.

Data from the analysis of nanoparticle-treated cells showed an initial rise in the analyte intracellular concentration followed by a maximum and a somewhat more gradual decrease of the intracellular analyte. Herein, the findings are consistent with a progressive nanoparticle uptake, which reached a steady state before a seeming depletion of the intracellular analyte. Two events that may account for the intracellular depletion of the gemini surfactant are its bio-transformation into metabolites and its exocytosis from the host cells. An advantage with LC-MS/MS includes its versatility that allows adapting the described method, with major or minor modifications, for the investigation of both bio-transformation and exocytosis. Accumulated data from such superior HILIC-LC-MS/MS bio-analyses of lipid-based nanoparticles should uncover structure-property-activity relationship. The knowledge can impact decision regarding the safe use of biomedical nanoparticles as well as provide insights into engineering new nanoparticles.

3.6 Conclusion

Sensitive, robust and simple HILIC-LC-MS/MS methods for the determination of the 16(Py)-S-2-S-(Py)16 and 16-3-16 gemini surfactants in cells have been developed and fully validated according to USFDA. A high-efficiency liquid-liquid extraction was adopted along with a ZIC-HILIC column to attain high sensitivity and a run time of merely 4 minutes. The validated method is suitable for monitoring the fate of therapeutic nano-lipoplex within cells. In addition to cellular uptake shown in this study, we are currently investigation the intracellular deposition of gemini surfactants as well as metabolite formation. Such knowledge can shed light into the varying toxicities reported for gemini surfactants.[19,33] Finally, it should be noted that gemini surfactants have many other industrial applications[34] such as detergents, cosmetics and

solubilisation agents. The newly developed versatile HILIC-LC-MS/MS can serve as a starting point for the analysis of gemini surfactants regardless of the application.

3.7 Acknowledgements

The authors acknowledge the technical assistance provided by Ms. Deborah Michel and Dr. Joshua Buse for the 4000 QTRAP LC/MS/MS system. Ms. Hanan Awad and Ms. Mays Al-Dulaymi are duly acknowledged for conduction parallel independent experiments that helped verify the reproducibility of the methodology and analytical results. We also acknowledge the assistance of Drs. Ildiko Badea and Jackson Chitanda for their help in designing the transfection experiments and the synthesis of gemini surfactants, respectively. The 4000 QTRAP LC/MS/MS system was acquired via a Canada Foundation for Innovation (CFI) grant. The project was supported by a Natural Science and Engineering Research Council of Canada (NSERC)-Discovery grant.

3.8 References

[1] W. Mohammed-Saeid, D. Michel, A. El-Aneed, R. Verrall, N.H. Low, I. Badea, Development of Lyophilized Gemini Surfactant-Based Gene Delivery Systems: Influence of Lyophilization on the Structure, Activity and Stability of the Lipoplexes, Journal of Pharmacy and Pharmaceutical Sciences 15 (2012) 548-567.

[2] I. Badea, R. Verrall, M. Baca-Estrada, S. Tikoo, A. Rosenberg, P. Kumar, M. Foldvari, In vivo cutaneous interferon-gamma gene delivery using novel dicationic (gemini) surfactant-plasmid complexes, J Gene Med 7 (2005) 1200-1214.

[3] M. Donkuru, S.D. Wettig, R.E. Verrall, I. Badea, M. Foldvari, Designing pH-sensitive gemini nanoparticles for non-viral gene delivery into keratinocytes, J. Mater. Chem. 22 (2012) 6232-6244.

[4] A.J. Kirby, P. Camilleri, J.B. Engberts, M.C. Feiters, R.J. Nolte, O. Soderman, M. Bergsma, P.C. Bell, M.L. Fielden, C.L. Garcia Rodriguez, P. Guedat, A. Kremer, C. McGregor, C. Perrin, G. Ronsin, M.C. van Eijk, Gemini surfactants: new synthetic vectors for gene transfection, Angew Chem Int Ed Engl 42 (2003) 1448-1457.

[5] C. Bombelli, L. Giansanti, P. Luciani, G. Mancini, Gemini Surfactant Based Carriers in Gene and Drug Delivery, Current Medicinal Chemistry **16** (2009) 171–183.

[6] M. Donkuru, I. Badea, S. Wettig, R. Verrall, M. Elsabahy, M. Foldvari, Advancing nonviral gene delivery: lipid- and surfactant-based nanoparticle design strategies, Nanomedicine (Future Medicine) 5 (2010) 1103−1127.

[7] S.D. Wettig, R.E. Verrall, M. Foldvari, Gemini surfactants: a new family of building blocks for non-viral gene delivery systems, Curr Gene Ther 8 (2008) 9-23.

[8] C. Barton, R.G. Kay, W. Gentzer, F. Vitzthum, S. Pleasance, Development of high-throughput chemical extraction techniques and quantitative HPLC-MS/MS (SRM) assays for clinically relevant plasma proteins, J Proteome Res 9 (2010) 333-340.

[9] U. Chiuminatto, F. Gosetti, P. Dossetto, E. Mazzucco, D. Zampieri, E. Robotti, M.C. Gennaro, E. Marengo, Automated online solid phase extraction ultra high performance liquid chromatography method coupled with tandem mass spectrometry for determination of forty-two therapeutic drugs and drugs of abuse in human urine, Anal Chem 82 (2010) 5636-5645.

[10] B. Singh, S. Sharma, N. Dubey, A. Dwivedi, R.S. Lokhandae, Bioanalytical method development and validation of alimemazine in human plasma by LC-MS/MS and its application in bioequivalence studies, J Pharm Bioallied Sci 5 (2013) 257-264.

[11] W. Mohammed-Saeid, J. Buse, I. Badea, R. Verrall, A. El-Aneed, Mass spectrometric analysis of amino acid/di-peptide modified gemini surfactants used as gene delivery agents: Establishment of a universal mass spectrometric fingerprint, *Int. J. Mass Spectrom.* 309 (2012) 182–191.

[12] J. Buse, I. Badea, R.E. Verrall, A. El-Aneed, Tandem mass spectrometric analysis of novel diquaternary ammonium gemini surfactants and their bromide adducts in electrospray-positive ion mode ionization, J Mass Spectrom 46 (2011) 1060-1070.

[13] J. Buse, I. Badea, E.R. Verrall, A. El-Aneed, Tandem Mass Spectrometric Analysis of the Novel Gemini Surfactant Nanoparticle Families G12-s and G18:1-s, Spectroscopy Letters 43 (2010) 447–457.

[14] M. Donkuru, M.J. Chitanda, E.R. Verrall, A. El-Aneed, Multi-stage tandem mass spectrometric analysis of novel β-cyclodextrin-substituted and novel bis-pyridinium gemini surfactants designed as nanomedical drug delivery agents., Rapid Commun Mass Spectrom. 28 (2014) 757–772.

[15] J. Buse, I. Badea, R.E. Verrall, A. El-Aneed, A general liquid chromatography tandem mass spectrometry method for the quantitative determination of diquaternary ammonium gemini surfactant drug delivery agents in mouse keratinocytes' cellular lysate, J Chromatogr A 1294 (2013) 98-105.

[16] J. Buse, R.W. Purves, R. Verrall, I. Badea, H. Zhang, C.C. Mulligan, K.M. Peru, J. Bailey, J.V. Headley, A. El Aneed, The Development and assessment of high-throughput mass spectrometry-based methods for the quantification of a nanoparticle drug delivery agent in cellular lysate, J Mass Spectrom 49 (2014) 1139-1147.

[17] B. Buszewski, S. Noga, Hydrophilic interaction liquid chromatography (HILIC)—a powerful separation technique, Analytical and Bioanalytical Chemistry 402 (2012) 231-247.

[18] Y. Guo, Analysis of Quaternary Amine Compounds by Hydrophilic Interaction Chromatography/Mass Spectrometry (HILIC/MS), Journal of Liquid Chromatography & Related Technologies 28 (2005) 497-512.

[19] A. Bhadani, S. Singh, Novel gemini pyridinium surfactants: synthesis and study of their surface activity, DNA binding, and cytotoxicity, Langmuir 25 (2009) 11703-11712.

[20] S. Singh, A. Bhadani, H. Kataria, G. Kaur, R. Kamboj, Synthesis of Glycerol-Based Pyridinium Surfactants and Appraisal of Their Properties, Industrial & Engineering Chemistry Research 48 (2009) 1673-1677.

[21] I. van der Woude, A. Wagenaar, A.A. Meekel, M.B. ter Beest, M.H. Ruiters, J.B. Engberts, D. Hoekstra, Novel pyridinium surfactants for efficient, nontoxic in vitro gene delivery, Proc Natl Acad Sci U S A 94 (1997) 1160-1165.

[22] M. Donkuru, Non-viral gene delivery with pH-sensitive gemini nanoparticles: synthesis of gemini surfactant Building blocks, characterization and *in vitros*creening of transfection efficiency and toxicity, College of Pharmacy & Nutrition, Univeristy of Saskatchewan, Saskatoon, SK, Canada, 2008, pp. 205.

[23] S.D. Wettig, R.E. Verrall, Thermodynamic studies of aqueous m-s-m gemini surfactant systems, J. Colloid Interface Sci. 235 (2001).

[24] E.J. Richards, F.M. Ausubel, Isolation of a higher eukaryotic telomere from *Arabidopsis thaliana*, Cell 53 (1988) 127–136.

[25] E.G. Bligh, W.J. Dyer, A rapid method of total lipid extraction and purification, Can J Biochem Physiol 37 (1959) 911-917.

[26] M. Whitmire, J. Ammerman, P. de Lisio, J. Killmer, D. Kyle, E. Mainstone, L. Porter, T. Zhang, LC-MS/ MS Bioanalysis Method Development, Validation, and Sample Analysis: Points to Consider When Conducting Nonclinical and Clinical Studies in Accordance with Current Regulatory Guidances, J Anal Bioanal Tech S4 (2011) 1–10.

[27] Guidance for Industry: Bioanalytical Method Validation, in: F.a.D.A. USFDA, Center for Drug Evaluation and Research (CDER), Center for Veterinary Medicine (CV) (Ed.), 2001.

[28] S.D.D. Wettig, RubenaAkbar, JavedKaur, TranumWang, HaitangSheinin, TatianaJoseph, Jamie W.Slavcev, Roderick A., Thermodynamic investigation of the binding of dissymmetric pyrenyl-gemini surfactants to DNA, Phys Chem Chem Phys. 12 (2010) 4821–4826.

[29] C. Wang, S.D. Wettig, M. Foldvari, R.E. Verrall, Synthesis, Characterization, and Use of Asymmetric Pyrenyl-Gemini Surfactants as Emissive Components in DNA-Lipoplex Systems, Langmuir 23 (2007) 8995–9001.

[30] B.K. Matuszewski, M.L. Constanzer, C.M. Chavez-Eng, Strategies for the Assessment of Matrix Effect in Quantitative Bioanalytical Methods Based on HPLC−MS/MS, Analytical Chemistry 75 (2003) 3019–3030.

[31] T. Jonsson, P. Appelblad, Separation of Polar and Hydrophilic Compounds Using a Zwitterionic Stationary Phase in Hydrophilic Interaction Liquid Chromatography Separation of Polar and Hydrophilic Compounds Using a Zwitterionic Stationary Phase, LC-GC Eur 17 (2004) 40–41.

[32] P. Appelblad, T. Jonsson, W. Jiang, K. Irgum, Fast hydrophilic interaction liquid chromatographic separations on bonded zwitterionic stationary phase, J. Sep Sci. 31 (2008) 1529−1536.

[33] S.D. Wettig, I. Badea, M. Donkuru, R.E. Verrall, M. Foldvari, Structural and transfection properties of amine-substituted gemini surfactant-based nanoparticles, J Gene Med 9 (2007) 649-658.

[34] N. Kumar, R. Tyagi, Industrial Applications of Dimeric Surfactants: A Review, Journal of Dispersion Science and Technology 35 (2014) 205-214.

3.9 Supplementary Information

Supplementary Figure S3.9.1

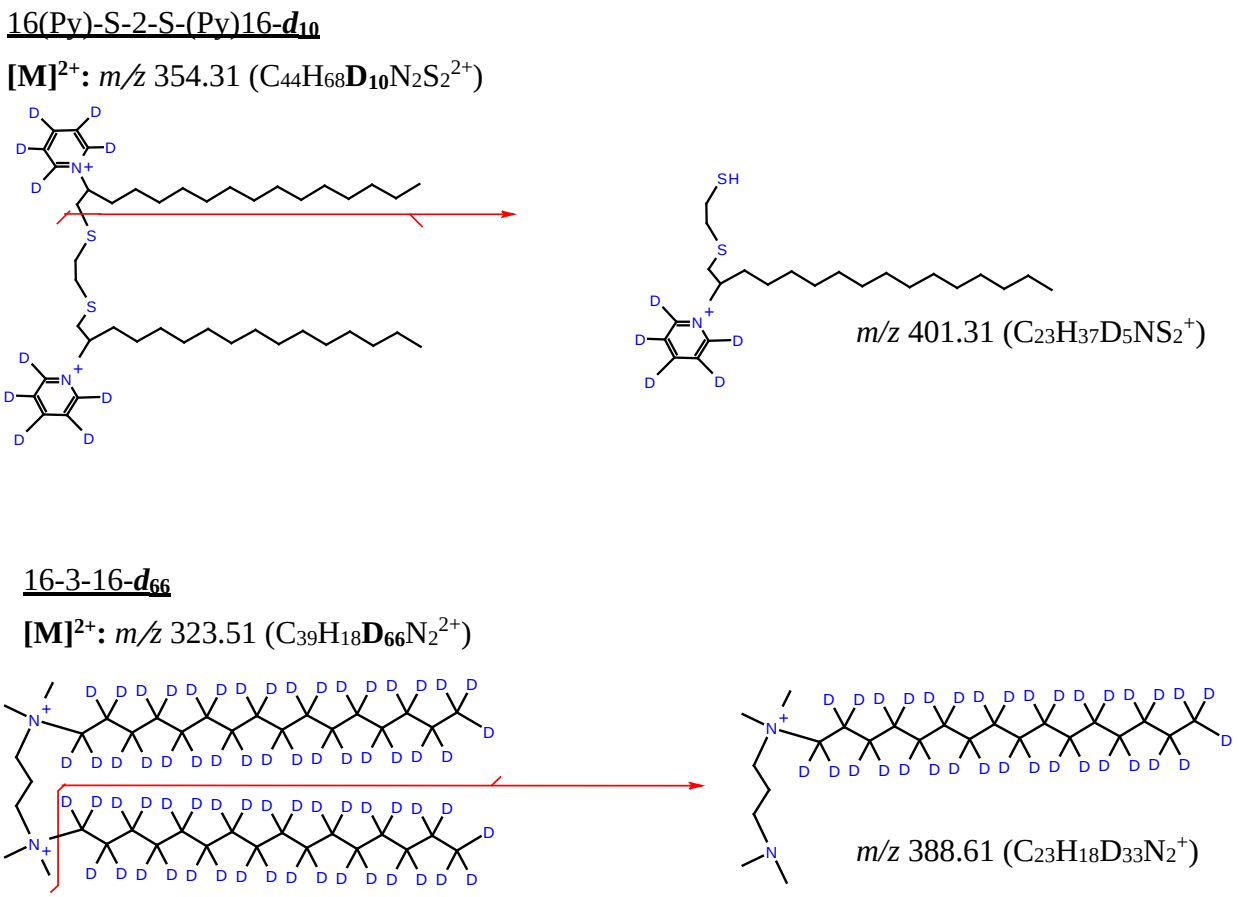

Figure S1.6: Product ions monitored for the internal standards 16(Py)-S-2-S-(Py)16-***d*₁₀ and 16-3-16-***d*₆₆ during HILIC-LC-MS/MS analysis.

Supplementary Figure S3.9.2

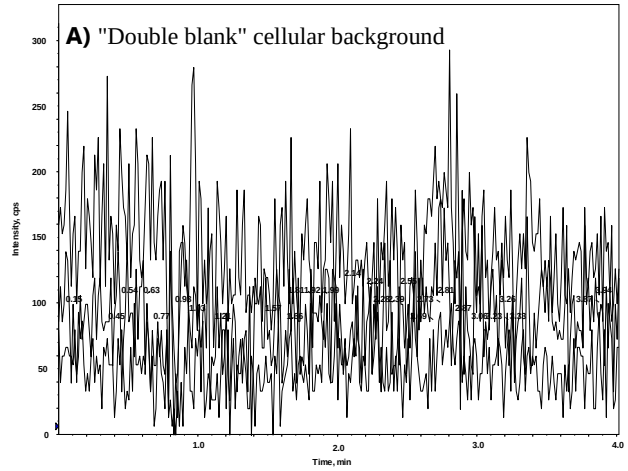

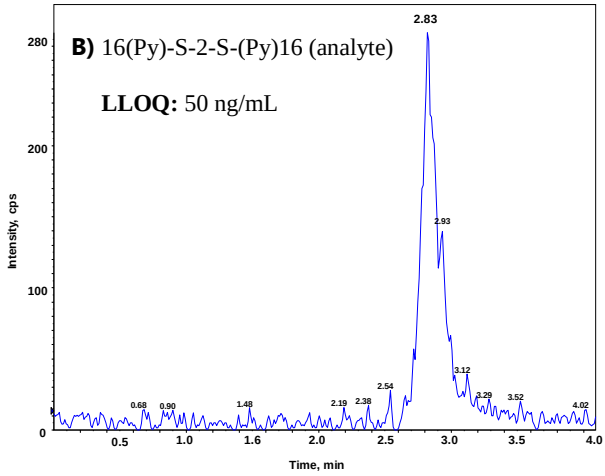

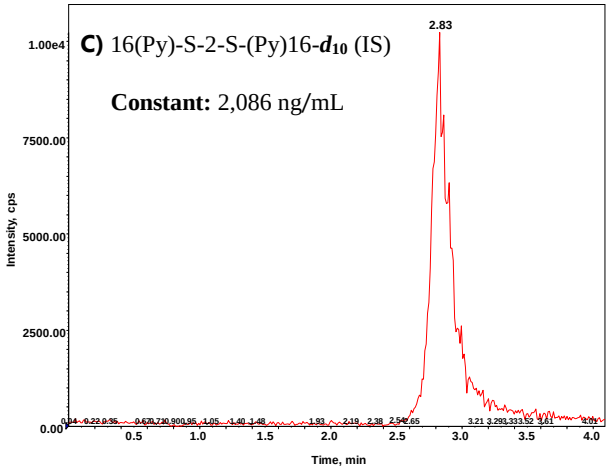

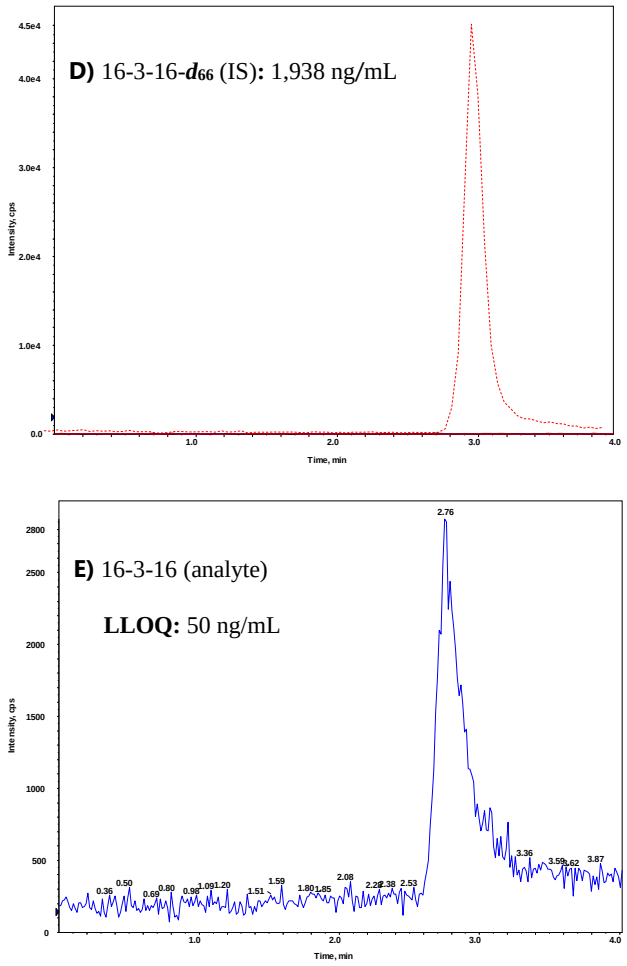

Figure S1.7: Chromatograms of the gemini surfactants, 16(Py)-S-2-S-(Py)16, 16-3-16, 16(Py)-S-2-S-(Py)16-d_{10}, 16-3-16-d_{66}. [Panel **A** indicates the absence of any interference against the selective determination of all four compounds by showing the detection of no signals around the established HILIC-LC-MS/MS elution times of these compounds within "double blank" cell samples. **B**) chromatogram from an injection of only 16(Py)-S-2-S-(Py)16-d_{10} and **C**) Chromatogram from an injection of only 16(Py)-S-2-S-(Py)16 at lower limit of quantitation, LLOQ. No cross-interference occurred between 16(Py)-S-2-S-(Py)16 and 16(Py)-S-2-S-(Py)16-d_{10}]. **D**) Chromatogram from an injection of only 16-3-

16; and, **E**) Chromatogram from an injection of only 16-3-16-$\boldsymbol{d_{66}}$. No cross-interference occurred between 16-3-16 and 16-3-16-$\boldsymbol{d_{66}}$ since the injections produced signal for only the respective but not both compounds. In general, the chromatograms showed symmetry and smoothness for quantitative analysis as shown.

Supplementary Figure S3.9.3

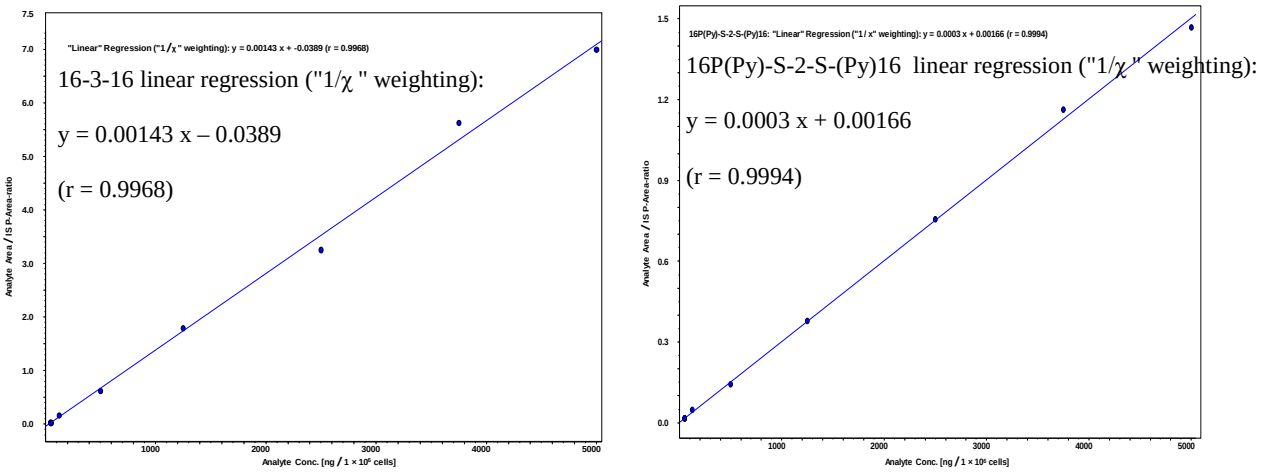

Figure S1.8: Calibration curves for the 16-3-16 and 16(Py)-S-2-S-(Py)16 gemini surfactants. In both cases, the linear range was 50 – 5000 ng/[1 × 10^6 cells], $r^2 \geq 0.99$.

Supplementary Figure S3.9.4

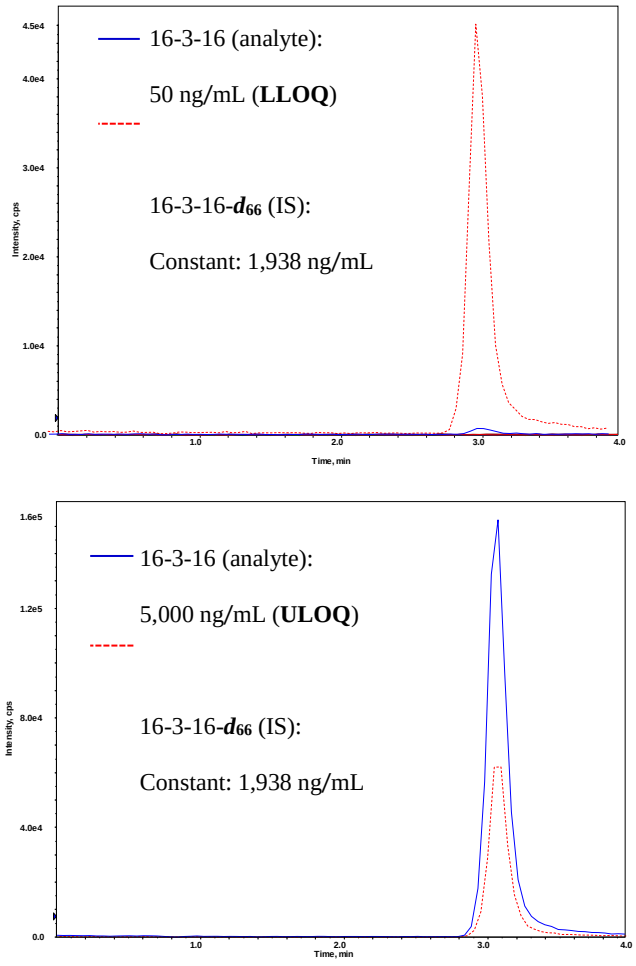

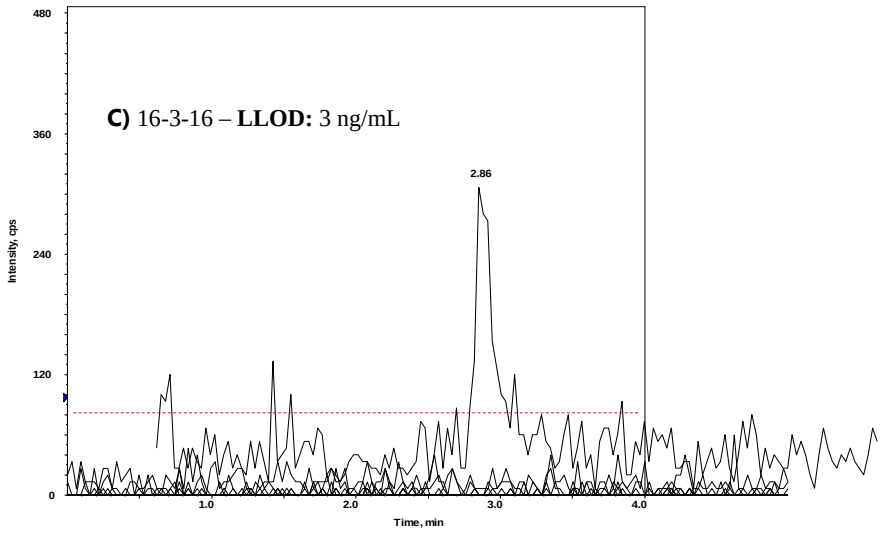

Figure S1.9: Chromatograms of the 16-3-16 gemini surfactant at LLOQ, ULOQ and LLOD. The relative response signal is shown for the analyte at: **A**) LLOQ and **B**) ULOQ in relation to the internal standard, 16-3-16-d_{66}, which was present at a constant concentration. **C**) Extracted chromatogram for 16-3-16 at LLOD.

Supplementary Figure S3.9.5

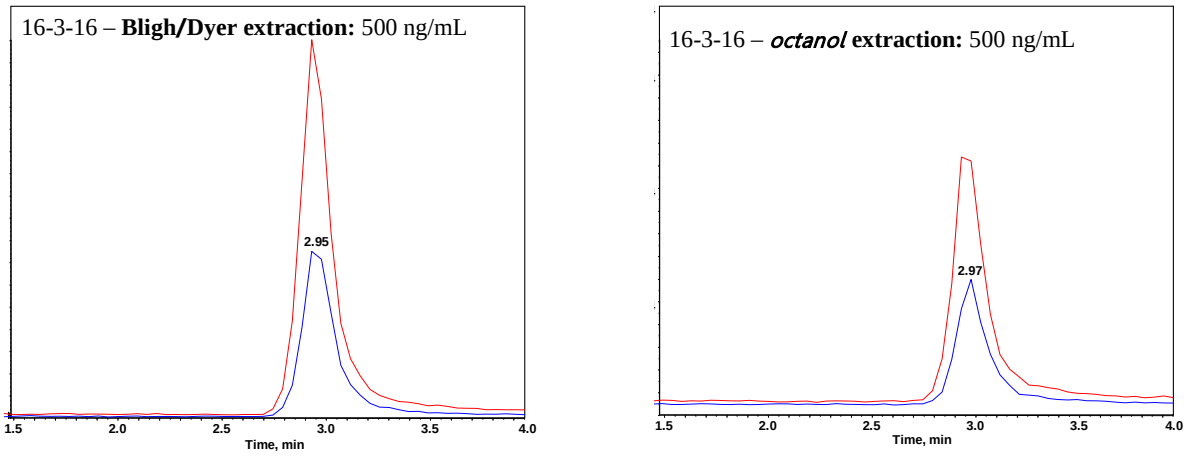

Figure S1.10: Contrasting analyte recovery efficiencies for Bligh/Dyer lipid extraction vs *octanol* extraction. Bligh/Dyer lipid extraction gave a better recovery (typically 98%) of the analyte and was the chosen liquid-liquid extraction method, departing from a recent report in which octanol extraction (70% efficiency) was used.

Table S1.6. Gemini surfactant mass concentrations equivalent to 3 mM molarity.

Gemini surfactant	Mass concentration (≈ 3 mM)
12(Py)-S-2-S-(Py)12	2.24 mg/mL
14(Py)-S-2-S-(Py)14	2.40 mg/mL
16(Py)-S-2-S-(Py)16	2.57 mg/mL
18(Py)-S-2-S-(Py)18	2.74 mg/mL
16-3-16	2.22 mg/mL
16-7-16	2.39 mg/mL
12-3-12	1.88 mg/ml
12-4-12	1.92 mg/mL
12-8-12	2.09 mg/mL
12-10-12	2.18 mg/mL
12-12-12	2.26 mg/mL
12-16-12	2.43 mg/mL
18-3-18	2.39 mg/ml
18-7-18	2.55 mg/mL
18:1-3-18:1	2.37 mg/mL
18:1-6-18:1	2.50 mg/mL
12-7NH-12	2.05 mg/mL
Py-3-12	2.24 mg/mL

Table S1.7. Overview of the HILIC-LC-MS/MS method validation parameters.

Analyte	16(Py)-S-2-S-(Py)16	16-3-16
Internal standard (IS)	16(Py)-S-2-S-(Py)16-d_{10}	16-3-16-d_{66}
Method description	LLE, HILIC-LC-MS/MS	LLE, HILIC-LC-MS/MS
QC range	150 – 4375 ng/mL	150 – 4375 ng/mL
Calibration curve range	50 – 5000 ng/mL	50 – 5000 ng/mL
Lower limit of detection (LLOD)	6 ng/mL	3 ng/mL
Average analyte recovery	97.7% (Bligh/Dyer method)	98.2% (Bligh/Dyer method)
Intra-day accuracy range	92 – 110%	92 – 110%
Intra-day precision range	3 – 11%	3 – 11%
Inter-day accuracy range	92 – 110%	92 – 110%
Inter-day precision range	3 – 11%	3 – 11%
Bench-top stability (hrs)	24	24
Autosampler stability (hrs)	48	48
Freeze-thaw stability (cycles)	3	3
Long-term stability (days)	105	105
Specificity (i.e., matrix effects)	No net matrix effects	No net matrix effects

Table S1.8. Recovery of 16-3-16 (analyte) from the aqueous cellular matrix.

Theoretical concentration	Bligh/Dyer extraction			***Octanol*** extraction		
	Extracted cells (mean ± SD, ng/mL)	**Spiked extracted cells** (mean ± SD, ng/mL)	Recovery (%)	**Extracted cells** (mean ± SD, ng/mL)	**Spiked extracted cells** (mean ± SD, ng/mL)	Recovery (%)
16-3-16						
50 ng/mL (LLOQ)	48.24 ± 5.73	49.38 ± 3.74	97.7	36.38 ± 5.02	52.21 ± 4.74	69.7
150 ng/mL (LQC)	147.19 ± 13.61	150.53 ± 15.31	97.8	114.51 ± 8.72	159.26 ± 11.38	71.9
375 ng/mL (MQC)	371.57 ± 51.33	383.46 ± 47.32	96.9	277.87 ± 33.16	385.06 ± 37.92	72.2
4375 ng/mL (HQC)	4359.45 ± 359.41	4368.17 ± 212.57	100.2	3210.64 ± 179.11	4528.22 ± 182.33	70.9

Table S1.9. Intra- and inter-day accuracy and precision in the analysis of 16-3-16.

Quality Control		Observed concentration (mean ± SD, ng/mL)	Accuracy (%)	Precision (%RSD)
INTRA-DAY:	Analysis Day (#)			
LLOQ: 50 ng/mL	Day 1	47.45 ± 4.22	94.9	8.9
	Day 2	49.61 ± 3.77	99.2	7.6
	Day 3	50.19 ± 3.31	100.4	6.6
LQC: 150 ng/mL	Day 1	160.95 ± 14.65	107.3	9.1
	Day 2	159.45 ± 13.39	106. 3	8.4
	Day 3	163.78 ± 14.58	109.2	8.9
MQC: 375 ng/mL	Day 1	343.88 ± 34.73	91.7	10.1
	Day 2	392.62 ± 33.37	104.7	8.5
	Day 3	336.75 ± 32.33	89.8	9.6
HQC: 4375 ng/mL	Day 1	4480.01 ± 456.96	102. 4	10.2
	Day 2	4536.88 ± 426.47	103.7	9.4
	Day 3	4738.13 ± 355.36	108.3	7.5
INTER-DAY:	Concentration			
LLQC	50 ng/mL	55.05 ± 5.84	110.1	10.6
LQC	150 ng/mL	145.955 ± 11.09	97.3	7.6
MQC	375 ng/mL	393.03 ± 34.19	104.8	8.7
HQC	4375 ng/mL	4475.63 ± 434.14	102.3	9.7

Table S1.10. Stability of the 16-3-16 gemini surfactant within the sample matrix.

Quality Control	Storage condition/ period	Observed concentrations (mean ± SD, ng/mL)	Accuracy (%)	Precision (%RSD)
LQC: 150 ng/mL	0 h	150.31 ± 11.57	100.2	7.7
	24 h on bench top	164.42 ± 10.69	109.6	6.5
	Three freeze/thaw cycles	135.45 ± 14.22	90.3	10.5
	–20 ˚C for 105 days (LT)	134.85 ± 8.23	89.9	6.1
	48 h extract in autosampler	144.15 ± 13.84	96.1	9.6
MQC: 375 ng/mL	0 h	362.63 ± 34.45	96.7	9.5
	24 h on bench top	353.62 ± 34.31	94.3	9.7
	Three freeze/thaw cycles	338.63 ± 32.17	90.3	9.5
	–20 ˚C for 105 days (LT)	345.38 ± 36.26	92.1	10.5
	48 h extract in autosampler	399.75 ± 37.58	106.6	9.4
HQC: 4375 ng/mL	0 h	4147.51 ± 443.78	94.8	10.7
	24 h on bench top	4379.38 ± 381.01	100.1	8.7
	Three freeze/thaw cycles	4038.13 ± 415.93	92.3	10.3
	–20 ˚C for 105 days (LT)	4239.38 ± 390.02	96.9	9.2
	48 h extract in autosampler	4392.51 ± 347.01	100.4	7.9

LT (long term): –20 ˚C for 105 days

CHAPTER 4:

RESEARCH MANUSCRIPT (PUBLICATION 3 - *PENDING*)

***Citation*:** McDonald Donkuru, Ildiko Badea, George Katselis, Anas El-Aneed. Evaluation of the subcellular distribution of gemini surfactant gene delivery nanoparticles using liquid chromatography-tandem mass spectrometry. *Finalized manuscript, April 2017; to be submitted for publication.*

The work presented in this chapter is a finished publication-standard manuscript aimed for publication in a pharmaceutical research-focused journal. The manuscript was drafted exclusively from work conducted within my Ph.D. research and describes the development/validation of standard addition–HILIC-MS/MS methods. It also presents the determination of gemini surfactant biodistribution in transfected PAM212 epidermal keratinocytes using the developed methods. I designed, initiated and completed all experimental work including development/assessment of the standard addition–HILIC-MS/MS methods, gemini surfactant-based cell transfection, isolation of subcellular compartments/organelles from treated cells and the determination of gemini surfactants present within the organelles/compartments. Co-author, Ildiko Badea and George Katselis made valuable inputs on efficient analyte recovery from samples/western blot analysis and on cellular data interpretation, respectively. As first author, I wrote all draft versions of the

manuscript and incorporated revision advised by co-authors. This work was fully supervised by Dr. Anas El-Aneed.

Manuscript:

4. Evaluation of the subcellular distribution of gemini surfactant gene delivery nanoparticles using liquid chromatography-tandem mass spectrometry.

McDonald Donkuru[1], Ildiko Badea[1], George Katselis[2] & Anas El-Aneed[1]

1. College of Pharmacy and Nutrition, University of Saskatchewan, 107 Wiggins Road, Saskatoon, SK S7N 5E5, Canada

2. Canadian Centre for Health and Safety in Agriculture (CCHSA), Department of Medicine, College of Medicine, University of Saskatchewan, 104 Clinic Place, Saskatoon, SK S7N 2Z4, Canada

4.1 Abstract

Introduction: The lipid molecules termed dicationic gemini surfactants have been explored successfully for the delivery of genetic materials into cells. However, the fate of the gemini surfactants after the delivery of their DNA cargo into cells remains poorly studied. Thus, the safe and efficient use of gemini surfactants requires a better understanding of their cellular and subcellular fate namely, cellular uptake, bio-distribution, metabolism and excretion.

Methods: The subcellular profiles of two lead gemini surfactants, denoted as 16(Py)-S-2-S-(Py)16 and of 16-3-16, was investigated using hydrophilic interaction liquid chromatography electrospray–ionization-tandem mass spectrometry (HILIC–ESI–MS/MS) employing the standard addition method. Keratinocytes were treated with gemini surfactant-based nanoparticles and subsequently fractionated using differential centrifugation, resulting in five subcellular fractions. The gemini surfactants were then extracted using the Bligh/Dyer method.

Results: The standard addition–HILIC–ESI–MS/MS platform was suitable for the quantification within multiple subcellular fractions as well as the whole-cell homogenates. The accuracy of the measurements was within ±15% as established by evaluation of quality control samples spiked within the various samples. Subcellular analysis showed a gemini surfactant distribution to all the cellular compartments, with an uneven distribution for 16(Py)-S-2-S-(Py)16 and a somewhat even distribution for its counterpart, 16-3-16.

Discussion/conclusions: The distinct subcellular distribution, observed for the first time, provides possible explanations for the different toxicities of the studied compounds, 16(Py)-S-2-S-(Py)16 and of 16-3-16. It also demonstrates a new approach for screening and toxicity elucidation for a vast array of bio-active gemini surfactants.

4.2 Introduction

In gene therapy, dicationic gemini surfactants are promising molecules used as non-viral vectors for nanoparticle-mediated gene delivery.[1] Gemini surfactants represent a versatile family of lipids, with a general structure of two monomer surfactants interconnected through a spacer, where both monomers contain a polar or ionic head-group and a hydrophobic alkyl tail (Figure 4.1A)[2]. Gemini surfactants are synthetically tailored for effective gene delivery through the rational design and selection of molecular building blocks (i.e. head-groups, hydrocarbon tails and spacers).[3-5] The aim is to increase gene transfection abilities and reduce undesired cytotoxic effects. The positively charged head-groups can be modified, for example, to di-pyridinium or di-quaternary amines for effective complexation of nucleic acids into nanoparticles to achieve efficient cell transfection.[6-8] More recently, amino acids were added within the spacer region to enhance biocompatibility.[3]

Despite their promising potency, the fate of the building blocks of gemini surfactant-based nanoparticles (herein, *gemini* nanoparticles) after entry into cells and release of their therapeutic cargo is poorly studied. It is possible to study their fate by adding a fluorescence tag to the gemini surfactant structure, such as pyrene.[9, 10] However, it was shown that the addition of such structure-modified moieties within the formulation alters the pharmacokinetics behaviour of the nanoparticles.[11, 12] In addition, gemini surfactants may degrade within biological systems and the fluorescence tag may detach from the parent molecule. Such limitations prompted us to develop multiple mass spectrometry (MS)-based methods to monitor the fate of gemini surfactants within cells.[13-15] Most recently, we reported a new hydrophilic interaction liquid

chromatography-tandem mass spectrometry (HILIC-MS/MS) method which, for the first time, allowed for monitoring the cellular uptake of structurally diverse gemini surfactants, such as 16(Py)-S-2-S-(Py)16 and 16-3-16 (Fig 1B, 1C).[15]

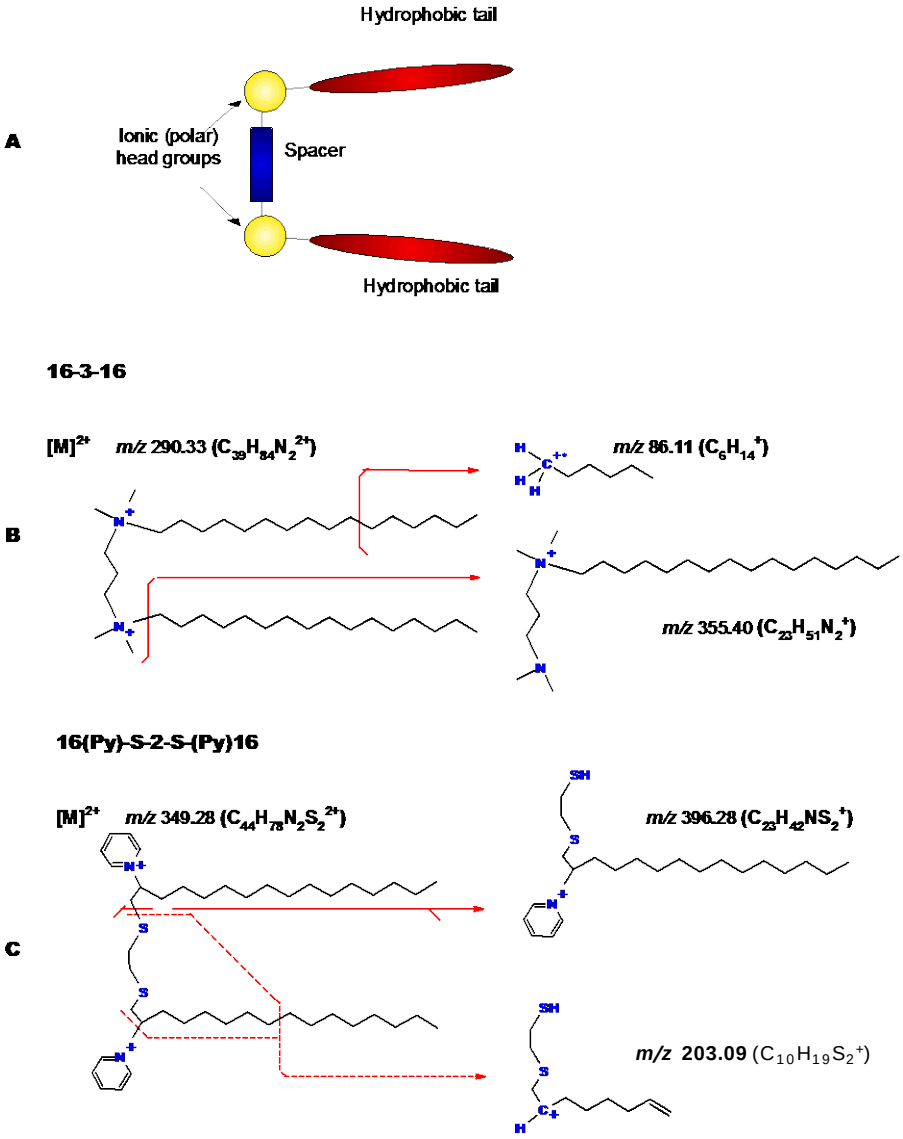

Figure 4.1: Gemini surfactant structures.

A) Schematic representation of gemini surfactant general structure; **B)** The exact molecular structures of intact compounds and monitored product ions during HILIC-MS/MS of 16-3-16: *N*,*N*-bis(dimethylhexadecyl)-1,3-propanediammonium; **C)** 16(Py)-S-2-S-(Py)16: 1,1'-[ethane-1,2-diylbis(sulfanediylhexadecane-1,2-diyl)]dipyridinium.

The gemini surfactant compounds 16(Py)-S-2-S-(Py)16 and 16-3-16, are: 1,1'-[ethane-1,2-diylbis(sulfanediylhexadecane-1,2-diyl)]dipyridinium and *N*,*N*-bis(dimethylhexadecyl)-1,3-propanediammonium, respectively (Figure 4.1B, 1C). Both surfactants contain saturated C-16 hydrocarbon tails; however, the former contains dipyridium head-groups and an ethane-1,2-dithiol spacer, whereas the latter has diquaternary ammonium head-groups along with a propyl spacer.[16] Despite both being promising gene delivery agents, the cytotoxicity associated with di-quaternary bearing gemini surfactants is relatively higher than that of their di-pyridinium counterparts.[8]

The determination of the intracellular-fate of 16(Py)-S-2-S-(Py)16 and 16-3-16 gemini surfactants using HILIC-MS/MS method revealed that both compounds rapidly accumulated in PAM 212 epidermal keratinocytes when their nanoparticles were administered to cultured cells.[15] Subsequently, both compounds depleted in a similar fashion when monitored up to 55 hours post transfection.[15] The identical trend in cellular uptake and degradation/elimination offers no explanation of the differential cytotoxicity between the two compounds as building blocks for the nanoparticles.

Theoretically, lipid-based nanoparticles can migrate freely within different compartments in cells[17-21] or can be targeted to specific subcellular organelles.[22-26] In general, the overall

process of nanoparticle–cell interaction is a complex, multi-step mechanism. It involves the initial binding of nanoparticles to the cells' outer plasma membrane and an uptake of the nanoparticles into cells through multiple pathways that predominantly includes endocytosis and occasionally includes non-endocytotic routes.[17-21] Within cells, the nanoparticles can transition through multiple steps that involve various organelles, resulting either in successful drug release or degradation of the nanoparticles with or without exocytosis into the extracellular surrounding.[17-21] Therefore, the nanoparticles or their encapsulated materials may deposit at several subcellular sites including plasma membrane,[18, 21, 27] endosomes/lysosomes,[28-31] cytoplasm,[18, 32-37] mitochondria[23, 38] and the nucleus.[39-41] The deposition into subcellular sites can be reasonably expected to change with time and to vary among different subcellular compartments and is dependent on the molecular structure of the gemini surfactants.

Therefore, investigation of the subcellular distribution profiles could explain the various cytotoxicity trends observed among various structures of gemini surfactants. In this reported work, a qualitative and quantitative HILIC-LC-MS/MS assessment of the subcellular distribution of gemini surfactants within PAM 212 cells is provided for the first time.

4.3 Materials and Methods

4.3.1 Materials

A dipyridinium gemini surfactant 16(Py)-S-2-S-(Py)16, its diquaternary ammonium counterpart 16-3-16, and their deuterated internal standards 16(Py)-S-2-S-(Py)16-$\boldsymbol{d_{10}}$ and 16-3-16-$\boldsymbol{d_{66}}$, respectively, were synthesized as described previously.[15] The deuterium atoms were located on the pyridinium ring in the case of the dipyridinium gemini surfactant and on the tail

regions in the case of 16-3-16. The zwitterionic phospholipid 1,2-dioleoyl-sn-glycero-3-phosphoethanolamine (DOPE) was supplied by Avanti Polar Lipids Inc. (Alabaster, AL, USA). Chloroform, methanol and 1-octanol (99%), ammonium formate, formic acid, mass spectrometric-grade water and acetonitrile were purchased from ThermoFisher Scientific (Ottawa, ON, Canada). PAM 212 cells were from an original cell passage kindly provided by Dr. S. Yuspa (NIH, Bethesda, MD, USA). Ingredients for cell culture medium, namely minimum essential media (MEM), fetal bovine serum albumin (FBS) and antibiotic-antimycotic were obtained from Sigma-Aldrich (Oakville, ON, Canada). Plasmid DNA (pGT·IFN-GFP) was constructed in-house, as described previously.[42] Western blotting kit containing primary and secondary antibody cocktail was obtained from Abcam (Cambridge, MA, USA), while protease inhibitor cocktail came from Invitrogen (Carlsbad, CA, USA). Tissue culture flasks and Petri dishes (with 150-cm^3 and 75-cm^3 capacities) were purchased from ThermoFisher Scientific (Ottawa, ON, Canada).

4.3.2 LC-MS/MS instrumentation

The hybrid LC-MS/MS analytical system is as described in previous work.[15] It comprised of an Agilent 1200 Series HPLC with a quaternary pump, a degasser and auto sampler (Agilent Technologies, Mississauga, ON, Canada) coupled to an AB Sciex API 4000 QTRAP mass spectrometer (AB Sciex, Concord, ON, Canada). A typical chromatographic 4-min separation run to analyze 2 µL injected aliquots involved a ZIC®-HILIC column (150 × 2.1 mm, 5 µm, 200 Å; Merck SeQuant AB, Umea, Sweden) held at 50 ˚C and an isocratic mobile phase flowing at 500 µL/min. The mobile phase consisted of 80:20 (v/v) acetonitrile:buffer, with the buffer containing 2.5 mM ammonium formate and 25 mM formic acid. Sample carryover was absent;

however, to eliminate matrix build-up in the column, a 2-min double blank injection was run between every two samples using the same mobile phase but with the ammonium formate modified to 12.5 mM. Increasing the ammonium formate concentration was to help eliminate potential in-column buildup of sucrose, which was used as a differential centrifugation medium in the subcellular fractionation process (described below).

The AB Sciex QTRAP 4000 mass spectrometer is equipped with an electrospray ionization (ESI) source set at 5500 V ionspray voltage and 600 ˚C at the ion source interface, with 55 psi being the pressure for the curtain gas pressure and 65 psi as the pressures for both GS1 and GS2. The mass spectrometer was operated in the multiple reaction monitoring (MRM) mode for the analytes and the deuterated internal standards as $[M]^{2+}$ species through the following transitions: 16-3-16 $[M]^{2+}$ *m/z* 290.33 → 355.40, 86.11; 16-3-16-$\boldsymbol{d_{66}}$ $[M]^{2+}$ *m/z* 323.54 → 388.61; and, 16(Py)-S-2-S-(Py)16 $[M]^{2+}$ *m/z* 349.28 → 396.28, 203.09; 16(Py)-S-2-S-(Py)16-$\boldsymbol{d_{10}}$ $[M]^{2+}$ *m/z* 354.31 → 401.31 (Figure 4.1, Figure 4.2S). The MRM conditions for the monitored precursor → product ion transitions are presented in Table S4.1 (supplementary information).[15]

4.3.3 Preparation of standard solutions

Aqueous 3 mM stock solutions of the gemini surfactants including the deuterated internal standards were used and routinely stored at −20 ˚C under darkness. The 3 mM molarity give the equivalence of 2.2227 mg/mL for 16-3-16, 2.4219 mg/mL for 16-3-16-$\boldsymbol{d}_{66}$, 2.5771 mg/mL for 16(Py)-2-S-2-(Py)16 and 2.6073 mg/mL for 16(Py)-2-S-2-(Py)16-$\boldsymbol{d_{10}}$. Liposomal DOPE solution at 1 mM was routinely prepared fresh in 9.25% w/v isotonic sucrose solution with pH 9. Plasmid DNA (pGT·IFN-GFP) solution at 200 µg/mL was prepared in ultrapure, organic-free water and was routinely stored at −20 ˚C.

4.3.4 Preparation of nanoparticle formulations

Nano-lipoplex formulations for cell transfection were prepared through a 1:10:100 molar ratio of plasmid DNA/gemini surfactant/lipid DOPE (P/G/L) as described.[7] A mole of DNA is calculated per DNA base-pair with an average molecular weight of 660 Da. Briefly, the required transfection dose of plasmid DNA, that is 4.5 µg for 10×10^6 cells/treatment, was mixed with the appropriate amount of gemini surfactant for a 30-minute incubation at room temperature. The appropriate amount of the liposomal DOPE was added to the binary mixture, followed by further 15-minute incubation at room temperature to obtain a ternary (final) P/G/L system.

4.3.5 PAM 212 cell treatment and sample collection

PAM 212 cells used in this study were routinely cultured to ~85% confluence in *s*-MEM (*i.e.*, MEM supplemented with 10% FBS and 1 unit/mL antibiotic-antimycotic) inside 37 ˚C-humidified 95% air/5% CO_2 incubator. At 24 h before treatment, cells were seeded at 10×10^6 cells/150-cm^3 Petri dish in *s*-MEM, which was changed to FBS-free MEM after a rinse with same media within 1 h to transfection. Freshly prepared nanoparticle formulations (*Section 2.4*) were added to the cell cultures and allowed to interact with cells by returning cells to the CO_2 incubator. All treatments were carried out in replicates (n = 3). The addition of the nanoparticle formulation to the cell marks the reference point for recording post-treatment events and time-points.

At 5 h post-treatment, the nanoparticle-dosed cell media was removed and cells were rinsed with phosphate-buffered saline (PBS). The cells were detached by trypsinization and collected into 40 mL volumes. The collected cells were pelleted (1,500 rpm, 5 min, 4 ˚C), rinsed

with PBS, resuspended in 500 µL of ice-cold 0.25 M sucrose-HEPES-EDTA (SHE) (0.25 M sucrose, 10 mM HEPES, pH 7.5, 1 mM EDTA, 1× Halt™ protease inhibitor) and cooled on ice prior to subsequent steps.

4.3.6 Subcellular fractionation and subcellular sample collection

The ice-cooled 500-µL treated cell samples were gently homogenized using a motorized tissue-grinder/pellet homogenization apparatus (Fisher Scientific, #12-141-361, 12-141-368; Toronto, ON, Canada). The cell homogenates were transferred into ice-cooled tubes and resuspended to a total of 1,200 µL using ice-cold homogenization buffer. A 200-µL aliquot was stored at –80 ˚C until further analysis.

The remaining 1,000-µL homogenates were then fractionated using established differential centrifugation schemes, Figure 4.2.[43] Briefly, the 1,000-µL homogenates were centrifuged at 1,000 × g for 10 min, 4 ˚C. The resulting supernatant S1 (~1,000-µL) was retrieved and maintained on ice. The pellet P1 was resuspended to a total of 1,000-µL with 1.8 M sucrose final concentration. This was through initial resuspension of pellet P1 into 310 µL of 0.3 M sucrose-Tris-magnesium (STM) buffer (0.30 M sucrose, 50 mM Tris, 3 mM $MgCl_2$, protease inhibitor), followed by addition of 690 µL of 2.5 M STM buffer (2.5 M sucrose, 50 mM Tris, 0.5 mM $MgCl_2$, protease inhibitor). The P1 suspension was centrifuged at 71,000 × g for 90 min, 4 ˚C.[43] The obtained plasma membrane supernatant S2 and the nuclear pellet P2, which was resuspended in 100 µL of PBS, and were subsequently stored at –80 ˚C until further analysis.

Next, the supernatant S1 from the first centrifugation round was centrifuged at 8,000 × g for 15 min, 4 ˚C.[43] A mitochondrial pellet P3 was obtained, and was resuspend in 100 µL PBS and stored at –80 ˚C until further analysis. The supernatant S3 was subjected to further

centrifugation at 125,000 × g, 30 min, 4 ˚C. The resulting products were cytosolic supernatant S4 and pellet P4,[43] which represents remnant fractionation residue and which was resuspended in 100 µL of PBS. Both were stored at –80 ˚C until further analysis.

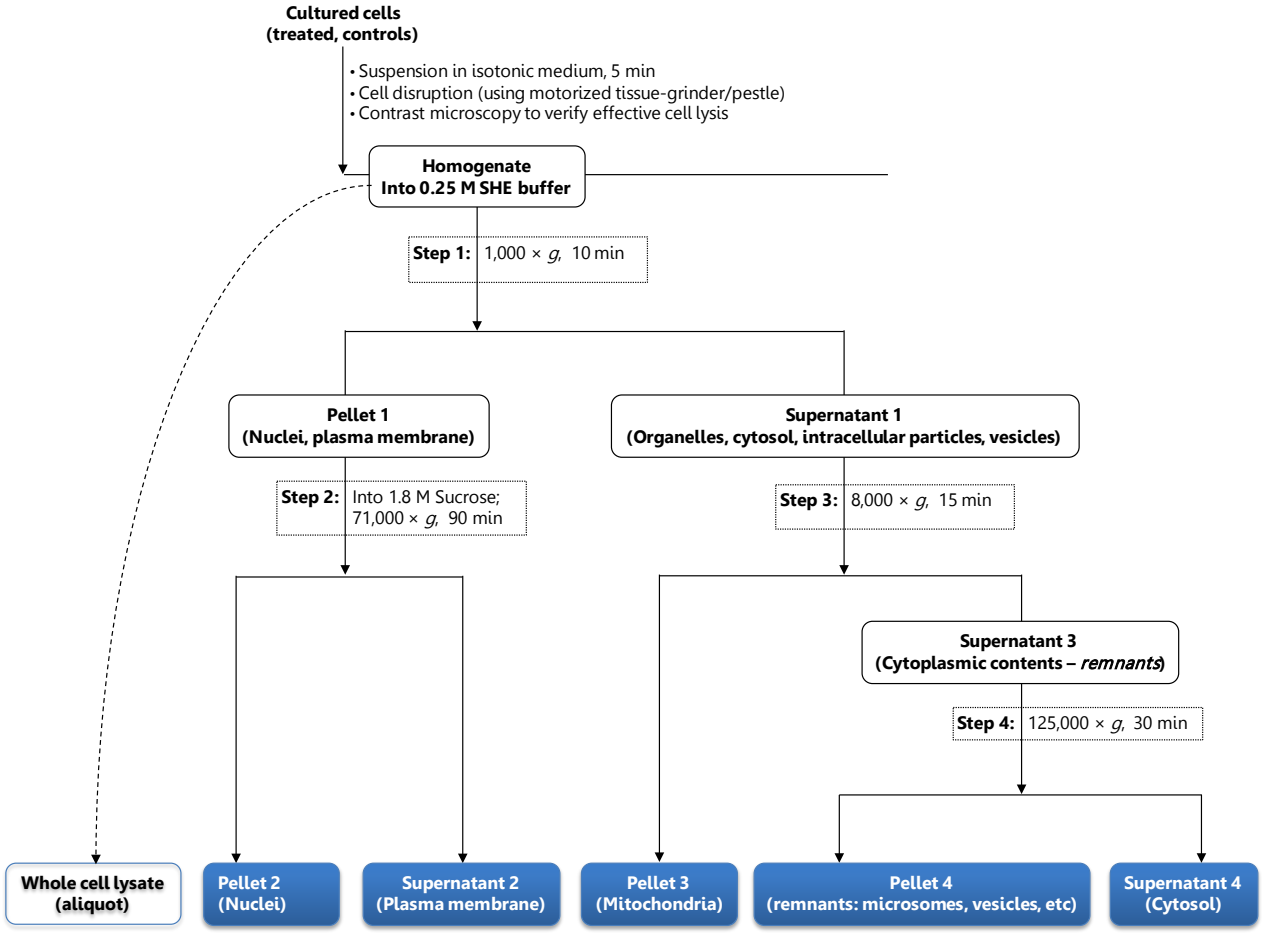

Figure 4.2: Subcellular fractionation scheme based on differential centrifugation.

Multiple subcellular fractions were isolated including nuclear, plasma membrane, mitochondrial and cytosolic fractions along with the leftover cellular residue. Adopted with

some modifications from refs.[43]

4.3.7 Protein recovery, 1-Dimensional SDS-PAGE and western blotting

Isolated subcellular fractions were analyzed to verify their composition and purity using immunoblot assays. The experimental procedure and the results are shown in supplementary materials (*Section 4.3 Supplementary Information*, ahead in this chapter).

4.3.8 Sample preparation for LC-MS/MS analysis

The whole-cell homogenates as well as the five subcellular fractions as shown in *Section 2.6* were processed for LC-MS/MS analysis according to the scheme shown in Figure 4.3. Briefly, the samples were retrieved from –80 ˚C, allowed to thaw and the volumes were brought to 1,000-µL for samples that were below this volume. All samples were then lysed by six freeze/thaw cycles along with 1-h sonication at 25 kHz. Each lysed sample was then divided in half to give two identical samples equal to 500-µL (Figure 4.3).

Standard addition method for quantification was carried out by adding known analyte concentration or appropriate blanks separately to the 500-µL samples. Briefly, either 16(Py)-2-S-2-(Py)16 or 16-3-16 was spiked at 5000 ng/mL within the corresponding treated cells into only one of each two identical samples while an equal volume of blank was added to the other. Internal standards were then added at 2086 ng/mL for 16(Py)-2-S-2-(Py)16-$\boldsymbol{d_{10}}$ and 938 ng/mL for 16-3-16 through equal-volume additions. All additions were within a 25-µL allocated volume, giving a resultant volume of 525 µL per sample prior to extraction.

For the construction of standard addition calibration curves, three levels of standard additions were prepared by spiking the standards into whole-cell lysate samples already containing a base concentration of the target analytes. Briefly, the concentrations 2500, 3750 and 5000 ng/mL were spiked into 500-µL whole-cell lysate samples with a base concentration (1250

ng/mL) of the target analytes. In addition, a zero addition (0 ng/mL) sample was prepared by adding equal volumes blank solutions in place of a standard solution. Then, equal volumes containing equimolar amounts of the appropriate internal standard as stated above, 16(Py)-S-2-S-(Py)16-d_{10} or 16-3-16-d_{66}, were added to all samples. As above, all additions were within a 25-µL allocated volume, giving a resultant volume of 525 µL per sample prior to extraction.

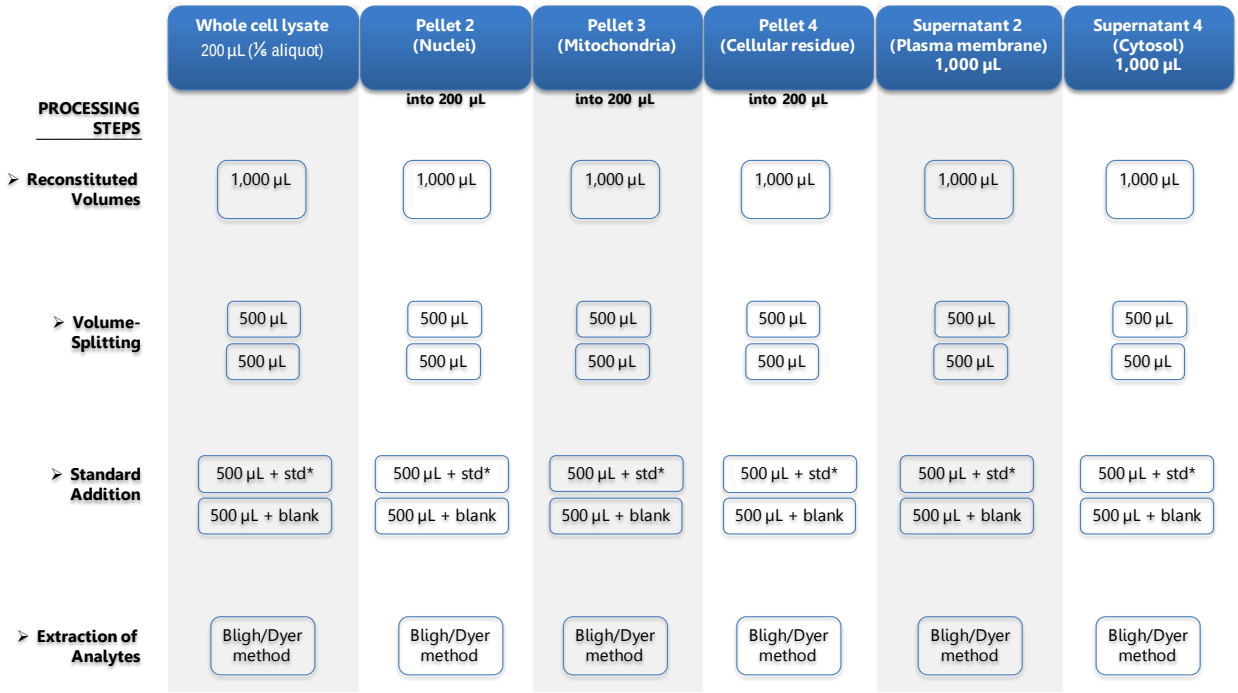

Figure 4.3: Subcellular and whole-cell sample processing steps prior to LC-MS/MS analysis. Topmost panel shows all samples as collected from differential centrifugation. 'Std*' indicates a standard addition where both the analyte and internal standard were added and 'blank' indicates a blank addition which involved only the internal standard.

All samples were then extracted using Bligh/Dyer method as described.[44] To the 525-µL samples, 1,900 µL (3.8 vols) of 2:1 (v/v) methanol/chloroform was added, followed by 625 µL (1.24 vols) of both chloroform and water, with vortexing in each case. The combined mixtures were centrifuged at 14,000 rpm for 10 min at room temperature to achieve aqueous/organic phase separation. A 1,000 µL of the bottom organic phase (i.e., 80% portion) was retrieved, dried using a gentle N_2 gas stream and the analytes deposited in microvials were reconstituted into in 200 µL of n-octanol. The reconstituted analytes were diluted 10 – 50× in the running mobile phase prior to LC-MS/MS analysis.

4.3.9 Assessment of the suitability of the Standard addition–LC-MS/MS method

The standard addition–HILIC-ESI-MS/MS method was validated for quantifying the target analytes within different subcellular fractions. It was suitable to apply the standard addition method since the HILIC-ESI-MS/MS, with linearity 50 – 5000 ng/mL, was fully validated in our previous report in accordance with USFDA guidelines.[15] Concentrations measured using the standard addition method should fall within the established linear range for reliable measurements.

Linearity within the standard addition method was established through a 4-point calibration line consisting of three standard additions and a zero point spiked into a base concentration of the analytes. The data was processed by least-squares method along with a $1/\chi$ weighting factor to obtain ratios of summed peak areas of the analytes, 16(Py)-S-2-S-(Py)16 and 16-3-16, to peak areas of the respective internal standards, 16(Py)-S-2-S-(Py)16-$\boldsymbol{d_{10}}$ and 16-3-16-$\boldsymbol{d_{66}}$.[15] The ratios

were then plotted against the standard addition concentrations (0, 2500, 3750, 5000 ng/mL) and the slope and coefficient of determination (R^2) were determined for the lines of best fit. Here, the *y*-intercept is the signal response due to a given (or unknown) original analyte concentration, which is determined by extrapolating the plotted line to zero signal response. After establishing linearity, routine analysis was performed timely with only one standard addition, utilizing validated mathematical equation.[45, 46]

For precision and accuracy determination, quality control (QC) samples of 4575 ng/mL of 16(Py)-S-2-S-(Py)16 were prepared and analyzed across all subcellular fractions as well as the whole-cell homogenates. In the case of the analyte 16-3-16, the QC concentration was 1250 ng/mL. All QC samples were analyzed in triplicates. Acceptance criterion for accuracy was ±15% of the nominal QC concentration, while the criterion for precision, computed as relative standard deviation (RSD), was ±15%. The minimum acceptable signal response was set at a signal-to-noise (S/N) ratio of 5.

4.3.10 Statistical analysis

Statistical analyses and comparisons were performed by unpaired t-test. Significant difference between compared cases was established at the $p < 0.05$ level of significance.

4.4 Results

4.4.1 Purity and Western blot characterization of subcellular fractions

Western blot results assessing the protein composition and purity of the subcellular fractions are presented in supplementary materials, Appendix B, Figure S4.1. It confirms the

separation of target organelles and indicates that the fractionation scheme employed allowed the isolation of intact organelles and cellular components. However, some cross contamination is observed and is actually expected in accordance with the manufacturer's specifications.

4.4.2 Standard addition–HILIC-LC-MS/MS for subcellular bio-analysis of gemini surfactants

A standard addition calibration plot obtained for typical validation samples containing the 16(Py)-S-2-S-(Py)16 and 16-3-16 compounds are shown in Figure 4.4. Four replicate injections were ran for each QC sample. On the other hand, triplicate injections of the samples were done after spiking with known concentrations of the analyte. The concentration of the analyte was obtained by extrapolating the calibration line to zero signal response. All calibration curves were linear with an R^2 of 0.99 (Figure 4.4).

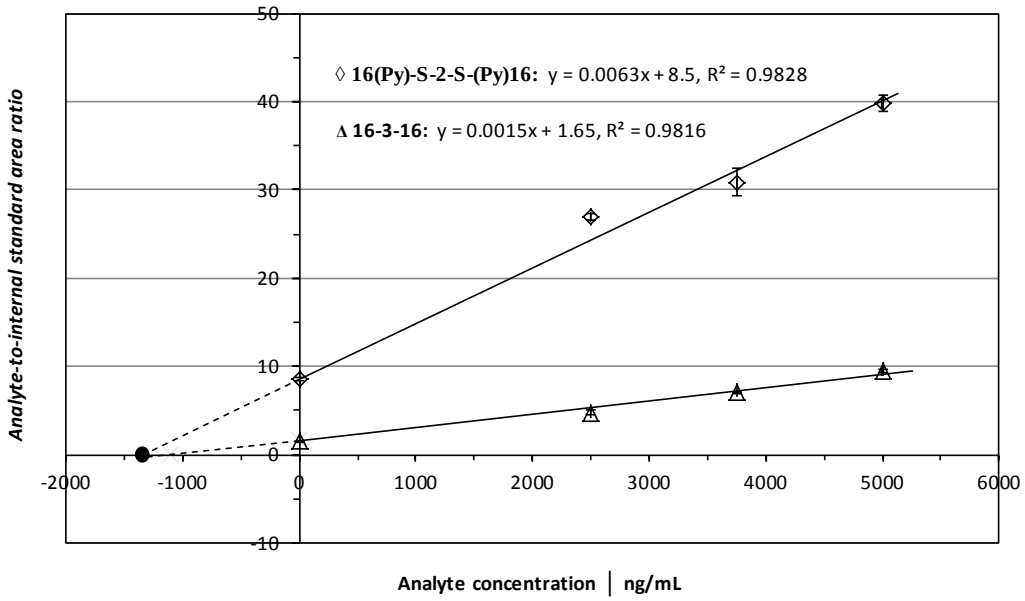

Figure 4.4: Four-point 'standard addition' calibration curve.

The original concentration of the analyte in the sample is found by extrapolating the calibration line to the zero signal response.

The standard addition–LC-MS/MS method adopted our in-house developed HILIC-ESI-MS/MS method (linearity 50 – 5000 ng/mL), which was validated as per the USFDA guidelines.[15] Analytical selectivity was gained from analyte-specific retention times and from monitoring of target analytes through the analyte's unique precursor → product ion transitions. No effect on the selectivity was observed in the use of the standard addition–LC-MS/MS method for different subcellular samples. This is evident from the absence of any interference or contaminant peaks from the LC-MS/MS chromatograms. The analytes co-eluted with their deuterated internal standards: 16(Py)-S-2-S-(Py)16 and 16(Py)-S-2-S-(Py)16-$\boldsymbol{d_{10}}$ co-eluted at 2.62 mins, while 16-3-16 and 16-3-16-$\boldsymbol{d_{66}}$ co-eluted at 2.42 mins.

Once linearity is established, it is deemed suitable to perform routine analysis with only a single standard addition point (5000 ng/mL) which should ideally be greater than the expected unknown concentration by at least one order of magnitude. Such "one-level" standard addition approach is valid as long as the analyte concentrations in both the original and the standard addition sample falls within an established linear calibration range.[46] In our previous work, we demonstrated that the calibration curves for the two analytes, 16(Py)-S-2-S-(Py)16 and 16-3-16, were linear within the concentration range of 50 – 5000 ng/mL.[15] The original analyte concentration (unknown) in samples was calculated using the established equation:[45]

$$\frac{[X]_i}{[S]+[X]_i} = \frac{I_X}{I_{S+X}} \quad \ldots \quad \ldots \quad \ldots \quad (1)$$

where $[X]_i$ denotes the initial (original) concentration of analyte in the sample before spiking, [S] is the known concentration spiked into the sample, I_X is the signal response from the initial sample before spiking, and $I_{(S+X)}$ is the signal response from the sample after it had been spiked with known analyte concentration. The one-level standard addition approach generated the needed results while at the same time significantly reducing the overall analysis time.

4.4.3 Matrix effects, accuracy and precision in standard addition–LC-MS/MS

Precision and accuracy results of QC samples analyzed across all subcellular fractions are given on Table 4.1. The results show that for samples containing the 16(Py)-S-2-S-(Py)16 and 16-3-16 gemini surfactants, accuracy for the QC samples were all within ~88 – ~ 110% of the nominal values. The precision for both analytes, 16(Py)-S-2-S-(Py)16 and 16-3-16, were within 3 – 13% (RSD) in all cases. These values serve as indicators for assessing possible matrix effects across the subcellular and whole-cell samples. The values indicate that the analytical accuracy and precision of the standard addition–LC-MS/MS method was not affected by the subcellular and whole-cell matrices. A recent LC-MS/MS method for subcellular lipids also showed quantitative accuracy and precision with no matrix effects across mitochondria fractions and a cell-mimetic fraction based on bovine serum albumin.[47]

Table 4.1. Accuracy and precision of quality control samples in the standard addition–HILIC-ESI-MS/MS analysis gemini surfactants.

Gemini surfactant identity	Quality Control (concentration)	Subcellular/cellular matrix types	Observed concentrations (mean ± SD, ng/mL)	Accuracy (%)	Precision (%RSD)
16(Py)-S-2-S-(Py)16	4575 ng/mL	Plasma membrane fraction	4292.44 ± 236.81	93.82	5.18
		Cytosolic fraction	4382.85 ± 401.03	95.80	9.15
		Nuclear fraction	4198.02 ± 491.59	91.76	11.71
		Mitochondrial fraction	4651.35 ± 439.26	101.67	9.60
		ER/Cellular remnants	5014.16 ± 472.49	109.60	10.33
		Whole cell lysate	4780.88 ± 617.53	104.50	12.92
16-3-16	1250 ng/mL	Plasma membrane fraction	1106.21 ± 133.12	88.50	10.65
		Cytosolic fraction	1242.93 ± 105.43	99.43	8.48
		Nuclear fraction	1128.47 ± 030.72	90.28	2.46
		Mitochondrial fraction	1353.25 ± 161.18	108.26	11.91
		ER/Cellular remnants	1201.15 ± 159.36	96.09	13.27
		Whole cell lysate	1258.42 ± 153.23	100.67	12.26

4.4.4 Standard addition–HILIC-LC-MS/MS analysis of cellular and subcellular samples

The standard addition–HILIC-LC-MS/MS was applied to the analysis of five subcellular fractions along with the whole-cell homogenates from cell-treatments using DNA-encapsulated nanoparticles of the 16(Py)-S-2-S-(Py)16 and 16-3-16 gemini surfactants. The results in Figure 4.5 represent the gemini surfactant subcellular distribution after a 5-h duration in which cells remained in contact with a dose of nanoparticles containing the studied gemini surfactants. For both gemini surfactants, a large uptake into cells occurred: 70% uptake for 16(Py)-S-2-S-(Py)16 and 90% uptake for 16-3-16, determined by analysing the whole-cell homogenates. The 5-hour time point was chosen based on our published work on cellular uptake;[15] this point marks the

maximum uptake point which is followed by gradual elimination and/or degradation. It is also represents the ideal nanoparticle–cell contact time for transfection and gene expression in PAM 212 cells.[7]

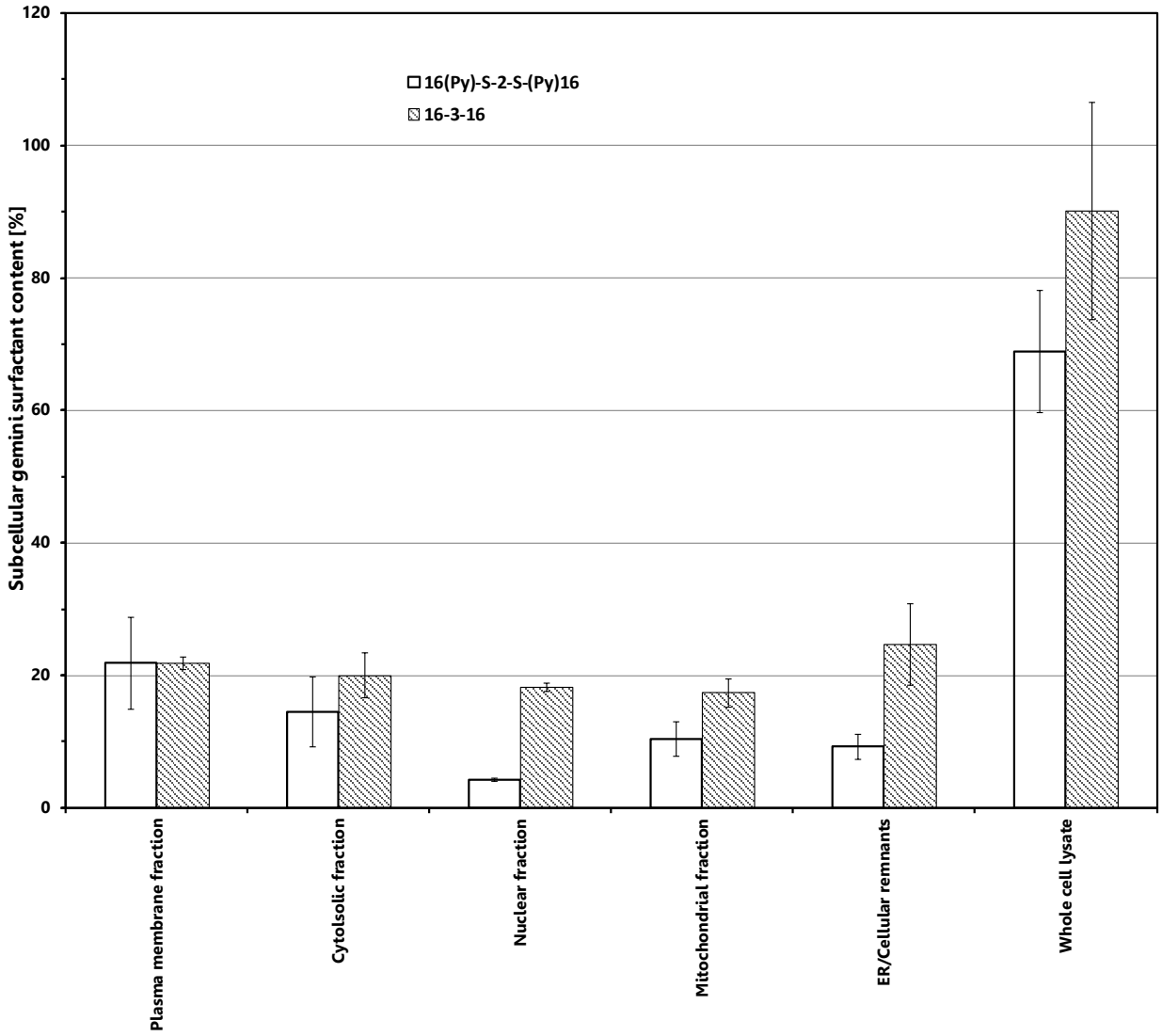

Figure 4.5: Subcellular distribution of the gemini surfactants, 16(Py)-S-2-S-(Py)16 and 16-3-16.

The subcellular concentrations were determined after 5-hour treatment duration in which cultured PAM 212 epidermal keratinocytes had an administered dose of gemini surfactant/DNA nanoparticles. Each plotted data point represents mean ± SD, n = 3.

As shown in Figure 4.5, the 16(Py)-S-2-S-(Py)16 compound showed its highest distribution to the plasma membrane (22%), followed by its distribution to cytosol (15%), mitochondria (10%) and the nucleus (5%) (Figure 4.5). The distribution to the remnant subcellular residue which was not further 'fractionatable' was 9%. In the case of the 16-3-16 compound, it was distributed across the subcellular compartments within a rather narrow variation margin of 18 – 24% among various compartments. It had a slightly higher distribution to the remnant subcellular residue (24%), followed by plasma membrane (22%), cytosol (20%), nucleus (19%), and mitochondria (18%) (Figure 4.5).

Evidently, both compounds showed unequal distribution across the subcellular compartments. However, the 16-3-16 compound *versus* its counterpart 16(Py)-S-2-S-(Py)16 showed particularly high distribution to the mitochondria (19% vs. 5%; $p < 0.05$), nucleus (18% vs. 10%; $p < 0.05$) and the remnant subcellular residue (24% vs. 9%; $p < 0.05$) (Figure 4.5). The distribution among other compartments including the membrane showed insignificant variation among the two structures. We initially hypothesized that the reported increased cytotoxicity associated with diquaternary gemini surfactants in comparison to the dipyrdinium surfactants was due to their disruptive effects on cell membranes. However, the membrane-distribution of the two gemini surfactants was not significantly different.

The obtained data may suggest that association with the mitochondria or the nucleus could be the reason for the varying toxicities. Distribution to mitochondria or nucleus may either be due to the entry of the gemini surfactants into these subcellular compartments or their association with the membranes of these organelles. Our findings provide the only qualitative and quantitative distinction in subcellular profile between the two compounds, without the need for fluorescence tag. It may provide the first experimental explanation on the cytotoxicity difference among these two promising gene delivery agents.

In Figure 4.5, the data obtained for the different subcellular fractions was compared with that for the whole-cell homogenate. Theoretically, the combined content of the analyte from the five subcellular fractions can be equated to the content of the analyte within the whole-cell homogenate. For the 16(Py)-S-2-S-(Py)16 gemini surfactant, its combined content from the five fractions was 61% while its content within the whole-cell homogenate was found to be 70% of the initial dose. The resultant percentage difference is 13.7%. In the case of the 16-3-16 gemini surfactant, its combined content from the five subcellular fractions was 103% while its content within the whole-cell homogenate was 90%. This gives a difference of 13.5%. In both cases, values for the percentage difference fall below the widely accepted ± 15% accuracy standard, as per USFDA regulatory guidelines in bioanalytical methods.

4.5 Discussion

This study evaluated the subcellular distribution and fate of gemini surfactants within PAM 212 epidermal keratinocytes with the aim of understanding the reasons behind the varying toxicities of two distinct gemini surfactant structures, namely 16(Py)-S-2-S-(Py)16 and of 16-3-

16 (Figure 4.1). We previously assessed the cellular uptake of these gemini surfactants, reporting an almost identical intracellular accumulation and subsequent, more gradual depletion trend for the two structures.[15] As such, the similar intracellular accumulation and depletion did not explain the different toxicities, therefore, we focused in the present study on investigating the gemini surfactant subcellular distribution.

Theoretically, to determine the subcellular distribution of gemini surfactants, different LC-MS/MS methods with internal calibration must be developed/validated for application to the different subcellular fractions. This is because the subcellular organelles are different in their bio-complexity and therefore can possibly pose different matrix effects. This can be time consuming and challenging to achieve.

Therefore, we implemented a simple standard addition method in using HILIC-LC-MS/MS method as reported[15] in terms of mobile phase and experimental conditions. The use of standard addition with LC-MS/MS was only recently demonstrated in few reports;[45, 48, 49] however, the standard addition approach has been commonly combined with techniques such as atomic spectroscopy,[50-52] UV-Visible spectroscopy[53, 54] and fluorescent spectroscopy.[55] The standard addition approach requires no blank matrix; herein it eliminates the need for blank subcellular matrix and the time-consuming subcellular fractionation. It compensates for effects of varying matrix is as each sample is analyzed against its own matrix and the measured signal is calibrated against an added standard of the analyte. The method simultaneously allowed the analysis of different subcellular fractions as well as whole-cell samples. A key advantage of such method is the compensation of matrix effect since identical matrix is present in both the spiked samples (serving as calibration standards) and unspiked samples (*i.e.*, actual samples).[45, 46]

Though no guidelines are yet available for bio-analytical method validation involving standard addition methods, we opted for establishing precision and accuracy to demonstrate the robustness of the analytical approach including matrix effects compensation across the subcellular and whole-cell lysates. Precision and accuracy were acceptable as shown in Table 4.1 and were established by analyzing QC concentration of 4575 ng/mL for 16(Py)-S-2-S-(Py)16 and 1250 ng/mL for 16-3-16 across the different subcellular and whole-cell samples (Table 4.1). The QC concentrations were chosen such that they fall in the range of analyte concentrations found within the studied subcellular samples for the respective analytes. Overall, the analytical accuracy and precision (Table 4.1) across the different subcellular and whole-cell samples suggest that the matrix effects did not affect signal response within the standard addition method.

Subcellular data from the standard addition–HILIC-ESI-MS/MS analyses of nanoparticle-treated cell samples showed a high cellular uptake of the test compounds, 16(Py)-S-2-S-(Py)16 and 16-3-16 (70% and 90% uptake, respectively; Figure 4.5). The total uptake amount was found to be distributed across the studied subcellular organelles (or compartments), namely plasma membrane, cytosol, mitochondria, nucleus and the remnant subcellular residue. The amount of test compound per subcellular compartment ranged from 5 – 24%, and the combined content from the subcellular compartments was equal to the total uptake amount (within ± 15% margin of error).

The subcellular distribution profiles (Figure 4.5) showed a significantly higher distribution to the mitochondria, nucleus and the remnant subcellular residue for 16-3-16 as compared to its counterpart 16(Py)-S-2-S-(Py)16 (Figure 4.5). Though 16-3-16 is reportedly more toxic than 16(Py)-S-2-S-(Py)16,[8] studies to account for toxicity difference have been lacking. Herein, the

distinct subcellular distribution observed between these compounds may explain the reported difference in toxicity.

The higher cellular uptake observed for the 16-3-16 compound is a plausible explanation of its reported higher toxicity relative to the 16(Py)-S-2-S-(Py)16 compound. Studies show that the cytotoxicity of gemini surfactants is concentration-dependent, where higher concentration leads to higher cytotoxicity.[6, 8] Herein, the 16(Py)-S-2-S-(Py)16 and 16-3-16 gemini surfactants were used for cellular gene transfection at equimolar concentrations, thus, the higher cellular uptake for 16-3-16 implies higher concentration in host cells and is consistent with its reported higher toxicity. The observed difference in cellular uptake was accompanied by different subcellular distribution that further accounts for different gemini surfactant toxicities.

The subcellular distribution of 16-3-16 compound with higher overall uptake into cells showed higher accumulation within the mitochondria, nucleus and the remnant subcellular residue. The mitochondria and nucleus have crucial functions within cells, including cellular metabolism and energy generation; and, control of a cell's machinery by storage/regulation of genes, respectively.[56] The remnant subcellular residue encompasses such subcellular structures as ribosomes (sites of protein synthesis) and vesicular systems (for transport and defense against foreign particles).[56] Therefore, an accumulation of gemini surfactants (whether as nanoparticles or free-separate molecules) into these compartments could impact their outer membrane integrity and their normal function. Herein, it is reasonable to argue that the increased accumulation of 16-3-16 particularly within the mitochondria and nucleus provides a basis for its higher toxicity relative to 16(Py)-S-2-S-(Py)16.

4.6 Conclusion

Standard addition–HILIC-ESI-MS/MS was successfully implemented for the determination of the subcellular distribution of the 16(Py)-S-2-S-(Py)16 and 16-3-16 gemini surfactants within cells, possibly shedding light for their varying toxicities. Obtained subcellular data showed that the 16-3-16 gemini surfactant showed increased distribution to the nucleus, mitochondria and the remnant subcellular residue. This distinction may thus account for the higher toxicity exhibited by this compound in relation to its counterpart 16(Py)-S-2-S-(Py)16.

The analytical strategy applied in this study is applicable for the analysis of gemini surfactants not only for cell cultures but also for the case of tissues, organs and organisms; here, the analyte accumulation into and depletion from biological sub-compartments and sub-structures can both be evaluated. It is also applicable to environmental samples where the exposure and biodistribution pathways can be studied. We are currently evaluating additional gemini surfactant structures, assessing their cellular biodistribution to possibly provide new insights to both toxicity and transfection efficiency.

4.7 Acknowledgements

The authors acknowledge the technical assistance provided by Dr. Joshua Buse to Mr. Donkuru for the 4000 QTRAP LC/MS/MS system. We also acknowledge the assistance of Jackson Chitanda for his help in the synthesis of gemini surfactants. The 4000 QTRAP LC/MS/MS system was acquired through a Canada Foundation for Innovation (CFI) grant. The project was supported by a Natural Sciences and Engineering Research Council of Canada (NSERC) Discovery grant.

4.8 References

[1] M. Donkuru, I. Badea, S. Wettig, R. Verrall, M. Elsabahy, M. Foldvari, Advancing nonviral gene delivery: lipid- and surfactant-based nanoparticle design strategies, Nanomedicine (Future Medicine), 5 (2010) 1103−1127.

[2] F.M. Menger, J.S. Keiper, Gemini Surfactants, Angewandte Chemie (International ed. in English)2000, pp. 1906-1920.

[3] P. Yang, J. Singh, S. Wettig, M. Foldvari, R.E. Verrall, I. Badea, Enhanced gene expression in epithelial cells transfected with amino acid-substituted gemini nanoparticles., European Journal of Pharmacuetics & Biopharmacuetics, 75 (2010) 311–320.

[4] S.D. Wettig, C. Wang, R.E. Verrall, M. Foldvari, Thermodynamic and aggregation properties of aza- and imino-substituted gemini surfactants designed for gene delivery, Physical chemistry chemical physics : PCCP, 9 (2007) 871-877.

[5] S.D. Wettig, I. Badea, M. Donkuru, R.E. Verrall, M. Foldvari, Structural and transfection properties of amine-substituted gemini surfactant-based nanoparticles, The journal of gene medicine, 9 (2007) 649-658.

[6] M. Donkuru, S.D. Wettig, R.E. Verrall, I. Badea, M. Foldvari, Designing pH-sensitive gemini nanoparticles for non-viral gene delivery into keratinocytes, J. Mater. Chem., 22 (2012) 6232-6244.

[7] I. Badea, R. Verrall, M. Baca-Estrada, S. Tikoo, A. Rosenberg, P. Kumar, M. Foldvari, *In vivo* cutaneous interferon-γ gene delivery using novel dicationic (gemini) surfactant–plasmid complexes, Journal of Gene Medicine, 7 (2005) 1200–1214.

[8] A. Bhadani, S. Singh, Novel gemini pyridinium surfactants: synthesis and study of their surface activity, DNA binding, and cytotoxicity, Langmuir : the ACS journal of surfaces and colloids, 25 (2009) 11703-11712.

[9] C. Wang, S.D. Wettig, M. Foldvari, R.E. Verrall, Synthesis, Characterization, and Use of Asymmetric Pyrenyl-Gemini Surfactants as Emissive Components in DNA-Lipoplex Systems, Langmuir, 23 (2007) 8995–9001.

[10] S.D.D. Wettig, RubenaAkbar, JavedKaur, TranumWang, HaitangSheinin, TatianaJoseph, Jamie W.Slavcev, Roderick A., Thermodynamic investigation of the binding of dissymmetric pyrenyl-gemini surfactants to DNA, Phys Chem Chem Phys., 12 (2010) 4821–4826.

[11] Torchilin, V. P., Recent approaches to intracellular delivery of drugs and DNA and organelle targeting, Annual Review of Biomedical Engineering, 8 (2006) 343–375.

[12] K. Rombouts, T.F. Martens, E. Zagato, J. Demeester, S.C. De Smedt, K. Braeckmans, K. Remaut, Effect of Covalent Fluorescence Labeling of Plasmid DNA on Its Intracellular Processing and Transfection with Lipid-Based Carriers, Molecular pharmaceutics, 11 (2015) 1359–1368.

[13] J. Buse, I. Badea, R.E. Verrall, A. El-Aneed, A general liquid chromatography tandem mass spectrometry method for the quantitative determination of diquaternary ammonium Gemini surfactant drug delivery agents in mouse keratinocytes' cellular lysate, Journal of Chromatography A, 1294 (2013) 98–105.

[14] J. Buse, R.W. Purves, R.E. Verrall, I. Badea, H. Zhang, C.C. Mulligan, K.M. Peru, J. Bailey, J.V. Headley, A. El-Aneed, The development and assessment of highthroughput mass

spectrometry-based methods for the quantification of a nanoparticle drug delivery agent in cellular lysate, Journal of Mass Spectrometry, 49 (2014) 1171–1180.

[15] M. Donkuru, D. Michel, H. Awad, G. Katselis, A. El-Aneed, HILIC-LC-MS/MS quantitative method for the cellular analysis of varying structures of gemini surfactants designed as nanomaterial drug carriers, Journal of Chromatography A, 1446 (2016) 114–124.

[16] R.K. Mahajan, S. Mahajan, A. Bhadani, S. Singh, Physicochemical studies of pyridinium gemini surfactants with promethazine hydrochloride in aqueous solution, Phys. Chem. Chem. Phys., 14 (2012) 887–898.

[17] I.A. Khalil, K. Kogure, H. Akita, H. Harashima, Uptake pathways and subsequent intracellular trafficking in nonviral gene delivery, Pharmacol Rev, 58 (2006) 32-45.

[18] R. Savić, L. Luo, A. Eisenberg, D. Maysinger, Micellar nanocontainers distribute to defined cytoplasmic organelles, Science, 300 (2003) 615–618.

[19] A. Elouahabi, J.M. Ruysschaert, Formation and intracellular trafficking of lipoplexes and polyplexes, Molecular therapy : the journal of the American Society of Gene Therapy, 11 (2005) 336-347.

[20] D. Niculescu-Duvaz, J. Heyes, C.J. Springer, Structure-activity relationship in cationic lipid mediated gene transfection, Current medicinal chemistry, 10 (2003) 1233-1261.

[21] D.D. Lasic, Recent developments in medical applications of liposomes: sterically stabilized liposomes in cancer therapy and gene delivery in vivo, Journal of Controlled Release, 48 (1997) 203–222.

[22] S.V. Boddapati, G.G. D'Souza, V. Weissig, Liposomes for drug delivery to mitochondria, Methods in molecular biology (Clifton, N.J.), 605 (2010) 295-303.

[23] A.M. Cardoso, C.M. Morais, A.R. Cruz, A.L. Cardoso, S.G. Silva, M.L. do Vale, E.F. Marques, M.C. Pedroso de Lima, A.S. Jurado, Gemini Surfactants Mediate Efficient Mitochondrial Gene Delivery and Expression, Molecular pharmaceutics, 12 (2015) 716-730.

[24] R. Mo, Q. Sun, J. Xue, N. Li, W. Li, C. Zhang, Q. Ping, Multistage pH-responsive liposomes for mitochondrial-targeted anticancer drug delivery, Adv. Mater., 24 (2012) 3659–3665.

[25] V. Weissig, G.G.M. D'Souza, Cationic Mitochondriotropic Vesicles for DNA Delivery to Mitochondria, Molecular Therapy, 9 (2004) S259–S259.

[26] V. Weissig, V.P. Torchilin, Mitochondriotropic cationic vesicles: a strategy towards mitochondrial gene therapy, Current pharmaceutical biotechnology, 1 (2000) 325-346.

[27] E. Garcia-Garcia, K. Andrieux, S. Gil, H.R. Kim, T.L. Doan, D. Desmaële, J. d'Angelo, F. Taran, D. Georgin, P. Couvreur, A methodology to study intracellular distribution of nanoparticles in brain endothelial cells, International journal of pharmaceutics, 298 (2005) 310-314.

[28] A. Sorkin, M. von Zastrow, Endocytosis and signalling: intertwining molecular networks, Nat Rev Mol Cell Biol, 10 (2009) 609-622.

[29] J. Singh, D. Michel, M.J. Chitanda, E.R. Verrall, I. Badea, Evaluation of cellular uptake and intracellular trafficking as determining factors of gene expression for amino acid-substituted gemini surfactant-based DNA nanoparticles, J. Nanobiotechnology, 10 (
2012) 1–14.

[30] R.E. Serda, A. Mack, A.L. van de Ven, S. Ferrati, K. Dunner, Jr., B. Godin, C. Chiappini, M. Landry, L. Brousseau, X. Liu, A.J. Bean, M. Ferrari, Logic-embedded vectors for

intracellular partitioning, endosomal escape, and exocytosis of nanoparticles, Small (Weinheim an der Bergstrasse, Germany), 6 (2010) 2691-2700.

[31] P. Saftig, J. Klumperman, Lysosome biogenesis and lysosomal membrane proteins: trafficking meets function, Nat Rev Mol Cell Biol, 10 (2009) 623-635.

[32] O. Zelphati, F.C. Szoka, Jr., Intracellular distribution and mechanism of delivery of oligonucleotides mediated by cationic lipids, Pharmaceutical research, 13 (1996) 1367-1372.

[33] C.J. Wheeler, P.L. Felgner, Y.J. Tsai, J. Marshall, L. Sukhu, S.G. Doh, J. Hartikka, J. Nietupski, M. Manthorpe, M. Nichols, M. Plewe, X. Liang, J. Norman, A. Smith, S.H. Cheng, A novel cationic lipid greatly enhances plasmid DNA delivery and expression in mouse lung, Proc Natl Acad Sci U S A., 93 (1996) 11454–11459.

[34] P.L. Felgner, G.M. Ringold, Cationic liposome-mediated transfection, Nature, 337 (1989) 387-388.

[35] I.M. Hafez, N. Maurer, P.R. Cullis, On the mechanism whereby cationic lipids promote intracellular delivery of polynucleic acids, Gene Ther, 8 (2001) 1188-1196.

[36] Y. Xu, F.C. Szoka, Jr., Mechanism of DNA release from cationic liposome/DNA complexes used in cell transfection, Biochemistry, 35 (1996) 5616-5623.

[37] E. Mastrobattista, G. Koning, L. Avan Bloois, A. Filipe, W. Jiskoot, G. Storm, Functional characterization of an endosome-disruptive peptide and its application in cytosolic delivery of immunoliposome-entrapped proteins, Journal of Biological Chemistry, 277 (2002) 27135–27143.

[38] S.V. Boddapati, P. Tongcharoensirikul, R.N. Hanson, G.G. D'Souza, V.P. Torchilin, V. Weissig, Mitochondriotropic liposomes, Journal of liposome research, 15 (2005) 49-58.

[39] D.A. Dean, D.D. Strong, W.E. Zimmer, Nuclear entry of nonviral vectors, Gene Ther, 12 (2005) 881-890.

[40] G.L. Lukacs, P. Haggie, O. Seksek, D. Lechardeur, N. Freedman, A.S. Verkman, Size-dependent DNA mobility in cytoplasm and nucleus, The Journal of biological chemistry, 275 (2000) 1625-1629.

[41] V. Escriou, M. Carrière, F. Bussone, P. Wils, D. Scherman, Critical assessment of the nuclear import of plasmid during cationic lipid-mediated gene transfer, The journal of gene medicine, 3 (2001) 179-187.

[42] Badea, Ildiko, Gemini cationic surfactant-based delivery systems for non-invasive cutaneous gene therapy College of Pharmacy & Nutrition, University of Saskatchewan, Saskatoon, 2006, pp. pp 237.

[43] P. Nikos, Subcellular Fractionation, Nature Methods, 3 (2013) 562.

[44] E.G. Bligh, W.J. Dyer, A rapid method of total lipid extraction and purification, Canadian journal of biochemistry and physiology, 37 (1959) 911-917.

[45] A.K. Hewavitharana, S.K. Tan, N.P. Shaw, Strategies for the Detection and Elimination of Matrix Effects in Quantitative LC–MS Analysis, LCGC North America, 32 (2014) 54–64.

[46] S.L. Ellison, M. Thompson, Standard additions: myth and reality, The Analyst, 133 (2008) 992–997.

[47] Kima, Junhwan, Hoppel, C. L., Comprehensive approach to the quantitative analysis of mitochondrial phospholipids by HPLC–MS Journal of Chromatography B, 912 (2013) 105–114.

[48] M. Gergov, T. Nenonen, I. Ojanperä, R.A. Ketola, Compensation of matrix effects in a standard addition method for metformin in postmortem blood using liquid chromatography–electrospray–tandem mass spectrometry, Journal of Analytical Toxicology, 39 (2015) 359–364.

[49] N. Cimetiere, I. Soutrel, M. Lemasle, A. Laplanche, A. Crocq, Standard addition method for the determination of pharmaceutical residues in drinking water by SPE-LC-MS/MS, Environmental Technology, 34 (2013) 3031–3041.

[50] P. Kościelniak, J. Kozak, M. Wieczorek, Calibration by the standard addition and indicative dilution method in flame atomic absorption spectrometry, J. Anal. At. Spectrom., 26 (2011) 1387–1392.

[51] P. Kościelniak, M. Wieczorek, J. Kozak, M. Herman, Generalized calibration strategy in analytical chemistry, Analytical Letters, 44 (2011) 411–430.

[52] M. Bader, A systematic approach to standard addition methods in instrumental analysis, Journal of Chemical Education, 57 (1980) 703–706.

[53] S. Altinöz, D. Tekeli, Analysis of glimepiride by using derivative UV spectrophotometric method, Journal of Pharmaceutical and Biomedical Analysis, 24 (2001) 507-515.

[54] M.H. Givianrad, M. Mohagheghian, Net analyte signal standard additions method for simultaneous determination of sulfamethoxazole and trimethoprim in pharmaceutical formulations and biological fluids, E-Journal of Chemistry, 9 (2012) 680–692.

[55] P. Valderrama, R.J. Poppi, Second order standard addition method and fluorescence spectroscopy in the quantification of ibuprofen enantiomers in biological fluids, Chemometrics and Intelligent Laboratory Systems, 106 (2011) 160-165.

[56] B. Alberts, A. Johnson, J. Lewis, D. Morgan, M. Raff, K. Roberts, P. Walter, Molecular Biology of the Cell, 6 ed., Garland Science, New York, NY, USA, 2014.

4.9 Supplementary Information

4.9.1 Supplementary Methods

4.9.1.1 *Protein recovery, 1-Dimensional SDS-PAGE and western blotting*

Isolated subcellular fractions were analyzed to verify their composition and purity using immunoblot assays.[1-3] First, to recover proteins from whole-cell cell pellet, nuclear pellet P2, mitochondrial pellet P3 and remnant subcellular pellet P4, the freshly collected pellets were resuspended in ice-cold 200 µL RIPA buffer for 30 mins. The protein-containing supernatants were collected after centrifugation at 15,000 rpm for 20 min, 4 ˚C. NOTE: The RIPA buffer contained 50 mM Tris-HCl, pH 8, 150 mM NaCl, 1% triton X 100, 0.5% sodium deoxycholate, 0.1% SDS and protease inhibitor. For proteins from plasma membrane fraction (isolated as supernatants, Figure 4.3), the supernatant S2 having 1.8 M sucrose was resuspended into sucrose-free 0.25 M SHE buffer to have 0.25 M sucrose.[1, 4] The pellet obtained upon centrifugation (5,000 × g, 10 min, 4 ˚C) was resuspended in ice-cold 200 µL RIPA buffer for 30 mins, followed further centrifugation at 15,000 rpm for 20 min, 4 ˚C to give the protein-containing supernatant. To obtain higher protein concentrations, the individual supernatants were combined with equal volume of –80 ˚C-cold acetone and the precipitated protein was reconstituted in a smaller volume of RIPA buffer. For the cytosolic fraction (also isolated as supernatant, Figure 4.3) no protein recovery steps were necessary.

For protein separation, protein from each fraction were mixed with equal volumes of 2× Leammli buffer and electrophoresed, 50 µg protein per lane, through 4-20% SDS-PAGE gels in tris-glycine running buffer. The resolved proteins were electrophoretically transferred to PVDF

membranes (GE Healthcare) at 400 mA for 1.75 h. The PVDF-bound proteins were blocked for 2 h in TTBS/milk buffer containing 20 mM Tris (pH 7.5), 150 mM NaCl, 0.1% Tween-20, and 5% nonfat dry milk.[1, 2] The membranes were then incubated in the same buffer with primary antibody cocktail (AB140365; Abcam, Canada) overnight at 4 ˚C, washed in TTBS and subsequently incubated for 2-h at room temperature in secondary antibody cocktail from same Abcam kit as instructed.[5] Finally, the blots were washed in TTBS, developed with enhanced chemiluminescence assay (Bio-Rad, Canada) and the protein bands were visualized with AlphaImager system (Bio-Rad, Canada) after up to 5-min exposure at ambient temperature.

4.9.2 *Supplementary Results*

4.9.2.1 *Purity and Western blot characterization of subcellular fractions*

Western blot results assessing the protein composition and purity of the subcellular fractions are presented in Figure S4.1. Organelle-specific protein antibodies were detected for the confirmation of the fractions, namely plasma membrane, mitochondria, cytosol, nucleus and the remnant subcellular residue. The lanes in Figure S4.1 show protein patterns as expected for the subcellular fractions and the whole-cell homogenate.

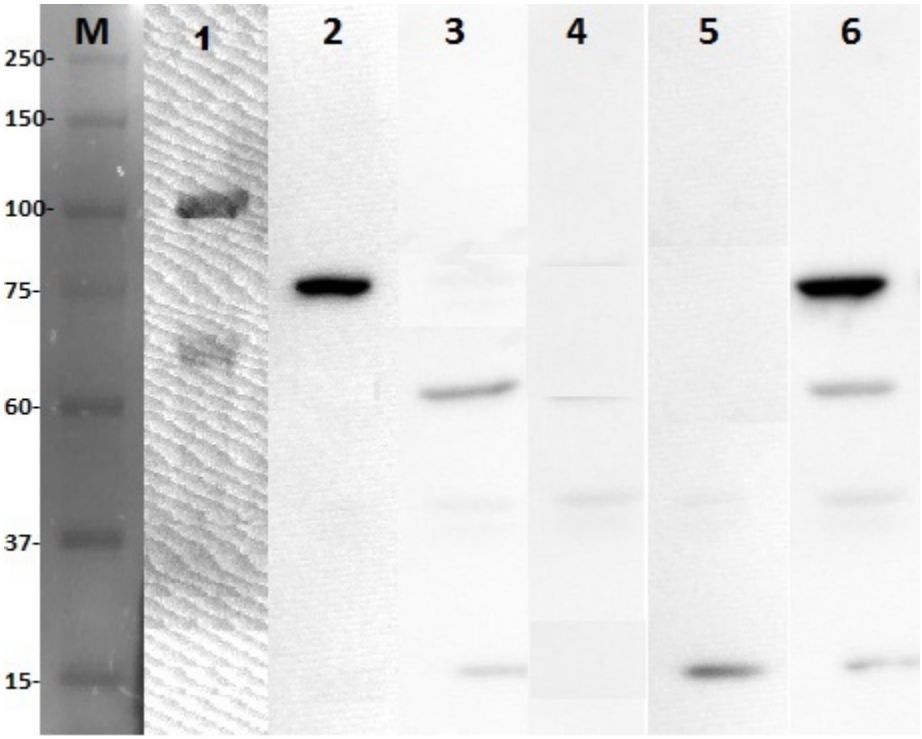

…

Figure S0.1: Immunoblot verification and assessment of the subcellular fractions from differential

centrifugation.

Lane M: protein molecular weight marker; **lane 1**: plasma membrane fraction; **lane 2**: endoplasmic reticulum (ER) fraction; **lane 3**: mitochondrial fraction; **lane 4**: cytosolic fraction; **lane 5**: nuclear fraction; **lane 6**: whole-cell homogenate. Samples in all lanes were probed with a single antibody cocktail containing all organelle-specific markers. The protein band sizes are: Na^+/K^+ ATPase ≈ 100 kDa, plasma membrane; GRP78 ≈ 78 kDa, ER; ATP5a ≈ 60 kDa, mitochondria; GAPDH ≈ 38 kDa, cytosol; histone H3 ≈ (di-methyl K9) ≈ 17 kDa, nucleus.

In the western blot experiments, the organelle-marker antibodies were applied in one-single cocktail to probe the subcellular fractions. So antibodies for one-organelle marker gives positive indication for that organelle while at the same time giving negative indication for the other organelles. There were few cross-contaminations in the subcellular fractions, especially the mitochondrial fraction, cytosolic fraction and nuclear fractions. However, the contamination did not in any way overwrite the distinct, relatively pure nature of the fractions. It should be noted that the subcellular fractions were isolated in parallel from the same cell-homogenate samples. The qualitative purity of organelles as shown by Figure S4.1 is consistent with the best purity limits observed when several, parallel subcellular fractions are isolated from single cell-homogenates.[6] Overall, the results show that the subcellular fractions were reasonably isolated, containing the right, intact organelles or cellular components.

4.9.3 *Supplementary Figure S1*

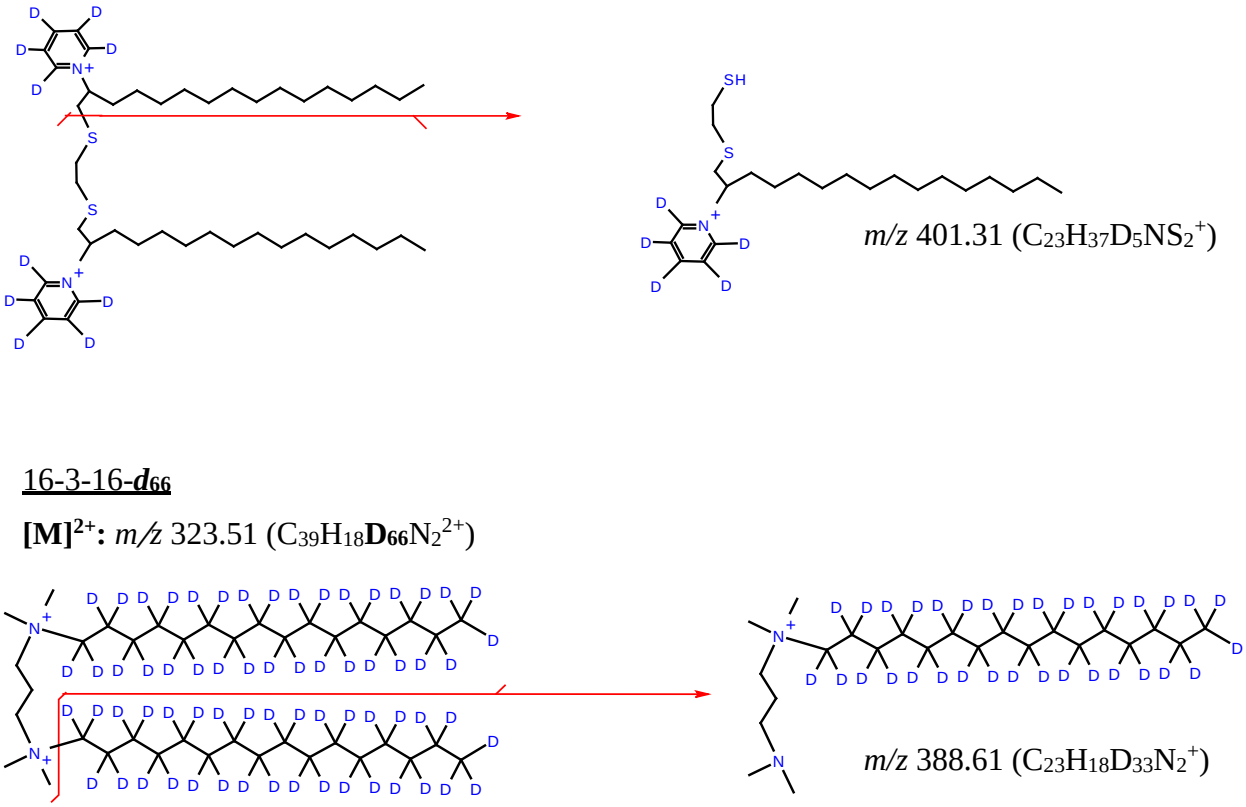

Figure S0.2: Product ions monitored for the internal standards 16(Py)-S-2-S-(Py)16-***d*$_{10}$ and 16-3-16-***d*$_{66}$ during HILIC-LC-MS/MS analysis.

4.9.4 Supplementary Table S4.1

Table S4.1. Conditions for MRM transitions of the analytes on AB Sciex 4000 QTRAP® System

Analyte		MRM Transition		DP*	CE*	CXE*
Gemini surfactant	Molecular Formula	$[M]^{2+} \rightarrow [M - X]^{+}$	*m/z* → *m/z*	(eV)	(eV)	(eV)
16(Py)-S-2-S-(Py)16	$C_{44}H_{78}N_2S_2^{2+}$	$[M]^{2+} \rightarrow [M - C_{21}H_{36}N]^{+}$	*m/z* 349 → 396	30	22	10
16(Py)-S-2-S-(Py)16	$C_{44}H_{78}N_2S_2^{2+}$	$[M]^{2+} \rightarrow [M - C_{34}H_{59}N_2]^{+}$	*m/z* 349 → 203	30	22	10
16(Py)-S-2-S-(Py)16-***d*$_{10}$**	$C_{44}H_{68}\mathbf{D_{10}}N_2S_2^{2+}$	$[M]^{2+} \rightarrow [M - C_{21}H_{31}\mathbf{D_5}N]^{+}$	*m/z* 354 → 401	30	25	10
16-3-16	$C_{39}H_{84}N_2^{2+}$	$[M]^{2+} \rightarrow [M - C_{16}H_{33}]^{+}$	*m/z* 290 → 355	40	21	10
16-3-16	$C_{39}H_{84}N_2^{2+}$	$[M]^{2+} \rightarrow [M - C_{33}H_{70}N_2]^{+}$	*m/z* 290 → 86	40	35	6
16-3-16-***d*$_{66}$**	$C_{39}H_{18}\mathbf{D_{66}}N_2^{2+}$	$[M]^{2+} \rightarrow [M - C_{16}\mathbf{D_{33}}]^{+}$	*m/z* 323 → 388	35	25	10

***Abbreviations:**

DP: declustering potential, CE: collision energy, CXE: collision cell exit potential; X: neutral loss

4.9.5 Supplementary References

[1] H.G. Nothwang, M. Becker, K. Ociepka, E. Friauf, Protein analysis in the rat auditory brainstem by two-dimensional gel electrophoresis and mass spectrometry, Molecular Brain Research, 116 (2003) 59-69.

[2] I. Guillemin, M. Becker, K. Ociepka, E. Friauf, H.G. Nothwang, A subcellular prefractionation protocol for minute amounts of mammalian cell cultures and tissue, Proteomics, 5 (2005) 35-45.

[3] D. Salvi, N. Rolland, J. Joyard, M. Ferro, Assessment of organelle purity using antibodies and specific assays: the example of the chloroplast envelope, Methods in molecular biology (Clifton, N.J.), 432 (2008) 345-356.

[4] P. Nikos, Subcellular Fractionation, Nature Methods, 3 (2013) 562.

[5] A. Scientific, Membrane Fraction WB Cocktail AB140365 (Product datasheet), 2016 (retrieved June 18), pp. 1–6.

[6] Y. Song, Y. Hao, A. Sun, T. Li, W. Li, L. Guo, Y. Yan, C. Geng, N. Chen, F. Zhong, H. Wei, Y. Jiang, F. He, Sample preparation project for the subcellular proteome of mouse liver, Proteomics, 6 (2006) 5269–5277.

…

CHAPTER 5:

DISCUSSIONS, CONCLUSION AND FUTURE WORK

5.1 General Discussion

Dicationic gemini surfactants have witnessed an intensive development and extensive exploration as non-viral vectors for nanoparticle-mediated delivery of therapeutic nucleic acids.[1] They have demonstrated promising gene transfection potencies through the ability to complex nucleic acids and compact them into nanoparticles, preserving the nucleic acid bioactivity and mediate the transport of the genetic cargo into target cells. This allows the expressing of therapeutic transgenes in host cells whereas such possibility is unachievable using control treatments involving *naked* nucleic acids.[2, 3] Along with this, gemini surfactants facilitate cellular internalization of other tested biomedical applications including anti-cancer drug delivery,[4] antimicrobial treatments[5-7] and bacterial transformations.[8]

While current gemini surfactant gene transfection efforts are advancing towards clinical trials, there is still little insights regarding the fate of gemini surfactant-based nanoparticles after entry into cells and release of their therapeutic cargo. In fact, gemini surfactants show varying degrees of cytotoxicity,[9, 10] which may, theoretically, be linked to their fate within cells. Cellular and subcellular fate of gemini surfactants encompasses the concept of quantitatively analyzing and understanding their cellular uptake, intracellular deposition, subcellular distribution, and possible metabolism and/or exocytosis. A better understanding of how intracellular/subcellular fate of the gemini surfactant relates to toxicity will aid in the

development of less toxic and more efficient compounds. To investigate the cellular and subcellular fate of gemini surfactants, effective bioanalytical methods are needed.

Therefore, my Ph.D. research investigated gemini surfactants using mass spectrometry, capitalizing on the specificity and selectivity of the technique for efficient detection and measurement of the target compound. Gemini surfactants bear permanent positive charges (i.e. quaternary amines) making them excellent candidates for MS analysis. Initially, compound-specific mass spectrometric fingerprints were established and adapted into bioanalytical methods for targeted analysis.

The gemini surfactant bioanalysis within nanoparticle-treated cells can benefit from analytical methods that offer a range of suitable capabilities. The developed and validated liquid chromatography-tandem mass spectrometric (LC-MS/MS) methods for gemini surfactant quantification were fast, sensitive and provided target analyte selectivity andspecificity. The mass spectrometric detection is suitable for the studied gemini surfactants which are not compatible with fluorescent/UV-detection due to the lack of fluorescent or UV-active structural features. On the other hand, the chromatographic step was necessary for target analyte separation from potential endogenous species co-extracted from cellular matrix and was a means for reducing matrix effects for better sensitivity.

5.1.1 Mass spectrometric characterization of dipyridinium and β-cyclodextrin-based diammonium gemini surfactants

The mass spectrometric characterization of gemini surfactants allowed for the confirmation of their molecular composition and structures, and for the identification of unique diagnostic product ions for each compound. To date, CID-MS/MS characteristics have been studied for a

number of traditional *m-s-m* quaternary ammonium gemini surfactants[11, 12] and their amino/dipeptide derivatives[13]; however, the vast majority of bioactive gemini surfactants are yet to studied. The gemini surfactants evaluated in my Ph.D. comprise novel β-cyclodextrin-based diquaternary ammonium and dipyridinium molecules, herein denoted as R-7N(*X*-suc-β-CD)-R and R̂(Py)-S-2-S-(Py)R̂, respectively (Figure 1.5). A combination of high-resolution single-stage (MS), tandem (MS/MS) and multi-stage (MS^n) analysis allowed for in-depth MS characterization. The high-resolution single-stage MS analysis showed abundant doubly-charged $[M]^{2+}$ species for the evlauted compounds at sub-1ppm mass accuracies and strongly confirmed/established the compound molecular formula and identity. This was achieved using a two-point internal calibration on an ESI-QqToF-MS system (Table 2.1).

The use of MS/MS and MS^3 analyses revealed comprehensive CID fragmentation beheviour of the gemini surfactants, including both universal and distinctive fragmentation patterns. The β-cyclodextrin-based diquaternary ammonium gemini surfactants showed a universal MS/MS fragmentation pattern as was the case for compounds from the dipyridinium gemini surfactant family. For example within one gemini surfactant family, the observed fragmentation included similar neutral loss of full alkyl tail moieties and alkyl-ammonium or alkyl-pyridinium neutral fragments by the individual compounds. The loss of alkyl tail moieties was also universal in the CID fragmentation of other gemini surfactants investigated in previous reports.[11, 12, 13]

However, there was a distinctive MS/MS pattern between compounds of these two families. The β-cyclodextrin-substituted compound fragmentation began with the loss of either one head-tail region or both head-tail regions; the resultant product ions, in both cases, further

dissociated through sequential cleavage of sugar moieties. For the bis-pyridinium gemini compounds, they either lost neutral pyridine(s) to give doubly-charged ions or formed complementary pyridinium alongside other singly-charged ions. For both gemini surfactant families, the MS/MS fragmentation generated compound-specific product ions marked by the presence of at least an intact alkyl tail portion.

The compound-specific product ions served as diagnostic ions and thus authenticated the molecular structures of the studied compounds and differentiated between isobaric compounds (with identical molecular mass). They confirmed the presence of unique structural features including pyridinium head-groups for the dipyridinium compounds and quaternary ammonium head-groups for the β-cyclodextrin-based diquaternary ammonium compounds.

Overall, at least eight diagnostic CID-MS/MS product ions were established for the β-cyclodextrin-based diquaternary ammonium and dipyridinium gemini surfactants. With this number, more diagnostic product ions were established for each investigated compound herein than for other gemini surfactants investigated in previous reports.[11, 12, 13] Based on the diagnostic CID-MS/MS fragment ions and distinctive fragmentation patterns, the dipyridinium and β-cyclodextrin-based based diquaternary ammonium gemini surfactants can be theoretically detected and unambiguously identified within any biological or environmental matrices.

5.1.2 Quantitative, hydrophilic interaction liquid chromatography tandem mass spectrometric method for of gemini surfactants

Cellular/subcellular fate investigation of gemini surfactants requires the development of effective validated analytical techniques. Liquid chromatography coupled to tandem mass spectrometry (LC-MS/MS) provides higher selectivity and sensitivity over other analytical

approaches for bioanalysis of gemini surfactants, their metabolites and endogenous molecules. Herein, zwitterionic hydrophilic interaction liquid chromatography-based (HILIC)-MS/MS methods were developed and validated for the separation of two lead gemini surfactants. The methods were also applicable to 18 compounds belonging to dipyridinium and diquaternary ammonium (m-s-m) gemini surfactant families (Table 3.2).

The HILIC-MS/MS analysis detected each gemini surfactant within PAM212 keratinocyte lysate with a distinctive retention time combined with selective MRMs based on abundant yet diagnostic product ions. The specific retention times coupled with analyte selectivity allowed for the differentiation of gemini surfactants with varying molecular structures. It was shown that gemini surfactants having an overall longer hydrophobic alkyl tails or longer alkyl spacer chains have shorter retention times on the HILIC column with a zwitterionic sulfoalkylbetaine stationary phase (Table 3.2).

The HILIC-MS/MS methods were fully validated as per the USFDA guidelines[14] for the quantitation of two lead dipyridinium and diquaternary ammonium gemini surfactants, designated as 16(Py)-S-2-S-(Py)16 and 16-3-16 respectively (Figure 2.1). The HILIC-MS/MS methods showed 60-fold higher sensitivity, 2-fold faster run times and are simplified with isocratic elution compared with other methods, most notably including a *cyano*-based LC-MS/MS method[15] which was only applicable to diquaternary ammonium gemini surfactants. The HILIC-MS/MS superiority is attributable to multiple factors that are related to sample preparation and the chromatographic separation. A 98%-efficient liquid-liquid extraction was achieved via the use of Bligh/Dyer lipid extraction method[16]. In addition, the sulfoalkylbetaine HILIC stationary phase is more compatible with the physicochemical properties of the studied

gemini surfactants. This compares with the *cyano*-based LC-MS/MS method[15] with 70% extraction efficiency using octanol and the unfavorable use of an ion-pairing reagent known for its ion suppressive effects.

Though the HILIC-MS/MS methods were effective for gemini surfactant determination at the whole-cell lysate, the ability to allow subcellular level analysis involving different subcellular fractions was also required. Therefore, a standard addition scheme in combination with HILIC-LC-MS/MS (*i.e.*, standard addition–HILIC-MS/MS) was developed to allow simultaneous analysis of different subcellular fractions and to compensate for matrix effects. The standard addition–HILIC-MS/MS method exhibited accuracy and precision (within accepted ± 15% margin), indicating that signal response was not affected by matrix effects across the different subcellular fractions. Overall, the HILIC-MS/MS and standard addition–HILIC-MS/MS methods were effective for the determination of gemini surfactants at both the whole-cell lysate and the subcellular level.

5.1.3 Bio-quantfication of 16(Py)-S-2-S-(Py)16 and 16-3-16 gemini surfactants: intracellular and subcellular fate in PAM 212 cells

To demonstrate their bioanalytical application, the developed/validated methods achieved effective quantification of the 16(Py)-S-2-S-(Py)16 and 16-3-16 gemini surfactants in PAM212 keratinocytes – through HILIC-MS/MS analysis of whole-cell lysates and standard addition–HILIC-MS/MS analysis of subcellular fractions. This allowed accurate determination of the cellular uptake of gemini surfactant-based nanoparticles, the gemini surfactant intracellular concentration-vs-time profiles and their subcellular distribution.

The *whole-cell* data revealed that both the 16(Py)-S-2-S-(Py)16 and 16-3-16 gemini surfactants were rapidly internalized by PAM212 keratinocytes during a 5-hour treatment period when gemini surfactant-based DNA nanoparticles were applied to the cells. Upon removal of the added nanoparticles, the intracellular gemini surfactant content underwent a depletion, with a 40-50% content remaining in cells after 54 hours. The depletion may indicate either gemini surfactant biodegradation or exocytosis from host cells, however, the overall similar trend presents no apparent explanation of a suggested toxicity difference between the 16(Py)-S-2-S-(Py)16 and 16-3-16 gemini surfactants.

Despite similar cellular uptake and intracellular depletion trends of the two compounds, their subcellular data showed different subcellular distribution profiles. The 16-3-16 gemini surfactant had a statistically significant increase in distribution to the mitochondria and nucleus relative to its 16(Py)-S-2-S-(Py)16 counterpart ($p < 0.05$), with the two having similar distribution to the cell membrane, cytosol and the remnant subcellular residue. This differential subcellular distribution, determined for the first time, may explain why 16-3-16 is apparently the more toxic compound. Its increased distribution to the mitochondria and nucleus may pose harmful effects to the biological integrity and function of the cells.

5.2 Summary and conclusions

The work accomplished in this research includes the mass spectrometric analysis of β-cyclodextrin-based diquaternary ammonium and dipyridinium gemini surfactants, including the establishment of universal CID-MS/MS fingerprints. The fingerprints defined diagnostic MRM

transitions for subsequently developing effective MRM bioanalytical methods required for gemini surfactant identification and quantitation.

The methods developed and validated were HILIC-MS/MS and the standard addition–HILIC-MS/MS; they were new for the gemini surfactants, sensitive, fast and simple. The HILIC-MS/MS and the standard addition–HILIC-MS/MS methods accomplished the quantification of target gemini surfactants, 16(Py)-S-2-S-(Py)16 and 16-3-16, within PAM212 whole-cell lysates and subcellular fractions after nanoparticle-based DNA transfection of cells. The generated data allowed a time-course monitoring of gemini surfactant internalization into cells along with their intracellular deposition and subcellular distribution. The rapid, initial cellular uptake of both gemini surfactants occurred as would be expected for successful entry of gemini surfactant-based DNA nanoparticles into cells.

Herein, the first time-observed depletion of the intracellular gemini surfactant content maybe indicative of biodegradation, exocytosis or both. Based on subcellular distribution, the increased distribution of 16-3-16 than its counterpart, 16(Py)-S-2-S-(Py)16, to the mitochondria and nucleus may explain its suggested higher toxicity. Together, this work and findings offer a new paradigm for future gemini surfactant development and exploration, establishing molecular fragmentation fingerprints of novel compounds and comprehensive MRM bioanalytical strategies for studying biological fate, elucidating varying toxicity and assessing the possible metabolite formation.

5.3 Future directions

The accomplished and described application of analytical mass spectrometric platforms for studying representative DNA transfection gemini surfactants highlight an effective investigative approach, at its pioneering stage, that can benefit future studies in two main directions. *First*, the CID-MS/MS analysis of fragmentation behaviour can be adapted and extended to other novel gemini surfactants, such as amino acid/peptide-based gemini surfactants. *Second*, fingerprint product ions established for the chosen and characterized compounds can then be adopted for developing/validating bioanalytical MS/MS methods for studying gemini surfactant biological fate.

5.3.1 Evaluation of the tandem mass spectrometric fragmentation across structural varieties of gemini surfactants

A wide variety of gemini surfactants developed for gene transfection represent worthy candidates for CID-MS/MS characterization to determine their fragmentation behaviour and establish unique product ions. For example, sub-categories of gemini surfactants with notable nucleic acid transfection abilities and low toxicity now include amine-/ammonium-containing compounds along with modified derivatives including sugar-based[17, 18], amino acid-/peptide-based[9, 19] and heterocyclic (imidazole, pyridinium) compounds.[20-22] Herein, the data generated will serve as a platform for CID-MS/MS fragmentation studies of new compounds including the above-mentioned gemini surfactant sub-categories.

Ultimately, the accumulation of fragmentation studies will build a library of diagnostic product ions for a vast range of gemini surfactants. This will offer unique MRM transitions for

different analytical scenarios including confirmation of synthetic target compounds, metabolite identification and identification/quantitation of compounds within complex bio-samples.

5.3.2 Quantitative assessment of *in vivo* and *in vitro* profiles of gemini surfactants

The systematic investigation of gemini surfactant cellular/subcellular (*in vitro*) fate using HILIC-MS/MS analysis in this work can be broadened to incorporate multiple data points: this includes multiple/extended post-transfection time-points at the whole-cell investigation level and the exploration of additional subcellular level components such as endosome/lysosome and extracellular media. This will help obtain more information about the cellular internalization, bio-distribution and toxicity of the 16(Py)-S-2-S-(Py)16 and 16-3-16 gemini surfactants. In particular, the observed depletion of the gemini surfactants after uptake into cells could be further probed by exploring the extracellular fluid to examine possible gemini surfactant exocytosis.

Beyond the PAM212 epidermal keratinocyte cellular model adopted for this work, the cellular/subcellular fate investigations can be extended to cover other cell lines so as to further explore the gemini surfactants studied herein. A noteworthy cell line is the breast cancer-derived cell, MCF-7, which has accounts for significant gemini surfactant-based anti-cancer gene delivery studies. Another cell line is the kidney fibroblast cell line, COS-7 cells[23], which has been widely used for evaluating the gene transfection and cytotoxic profiles of gemini surfactants, including 16-3-16. In addition, the investigations can be expanded into the *in vivo* biological fate, particularly for gemini surfactants tested in animal models for genetic and acquired diseases. Ultimately, the accumulation of data and insights into the *in vitro* and *in vivo*

fate of gemini surfactants will unearth and possibly help engineer desired relationships between compound structure, biological fate and toxicity.

An important aspect of studying the fate of gemini surfactants as constitutive element of gene delivery nanoparticles in biological hosts is our improved ability to determine the influence of nanoparticle properties on their bioactivity, toxicity and the biological fate. Although the molecular structure of the gemini surfactant is a significant influential factor with regards to the efficiency of gene delivery systems, the physicochemical properties of nanoparticles as a whole can exert equally strong or greater influence. Therefore, future gemini surfactant biological fate studies can be integrated with detailed physicochemical analysis of nanoparticle size, surface charge (termed zeta potential), pH sensitivity, bio-stability and aggregation. This allows a comprehensive evaluation of gemini surfactant biological fate and the effects of both compound structure and nanoparticle properties.

5.3.3 Investigation of gemini surfactant biodegradation and metabolite formation

Based on the first evidence of depletion of the studied 16(Py)-S-2-S-(Py)16 and 16-3-16 gemini surfactants within PAM212 epidermal keratinocytes as observed in this work, future research should evaluate the possible intracellular metabolism of gemini surfactants. Mass spectrometry offers an ideal tool for studying possible metabolites of the gemini surfactants due its ability to detect and identify structural modifications that accompany biotransformation of xenobiotics. That is, the capabilities of single-stage MS, CID-MS/MS and multi-stage MS^n can analyze biotransformations which are marked by differences in *m/z* values between parent compounds and their metabolites. In addition, neutral losses and precursor ion scans can be employed to aid in the identification of metabolites.

In addition to probing metabolite formation, the possibility of gemini surfactant exocytosis from host cells should be studied to determine its contribution to the observed intracellular depletion. In this case, the HILIC-MS/MS quantitations described in this work could be adopted for the analysis of extracellular matrix components. Knowledge of gemini surfactant exocytosis (under the wider scope of subcellular distribution) and gemini surfactant metabolism and metabolic pathways/sites will ultimately benefit the platform of gemini surfactant development for more efficiency and minimal toxicity.

5.4 References

[1] M. Donkuru, I. Badea, S. Wettig, R. Verrall, M. Elsabahy, M. Foldvari, Advancing nonviral gene delivery: lipid- and surfactant-based nanoparticle design strategies, Nanomedicine (Future Medicine) 5(7) (2010) 1103−1127.

[2] I. Badea, R. Verrall, M. Baca-Estrada, S. Tikoo, A. Rosenberg, P. Kumar, M. Foldvari, *In vivo* cutaneous interferon-γ gene delivery using novel dicationic (gemini) surfactant–plasmid complexes, Journal of Gene Medicine 7(9) (2005) 1200–1214.

[3] Badea, Ildiko, Gemini cationic surfactant-based delivery systems for non-invasive cutaneous gene therapy College of Pharmacy & Nutrition, University of Saskatchewan, Saskatoon, 2006, p. pp 237.

[4] D. Michel, J.M. Chitanda, R. Balogh, P. Yang, J. Singh, U. Das, A. El-Aneed, J. Dimmock, R. Verrall, I. Badea, Design and evaluation of cyclodextrin-based delivery systems to incorporate poorly soluble curcumin analogs for the treatment of melanoma, Eur J Pharm Biopharm, 2012 Elsevier B.V, Netherlands, 2012, pp. 548-56.

[5] S. He, B. Wang, H. Chen, C. Tang, Y. Feng, Preparation and antimicrobial properties of gemini surfactant-supported triiodide complex system, ACS Appl Mater Interfaces **4**(4) (2012) 2116–2123.

[6] L. Caillier, E. Taffin de Givenchy, R. Levy, Y. Vandenberghe, S. Geribaldi, F. Guittard, Polymerizable semi-fluorinated gemini surfactants designed for antimicrobial materials, J. Colloid. Interface Sci. **332**(1) (2009) 201-207.

[7] J. Chlebicki, J. Węgrzyńska, I. Maliszewska, M. Oświęcimska, Preparation, surface-active properties, and antimicrobial activities of bis-quaternary ammonium salts from amines and epichlorohydrin, Journal of Surfactants and Detergents **8**(3) (2005) 227–232.

[8] L. Horniak, F. Devínsky, P. Balgavý, I. Lacko, L. Ebringer, Quaternary ammonium halides for increased efficiency of
bacterial transformation, Commenius University in Bratislava, Czechoslovakia, 1990.

[9] J. Singh, P. Yang, D. Michel, R.E. Verrall, M. Foldvari, I. Badea, Amino acid-substituted gemini surfactant-based nanoparticles as safe and versatile gene delivery agents, Curr Drug Deliv, United Arab Emirates, 2011, pp. 299-306.

[10] M. Donkuru, S.D. Wettig, R.E. Verrall, I. Badea, M. Foldvari, Designing pH-sensitive gemini nanoparticles for non-viral gene delivery into keratinocytes, J. Mater. Chem. 22 (2012) 6232-6244.

[11] J. Buse, I. Badea, E.R. Verrall, A. El-Aneed, Tandem Mass Spectrometric Analysis of the Novel Gemini Surfactant Nanoparticle Families G12-s and G18:1-s, Spectroscopy Letters 43 (2010) 447–457.

[12] J. Buse, I. Badea, R.E. Verrall, A. El-Aneed, Tandem mass spectrometric analysis of novel diquaternary ammonium gemini surfactants and their bromide adducts in electrospray-positive ion mode ionization, J Mass Spectrom 46(10) (2011) 1060-70.

[13] W. Mohammed-Saeid, J. Buse, I. Badea, R. Verrall, A. El-Aneed, Mass spectrometric analysis of amino acid/di-peptide modified gemini surfactants used as gene delivery agents: Establishment of a universal mass spectrometric fingerprint, *Int. J. Mass Spectrom.* 309 (2012) 182–191.

[14] J. Kadavil, B. Booth, Bioanalytical Method Validation - Biopharmaceutics (guidance for Industry), Food and Drugs Administration, United States of America, 2013, pp. 1–28.

[15] J. Buse, I. Badea, R.E. Verrall, A. El-Aneed, A general liquid chromatography tandem mass spectrometry method for the quantitative determination of diquaternary ammonium Gemini surfactant drug delivery agents in mouse keratinocytes' cellular lysate, Journal of Chromatography A 1294 (2013) 98–105.

[16] E.G. Bligh, W.J. Dyer, A rapid method of total lipid extraction and purification, Can J Biochem Physiol 37(8) (1959) 911-7.

[17] M.L. Fielden, C. Perrin, A. Kremer, M. Bergsma, M.C. Stuart, P. Camilleri, J.B. Engberts, Sugar-based tertiary amino gemini surfactants with a vesicle-to-micelle transition in the endosomal pH range mediate efficient transfection in vitro, Eur J Biochem, Germany, 2001, pp. 1269-79.
[18] L. Wasungu, M. Scarzello, G. van Dam, G. Molema, A. Wagenaar, J.B. Engberts, D. Hoekstra, Transfection mediated by pH-sensitive sugar-based gemini surfactants; potential for in vivo gene therapy applications, J Mol Med (Berl) 84(9) (2006) 774-84.
[19] P. Yang, J. Singh, S. Wettig, M. Foldvari, R.E. Verrall, I. Badea, Enhanced gene expression in epithelial cells transfected with amino acid-substituted gemini nanoparticles., European Journal of Pharmacuetics & Biopharmacuetics 75(3) (2010) 311–320.
[20] V.D. Sharma, M.A. Ilies, Heterocyclic cationic gemini surfactants: a comparative overview of their synthesis, self-assembling, physicochemical, and biological properties, Medicinal Research Reviews 34(1) (2014) 1–44.
[21] A. Bhadani, S. Singh, R. Kamboj, V. Chauhan, Synthesis and self-aggregation properties of ester-functionalized heterocyclic pyrrolidinium surfactants, Colloid and Polymer Science 291(10) (2013) 2289–2297.
[22] A. Bhadani, S. Singh, H. Sakai, M. Abe, Synthesis and Properties of Heterocyclic Cationic Gemini Surfactants, in: H. Ohshima (Ed.), Encyclopedia of Biocolloid and Biointerface Science, John Wiley & Sons, Inc., Hoboken, NJ, USA, 2016.
[23] L. Li, Y. Nie, D. Ye, G. Cai, An easy protocol for on-chip transfection of COS-7 cells with a cationic lipid-based reagent, Lab Chip 9 (2009) 2230–2233.

…